

Chemistry-Climate Interactions
in the Coupled Atmosphere-Chemistry-Ocean
Model SOCOL-MPIOM

INAUGURALDISSERTATION
der Philosophisch-naturwissenschaftlichen Fakultät
der Universität Bern

vorgelegt von

Stefan Muthers

Leiter der Arbeit:

PD. Dr. Christoph C. Raible
Prof. Dr. Thomas F. Stocker

Abteilung für Klima- und Umweltphysik
Physikalisches Institut der Universität Bern

Chemistry-Climate Interactions
in the Coupled Atmosphere-Chemistry-Ocean
Model SOCOL-MPIOM

INAUGURALDISSERTATION
der Philosophisch-naturwissenschaftlichen Fakultät
der Universität Bern

vorgelegt von

Stefan Muthers

Leiter der Arbeit:

PD. Dr. Christoph C. Raible
Prof. Dr. Thomas F. Stocker

Abteilung für Klima- und Umweltphysik
Physikalisches Institut der Universität Bern

Von der Philosophisch-naturwissenschaftlichen Fakultät angenommen.

Bern, 17. Juni 2014

Der Dekan
Prof. Dr. Silvio Decurtins

Wissen bringt neues Unwissen hervor.

Terry Pratchett, I. Stewart, and J. Cohen «Die Gelehrten der Scheibenwelt».

*Eine neue Doktorarbeit ist immer auch eine Art Orgie
von alten Doktorarbeiten, die sich
untereinander, ähm, befruchten, damit etwas
Neues noch nie Dagewesenes aus ihnen hervorgeht.*

Dr. Oztafan Kolibril in Walter Moers «Rumo & Die Wunder im Dunkeln».

Contents

Thesis summary	iii
Abbreviations	vii
1. Introduction	1
1.1. Motivation	1
1.2. The climate system	1
1.3. Climate variability and external forcings	5
1.3.1. Solar variability	7
1.3.2. Volcanic activity	11
1.4. Stratospheric ozone chemistry and chemistry-climate interactions	14
1.4.1. Stratospheric ozone chemistry	17
1.4.2. Chemistry-climate interactions	20
1.5. Modelling of chemistry-climate interactions	23
1.5.1. The atmosphere-ocean-chemistry-climate model SOCOL-MPIOM	26
1.5.2. Overview of the simulations used in this thesis	27
1.6. Outline	31
Bibliography	32
2. The coupled atmosphere-chemistry-ocean model SOCOL-MPIOM	47
2.1. Introduction	49
2.2. Model description and experimental setup	51
2.2.1. Model description	51
2.2.2. Experiments	53
2.2.3. Observational data sets	59
2.3. Pre-industrial model climatology and imprint of atmospheric chemistry	59
2.3.1. Stratospheric changes with interactive chemistry	61
2.3.2. Tropospheric and surface changes	66
2.3.3. Climate sensitivity of SOCOL-MPIOM	69
2.4. Transient climate simulations	71
2.4.1. Temperature variability in the pre-industrial period	71
2.4.2. Temperature trends after 1850	75
2.5. Discussion and Conclusions	79
Bibliography	82
3. Northern hemispheric winter warming pattern after tropical volcanic eruptions: Sensitivity to the ozone climatology	91
Supplementary material	108

4. Dynamical and chemical ozone perturbations after large volcanic eruptions:	
Role of the climate state and the strength of the eruption	111
4.1. Introduction	112
4.2. Model and experiments	114
4.2.1. Model	114
4.2.2. Experiments	115
4.2.3. Observations	117
4.3. Evaluation of the model	118
4.3.1. Global mean temperature response	118
4.3.2. Stratospheric response	119
4.3.3. Tropospheric response	122
4.4. Underlying mechanisms of response behavior	124
4.4.1. Dynamic effect vs. heterogeneous reactions	125
4.4.2. Dynamic response of the combined ozone changes	128
4.5. Influence of the climate state and the eruption strength	129
4.5.1. Ozone changes	129
4.5.2. Temperature and dynamic changes	130
4.6. Discussion and Conclusions	133
Bibliography	136
5. Outlook	141
Bibliography	143
A. Appendix	145
A.1. Impact of a potential 21st century "grand solar minimum" on surface temperatures and stratospheric ozone	145
Supplementary material	152
A.2. Forcing of stratospheric chemistry and dynamics during the Dalton Minimum Supplementary material	155
Supplementary material	173
A.3. Impact of solar vs. volcanic activity variations on tropospheric tempera- tures and precipitation during the Dalton Minimum	177
Supplementary material	196
Acknowledgements	199
Publications	201
Erklärung gemäss Reglement RSL 05 Art. 28 Abs. 2	203
Curriculum Vitae	205

Thesis summary

Understanding natural variations in the climate system and the influence of different components of the climate system on these variations is an important prerequisite to interpret past changes in the climate system and projections for the future. In this thesis an atmosphere-ocean-chemistry-climate model (AOCCM) is developed by coupling a chemistry-climate model (CCM) to an ocean model, which is then used to analyse the influence of the atmospheric chemistry in various case studies. A particular focus is on interactions between the atmospheric chemistry and the external forcings, motivated by the questions whether the atmospheric chemistry reinforces or balances changes in the climate system. Furthermore, the role of solar variations and volcanic activity for past and future climates is addressed in simulations for the past 400 and the upcoming 100 years. These simulations are forced by a state-of-the-art spectral solar forcing reconstruction with a large amplitude and the results are compared against proxy based temperature reconstructions.

The **introductory chapter** gives an overview of the climate system and the components and processes relevant for this thesis. Furthermore, the current state of knowledge of the past (and future) solar and volcanic activity as well as the principles of the stratospheric ozone chemistry and their interactions with the climate system are summarised.

In **Chapter 2** the model SOCOL-MPIOM is presented and the characteristic of the AOCCM is evaluated using a number of pre-industrial control simulations and transient experiments for the period 1600-2000 AD. A pre-industrial time-slice simulation with interactive chemistry is used to analyse the characteristics of the coupled model, which is compared to a second control simulation forced by the same boundary conditions, but without interactive chemistry. By comparing both simulations, we find an overall minor influence of the interactive chemistry on the climate state and the variability. Temperatures differ in the mesosphere and the higher stratosphere. These changes are related to a parametrisation for UV absorption by oxygen and ozone and to diurnal variations in the ozone concentrations in the mesosphere, both are included in the model with interactive chemistry only. The influence of these temperature differences on the dynamics is small and limited to the stratosphere. Furthermore, SOCOL-MPIOM is used in transient simulation for the period 1600-2000 AD, forced by two spectral solar irradiance (SSI) reconstructions with medium and large centennial scale variations, respectively. The influence of the solar forcing is obvious in the pre-industrial temperature variations, although the differences between the two forcings is not always detectable. Overall, the Northern Hemispheric scale temperature variations are within the uncertainty range of proxy based temperature reconstructions, but the spatial patterns for the Maunder and the Dalton Minimum suggest an overestimation in many regions. In the industrial period the simulations undergo a pronounced and globally uniform increase of surface air temperature. In comparison to observations the temperature trends are overestimated by about a factor of two. In sensitivity experiments, the relative importance of the major greenhouse gases (GHGs), the solar forcing, stratospheric and tropospheric aerosols,

as well as the simulated ozone changes are assessed. Furthermore, climate sensitivity experiments are performed to estimate the climate sensitivity of SOCOL-MPIOM. In summary, the simulated temperature trends from 1850 onwards can be understood by a combination of the GHGs induced warming with additional positive contributions from the comparable large solar forcing used and the simulated ozone changes. All of them are amplified by the comparable high climate sensitivity of the model (transient climate response: 2.2 K). This study is published as a discussion paper in *Climate of the Past Discussions* and is currently under review for publication in *Climate of the Past*.

Chapter 3 presents a study published in the *Journal of Geophysical Research*, in which we use a configuration of SOCOL-MPIOM without interactive chemistry to analyse the role of different ozone climatologies in the dynamic response to strong tropical volcanic eruptions. Ozone climatologies are commonly used in models without interactive chemistry to consider seasonal variations in the ozone concentrations in the radiation schemes. Here, we compare a climatology with stronger and weaker meridional ozone gradients. Ensemble simulations were conducted with a single strong volcanic eruption in the beginning and compared to a set of ensemble control simulations without volcanic eruptions, for each climatology separately. With larger meridional gradients in stratospheric ozone, the northern polar vortex is stronger in the background state and the eruption leads to an additional intensification. This intensification results in a significant increase in the coupling of wind anomalies between stratosphere and troposphere and a highly significant positive phase of the North Atlantic Oscillation (NAO) in the first winter after the eruption. With weaker meridional ozone gradients the response is qualitatively similar but weaker and not significant. The comparison of the number of coupling events in the ensemble simulations reveals indications for non-linear interactions between the ozone gradient and the perturbation by the volcanic aerosols.

Following from these results **Chapter 4** focuses on the ozone changes after a strong volcanic eruption in the model with interactive chemistry. Ozone changes are in general influenced by two different processes. Firstly, stratospheric dynamics and chemical reactions rates are affected by the warming in the tropical lower stratosphere, which we summarise as dynamical processes. Secondly, the volcanic aerosols provide surfaces for a number of heterogeneous chemical reactions in the aerosol clouds, that modify the chemical ozone balance of the stratosphere. In idealised simulations the importance of these two processes as well as the combination of both for the ozone changes and the dynamics is addressed by a number of ensemble simulations. Furthermore, the influence of the eruption strength and the climate state, i.e. a present day atmosphere vs. a pre-industrial atmosphere, is simulated. The two climate states differ in their amount of GHGs and ozone depleting substances in the atmosphere. We find that dynamical processes result in rapid changes in the ozone concentrations in the tropics and mid latitudes, almost independent of the climate state. The dynamical mechanism has the largest effect on the dynamics with the intensification of the polar vortex and the following changes in the tropospheric circulation of the northern high latitudes. Significant influences of the second mechanism, heterogeneous chemical reactions are only found in the present day climate state, with a general reduction of the ozone concentrations that is amplified in the high latitudes during polar night and spring. The reaction of the chemistry is slower in comparison to the dynamic mechanism, but longer lasting. With larger eruption strength the amplitude and the duration of the ozone depletion increases. The ozone changes lead to a slight but significant weakening of the polar vortex in mid

winter and a slight intensification in spring. The results of this study are currently under review for publication in the *Journal of Geophysical Research*.

The appendix of this thesis covers three publications addressing mainly the role of solar variability. In **Chapter A.1**, published in the *Geophysical Research Letters*, the influence of a possible grand solar minima within the 21th century is simulated under the RCP 4.5 scenario. Two different reduction scenarios are compared to simulations without reduced solar forcing. With solar minima the temperatures at the end of the 21th century increase by 1.61°C, 1.75°C for a strong and weak minimum, respectively, in comparison to 1.96°C without solar minimum. Furthermore, a significant delay of the stratospheric ozone recovery is found with solar minimum, in particular in the tropics and subtropics. Finally, sensitivity experiments for the Dalton Minimum (DM) are presented in **Chapter A.2** and **A.3**, published in *Atmospheric Chemistry and Physics* and *Climate of the Past*, separately for the stratospheric dynamics and chemistry and dynamical changes in the troposphere. Here, we explore the relative importance of the top-down (UV variability only), bottom-up (visible and near infrared variability only), volcanic aerosols, and energetic particle precipitation (EPP) for climate change in the period 1780-1840. In the stratosphere, UV variability significantly reduces the ozone concentrations and cools the middle atmosphere, but the influence on the dynamics is weak. Dynamical changes are mainly a result of the volcanic aerosols, which heat the lower tropical stratosphere and intensify the polar vortices in both hemispheres. Volcanic aerosols further have opposing effects on stratospheric ozone. Increased stratospheric water vapour concentrations enhance the catalytic ozone destruction by HO_x whereas heterogeneous chemical reactions increase ozone in the tropical stratosphere. Variation in the visible spectrum and EPP have only very small influence on the stratosphere during the DM. In the troposphere, however, the volcanic eruptions together with variations in the visible and near infrared are the driver of the temperature variability, whereas the influence of the top-down mechanism is low. Volcanic eruptions, furthermore, significantly affect the dynamics, visible in a widening of the Hadley cell and the winter warming pattern in the northern high latitudes.

Abbreviations

AMO Atlantic Multidecadal Oscillation.

AMOC Atlantic Meridional Overturning Circulation.

AO Arctic Oscillation.

AOCCM atmosphere-ocean-chemistry-climate model.

AOGCM atmosphere-ocean-general-circulation model.

BDC Brewer-Dobson circulation.

CCM chemistry-climate model.

CFCs chlorofluorocarbons.

DM Dalton Minimum.

EBM energy balance model.

ECMWF European Centre of Medium-Range Weather Forecasts.

ECS equilibrium climate sensitivity.

ENSO El-Niño Southern Oscillation.

EOF empirical orthogonal function.

GCM general circulation model.

GCR galactic cosmic rays.

GHG greenhouse gas.

LIA Little Ice Age.

LW long-wave.

MM Maunder Minimum.

NAM Northern annular mode.

NAO North Atlantic Oscillation.

NH Northern Hemisphere.

ODS ozone depleting substances.

PSC polar stratospheric cloud.

QBO Quasi-Biennial Oscillation.

RCP Representative Concentration Pathways.

RF radiative forcing.

SAD surface area density.

SAM Southern annular mode.

SEP solar energetic particle.

SH Southern Hemisphere.

SSI spectral solar irradiance.

SSW sudden stratospheric warmings.

SW short-wave.

TCR transient climate response.

TOA top-of-the-atmosphere.

TSI total solar irradiance.

UV ultra-violet radiation.

Chapter 1.

Introduction

1.1. Motivation

Human activity has changed the composition of the atmosphere faster and more fundamental than any time in the last 800 000 years (IPCC, 2013). By the emission of more than 550 Gt of carbon, the radiative forcing has undergone rapid changes making it *extremely likely* that the observed temperature increase is due to human emitted greenhouse gases (IPCC, 2013). Furthermore, the emission of ozone depleting substances has dramatically changed the chemical composition of the stratosphere, resulting in a serious loss of stratospheric ozone (WMO, 2002). The fingerprint of human influence is obvious almost everywhere on our planet, leading to the discussion whether the Earth has entered a new era, the Anthropocene (Crutzen and Stoermer, 2000). While the Montreal protocol (1987) implemented a fast and rigorous reaction to the stratospheric ozone depletion, a similar agreement for the emission of GHG is still outstanding.

A comprehensive understanding of the climate system, the processes driving climate change, and the underlying uncertainties is fundamental to project future changes in the climate system, the regional impacts, and to develop and implement mitigation and adaptation strategies. This involves in particular knowledge about natural changes, both due to internal variations of the climate system and due to changes caused by variations in the external forcings. Moreover, the climate system is a complex system of interacting components. Therefore, also interactions between different components are important, since changes may be amplified (damped) by positive (negative) feedbacks in other components of the climate system.

This thesis focuses on the influence of atmospheric chemistry on the climate in coupled AOCCM simulations. Therefore, a CCM has been coupled to an interactive ocean model. Of particular interest is the response of the model to solar variability and volcanic activity on past and future climate and the role of atmospheric chemistry in shaping this response. The following chapter gives an overview of the climate system and the processes relevant for this thesis. Furthermore, the model used and the simulations conducted are introduced. An outline of the following chapters is given at the end.

1.2. The climate system

Climate is the pattern of variations (statistic) of the weather for a specific area and a sufficient long period of time (Cubasch et al., 2013). The weather can be described by a set of meteorological variables (temperature, sea level pressure, precipitation, etc.) that characterise the current state of the atmosphere for a particular moment in time. *Climate*

1. Introduction

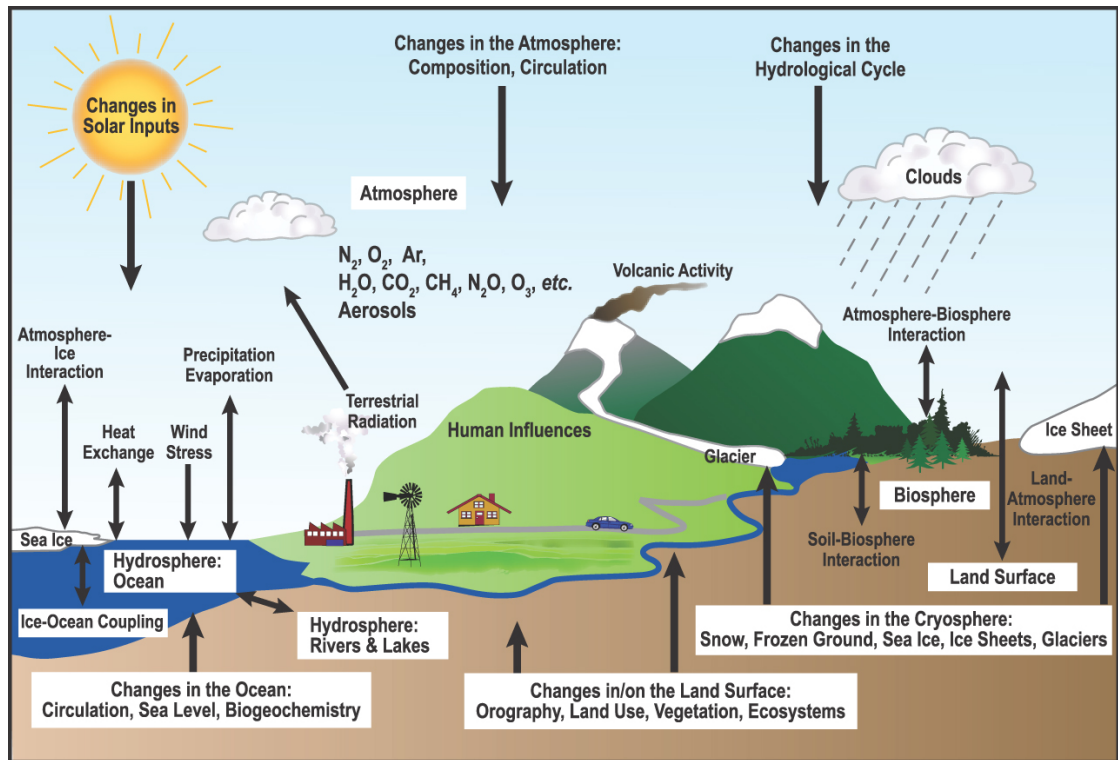


Figure 1.1.: Schematic overview of the climate system with the most important climate components and their interactions (Fig. from Le Treut et al., 2007).

change refers to a change in the statistic of the climate, which can reflect, e.g., in a change of the average or the extreme values. The term *climate system* is appropriate, since climate is the result of interactions between several components. The major components of the climate system are the atmosphere, the ocean, the cryosphere, the land surface, and the biosphere (Fig. 1.1). Each of them, however, can be divided further, e.g., the atmosphere into a physical and a chemical component. All of these components exchange energy, mass, momentum, and freshwater with each other. Changes in the fluxes alter the internal dynamics of each component, which in turn affect the exchange with other components. The climate system therefore is a coupled system. Each component is characterised by a different response time scale. The atmosphere usually adjusts very rapidly to changes, the ocean on the other side needs several millennia until a change is balanced and a new equilibrium is reached. In reality, the climate system is never in equilibrium, since the boundary conditions are changing throughout the time.

The atmosphere is a thin gaseous layer around the Earth, consisting of nitrogen (N₂, 78.08%), oxygen (O₂, 20.95%), argon (Ar, 0.93%) and a large number of trace gases. Important trace gases are carbon dioxide (CO₂), with concentrations of 0.039% or 390.5 ppm (parts per million) in 2011 (Hartmann et al., 2013), and water vapour, the latter undergoes pronounced variations in time and space. Besides the gaseous components, the atmosphere also contains various aerosols, which are important for cloud formation and in the absorption and reflection of radiation.

Different metrics exist to describe the vertical structure of the atmosphere. A common criterion is the vertical temperature profile, which divides the atmosphere into spheres

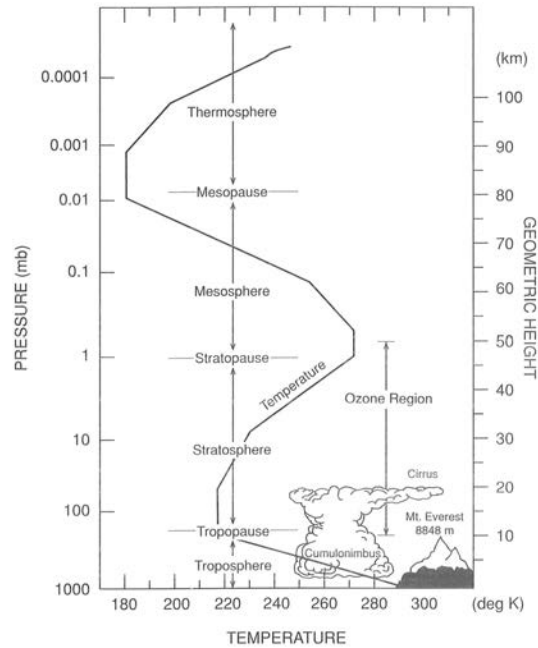


Figure 1.2.: Vertical temperature structure of the atmosphere and related atmospheric layers (Fig. from Brasseur et al., 1999).

with homogeneous temperature gradients (Fig. 1.2). Following this, the lowermost part of the atmosphere is the troposphere, where temperatures in general continuously decrease up to the tropopause. The altitude of the tropopause depends on the latitude with up to 17 km in the tropics and about 9 km in the high latitudes. Besides this decline of the tropopause height from low to high latitudes, pronounced variability in the tropopause level exists. The troposphere stores most of the atmospheric water vapour and is the sphere where weather takes place. Above the tropopause in the stratosphere, temperatures increase again, up to the stratopause at about 50 km. Increasing temperatures are related to the absorption of radiation linked with stratospheric chemistry, most important the ozone chemistry. The water vapour pressure in the stratosphere is in general very low, but under extreme cold conditions of the polar stratosphere, specific types of polar stratospheric clouds (PSCs) can develop. The stratosphere is also important in the context of understanding the global impact of strong volcanic eruptions. In the troposphere, volcanic aerosols are usually deposited after several days or a few weeks. Their influence on the climate is therefore only short lived. However, if the emitted eruption products are transported across the tropopause they can stay in the stratosphere for several years. Furthermore, the stratospheric circulation distributes the aerosols globally with impacts on the large scale radiance balance. Although the weather is mainly limited to the troposphere, the dynamics in the stratosphere can also influence the troposphere and vice versa. Above the stratopause in the mesosphere, temperatures decrease again up to the mesopause (80 km). From there on in the thermosphere, the sign of the temperature profile changes again.

An alternative metric for the vertical structure of the atmosphere divides the atmosphere into the well mixed homosphere and the heterosphere, where molecular diffusion dominates. The transition zone between homosphere and heterosphere is called tur-

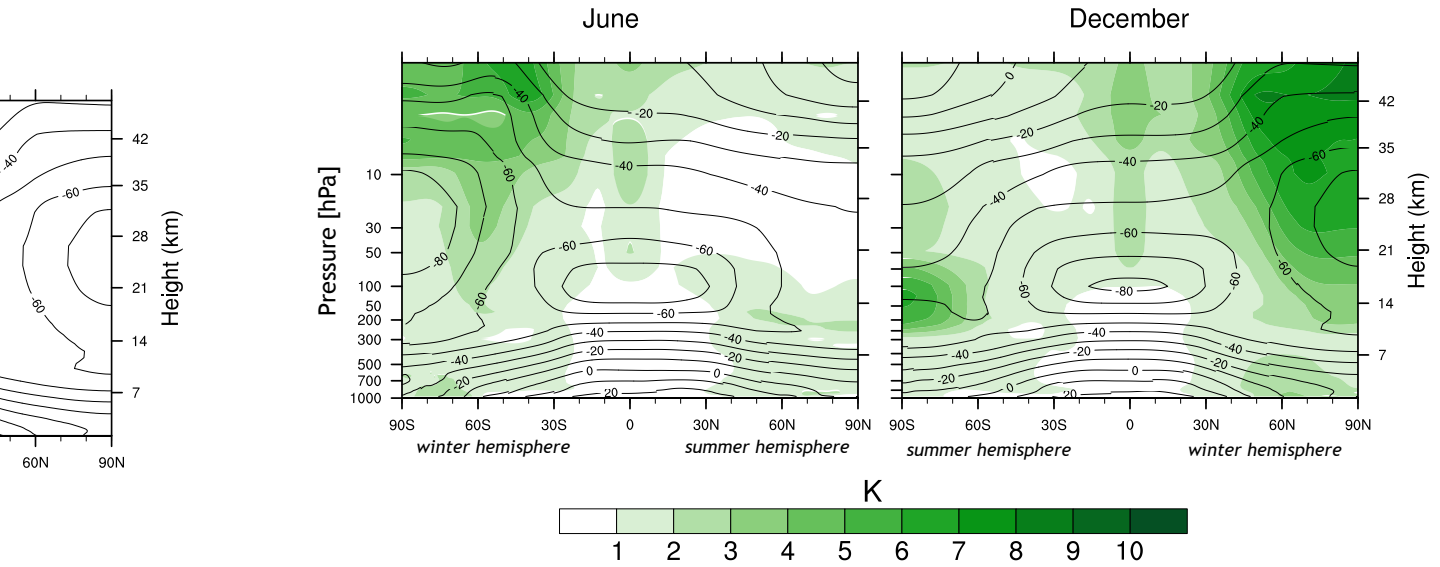


Figure 1.3.: Monthly mean zonally averaged temperature (contours) and standard deviation (colours) for (left) June and (right) December in ERA Interim (Dee et al., 2011) averaged over the period 1979-2012.

bopause (80-100 km). Furthermore, the radio-electrical properties allow a separation into the neutrosphere, with mainly neutral gases and the ionosphere, where solar UV and shorter wavelength produce free electrons and electrically charged atoms and molecules.

The word climate originates from Greek word for *incline* (*κλίμα*, *κλίματις*), which already refers to the primary driver of the climate system the Sun. A small fraction (a billionth) of the energy emitted by the Sun reaches our planet where it is either reflected back to space or absorbed in the atmosphere or at the surface. The amount of solar radiation that reaches the surface, however, depends on the inclination angle (path length through the atmosphere), which is a product of the time of the day, the season and the latitude. The short-wave (SW) radiation available at the surface is therefore not equally distributed, but is larger in low than in high latitudes and greater in summer than in winter.

The spatial and temporal differences in the energy input from the Sun result in temperature differences (Fig. 1.3), which drive the dynamics in the atmosphere and the ocean. In the troposphere, the highest temperatures are found in the tropics, almost independent of the season. Towards the poles, the seasonal differences become larger for both hemispheres. In the stratosphere, the differences between summer and winter are even more pronounced. Very cold conditions ($< -70^{\circ}\text{C}$) are found in the winter polar stratosphere facilitating the formation of PSCs, while temperatures in the summer polar stratosphere are in the order of -40°C . Persistent cold conditions are present in the lower tropical stratosphere during the entire year. Emphasis is put here on the fact that the climatological mean temperature exhibits profound month-to-month and year-to-year variability. The largest temperature variability in the stratosphere occurs in the high latitudes during the winter months, similar to the troposphere, although the variability in the stratosphere is overall more pronounced.

The temperature differences between high and low latitudes and the seasonal variations drive characteristic circulation patterns, depicted in Figure 1.4. The general tendency of the circulation is to balance the temperature contrasts by the transport of heat from

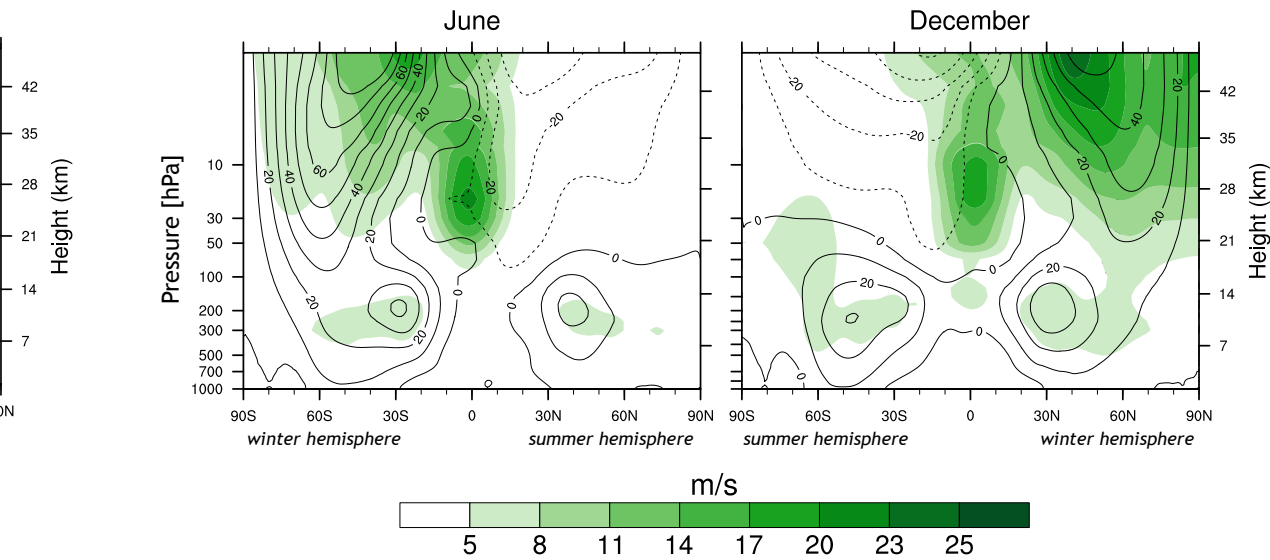


Figure 1.4.: Monthly mean zonally averaged zonal mean wind component (contours) and standard deviation (colour) for (left) June and (right) December in ERA Interim (Dee et al., 2011) averaged over the period 1979-2012.

warmer to colder regions. This type of circulation is called the diabatic circulation (Andrews et al., 1987). In the lower atmosphere, the heating is in all seasons larger in the low than in the high latitudes leading to a meridional circulation towards the poles. In a rotating system the Coriolis torque applied to this circulation results in a westerly flow in both hemispheres. The position of the maximum westerlies, i.e., the subtropical jet changes with the season. In the stratosphere, where the seasonal variation in the temperatures is larger, the temperature differences between high and low latitudes lead to an easterly circulation in summer, while the winter hemisphere is dominated by westerlies. This characteristic stratospheric westerly flow includes also the stratospheric polar vortex. The mean circulation differs between the Northern Hemisphere (NH) and the Southern Hemisphere (SH) in several aspects. In general, the zonal velocities are larger in the SH and the variability is lower. These differences are mainly a result of the different lower boundary conditions of the atmosphere, in particular the large amount of ocean surface and only a few meridional oriented mountain ridges in the SH. Pronounced variations in the zonal wind are obvious for the westerly circulation in the northern stratosphere during December. A second maxima is found in tropical latitudes, related to the Quasi-Biennial Oscillation (QBO) a pattern of alternating westerly and easterly wind regimes, with a period of approximately 28 months (Baldwin et al., 2001). In the SH the variability in the stratospheric circulation is lower. In the troposphere, variability maxima are found for the subtropical jets.

1.3. Climate variability and external forcings

Climate variability is associated with a wide range of time scales. Pronounced variations are related to the daily cycle, a consequence of the rotation of the Earth around its axis and to the annual cycle, caused by the rotation of the Earth around the Sun (ecliptic) and the tilt of the Earth's axis (obliquity). The characteristics and relative importance

of both, however, depends on the latitude. These variations related to cyclic changes in the boundary conditions are well understood and predictable.

A major source of uncertainty and thus a challenge for the climate sciences are internal variations generated by the climate system itself as well as climate variations caused by changes in the external forcings. The climate system is a complex and chaotic system of interacting components that produce a number of non-linear phenomena including positive (amplifying) and negative (controlling) feedbacks (Rind, 1999; Rial et al., 2004). Furthermore, the non-linearity is associated with a high sensitivity to the initial state, meaning that very small differences in the beginning can result in large differences in later states (Lorenz, 1963). These characteristics produce a number of so-called modes of variability. These modes can be generated by the atmosphere only (e.g., NAO, QBO), result from atmosphere-ocean interactions (e.g., El-Niño Southern Oscillation (ENSO)), or are produced internally by the ocean (e.g., Atlantic Meridional Overturning Circulation (AMOC), Atlantic Multidecadal Oscillation (AMO)). For some of these patterns, however, it is not completely clear whether the variations originate from internal processes or whether they are externally forced (e.g., AMO; Otterå et al., 2010; Booth et al., 2012; Zhang et al., 2013). Several of the variability modes are not completely chaotic, but are characterised by oscillations between a number of quasi-stationary states (e.g., QBO).

The NAO is the leading mode of variability in the Atlantic-European region on time scales of weeks to decades (Hurrell, 1995; Wanner et al., 2001), in particular during the winter months. The classical station based definition of the NAO index is expressed by the sea level pressure difference between Iceland and the Azores or Lisbon. Alternative definitions use the first empirical orthogonal function (EOF) of the sea level pressure or 500 hPa geopotential field of the North Atlantic. A positive phase of the NAO is associated with a higher pressure gradient between north and south, an enhanced westerly flow, increasing temperatures and precipitation in Northern Europe, and colder and dryer than average conditions in Southern Europe. For negative NAO indices these pattern shift to its opposite phase. Several attempts have been made to reconstruct the NAO back in time (compare review of Pinto and Raible, 2012). General circulation model (GCM) simulations for the last millennium and comparison studies for different reconstructions, however, have questioned the assumption of stationarity of the atmospheric circulation pattern and teleconnections over time (Schmutz et al., 2000; Raible et al., 2006; Lehner et al., 2012; Raible et al., 2014).

The NAO is closely related to the Arctic Oscillation (AO) or the Northern annular mode (NAM), covering the entire NH and the middle atmosphere (Thompson and Wallace, 1998, 2001). In fact, variations in the stratospheric NAM are manifestations of variations in the intensity of the stratospheric northern polar vortex and the surface modes are modulated by the stratospheric circulations (Baldwin and Thompson, 2009). A stronger polar vortex is typically associated with a positive phase of the AO and also the NAO in the troposphere, whereas a weakening of the vortex is often followed by a negative phase of the AO/NAO. The exchange of momentum between the stratosphere and the troposphere is called stratosphere-troposphere coupling (Baldwin et al., 1994; Baldwin and Dunkerton, 2001; Thompson et al., 2005). Often, stratosphere-troposphere coupling is described statistically, e.g., by composite or correlations between the stratospheric and tropospheric NAM (e.g., Baldwin and Thompson, 2009) or zonal wind anomalies for different levels (e.g., Christiansen, 2001, 2005). Several mechanisms

have been proposed to be involved in the coupling (Shepherd, 2002; Song and Robinson, 2004; Haynes, 2005), but the theoretical understanding of the governing processes is still limited (Thompson et al., 2011; Gerber et al., 2012).

Another type of variability of the climate system is driven by changing external forcings, e.g., volcanic eruptions. Furthermore, changes in the boundary conditions, e.g., land use or the orbital parameters can be attributed to this kind of variability. The non-linearity of the climate system is relevant for these variations as well, since feedbacks can amplify or weaken the response. This thesis focuses on the role of solar variability and volcanic activity for the climate. The current state-of-knowledge about past (and future) variations of both forcings, the associated uncertainties, and the mechanisms of solar and volcanic influence on the climate are summarised below.

1.3.1. Solar variability

The Sun is known to vary on different time scales (Gray et al., 2010). Most prominent and best understood is the (on average) 11-yr cycle of solar variability (Schwalbe cycle), but evidence for variability on longer time scales is found in documentary data, e.g., for the observed sunspot numbers or in proxy archives (Beer et al., 2006). In the following, different techniques to reconstruct solar variability for the past millennium are presented and the uncertainties involved are discussed. Furthermore, the possibility of a grand solar minima in the near future is reviewed. In the second part, the general mechanisms how solar variability influences the climate are presented.

Current, past, and future solar variability

For the 11-yr cycle, satellite observations for more than 30 years are available. Therefore, the amplitude of total solar irradiance (TSI) variability on this time scale is well established, although the spread between different instruments is large for the absolute value (Rottman, 2006). To overcome this artefact, several groups generated TSI composites by correcting for instrumental biases and drifts, e.g., the PMOD composite (Fröhlich, 2006). Based on measurements from recent instruments operating in space, the TSI is estimated at $1361.8 \pm 0.5 \text{ Wm}^{-2}$ (Kopp and Lean, 2011). For the last two solar cycles, the TSI varied about $\sim 1.1 \text{ Wm}^{-2}$ or 0.08% (Haigh, 2007). Evidence for variations on decadal and centennial time scales is found in historical documents, e.g., in documented sunspot observations (Wolf, 1861). These documents suggest several periods of reduced solar activity during the last centuries, so-called grand solar minima (Eddy, 1976). The last two grand minima are the Maunder Minimum (MM) between 1655 and 1710 and the DM from 1790 to 1830. However, the amplitudes of the TSI reduction during these minima remain uncertain. Besides the variations in the TSI also the spectral composition varies. Particularly, the variation of the solar spectrum on shorter wavelength (ultra-violet, UV) are much stronger than the variations in the visible and near infrared (Lean, 2000; Ermolli et al., 2013).

Evidence for solar variability on time scales of centuries and longer is based mainly on cosmogenic radionuclides derived from proxies, i.e., ^{10}Be concentrations from ice cores and ^{14}C from tree rings (Beer et al., 2006; Steinhilber et al., 2008, 2009, 2012). Cosmogenic radionuclides are produced in the upper atmosphere by galactic cosmic rays (GCR), the amount of GCR that enters the atmosphere, however, is modulated by the magnetic

field of the Earth and the geomagnetic field of the Sun. During periods with higher solar activity, the geomagnetic field of the Sun is stronger and less GCR enter the atmosphere. After production, ^{10}Be is attached to aerosols and deposited within approximately one to two years. ^{14}C is oxidised to $^{14}\text{CO}_2$, thus deposition and transport depend on the state of the carbon cycle and knowledge about past variations in the carbon cycle is needed to interpret ^{14}C records (Roth and Joos, 2013). Nevertheless, ^{10}Be and ^{14}C can act as two (independent) proxies for the activity level of the Sun. Uncertainties are involved in the transport and deposition of the cosmogenic radionuclides (Field et al., 2006; Heikkilä et al., 2009, 2011; Abreu et al., 2012b), in the assumptions made for the state of the carbon cycle (Roth and Joos, 2013), and in the reconstructed geomagnetic field (Knudsen et al., 2008). Furthermore, some of the recent changes, like opposite ^{10}Be trends in ice core records from Antarctica and Greenland during the 20th century are not understood so far (Muscheler et al., 2007). Nevertheless, the cosmogenic radionuclides measurements allow the reconstruction of past solar activity, typically expressed by the solar modulation potential Φ , which can further be used to reconstruct the TSI and the SSI. Depending on the reconstruction method, different assumptions about the activity level of the Sun are required (e.g., Schmidt et al., 2011, 2012). The differences between the assumptions explain the large diversity in the available TSI reconstructions. Schrijver et al. (2011), for instance, assume that the quietest level of the entire Sun was observed in the year 2009. A solar activity reconstruction based on this assumption leads then to similar TSI values for the MM as observed in 2009. Contrary, Shapiro et al. (2011) assume that the quietest area on the present day Sun identified in observations corresponds to the lowest possible activity level of the entire Sun. Their spectrally resolved reconstruction proposes a TSI amplitude of $6 \pm 3 \text{ Wm}^{-2}$, expressed by the TSI differences between MM and present day.

To some extent, reconstructions are based on physical models for the Sun. The observed variations in the solar activity originate from changes in the magnetic field of the Sun. By using this information, so-called solar dynamo models can reproduce the observed TSI variations reasonable well (Solanki et al., 2013). Still, deficits are found for the long-term variability, where the characteristic periodicities of solar variability as found in proxy records can not be sufficiently reproduced. Recently, Abreu et al. (2012a) proposed that solar variability may be modulated by the planets of the Solar System by applying a torque on the Sun. Using orbital information for the past they were able to reproduce the spectral characteristic of solar variability. Still, the force applied by the planets is too low to have significant direct effects in the Sun. Therefore, some amplifying, non-linear interactions in the Sun are required.

Nowadays, the understanding of the physical processes that influence the activity level of the Sun are not large enough to produce predictions of the future solar activity using dynamical models. Still, the information from the past, as it is conserved in observations or proxies, could be used to predict solar activity for the future by the application of statistical models (Abreu et al., 2008; Lockwood, 2010; Steinhilber and Beer, 2013). The satellite instrument records cover now three complete solar cycles from cycle 21 to 23. In this period, the long-term change in the activity of the Sun is rather low. Still, in the minimum level for each cycle is decreasing (Fröhlich, 2009). Furthermore, the transition phase between the end of the last and the start of the current cycle was longer than expected. These two metrics already indicate that the current period with high solar activity may end in the near future (Russell et al., 2010). Indeed, when using

the spectral characteristic from solar reconstructions for statistically based predictions, a solar minimum within the 21th century is likely (Lockwood, 2010; Roth and Joos, 2013; Steinhilber and Beer, 2013). Still, the amplitude of the TSI reduction is difficult to predict, since the periodicities used are stable in time but the amplitudes of the variations change (Steinhilber and Beer, 2013).

Solar influences on the climate system

With the Sun being the primary driver of the climate, the idea that variations in the solar activity may influence the climate on the Earth was already discussed more than 200 years ago (Herschel, 1801). Since then fingerprints of solar variability have been identified in an enormous number of studies covering many different components of the climate system and time scales (see reviews of Haigh, 2003, 2007; Gray et al., 2010; Lockwood, 2012; Roy, 2013). Two mechanisms have been proposed for the influence of irradiance variability on the climate (Fig. 1.5). Note that these mechanisms are not exclusively related to the solar forcing, but are, e.g., also involved in the response to volcanic eruptions. The *bottom-up* mechanism assumes that the variations in the solar forcing mainly affect the surface. In this case different feedback mechanisms, e.g., cloud feedback and air-sea interactions, may modulate or amplify the response (Meehl et al., 2003, 2008; Misios and Schmidt, 2013; Zhou and Tung, 2013). In the *top-down* mechanism, variability in the ultra-violet radiation (UV) influences ozone production, heating rates, and the meridional temperature profile in the stratosphere (Haigh, 1996). By interactions between stratosphere and troposphere (see Baldwin and Dunkerton, 2005, for a review) the solar signal in the stratospheric heating rates affects the tropical Hadley circulation (Shindell et al., 1999; Kodera and Kuroda, 2002; Haigh et al., 2005) and via the winter polar vortex the annual modes in the high latitudes (Kodera, 2003; Ineson et al., 2011). In reality, the separation of both effects is difficult and GCM results indicate that both processes are needed to reproduce a realistic response (Rind et al., 2008; Meehl et al., 2009).

Besides irradiance variability, solar variability is also reflected in the amount of energetic particles that enter the climate system. Although energetic particles are not in the focus of this thesis a brief overview is given in the following. Energetic particles come either from outside of the planetary system or from the Sun. The former are GCRs, which interact with atmospheric constituents when they enter the atmosphere and have been proposed to affect cloud formation (Dickinson, 1975; Svensmark et al., 2009). However, evidence for a link between GCRs and clouds is low (Laken et al., 2012) and the effect is probably too weak to influence climate significantly (Myhre et al., 2013). Solar energetic particles (SEPs) are energetic particles emitted by the Sun during solar flare events, i.e., massive magnetic eruptions on the Sun. Furthermore, the solar wind transports so-called energetic electrons to the Earth's atmosphere. Both cause ionisation, dissociation, and the production of species that are involved in different catalytic ozone destruction cycles (e.g., Solomon et al., 1982; Jackman et al., 2008).

There is an ongoing discussion whether the Little Ice Age (LIA), a relatively cold period between the 15th and the 18th century, is related to external influences (reduced solar and increased volcanic activity) or a result of internal variability in the climate system and whether the LIA was a global phenomena (e.g., Wanner et al., 2008; Mann et al., 2009). For the last two grand solar minima of the LIA (MM and DM) the associated

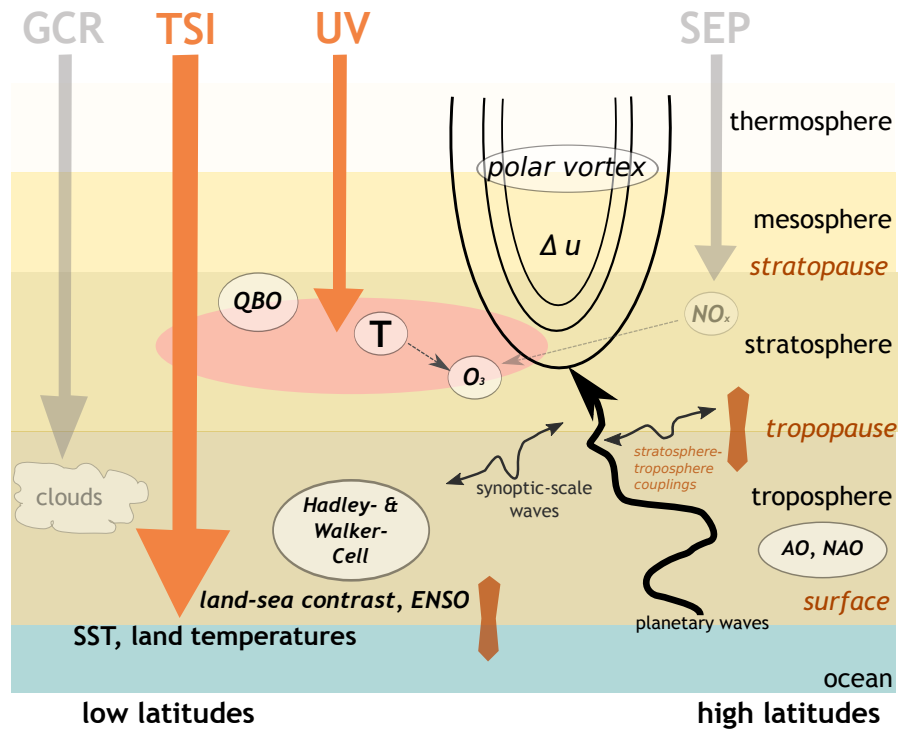


Figure 1.5.: Schematic overview of the different influences of solar variability on the climate based on Kodera and Kuroda (2002) and Gray et al. (2010). Processes not directly considered in this thesis (GCR and SEP) are shown in grey.

temperature changes have been evaluated in several GCM studies using different reconstructions for the TSI (e.g., Shindell et al., 2001; Rind et al., 2004; Zorita et al., 2004; Yoshimori et al., 2005; Jungclaus et al., 2010; Spanghel et al., 2010; Swingedouw et al., 2011). Other studies analysed the climate characteristics of these periods in proxy based reconstructions (e.g., Shindell et al., 2001; Luterbacher et al., 2002, 2004; Waple et al., 2002; Guiot et al., 2010; Mann et al., 2009). For Europe, several studies report evidence for colder temperatures associated with periods of reduced solar activity (Shindell et al., 2001; Waple et al., 2002; Luterbacher et al., 2004), while others do not find an influence on temperatures (Guiot et al., 2010). Globally, there is little evidence for a synchronised onset of the LIA on both hemispheres (PAGES 2k Network, 2013). Fernández-Donado et al. (2013) compared several model simulations for the last millennium to a large number of proxy reconstructions found broad agreement on a hemispheric scale, but large differences in the spatial patterns of the temperature anomalies. They concluded, that either internal variability is a major player for temperature variability in the last millennium or the models do not allow for realistic response pattern to external forcings.

Regional cold anomalies in Europe, e.g. in the MM, may be related to bottom-up mechanisms or to circulation changes related to the top-down process. During solar minima, the top-down mechanism is expected to lead to negative AO phases. Several NAO reconstructions indeed report a more negative phase for the MM (Luterbacher et al., 1999; Glueck and Stockton, 2001; Rodrigo et al., 2001; Cook et al., 2002; Luterbacher et al., 2002; Trouet et al., 2009), but the results for other grand solar minima differ substantially between the reconstructions. Negative AO/NAO phases during grand solar

minima have also been found in model simulations (Cubasch et al., 1997; Shindell et al., 2001, 2003; Zorita et al., 2004; Spanghehl et al., 2010; Swingedouw et al., 2011). However, while some studies indicate an instantaneous response for the MM (Shindell et al., 2003; Rind et al., 2004; Spanghehl et al., 2010) others find a lagged response with lags of 20 years or longer (Shindell et al., 2001; Swingedouw et al., 2011). Yet others found a shift of the NAO from a negative to a positive state in the middle of the solar minima (Zorita et al., 2004). Furthermore, Spanghehl et al. (2010) showed that a better representation of the stratosphere is not necessarily needed to reproduce the NAO response to solar forcing during the last 400 years, which contradicts the top-down hypothesis to some extent. In summary, evidence for a consistent response of the NAO to a reduced solar forcing is weak for the grand solar minima of the last millennium (Pinto and Raible, 2012).

In recent years, the possibility of a grand solar minima in the near future has motivated several modelling studies with focus on the reduction of the GHGs induced warming (Feulner and Rahmstorf, 2010; Jones et al., 2012; Meehl et al., 2013). They all agree on a weak slow-down of the temperature increase. After the end of the solar minimum the global mean temperature quickly recovers and the solar minimum has no prolonged effect on the temperature increase (Meehl et al., 2013).

In Chapter 2 of this thesis the temperature response to solar forcing is analysed in transient simulations for the period 1600-2000 AD. Furthermore, sensitivity studies assess the relative importance of the top-down and bottom-up mechanisms for the response to solar variability as well as the role of volcanic activity for climate variations during the DM (Chapter A.2 and A.3). The possible effect of a near future grand solar minima on temperatures and the recovery of the stratospheric ozone concentrations is presented in Chapter A.1.

1.3.2. Volcanic activity

Volcanic activity is the dominant cause of natural climate variability on time scales from years to decades (Myhre et al., 2013). Large volcanic eruptions emit massive amounts of volcanic products into the atmosphere, the most important ones are ash, sulphur dioxide (SO_2), water vapour, and carbon dioxide (CO_2). The ash is typically removed from the atmosphere within several days or weeks by dry or wet deposition. The amount of water vapour and carbon dioxide are normally not large enough to substantially influence the climate (Cole-Dai, 2010), although changes in the stratospheric water vapour may significantly affect the stratospheric chemistry (compare appendix A.2, Anet et al., 2013a). The emitted sulphur dioxide, however, can have pronounced effects on the climate system over time scales ranging from one to several years (Robock, 2000) and a series of several volcanic eruptions might even lead to a centennial climate change (Zhong et al., 2010; Miller et al., 2012).

The climate effect of SO_2 is of particular importance for large tropical volcanic eruptions if the volcanic gases are injected into the stratosphere (Coffey, 1996), where they are oxidised to sulphate aerosols (see Section 1.4.2). In the stratosphere the residence time of the volcanic aerosols is much longer than in the troposphere. Furthermore, in the tropical stratosphere the aerosols are lifted and transported to the higher latitudes by the residual meridional circulation named the Brewer-Dobson circulation (BDC). With the seasonal changes in the stratospheric circulation, the date of the eruption influences the shape and the hemispheric partitioning of the aerosol cloud (Holton et al., 1995).

For smaller eruptions typically, the emitted volcanic gases do not reach the stratosphere. Larger eruptions at high latitudes may inject their products into the stratosphere, but at high latitudes the downwelling branch of the BDC suppresses an effective global distribution of the aerosols. The climate effect of both is, therefore, smaller compared to tropical volcanic eruptions.

Reconstructing past volcanic activity

Similar to the solar variability, the understanding of the climate influence of large volcanic eruptions has significantly improved in the last decades. Reliable measurements of stratospheric aerosols began in the early 1970s (SPARC, 2006). Two large tropical volcanic eruptions were observed by instruments operating on satellites, the eruptions of El Chichón (Mexico) in March 1982 and Mt Pinatubo (Philippines) in June 1991. For these two eruptions the spatial and temporal characteristic of the aerosol cloud is therefore reasonably well established (SPARC, 2006). For eruptions before 1979, surface based observations of the solar optical depths could be used to characterise the eruption, but only until 1883 and the observations are mainly limited to the NH (Sato et al., 1993). The reconstruction of eruptions before 1883 need to rely mainly on ice core data (Sato et al., 1993; Ammann, 2003; Crowley et al., 2008; Gao et al., 2008) or historical documents (e.g., Lamb, 1970). Ice sheets in Greenland or Antarctica conserve the sulphuric acid or sulphate aerosols that are deposited on/in the snow after the eruption. Measurements of the sulphate concentrations or the acidity in ice cores are used to quantify the volcanic signal in the ice (Hammer et al., 1980). The individual signal in a single core, however, is influenced by several factors, like the variability in the circulation or the accumulation rate. Furthermore, the amounts of deposited material can differ substantially between the NH and the SH and not all eruptions are recorded in both hemispheres (Sigl et al., 2013). Additionally, an ice core may be “contaminated” by small eruptions close to the ice sheet (e.g., Iceland in the case of Greenland). Therefore, a larger number of ice cores need to be combined to increase the signal-to-noise ratio (Gao et al., 2008) and several correction factors (e.g., for the hemispheric partitioning) are needed if the total mass of stratospheric aerosol should be estimated from the deposited signals.

Early approaches implemented the volcanic perturbation by a simple reduction of the TSI (e.g., González-Rouco et al., 2006; Yoshimori et al., 2005; Spanghel et al., 2010; Phipps et al., 2012), however, this approach can not account of the stratospheric warming and the following circulation changes. For more realistic GCM simulations the total aerosol mass is not sufficient and information about the optical properties of the aerosols are needed for every latitude and altitude (Timmreck, 2012). Further, GCMs with interactive chemistry need surface area density (SAD) of the aerosols to consider heterogeneous reactions on the aerosol surfaces. Information of the shape and development of the aerosol cloud (and the size distribution of the aerosols) is therefore necessary to derive the optical properties. These properties are estimated from simple parametrisation for the transport or from observation for the most recent eruptions with additional scaling for the eruption size. However, often used linear relationships between aerosol loading and optical properties have been questioned (Timmreck et al., 2009, 2010).

Recently, Arfeuille et al. (2014) developed a new volcanic forcing data set for GCMs by simulating the formation of the aerosol clouds for the last 26 large eruption in a two-dimensional microphysical model using the aerosol mass estimates from Gao et al.

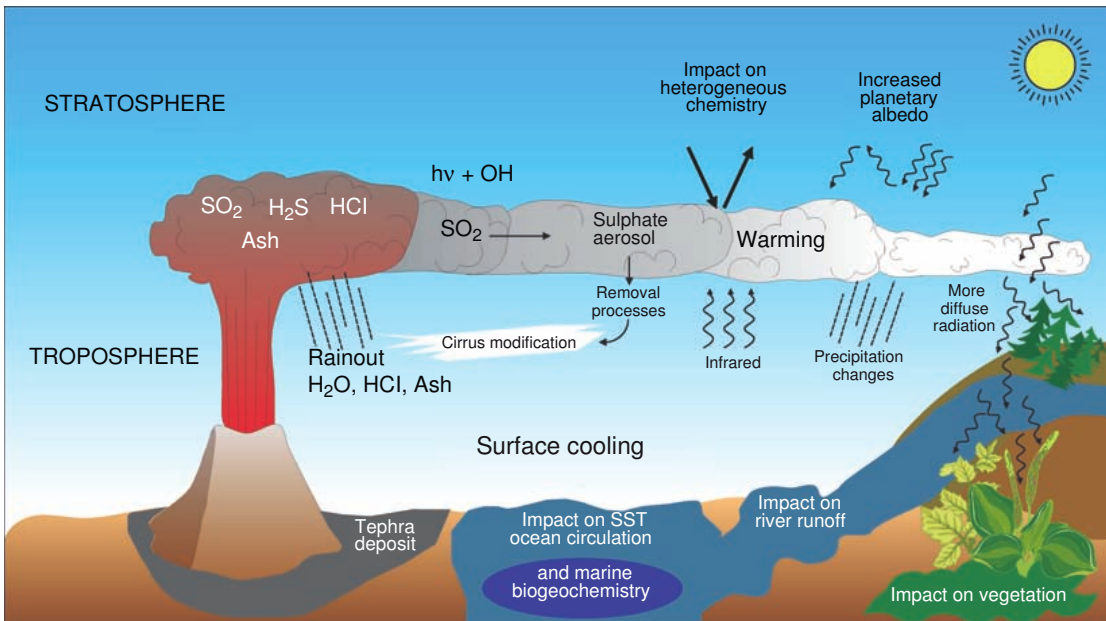


Figure 1.6.: Schematic overview of the different influences of volcanic activity on the climate system (Fig. from Timmreck, 2012).

(2008). The model simulates the transport, the nucleation, condensation, coagulation and sedimentation of the aerosols. Furthermore, the model considers the date of the eruption, the latitude, and the altitude of the aerosol injection. The size distribution and the optical properties of the aerosols are then directly calculated in the model. This forcing is used in most of the simulations performed for this thesis.

Overall it should be emphasised that the knowledge about volcanic forcing in the last millennium is associated with large uncertainties. In particular, the strength of the individual eruptions and the spatial pattern of the forcing is poorly constrained (Forster et al., 2007; Schmidt et al., 2011).

Volcanic influences on the climate system

A large volcanic eruption with aerosols injected into the stratosphere influences the climate by four distinct mechanisms (Fig. 1.6; Forster et al., 2007).

- The aerosol cloud in the stratosphere affects the radiation balance by reflecting and absorbing short-wave radiation from the Sun and reduces the surface temperatures.
- The aerosols further absorb in the near-infrared, therefore heating rates in the aerosol cloud increase, which alter the meridional and vertical temperature gradients in the stratosphere and thus the circulation.
- The forcing interacts with internal modes of variability, like ENSO or NAO.
- The aerosols affect chemical reactions in the stratosphere and modify the ozone concentrations (see section 1.4.2).

The sulphate aerosols remain in the stratosphere for 2-3 years, depending on the eruption size, and the surface cooling effect is limited by this residence time. A single eruption therefore reduces the global mean surface temperature for a few years up to a decade

(Robock, 2000). The cooling also reduces evaporation and leads to a significant reduction in global mean precipitation (Gillett, 2004; Trenberth and Dai, 2007; Iles et al., 2013). After tropical eruptions the temperature reduction is larger in the tropics than in higher latitudes and the meridional temperature gradient towards higher latitudes is modified as well. This weakens the Hadley circulation and the monsoon circulation (Wegmann et al., 2014) with the side effect of increasing precipitation in Europe, as reported for the "year without summer" (1816) after the eruption of Mt Tambora (1815). The cooling also reduces the heat content of the ocean – an effect which can last for many decades (Stenchikov et al., 2009). Furthermore, the AMOC may be influenced by the cooling (Mignot et al., 2011), with a strengthening of the overturning a few years after the eruption.

Although the surface temperature effect of a single eruption is limited to a few years, the accumulated effect of several eruptions could last much longer. A series of large volcanic eruptions has been proposed to be involved in the transition into the LIA (Zhong et al., 2010; Miller et al., 2012) amplified by positive sea-ice-ocean feedbacks (Lehner et al., 2013).

After an eruption, the winter season in the NH high latitudes can be warmer than average (Robock and Mao, 1992; Shindell et al., 2004; Fischer et al., 2007; Christiansen, 2008; Zanchettin et al., 2012), which is counter-intuitive given the surface cooling mechanism, but can be understood by dynamic effects. The stratospheric warming increases the meridional temperature gradient in the lower stratosphere, which is the driver for the polar vortices in the winter season. The eruption therefore effectively strengthens the polar vortices (Kodera, 1994). In the NH, positive zonal wind anomalies in the stratosphere influence the circulation in the troposphere (Graf et al., 1993) and increase the probability for positive phases of the NAO/AO and positive temperature anomaly in the high latitudes (Robock, 2000; Shindell et al., 2004). Although this mechanism is initiated by the warming in the tropical stratosphere, GCM simulations show that a positive phase of the AO phase after volcanic eruption can also be initiated by the surface cooling effect (Yoshimori et al., 2005; Stenchikov et al., 2002).

In this thesis the role of the ozone chemistry for the dynamic response after large volcanic eruptions is analysed in Chapters 3 and 4, with Chapter 3 focusing on ozone as passive forcing, i.e., an ozone forcing used in a GCM without interactive chemistry, and Chapter 4 assessing the different processes responsible for the ozone changes in a coupled atmosphere-chemistry-ocean model and their influences on the dynamics. How the ozone chemistry is affected by a volcanic eruption is reviewed in Section 1.4.2.

1.4. Stratospheric ozone chemistry and chemistry-climate interactions

The stratosphere has received more and more attention in climate change studies in the recent years, also the atmospheric chemistry and interactions between chemistry and climate have brought into focus of the climate sciences (Baldwin et al., 2007; Gerber et al., 2012). In particular, the ozone chemistry is directly affected by climate change, but also induce changes in the climate system. In this section, the principles of the most important chemical component for chemistry-climate interactions in the stratosphere, the ozone chemistry are summarised. The chemical cycles of tropospheric ozone are not

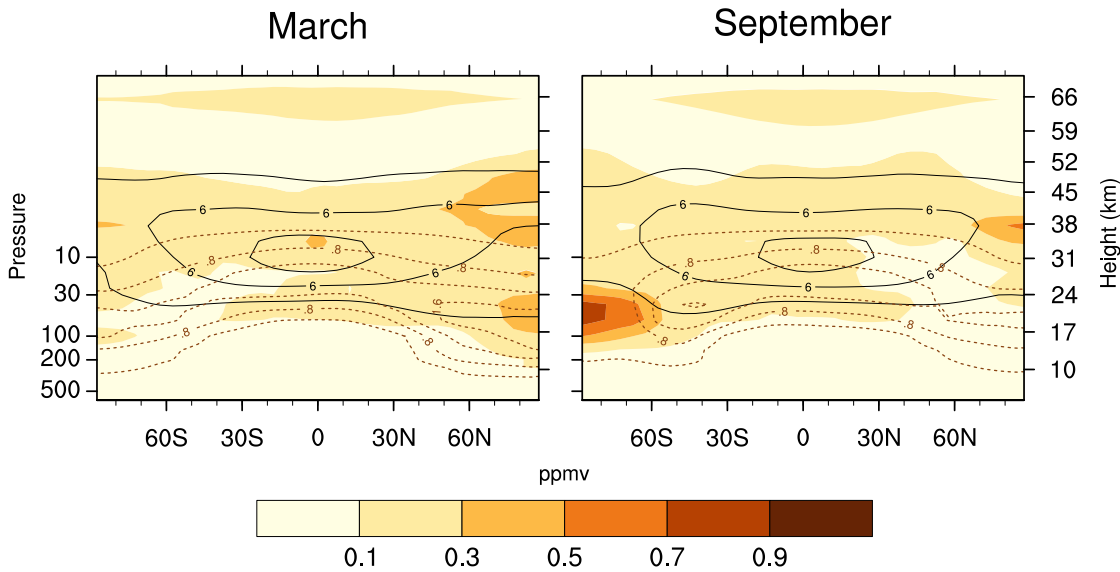


Figure 1.7.: Zonal mean climatological ozone mixing ratios in ppmv (solid contours) averaged over the period 1980-2007 (Hassler et al., 2008) for the month (left) March and (right) September (contours step 3 ppmv). Dashed contours: ozone partial pressure in 10^{-4} hPa (contour step $0.4 \cdot 10^{-4}$ hPa). Shading denotes the standard deviation of the corresponding months.

described as they are not considered in this thesis.

Above the tropopause, ozone mixing ratios increase until they reach their highest concentrations in the lower to middle stratosphere. The ozone concentrations in Figure 1.7 and in the following are shown for the end of the winter season on the NH (March) and SH (June), since variability and the differences between the hemispheres are most pronounced for these months (Brasseur and Solomon, 2005). Globally, the highest ozone mixing ratios are found in the tropics, where the ozone production is at its maximum. The vertical profile of the ozone concentrations or the partial pressure of ozone, however, reveals distinct differences between the high and low latitudes (dashed contours in Fig. 1.7). In the tropics, the highest concentrations are found at approximately 25 km. In the mid to high latitudes the maximum is found in lower levels of about 15 km (Hobbs, 2000). Furthermore, the partial pressure in the higher latitudes is larger than in the tropics, in particular in late winter and early spring. This explains why the largest total ozone column abundance, which is the vertically integrated ozone, is found in the mid to high latitudes in spring (Fig. 1.8). Ozone abundance is larger in the NH high latitudes than in the corresponding latitudes of the SH, which is an imprint of the "Antarctic ozone hole" since the mid 1980s. This characteristic ozone pattern with higher abundances in the mid- to high latitudes and highest mixing ratios in the lower latitudes builds the ozone layer that protects life on Earth from the carcinogenic UV radiation. It is responsible for the vertical temperature profile in the stratosphere and is involved in a large number of chemical reactions taking place in the stratosphere (Hobbs, 2000). The described idealised ozone distribution, however, is highly variable and changes with the season but also from year to year. Figure 1.7 and 1.8 depict also the inter-annual variability for the corresponding months in terms of their standard deviation. In the high latitudes the change in the column ozone abundances, but also in the vertical resolved mixing ratios is

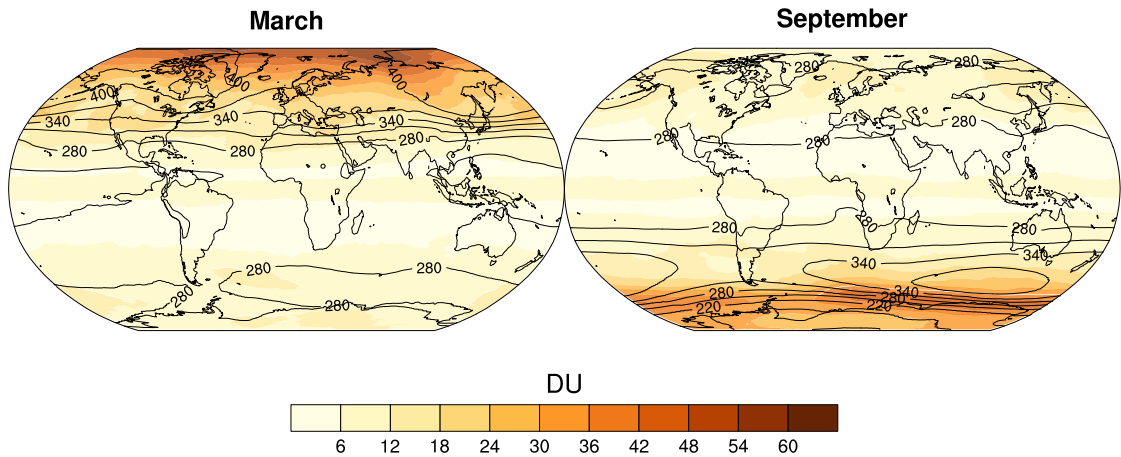


Figure 1.8.: Contours: Climatological column ozone values in DU averaged over the period 1980-2007 for the month (left) March and (right) September (Bodeker et al., 2005). Shading denotes the standard deviation of the corresponding months.

largest. Furthermore, the variability is larger in the NH compared with the SH, which can be understood by the enhanced variability of the stratospheric circulation in the NH and the stronger stratospheric zonal winds in the SH. The stable conditions in the SH is also the cause for the stronger ozone depletion over the Antarctic continent. Temperatures in the centre of the vortex are colder, which makes the depletion mechanisms more efficient. Furthermore, a stronger vortex is better isolated against the inflow of ozone enhanced air from low latitudes.

Ozone acts also as a GHG and concentration changes therefore affect the radiation balance. Whether the radiative forcing (RF) of the recent ozone changes is positive or negative depends on the altitude of the changes. In the stratosphere, ozone decreased since the 1970s due to the enhanced ozone depletion by halogens. The radiative effect of this change is associated with large uncertainties, but most likely negative, with $-0.05 \pm 0.1 \text{ Wm}^{-2}$ (Myhre et al., 2013). In the troposphere, concentrations have increased steadily in the industrial era, with intensified trend since 1950, related to the enhanced emission of ozone precursor gases. The RF from this change is estimated to be $0.4 \pm 0.2 \text{ Wm}^{-2}$ (Myhre et al., 2013). Both RF estimates are expressed by the difference in the radiative forcing between 1750 and 2011, as in (Myhre et al., 2013). Consequently, the net RF from the ozone changes is most likely positive and contributes significantly to temperature increase of the 20th century (Shindell et al., 2006; Stevenson et al., 2013). Note, these values are small in comparison to the radiative forcing from other GHGs. The CO_2 increase between 1750 and 2011, for instance, is associated with a RF of $1.82 \pm 0.19 \text{ Wm}^{-2}$ and the CO_2 related forcing increase in the last decade is of similar magnitude as the forcing from ozone changes between pre-industrial and present day (Myhre et al., 2013). Nevertheless, the changes in the RF from ozone have implications for coupled atmosphere-chemistry models, as will be shown for the temperature trends of the 20th century in Chapter 2.

1.4.1. Stratospheric ozone chemistry

This Section summarises the principles of the ozone chemistry and the major catalytic cycles that are needed to understand the ozone changes after volcanic eruptions described in Chapter 4 and the changes in the DM presented in A.2 and A.3 in the appendix.

Ozone (O_3) is mainly confined to the stratosphere, where about 90% of the global ozone mass is found. The formulation of the mean mechanism for ozone production and destruction goes back to the year 1930, when Sydney Chapman formulated his equations (Jacob, 1999; Hobbs, 2000). Ozone is produced by the photolysis of molecular oxygen (O_2) by UV.



with M being an arbitrary atom or molecule, typically N_2 or O_2 , carrying the excess energy of the reaction. At the same time, ozone is also destroyed by UV.



Both processes together generate an equilibrium of the global amount of ozone. The Chapman mechanism given in Equation 1.1 to 1.4, however, is not sufficient to explain the real ozone concentrations found in the stratosphere. In fact it overestimates the concentrations by a factor of 2 or more (Jacob, 1999). Therefore, several other chemical components were identified to be involved in the destruction of ozone (e.g., Crutzen (1970) described the role of nitrogen and Molina and Rowland (1974) the importance of chlorine for modern ozone depletion). They all share the same form, where a radical X is included as catalyst in the destruction of ozone:



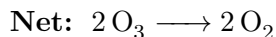
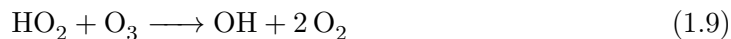
X can be a radical from the families of HO_x (OH, HO_2), NO_x (NO, NO_2), ClO_x (Cl, ClO, ClOOCl), and Br_x (Br, BrO). For each of these families specific reaction cycles exists.

The HO_x cycle

The HO_x cycle was the first catalytic cycle that was identified in the 1950s (Bates and Nicolet, 1950; Jacob, 1999). It is based on the two radicals OH and HO_2 . HO_x is produced by the oxidation of water vapour, which is available in the stratosphere due to the oxidation of methane (CH_4) and transport from the troposphere.



OH in turn converts ozone to oxygen.

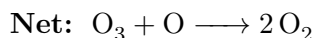


The reaction given in Equation 1.9 mainly takes place in low HO_x regimes, i.e., at altitudes below 20 km (Brasseur and Solomon, 2005). In high HO_x regimes, where intense radiation and high-energetic O is available, the Reaction 1.10 dominates over 1.9. Sufficient conditions for high HO_x regimes are found at altitudes above 40 km (Brasseur and Solomon, 2005).



The NO_x cycle

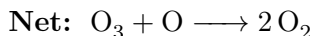
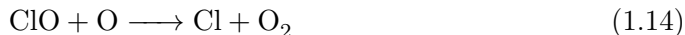
The NO_x cycle is based on the two components NO and NO_2 (Crutzen, 1970). They are generated in the stratosphere by the oxidation of nitrous oxide (N_2O) coming from nitrification and denitrification processes in the biosphere.



This cycle dominates at altitudes between 35 and 45 km. Below 35 km the lack of high-energy O builds the limit for the reaction and above 45 km NO reacts with atomic N to produce N_2 and O (Brasseur and Solomon, 2005). With the HO_x and the NO_x cycle, the gap between the observed ozone concentrations and the values calculated following the Chapman mechanism could be closed in the late 1970s (Jacob, 1999).

The ClO_x and BrO_x cycles

In the mid of the 1970s, the idea was born that human emitted chlorofluorocarbons (CFCs) can influence the ozone chemistry (Molina and Rowland, 1974). CFCs are chemical molecules containing Cl, F, and C with CFC-11 (CFCl_3) and CFC-12 (CF_2Cl_2) being the most common ones. They have a very long residence time in the atmosphere. Furthermore, CFCs have a very high global warming potential, meaning that their RF per mass is much larger than the reference forcing of CO_2 , and contribute about 11% to the RF of well-mixed GHG despite their low concentrations (Myhre et al., 2013). In the stratosphere CFCs are photolysed to chlorine (Cl) atoms. Cl atoms together with ClO are the two important components of the ClO_x family and the starting point for the ClO_x cycle.

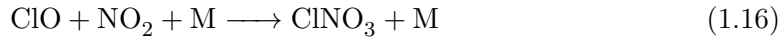
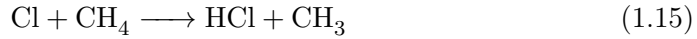


The chlorine cycle is very effective in the upper stratosphere (Brasseur and Solomon, 2005). Below 30 km the amount of Cl and ClO is in general too low, since the formation into reservoir molecules (see below) dominates. However, with heterogeneous reactions on aerosol surfaces the Cl_x cycle becomes important in the lower stratosphere, in particular in the polar regions. A similar cycle to the chlorine cycles exists for bromine (Wofsy et al., 1975). Furthermore, chlorine and bromine have been found to interact with each other and further increase the ozone destruction (Yung et al., 1980).

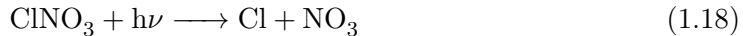
Cl radicals can also origin from a natural sources (Chloromethane, CH₄Cl), however, their concentrations are very low compared to the anthropogenic sources. With the Montreal protocol (1987) the emission of CFCs has been strictly reduced and a recovery of the stratospheric ozone concentrations is projected for the future (Austin and Wilson, 2006; Eyring et al., 2007; Austin et al., 2010).

Ozone depletion in the polar stratosphere

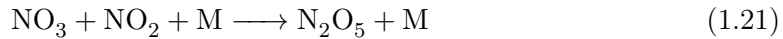
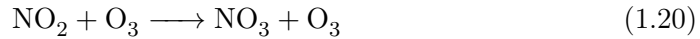
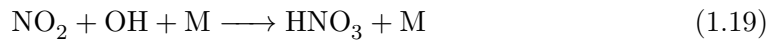
The mechanisms of ozone depletion described above could not explain the ozone depletion in the SH polar stratosphere in spring. Since the amount of UV radiation entering the polar stratosphere is extremely low, none of the known mechanisms was sufficient to explain this phenomena when it was discovered in the 1980s (Solomon, 1999). To understand the specific chemical reactions taking place in the winter and spring polar stratosphere, the term reservoir species need to be introduced. Since the radicals are preserved in Equation 1.11 to 1.14 the only possibility to stop the catalytic reaction (besides the complete consumption of ozone) is the conversion of the radicals into non-radical reservoir species. In case of the ClO_x family, this is the conversion into HCl and ClNO₃.



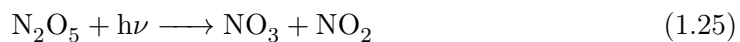
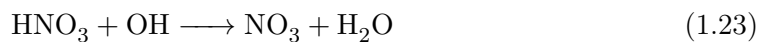
However, this species can be converted into ClO_x again.



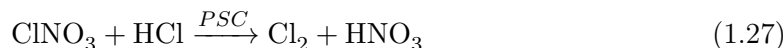
For NO_x, the corresponding reservoir species are HNO₃ and N₂O₅.



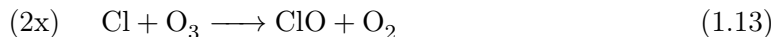
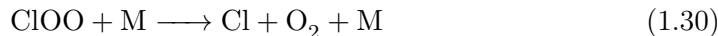
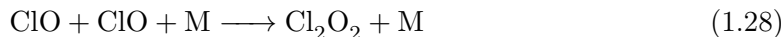
Under the influence of UV radiation, these reservoir species for NO_x can also eventually be converted back to NO_x.



For the polar ozone depletion, the reservoir molecules of the ClO_x become important. Under the extreme cold conditions of the southern polar stratosphere during winter time (< 200 K), persistent clouds, the PSCs, are formed in altitudes between 20-30 km (Solomon, 1999). PSCs consist of nitric acid (HNO_3) and H_2O , but depending on the exact chemical composition and the physical state different types of PSCs can be distinguished. For the ozone chemistry, PSCs are relevant, because they provide surfaces for the conversion of chlorine reservoir molecules into reactive compounds (Brasseur and Solomon, 2005). The first Reaction (1.26) on PSCs involves the hydrolysis of chlorine nitrate, for colder temperatures Reaction 1.27 becomes more important.



Both reactions are highly efficient and remove either all HCl and H_2O or all ClNO_3 from the polar air and accumulate Cl_2 and HOCl in the polar vortex region. In spring, when the first sunlight hits the polar stratosphere HOCl and Cl_2 are rapidly photolysed and a large amount of Cl radicals is produced. These radicals initiate ozone depletion via Reactions 1.13 and 1.14. The ozone depletion in turn accumulates high concentrations of ClO in the polar stratosphere. With high ClO load in the lower stratosphere another catalytic cycle becomes important.



Reaction 1.13 then forms again a catalytic cycle with ClO as catalyst. Note that this catalytic cycle does not depend on atomic oxygen, which makes it very efficient and the dominant reaction for the polar ozone depletion (Brasseur and Solomon, 2005). The depletion in the polar stratosphere is also further amplified by the above mentioned interactions between the bromine cycle and the chlorine cycle.

The depleting mechanisms are similar for both polar stratospheres. In the Arctic, however, the depletion signal is less severe compared to Antarctica (Solomon, 1999) as temperatures in the winter NH polar stratosphere are less cold and less PSCs are formed. Additionally, the polar vortex is weaker and more variable and the exchange of ozone with mid latitudes is larger. Consequently, also the variability in the ozone concentrations in the northern polar stratosphere is overall larger, therefore change signals are harder to detect. Nevertheless, signals of ozone depletion are apparent for the Arctic as well (von Hobe et al., 2006; Manney et al., 2011; Strahan et al., 2013).

1.4.2. Chemistry-climate interactions

A pronounced perturbation in the chemical equilibrium of the stratosphere is associated with the emission of CFCs (Solomon, 1999). Severe changes were observed in austral spring over Antarctica, where ozone was reduced by about 50% in the late 1990th (Staelin et al., 2001). In the next decades, stratospheric ozone is expected to recover to pre 1980 values (Austin and Wilson, 2006; Eyring et al., 2007), although the stratospheric

changes associated with the tropospheric warming delay the recovery regionally (Austin et al., 2010). Still, the differences between the model projections are large (Karpechko and Gillett, 2010). An additional slow-down of the recovery may result from a possible grand solar minima within the 21th century (see Chapter A.1).

The observed ozone changes lead to the question whether or not these chemical changes influence the dynamics in the stratosphere, but maybe also in the troposphere and at the surface (Baldwin et al., 2007). The difficulty for such detection and attribution studies is the separation of the effect of ozone depletion from the changes related to increasing GHG emissions. With rising levels of carbon dioxide the troposphere is expected to warm and the stratosphere is expected to cool. Similar effects are associated with the tropospheric and stratospheric ozone changes. Model studies indicate that the ozone changes are needed to match the observed temperature trends in the lower stratosphere and a combination of ozone changes and CO₂ effect is responsible to the temperature trends in the middle and upper stratosphere (Shine et al., 2003). Recently, however, the reliability of the observed temperature trends has been questioned (Thompson et al., 2012).

A pronounced influence of the ozone depletion on the dynamics in the troposphere and at the surface has been found for the SH. Climate in the SH mid and high latitudes is to a large extent determined by the Southern annular mode (SAM), the southern hemispheric counterpart of the NAM. Influenced by the strengthening of the southern polar vortex, which is mostly driven by the cooling of the lower polar stratosphere associated with the ozone depletion, the SAM has undergone a pronounced positive trend in recent decades (Thompson and Solomon, 2002; Thompson et al., 2011). GCMs can reproduce this trend if forced by observed ozone changes only (Gillett and Thompson, 2003; Son et al., 2010). A stronger SAM explains a number of the observed changes at the surface, e.g., a large fraction of the warming of the Antarctic Peninsula (Thompson and Solomon, 2002), the changed precipitation patterns in high to mid latitudes (Purich and Son, 2012) and in the subtropics (Kang et al., 2011), as well as extreme precipitation events (Kang et al., 2013). With the ozone recovery the SAM is expected to shift to a negative phase in summer, but the trend expected from the GHG increases is positive for all seasons (McLandress et al., 2011).

In the NH the climate change associated with ozone depletion is weaker and difficult to detect, since the variability in both ozone and the dynamics is more pronounced. However, changes in the temperature trends and the dynamics can be found as well (Randel and Wu, 1999; Hu and Tung, 2003; Langematz et al., 2003).

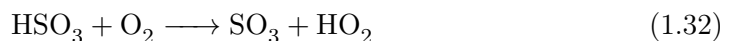
Another type of chemistry-climate interactions involves positive (negative) feedbacks of the chemistry that amplify (weaken) changes in the climate system. Recently, a positive feedback to increasing temperatures has been found in climate sensitivity experiments with the CCM MESSy (Dietmüller et al., 2014). In a double CO₂ experiment the temperature response is 3.4% weaker with interactive chemistry compared to an experiment without interactive chemistry. The strength of the feedback further grows with the size of the CO₂ perturbation. The negative feedback to the RF change is related to reduced ozone concentrations in the lower tropical stratosphere by enhanced tropical upwelling and an intensification of the BDC. As negative feedback of similar size is also estimated using with AOCCM used in this thesis (Chapter 2).

Solar influences on the atmospheric chemistry

Stratospheric chemistry is mainly affected by variability in the UV part of the solar spectrum, since this spectral interval modulates the production of ozone (Haigh, 1994). Over an 11-yr cycle the variability in the UV is higher compared to the longer wavelength (Ermolli et al., 2013) and signatures of this variability are clearly visible in ozone observations, both in the column ozone and in the vertical distribution (Soukharev and Hood, 2006; Brönnimann et al., 2013). The ozone variations affect the stratospheric heating rates, the meridional and vertical temperature gradients and the circulation in particular in the upper stratosphere (Austin et al., 2008; Gray et al., 2009; Frame and Gray, 2010). Circulation changes in the stratosphere may again affect the tropospheric circulation via influences on the polar vortex and the QBO (Kodera and Kuroda, 2002). This mechanism may also be relevant for long-term changes in the solar variability. Varma et al. (2012) found an amplified response of the SH westerlies to reduced solar forcing for the late MM, if solar induced ozone variations are considered in the model. In Chapter A.2 and A.3 the response of stratospheric chemistry and its influence on the dynamics is assessed for the UV reduction in the course of the DM.

Atmospheric chemistry and volcanic activity

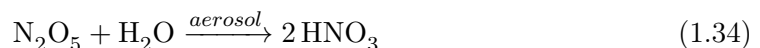
In the atmosphere, SO_2 emitted by a volcanic eruption is oxidised to sulphuric acid (H_2SO_4) by OH and water, which condenses and forms aqueous sulphate particles (Jacob, 1999; Hobbs, 2000).



These aerosols affect the ozone chemistry in the stratosphere in several ways:

- In the aerosol cloud, the reaction rates are influenced by the temperature changes, for example an acceleration of the catalytic cycles of ozone destruction is found.
- The transport of ozone is modified by dynamical changes in the stratosphere.
- The absorption and reflection by the aerosols affects the photolysis rates.
- On the surface of the aerosol particles different chemical reactions take place, so-called heterogeneous chemical reactions.
- In the polar stratosphere, the aerosols facilitate the formation of an additional type of PSCs. Furthermore, the cooling related to the stronger polar vortex intensifies also the mechanisms of polar ozone depletion described above.

An important heterogeneous reaction on the aerosol surfaces is the conversion of N_2O_5 to HNO_3 .



N_2O_5 and HNO_3 are both reservoir molecules in the NO_x cycle, but the residence time of HNO_3 is longer than the residence time of N_2O_5 . Reaction 1.34, therefore, effectively slows down the NO_x cycle. The net effect of this process is a reduction of the ozone

depletion, but only as long as the reaction is not saturated, i.e., all N_2O_5 is consumed (Tie and Brasseur, 1995). Furthermore, in case of high chlorine loads the ClO_x cycle may dominate over the changes to the NO_x cycle. In a pre-industrial atmosphere, however, the expected effect of a volcanic eruption on the ozone chemistry is an increase of the ozone concentrations (Brasseur and Solomon, 2005) and indeed a similar behaviour can be found in climate model experiments for pre-industrial atmospheres (compare Chapter 4 and A.2). In a modern atmosphere, the ClO_x cycle needs to be considered. Lower NO_x concentrations affect also the chlorine cycle and slow down the deactivation of chlorine expressed in Reaction 1.16. Moreover, in the modern polar stratosphere ozone depleting effects are intensified inside the stronger polar vortex by different types of PSCs. The ozone depletion is consequently stronger after volcanic eruptions and in a modern atmosphere this effect dominates over the NO_x effect (Tie and Brasseur, 1995).

In Chapter 4 the relative role of dynamical ozone changes, induced by the heating in the lower tropical stratosphere, and chemical ozone changes related to heterogeneous reactions is addressed and their relative importance in a pre-industrial and a present day atmosphere is analysed.

1.5. Modelling of chemistry-climate interactions

The current state of the climate system and the changes of the recent past are recorded in an enormous database of observed climate variables for many locations on the Earth (Hartmann et al., 2013). Since around the mid of the 19th century, the quality and coverage of climate observation is sufficient to derive global climate parameters, e.g., a global mean surface air temperature (Brohan et al., 2006; Hansen et al., 2010; Rohde et al., 2012; Vose et al., 2012). Changes in the climate system before the observational period can be extracted from sparse documentary data (e.g., Pfister et al., 2009; Matuschek, 2014) for the last several centuries or from natural climate archives (like, for instance, tree rings, lake sediments, or ice cores). Using advanced statistical methods proxy records are combined to represent large scale or global climate conditions (e.g. PAGES 2k Network, 2013). These estimates, however, are not necessarily physical consistent and for the future development of the climate system their use is limited to analog approaches.

A valuable tool to produce physical consistent, global climate information with high spatial and temporal resolution for the past and the present as well as projections for the future are climate models (Flato et al., 2013). Furthermore, contrary to nature these models enable us to gain understanding of the climate effect of individual forcings (e.g., solar variability) or boundary conditions (e.g., movement of continents). Climate models are mathematical representations of the climate system (McGuffie and Henderson-Sellers, 2005; Stocker, 2011). Depending on their complexity, they can be classified into a hierarchy from one layer energy balance models (EBMs) (e.g., Held et al., 2010), over climate models of reduced complexity (e.g., Petoukhov et al., 2000; Ritz et al., 2011), to GCMs or atmosphere-ocean-general-circulation models (AOGCMs) (e.g., Collins et al., 2006; Giorgetta et al., 2013). With more and more components incorporated into the latter, these models progressively transform into Earth system models (Fig. 1.9).

In a GCM, the model domain, typically the entire atmosphere or ocean, is divided into a three-dimensional grid (Fig. 1.10) and at each time step a set of differential equations describing the fluxes of energy, momentum and different tracers is solved for

1. Introduction

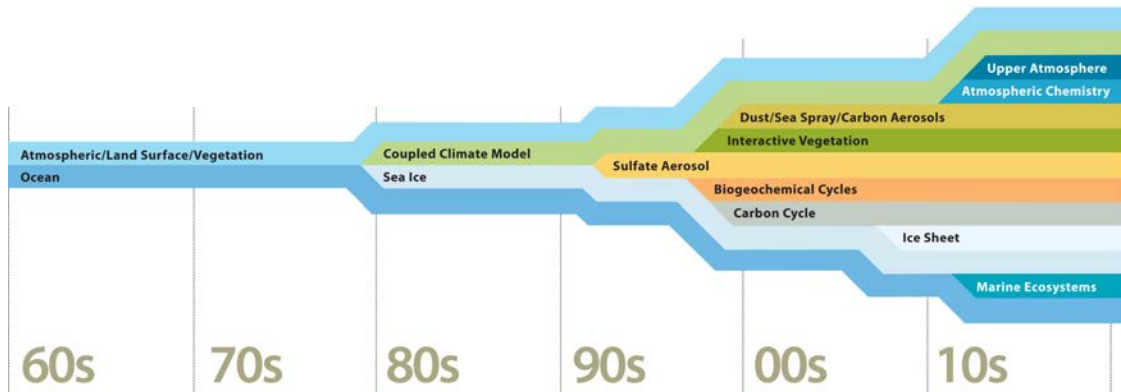


Figure 1.9.: Schematic overview of the development of climate models (adapted and modified from UCAR Climate Change - Multimedia Gallery¹).

each grid box (McGuffie and Henderson-Sellers, 2005; Stocker, 2011). The choice of the spatial discretisation depends on the scientific question, but also on the computational resources. Processes acting on spatial scales smaller than the spatial resolution of the model (subgrid scales) can not directly be considered in the equations and need to be parametrised. An example for a parametrisation is the treatment of convection and clouds in GCMs. These parametrisations differ between climate models and are the main reason for different model response to the same forcing, for instance, different temperature responses to a doubling of CO_2 (e.g. Webb et al., 2013).

For a realistic representation of the climate system in the model, all important model components and processes need to be considered (Fig. 1.1). But which components and processes are important for a realistic simulation of the climate system? The answer to this question has steadily changed since the development of the first climate models following the increasing knowledge about the climate system and the development of computational power (Fig. 1.9). Furthermore, the answer depends again on the scientific question addressed. Model simulations of glacial-interglacial cycles, for instance, can not implement the same complexity as simulations for the last decades of the 20th century.

Climate models are simplified representations of the real world and results from climate models are associated with uncertainties in several aspects. As stated before, subgrid processes are parametrised based on simplified physical models or empirical estimates and typical include parameters that can not or only within a certain range be defined by measurements (Randall et al., 2007). These "free" parameters are used in the model tuning to improve the agreement between simulated climate and observations (e.g., Mauritsen et al., 2012). The parametrisation and the tuning differs between the state-of-the-art climate models. Intercomparison projects are initiated with the goal to compare models and identify systematic errors in the simulations (e.g., CMIP5 for coupled AOGCMs or CCMVal2 for CCM). Climate models, furthermore, need information on the boundary conditions and forcings, such as solar variability, volcanic activity, land use changes, GHG concentrations, and others. As described above for the solar and volcanic forcing, these boundary conditions are subjected to different uncertainties, which introduce another level of uncertainty to the model simulations. In particular for the simulations of the

¹<https://www2.ucar.edu/news/understanding-climate-change-multimedia-gallery> (accessed on 08 May 2014)

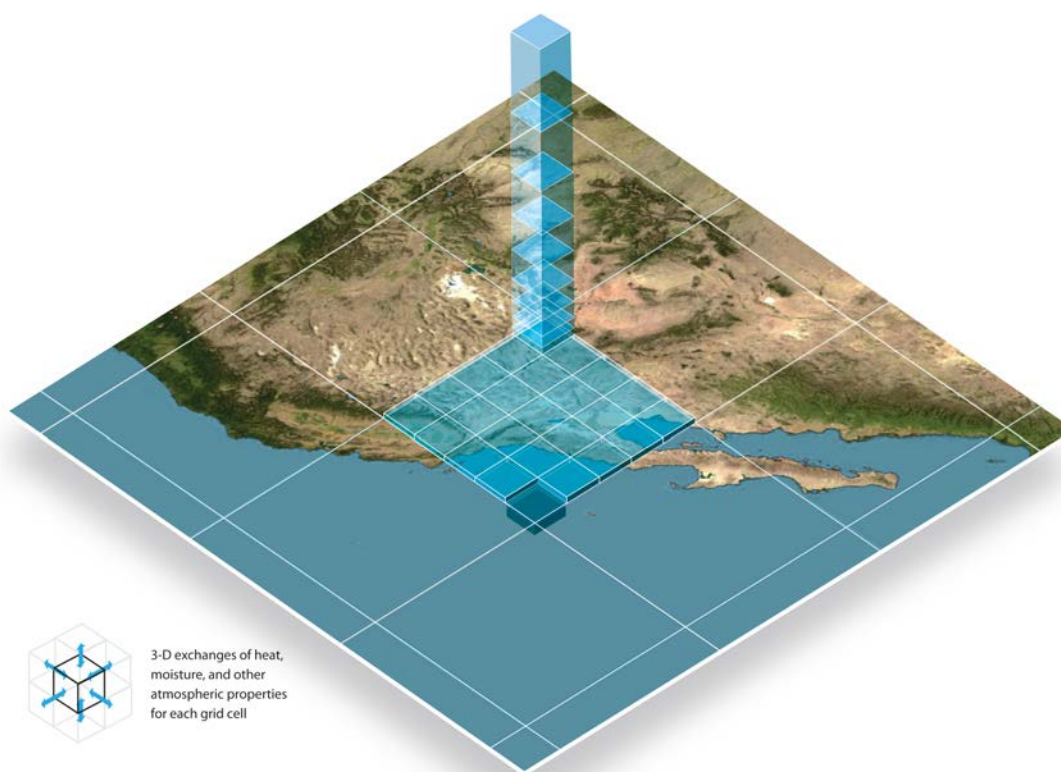


Figure 1.10.: Spatial discretisation of the atmosphere and the ocean in a climate model (adapted and modified from UCAR Climate Change - Multimedia Gallery²).

last millennium, some of the forcing are highly uncertain. For simulations of the future, the forcings are unknown and only projections of several even likely futures are possible (e.g., Representative Concentration Pathways (RCP)). A last level of uncertainty finally, is associated with the models internal variability. On the one hand, the models internal variability may differ from the one of the real climate system, e.g., by differences in the periodicities of ENSO. On the other hand, differences can arise from phase differences between model and observations, e.g., the Tambora eruption of 1815 occurs during El-Niña conditions in the coupled model simulation, whereas the real eruption might have occurred in an El-Niño state. The different levels of uncertainty are not equally distributed, but change in time (Hawkins and Sutton, 2009). For future projections of the global mean temperature, for instance, the model uncertainty is the dominant uncertainty in the beginning, but the uncertainties in the boundary conditions and forcings grow in time and are the major causes of uncertainty from the mid of the 21th century on. On a regional scale, the uncertainty is overall increased and the internal variability can become very important (e.g., Deser et al., 2010).

²<https://www2.ucar.edu/news/understanding-climate-change-multimedia-gallery> (accessed on 08 May 2014)

1.5.1. The atmosphere-ocean-chemistry-climate model SOCOL-MPIOM

For this thesis, an atmosphere-chemistry model has been coupled to an ocean model. In the following the components of the coupled model SOCOL-MPIOM are briefly described and the experiments used throughout this thesis are introduced. An detailed evaluation of SOCOL-MPIOM is given in Chapter 2.

SOCOL-MPIOM consists of the CCM SOCOL (Stenke et al., 2013) coupled to the ocean model MPIOM (Jungclaus et al., 2006). The atmospheric-chemistry component SOCOL in version 3 is based on the GCM ECHAM5 (Roeckner et al., 2003) in its middle atmosphere configuration (Manzini et al., 2006), which is coupled to the CCM MEZON (Rozanov et al., 1999, 2001; Egorova et al., 2003).

The dynamical core of SOCOL is identical with ECHAM5 and is based on the primitive equations with temperature, vorticity, divergence, surface pressure, humidity, and cloud water as prognostic variables (Schraner et al., 2008; Stenke et al., 2013). For the horizontal discretisation the spectral-transform methods (Simmons et al., 1989) are used. The vertical is discretised using a hybrid sigma-pressure coordinate system on a Lorenz grid (Simmons and Burridge, 1981). The SW radiation scheme originates from the scheme of the European Centre of Medium-Range Weather Forecasts (ECMWF) model IFS and considers wavelength between 185-4000 nm, divided into six intervals. Contrary to ECHAM5, SOCOL allows for variations in the spectral composition of the solar forcing. Furthermore, the absorption of oxygen and ozone in different wavelength intervals (Lyman-alpha, Schumann-Runge, Hartley, and Higgins) is parametrised following an approach by Egorova et al. (2004). The long-wave (LW) scheme of SOCOL is identical to ECHAM5 and follows the rapid radiative transfer model (RRTM) scheme (Mlawer et al., 1997) for the calculation of heating rates and radiation fluxes over 16 spectral bands from 10 to 3000 cm^{-1} .

The chemistry module considers 31 chemical species that react together in 140 gas-phase-, 46 photolysis, and 16 heterogeneous reactions. Heterogeneous reactions can take place on three types of PSC and on sulphate aerosols. The effect of energetic particle precipitation on the chemistry is implemented by different parametrisation for GCR, low energetic electrons (LEE), and SEP (Calisto et al., 2011; Rozanov et al., 2012). The coupling of the physical and the chemical components is implemented directly in SOCOL.

Furthermore, the chemistry module can be deactivated to enable simulation without interactive chemistry, e.g., in sensitivity studies. In this case, daily three dimensional ozone concentrations are applied as forcing. These can either origin from observation (e.g., Fortuin and Kelder, 1998) or from a simulation with interactive chemistry. For the latter, the forcing is extracted and applied directly on the model levels, since the errors introduced by vertical interpolation on the model levels can be quite substantial.

The ocean model MPIOM (Marsland, 2003; Jungclaus et al., 2006) is a free surface ocean general circulation model using an Arakawa-C grid in the horizontal and a z-grid in the vertical. MPIOM includes a dynamic sea-ice components following viscous-plastic rheology of Hibler (1979). The oceanic and the atmospheric component are coupled every 24 hours without flux correction by the OASIS3 coupler (Budich et al., 2010; Valcke, 2013).

All experiments with SOCOL-MPIOM are performed with a resolution of T31 ($3.75^\circ \times 3.75^\circ$) with 39 vertical levels (up to 0.01 hPa, approx 80 km) in the atmosphere and GR30 with 40 level in the ocean only. GR30 refers to a rotated grid with a nominal

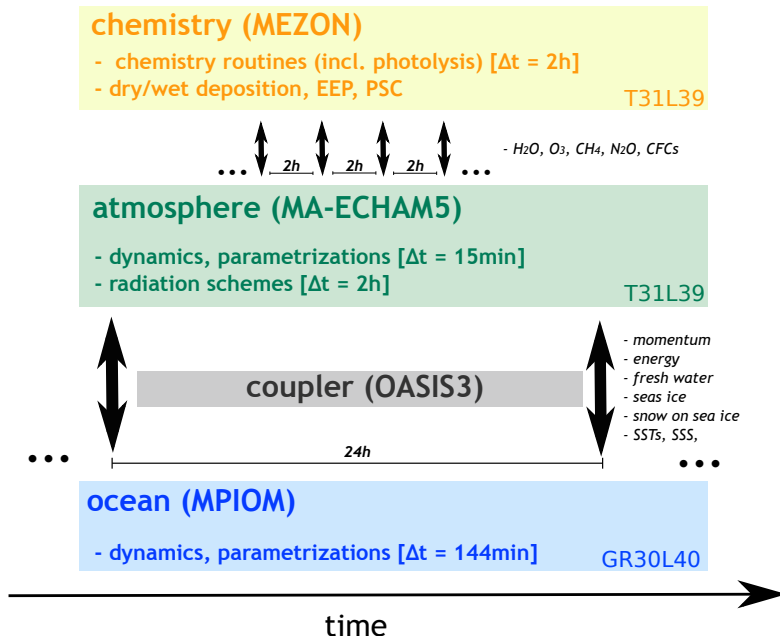


Figure 1.11.: Summary of the model components and the time steps for the different routines. Time steps given correspond to a spectral truncation of T31 and an ocean grid spacing of nominal 3° .

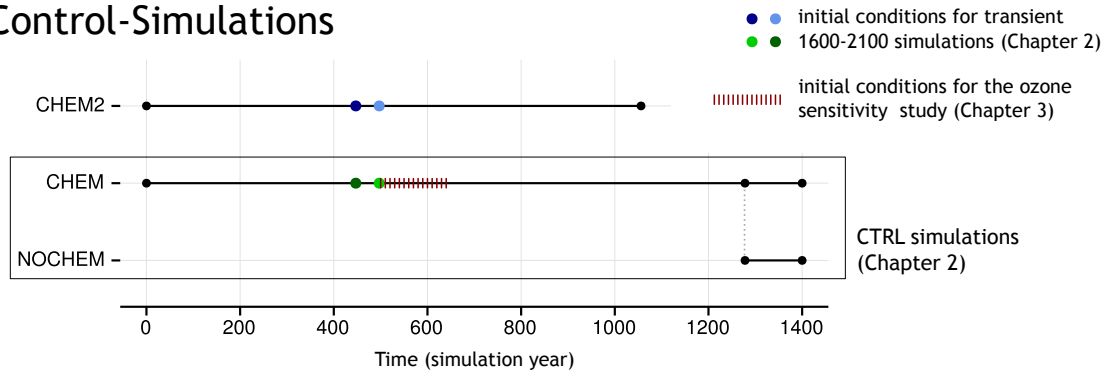
resolution of 3° . In this grid the poles are centred over land (Antarctica and Greenland) to avoid numerical instabilities at the poles and to reach a higher resolution in the freshwater formation regions of the North Atlantic. The vertical levels in the ocean are unevenly spaced, from 12 m near the surface to several hundred meters in the deep ocean. The model components, the coupler and the time-steps for the different components are depicted in Figure 1.11.

1.5.2. Overview of the simulations used in this thesis

A number of simulations have been performed for this thesis, which are summarised in the following. A detailed description of the forcings, boundary conditions, and initialisation techniques is given in the corresponding chapters. An overview of the simulations is given in Figure 1.12 and Table 1.1.

In Chapter 2 several simulations are used to evaluate the newly coupled model. CHEM is a long-term control simulation under perpetual 1600 AD conditions with a length of 1400 years performed with interactive chemistry. Initialisation files for the ocean are taken from transient simulations for the last millennium from the COSMOS model (Jungclaus et al., 2010). To assess the influence of the interactive chemistry in a control setup, i.e., without changing external forcings, a second control experiment (NOCHEM) without interactive chemistry is branched off from CHEM in the year 1178. The length of this experiment is 222 years and the climatological ozone forcing used in NOCHEM is extracted from the same 222 years of CHEM. Furthermore, CHEM performs as spin-up for transient simulations for the period 1600-2000 AD. For this period an ensemble of four simulations is performed, each two of them forced by a medium (M1, M2) or large (L1, L2) amplitude SSI forcing. The medium and large amplitude solar

Control-Simulations



Transient Simulations

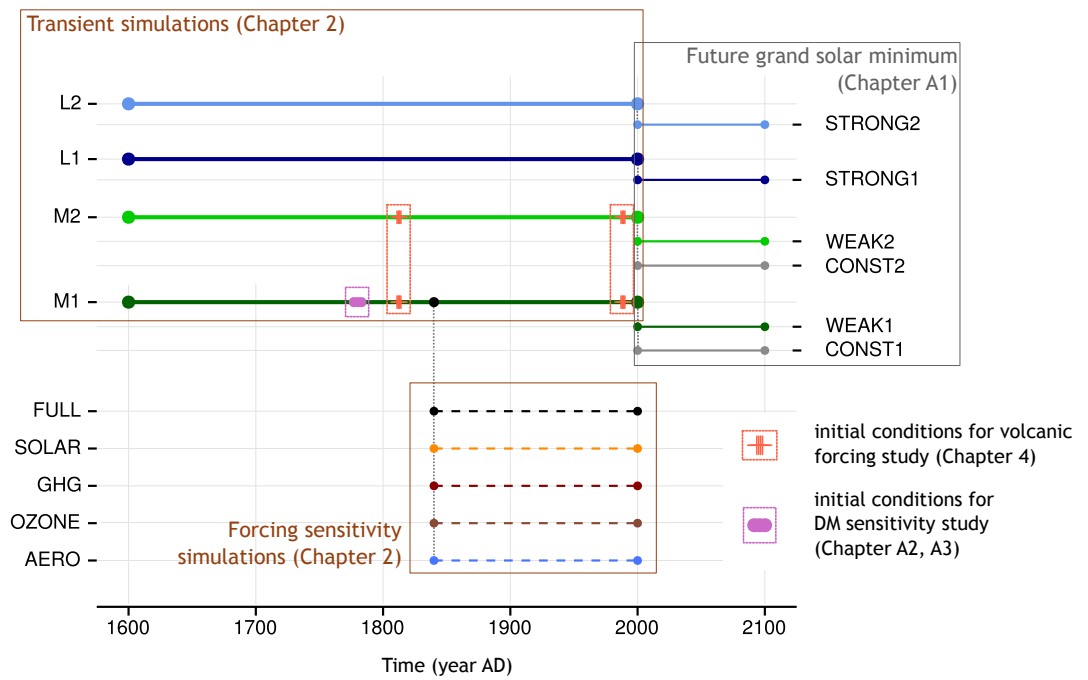


Figure 1.12.: Overview of the main simulations performed for this thesis (vgl. Table 1.1).

Table 1.1.: Overview of the main experiments and ensemble simulations used in this thesis. Forcings: mS: medium solar (mS_{UV}: UV only, mS_{VIS,NIR}: VIS and near-infrared only, mS_{EPP}: energetic particles only), lS: large solar, G: greenhouse gases, A: stratospheric and tropospheric aerosols, O: ozone (in case of simulation without interactive chemistry only). Simulations performed for the study presented in Chapter 4 are summarized in Table 4.1 on page 118.

Label	with chem	period/length (ensemble size)	forcings	Chapter
CHEM	yes	1400 yrs	const. 1600 AD	2
CHEM2	yes	1056 yrs	const 1600 AD	2
NOCHEM	no	222 yrs	const 1600 AD	2
M1	yes	1600-2000 AD	mSGA	2
M2	yes	1600-2000 AD	mSGA	2
L1	yes	1600-2000 AD	lSGA	2
L2	yes	1600-2000 AD	lSGA	2
FULL	no	1840-2000 AD	mSGAO	2
SOLAR	no	1840-2000 AD	mS	2
GHG	no	1840-2000 AD	G	2
AERO	no	1840-2000 AD	A	2
OZONE	no	1840-2000 AD	O	2
O ₃ ^{strong}	no	8 yrs (15)	AO	3
O ₃ ^{weak}	no	8 yrs (15)	AO	3
CTRL.O ₃ ^{strong}	no	8 yrs (15)	O	3
CTRL.O ₃ ^{weak}	no	8 yrs (15)	O	3
CONST	yes	2000-2100 AD (2)	GA	A.1
WEAK	yes	2000-2100 AD (2)	mSGA	A.1
STRONG	yes	2000-2100 AD (2)	lSGA	A.1
CTRL1780	yes	60 yrs (3)	const. 1780 AD	A.2, A.3
ALL	yes	1780-1840 AD (3)	mSGA	A.2, A.3
TD	yes	1780-1840 AD (3)	mS _{UV} G	A.2, A.3
BU	yes	1780-1840 AD (3)	mS _{VIS,NIR} G	A.2, A.3
VOLC	yes	1780-1840 AD (3)	GA	A.2, A.3
EPP	yes	1780-1840 AD (3)	mS _{EPP} G	A.2, A.3

forcings correspond to a TSI differences of 3 and 6 Wm^{-2} between MM and present day. Since the TSI for the year 1600 differs between the two forcings, a second control simulation (CHEM2) forced by a lower solar forcing is conducted to initialise L1 and L2. The transient experiments are initialised using restart conditions from the years 450 and 500 from CHEM and CHEM2, respectively and are carried out with interactive chemistry. For the period 1840-2000 AD, an additional set of sensitivity experiments is performed, to analyse the pronounced temperature increase during this period found in the four transient experiments (M1, M2, L1 and L2). Five sensitivity experiments with different forcings (solar, GHGs, aerosols, ozone, and all forcings together) are used to assess the temperature change associated with each forcing. These experiments are conducted without interactive chemistry to include or exclude the influence of the simulated ozone changes from the interactive model in the simulations. Finally, several climate sensitivity experiments with increasing 1 $\% \text{yr}^{-1}$ CO_2 increase or abrupt quadrupling of the CO_2 concentrations are carried out to estimate the climate sensitivity of SOCOL-MPIOM.

In Chapter 3 the sensitivity of the dynamical perturbations after large volcanic eruptions to the stratospheric ozone concentrations is assessed. Therefore, SOCOL-MPIOM without interactive chemistry is forced by two different ozone climatologies, characterised by different meridional ozone gradients. For each of the two climatologies an ensemble of control simulations and an ensemble of simulations perturbed by a single volcanic eruptions is performed, with 15 members each. Initial conditions for the ensemble experiments are extracted in 10-yr steps between the years 500-640 of CHEM, to consider a large number of different states of the climate system, e.g., in terms of the ENSO phase.

The study presented in Chapter 4 focuses again on the role of ozone changes for the dynamic response after a large volcanic eruption, but in this case in the model with interactive chemistry. Here, ozone concentrations respond to the volcanic perturbation and modulate the stratospheric dynamics. Furthermore, this study addresses the influence of the eruption strength and the climate state on the response and the relative importance of different processes (warming in the aerosol cloud vs. heterogeneous reaction of the aerosol surfaces) resulting in a large number of ensemble simulations, described in detail in Chapter 4. Each of the ensembles contains 8 members. The initial states of the atmosphere and the ocean are taken from M1 and M2 for the years 1987-1990 for the present day ensembles and the years 1811-1814 for the pre-industrial climate state.

The appendix finally covers simulations of a possible grand solar minimum in the near future (chapter A.1) and two sensitivity studies for the DM (chapter A.2 and A.3). For the future solar minimum the transient simulations M1, M2, L1, and L2 is continued to the year 2100 AD, with M1 and M2 resembling a medium reduction of the TSI and L1 and L2 a strong reduction. The two sets are named WEAK and STRONG in the corresponding study. Additionally, two experiments without solar minimum are performed (CONST). The GHG scenario used is the RCP 4.5. The sensitivity studies for the DM cover the period 1780-1840 AD. For these two studies, three member ensembles are conducted for different forcings to analyse their contribution to the climate variation during the DM. TD implements variations in UV part of the solar spectrum, BU variations in the visible and near infrared. VOLC is driven by forcing from volcanic aerosols only and EPP is exclusively forced by energetic particles. Furthermore, the ALL ensemble includes all of the above mentioned forcings and CONST perpetual 1780 conditions. These experiments are initialised using M1 and M2; the solar forcing used is the medium amplitude solar forcing of M1 and M2.

1.6. Outline

Within this thesis the following main research questions are addressed:

- i) What is the influence of atmospheric chemistry on the climate?
- ii) What is the role of solar and volcanic activity for past and future changes in the climate system?
- iii) How do atmospheric chemistry and external forcings interact and how does the response of the chemistry modulate the response of the climate system?

This thesis is structured as follows:

Chapter 2 introduces the AOCCM SOCOL-MPIOM coupled during this thesis. Within this chapter the influence of the chemistry on the climate is addressed by comparing 1600 AD time slice (control) simulations with and without interactive chemistry (CHEM and NOCHEM in Table 1.1). Transient simulations for the period 1600-2000 using the model with interactive chemistry and sensitivity experiments for different external forcings covering the period 1840-2000 are used to gain insights into the role of solar variability and other forcing for the simulated climate. This study is published as discussion paper in *Climate of the Past Discussions* (Muthers et al., 2014b) and in review for *Climate of the Past*.

In **Chapter 3** a number of sensitivity experiments is performed to identify the role of ozone in the model configuration without interactive chemistry. Most of the current AOGCMs do not include interactive ozone chemistry, but consider spatial and temporal ozone variations by prescribing ozone as forcing (e.g., Fortuin and Kelder, 1998; Cionni et al., 2011). However, considerable differences exist between different ozone forcing datasets. In this study, the response of SOCOL-MPIOM to large tropical volcanic eruptions is compared for different ozone climatologies. This study is published in the *Journal of Geophysical Research* (Muthers et al., 2014a).

Chapter 4 also focuses on stratospheric ozone and volcanic eruptions, but using model simulations with interactive chemistry. Here, ozone changes after a strong volcanic eruption are analysed and the influence of these changes on the dynamic response in the stratosphere with possible influences on the troposphere is evaluated. Furthermore, the question is raised how the responses differ between different climate states and eruption sizes. This study is submitted to the *Journal of Geophysics Research* (Muthers et al., 2014c).

The appendix contains three publications, where I was involved as co-author. In **Chapter A.1** the influence of a possible grand solar minima in the 21th century on the projected climate change is examined. This study is published in the *Geophysical Research Letters* (Anet et al., 2013b). **Chapters A.2** and **A.3** present results from sensitivity studies for the DM separately for stratospheric changes (published in *Atmospheric Chemistry and Physics*, Anet et al., 2013a) and the troposphere (*Climate of the Past*, Anet et al., 2014).

Bibliography

- Abreu, J. A., Beer, J., Steinhilber, F., Tobias, S. M., and Weiss, N. O.: For how long will the current grand maximum of solar activity persist?, *Geophys. Res. Lett.*, 35, 1–4, doi:10.1029/2008GL035442, 2008.
- Abreu, J. A., Beer, J., Mccracken, K. G., and Steinhilber, F.: Is there a planetary influence on solar activity?, *Astronomy & Astrophysics*, 548, 1–9, 2012a.
- Abreu, J. A., Beer, J., Steinhilber, F., Christl, M., and Kubik, P. W.: 10Be in ice cores and 14C in tree rings: Separation of production and climate effects, *Space Science Reviews*, 176, 343–349, doi:10.1007/s11214-011-9864-y, 2012b.
- Ammann, C. M.: A monthly and latitudinally varying volcanic forcing dataset in simulations of 20th century climate, *Geophys. Res. Lett.*, 30, 1657, doi:10.1029/2003GL016875, 2003.
- Andrews, D. G., Holton, J. R., and Leovy, C. B.: *Middle atmosphere dynamics*, Academic, 1987.
- Anet, J. G., Muthers, S., Rozanov, E., Raible, C. C., Peter, T., Stenke, A., Shapiro, A. I., Beer, J., Steinhilber, F., Brönnimann, S., Arfeuille, F., Brugnara, Y., and Schmutz, W. K.: Forcing of stratospheric chemistry and dynamics during the Dalton Minimum, *Atmos. Chem. Phys.*, 13, 10951–10967, doi:10.5194/acp-13-10951-2013, 2013a.
- Anet, J. G., Rozanov, E. V., Muthers, S., Peter, T., Brönnimann, S., Arfeuille, F., Beer, J., Shapiro, A. I., Raible, C. C., Steinhilber, F., and Schmutz, W. K.: Impact of a potential 21st century “grand solar minimum” on surface temperatures and stratospheric ozone, *Geophys. Res. Lett.*, 40, 4420–4425, doi:10.1002/grl.50806, 2013b.
- Anet, J. G., Muthers, S., Rozanov, E. V., Raible, C. C., Stenke, A., Shapiro, A. I., Brönnimann, S., Arfeuille, F., Brugnara, Y., Beer, J., Steinhilber, F., Schmutz, W., and Peter, T.: Impact of solar vs. volcanic activity variations on tropospheric temperatures and precipitation during the Dalton Minimum, *Climate of the Past*, 10, 921–938, doi:10.5194/cp-10-921-2014, 2014.
- Arfeuille, F., Weisenstein, D., Mack, H., Rozanov, E., Peter, T., and Brönnimann, S.: Volcanic forcing for climate modeling: a new microphysics-based data set covering years 1600–present, *Climate of the Past*, 10, 359–375, doi:10.5194/cp-10-359-2014, 2014.
- Austin, J. and Wilson, R. J.: Ensemble simulations of the decline and recovery of stratospheric ozone, *J. Geophys. Res.*, 111, D16 314, doi:10.1029/2005JD006907, 2006.
- Austin, J., Tourpali, K., Rozanov, E., Akiyoshi, H., Bekki, S., Bodeker, G. E., Brühl, C., Butchart, N., Chipperfield, M., Deushi, M., Fomichev, V. I., Giorgetta, M. A., Gray, L., Kodera, K., Lott, F., Manzini, E., Marsh, D., Matthes, K., Nagashima, T., Shibata, K., Stolarski, R. S., Struthers, H., and Tian, W.: Coupled chemistry climate model simulations of the solar cycle in ozone and temperature, *J. Geophys. Res.*, 113, 1–20, doi:10.1029/2007JD009391, 2008.
- Austin, J., Scinocca, J., Plummer, D., Oman, L., Waugh, D., Akiyoshi, H., Bekki, S., Braesicke, P., Butchart, N., Chipperfield, M., Cugnet, D., Dameris, M., Dhomse, S., Eyring, V., Frith, S., Garcia, R. R., Garny, H., Gettelman, A., Hardiman, S. C., Kinnison, D., Lamarque, J. F., Mancini, E., Marchand, M., Michou, M., Morgenstern, O., Nakamura, T., Pawson, S., Pitari, G., Pyle, J., Rozanov, E., Shepherd, T. G., Shibata, K., Teyssède, H., Wilson, R. J., and Yamashita, Y.: Decline and recovery of total column ozone using a multimodel time series analysis, *J. Geophys. Res.*, 115, D00M10, doi:10.1029/2010JD013857, 2010.
- Baldwin, M. P. and Dunkerton, T. J.: Stratospheric harbingers of anomalous weather regimes., *Science*, 294, 581–4, doi:10.1126/science.1063315, 2001.
- Baldwin, M. P. and Dunkerton, T. J.: The solar cycle and stratosphere–troposphere dynamical coupling, *Journal of Atmospheric and Solar-Terrestrial Physics*, 67, 71–82, doi:10.1016/j.jastp.2004.07.018, 2005.
- Baldwin, M. P. and Thompson, D. W. J.: A critical comparison of stratosphere – troposphere coupling indices, *Quart. J. Roy. Meteor. Soc.*, 1672, 1661–1672, doi:10.1002/qj, 2009.

- Baldwin, M. P., Cheng, X., and Dunkerton, T. J.: Observed correlations between winter-mean tropospheric and stratospheric circulation anomalies, *Geophys. Res. Lett.*, 21, 1141–1144, 1994.
- Baldwin, M. P., Gray, L. J., Dunkerton, T. J., Hamilton, K., Haynes, P. H., Holton, J. R., Alexander, M. J., Hirota, I., Horinouchi, T., Jones, D. B. A., Marquardt, C., Sato, K., and Takahashi, M.: The Quasi-Biennial Oscillation, *Rev. Geophys.*, 39, 179–229, 2001.
- Baldwin, M. P., Dameris, M., and Shepherd, T. G.: How will the stratosphere affect climate change?, *Science*, 316, 1576–1577, 2007.
- Bates, D. R. and Nicolet, M.: The photochemistry of atmospheric water vapor, *J. Geophys. Res.*, 55, 301–327, 1950.
- Beer, J., Vonmoos, M., and Muscheler, R.: Solar variability over the past several millennia, *Space Science Reviews*, 125, 67–79, doi:10.1007/s11214-006-9047-4, 2006.
- Bodeker, G. E., Shiona, H., and Eskes, H.: Indicators of Antarctic ozone depletion, *Atmos. Chem. Phys.*, 5, 2603–2615, 2005.
- Booth, B. B. B., Dunstone, N. J., Halloran, P. R., Andrews, T., and Bellouin, N.: Aerosols implicated as a prime driver of twentieth-century North Atlantic climate variability., *Nature*, 484, 228–32, doi:10.1038/nature10946, 2012.
- Brasseur, G. P. and Solomon, S.: *Ozone perturbations*, Kluwer Academic Publishers, Dordrecht, Netherlands, 2005.
- Brasseur, G. P., Orlando, J. J., and Tyndall, G. S.: *Atmospheric chemistry and global change*, Oxford University Press, 1999.
- Brohan, P., Kennedy, J. J., Harris, I., Tett, S. F. B., and Jones, P. D.: Uncertainty estimates in regional and global observed temperature changes: A new data set from 1850, *J. Geophys. Res.*, 111, D12 106, doi:10.1029/2005JD006548, 2006.
- Brönnimann, S., Bhend, J., Franke, J., Flückiger, S., Fischer, A. M., Bleisch, R., Bodeker, G. E., Hassler, B., Rozanov, E., and Schraner, M.: A global historical ozone data set and prominent features of stratospheric variability prior to 1979, *Atmos. Chem. Phys.*, 13, 9623–9639, doi:10.5194/acp-13-9623-2013, 2013.
- Budich, R., Giorretta, M., Jungclaus, J., Redler, R., and Reick, C.: *The MPI-M Millennium Earth System Model: An assembling guide for the COSMOS configuration*, MPI report, Max-Planck Institute for Meteorology, Hamburg, Germany, 2010.
- Calisto, M., Usoskin, I., Rozanov, E., and Peter, T.: Influence of galactic cosmic rays on atmospheric composition and dynamics, *Atmos. Chem. Phys.*, 11, 4547–4556, doi:10.5194/acp-11-4547-2011, 2011.
- Chapman, S.: A theory of upper-atmospheric ozone, *Memoirs of the Roy. Meteor. Soc.*, 3, 103–123, 1930.
- Christiansen, B.: Downward propagation of zonal mean zonal wind anomalies from the stratosphere to the troposphere: Model and reanalysis, *J. Geophys. Res.*, 106, 27 307, doi:10.1029/2000JD000214, 2001.
- Christiansen, B.: Downward propagation and statistical forecast of the near-surface weather, *J. Geophys. Res.*, 110, D14 104, doi:10.1029/2004JD005431, 2005.
- Christiansen, B.: Volcanic eruptions, large-scale modes in the northern hemisphere, and the El Niño–Southern oscillation, *J. Climate*, 21, 910–922, doi:10.1175/2007JCLI1657.1, 2008.
- Cionni, I., Eyring, V., Lamarque, J. F., Rand el, W. J., Stevenson, D. S., Wu, F., Bodeker, G. E., Shepherd, T. G., Shindell, D. T., and Waugh, D. W.: Ozone database in support of CMIP5 simulations: results and corresponding radiative forcing, *Atmos. Chem. Phys.*, 11, 11 267–11 292, doi:10.5194/acp-11-11267-2011, 2011.
- Coffey, M. T.: Observations of the impact of volcanic activity on stratospheric chemistry, *J. Geophys. Res.*, 101, 6767, doi:10.1029/95JD03763, 1996.
- Cole-Dai, J.: *Volcanoes and climate*, Wiley Interdisciplinary Reviews: Climate Change, 1, 824–839, doi:10.1002/wcc.76, 2010.

- Collins, W. D., Bitz, C. M., Blackmon, M. L., Bonan, G. B., Bretherton, C. S., Carton, J. A., Chang, P., Doney, S. C., Hack, J. J., Henderson, T. B., Kiehl, J. Y., Large, W. G., McKenna, D. S., Santer, B. D., and Smith, R. D.: The Community Climate System Model version 3 (CCSM3), *J. Climate*, 19, 2122–2143, 2006.
- Cook, E. R., D’Arrigo, R. D., and Mann, M. E.: A well-verified, multiproxy reconstruction of the winter North Atlantic Oscillation index since A.D 1400, *J. Climate*, 15, 1754–1764, 2002.
- Crowley, T., Zielinski, G., Vinther, B., Udisti, R., Kreutz, K., Cole-Dai, J., and Castellano, E.: Volcanism and the Little Ice Age, *PAGES news*, 16, 4–5, 2008.
- Crutzen, P. J.: The influence of nitrogen oxides on the atmospheric ozone content, *Quart. J. Roy. Meteor. Soc.*, 96, 320–325, 1970.
- Crutzen, P. J. and Stoermer, E. F.: The ‘Anthropocene’, *Global Change Newsletter*, 41, 17–18, 2000.
- Cubasch, U., Voss, R., Hegerl, G. C., Waszkewitz, J., and Crowley, T. J.: Climate dynamics simulation of the influence of solar radiation variations on the global climate with an ocean-atmosphere general circulation model, *Climate Dyn.*, 13, 757–767, 1997.
- Cubasch, U., Wuebbles, D., Chen, D., Facchini, M., Frame, D., Mahowald, N., and Winther, J.: Introduction, in: *Climate Change 2013: The Physical Science Basis. Contribution of Working Group I to the Fifth Assessment Report of the Intergovernmental Panel on Climate Change*, edited by Stocker, T., Qin, D., Plattner, G.-K., Tignor, M., Allen, S., Boschung, J., Nauels, A., Y. Xia, V. B., and Midgley, P., chap. 1, pp. 119–158, Cambridge University Press, Cambridge, United Kingdom and New York, NY, USA, 2013.
- Dee, D. P., Uppala, S. M., Simmons, A. J., Berrisford, P., Poli, P., Kobayashi, S., Andrae, U., Balmaseda, M. A., Balsamo, G., Bauer, P., Bechtold, P., Beljaars, A. C. M., van de Berg, L., Bidlot, J., Bormann, N., Delsol, C., Dragani, R., Fuentes, M., Geer, A. J., Haimberger, L., Healy, S. B., Hersbach, H., Hólm, E. V., Isaksen, I., Kållberg, P., Köhler, M., Matricardi, M., McNally, A. P., Monge-Sanz, B. M., Morcrette, J.-J., Park, B.-K., Peubey, C., de Rosnay, P., Tavolato, C., Thépaut, J.-N., and Vitart, F.: The ERA-Interim reanalysis: Configuration and performance of the data assimilation system, *Quart. J. Roy. Meteor. Soc.*, 137, 553–597, doi:10.1002/qj.828, 2011.
- Deser, C., Alexander, M. A., Xie, S.-P., and Phillips, A. S.: Sea surface temperature variability: Patterns and mechanisms, *Annual Review of Marine Science*, 2, 115–143, doi:10.1146/annurev-marine-120408-151453, 2010.
- Dickinson, R. E.: Solar variability and the lower atmosphere, *Bull. Amer. Meteor. Soc.*, 56, 1240–1248, 1975.
- Dietmüller, S., Ponater, M., and Sausen, R.: Interactive ozone induces a negative feedback in CO₂ driven climate change simulations, *J. Geophys. Res.*, 119, 1796–1805, doi:10.1002/2013JD020575, 2014.
- Eddy, J. A.: The Maunder Minimum, *Science*, 192, 1189–1202, 1976.
- Egorova, T., Rozanov, E., Zubov, V., and Karol, I. L.: Model for investigating ozone trends (MEZON), *Izvestiya, Atmospheric and Oceanic Physics*, 39, 277–292, 2003.
- Egorova, T., Rozanov, E., Manzini, E., Schmutz, W., and Peter, T.: Chemical and dynamical response to the 11-year variability of the solar irradiance simulated with a chemistry-climate model, *Geophys. Res. Lett.*, 83, 6225–6230, doi:10.1029/2003GL019294, 2004.
- Ermolli, I., Matthes, K., Dudok de Wit, T., Krivova, N. A., Tourpali, K., Weber, M., Unruh, Y. C., Gray, L., Langematz, U., Pilewskie, P., Rozanov, E., Schmutz, W. K., Shapiro, A., Solanki, S. K., and Woods, T. N.: Recent variability of the solar spectral irradiance and its impact on climate modelling, *Atmos. Chem. Phys.*, 13, 3945–3977, doi:10.5194/acp-13-3945-2013, 2013.
- Eyring, V., Waugh, D. W., Bodeker, G. E., Cordero, E., Akiyoshi, H., Austin, J., Beagley, S. R., Boville, B. A., Braesicke, P., Brühl, C., Butchart, N., Chipperfield, M. P., Dameris, M.,

- Deckert, R., Deushi, M., Frith, S. M., Garcia, R. R., Gettelman, A., Giorgetta, M. A., Kinnison, D. E., Mancini, E., Manzini, E., Marsh, D. R., Matthes, S., Nagashima, T., Newman, P. A., Nielsen, J. E., Pawson, S., Pitari, G., Plummer, D. A., Rozanov, E., Schraner, M., Scinocca, J. F., Semeniuk, K., Shepherd, T. G., Shibata, K., Steil, B., Stolarski, R. S., Tian, W., and Yoshiki, M.: Multimodel projections of stratospheric ozone in the 21st century, *J. Geophys. Res.*, 112, D16 303, doi:10.1029/2006JD008332, 2007.
- Fernández-Donado, L., González-Rouco, J. F., Raible, C. C., Ammann, C. M., Barriopedro, D., García-Bustamante, E., Jungclaus, J. H., Lorenz, S. J., Luterbacher, J., Phipps, S. J., Servonnat, J., Swingedouw, D., Tett, S. F. B., Wagner, S., Yiou, P., and Zorita, E.: Large-scale temperature response to external forcing in simulations and reconstructions of the last millennium, *Climate of the Past*, 9, 393–421, doi:10.5194/cp-9-393-2013, 2013.
- Feulner, G. and Rahmstorf, S.: On the effect of a new grand minimum of solar activity on the future climate on Earth, *Geophys. Res. Lett.*, 37, L05 707, doi:10.1029/2010GL042710, 2010.
- Field, C. V., Schmidt, G. A., Koch, D., and Salyk, C.: Modeling production and climate-related impacts on ^{10}Be concentration in ice cores, *J. Geophys. Res.*, 111, D15 107, doi:10.1029/2005JD006410, 2006.
- Fischer, E. M., Luterbacher, J., Zorita, E., Tett, S. F. B., Casty, C., and Wanner, H.: European climate response to tropical volcanic eruptions over the last half millennium, *Geophys. Res. Lett.*, 34, 1–6, doi:10.1029/2006GL027992, 2007.
- Flato, G., Marotzke, J., Abiodun, B., Braconnot, P., Chou, S., Collins, W., Cox, P., Driouech, F., Emori, S., Eyring, V., Forest, C., Gleckler, P., Guilyardi, E., Jakob, C., Kattsov, V., Reason, C., and Rummukainen, M.: Evaluation of climate models, in: *Climate Change 2013: The Physical Science Basis. Contribution of Working Group I to the Fifth Assessment Report of the Intergovernmental Panel on Climate Change*, edited by Stocker, T., Qin, D., Plattner, G.-K., Tignor, M., Allen, S., Boschung, J., Nauels, A., Xia, Y., Bex, V., and Midgley, P., chap. 6, pp. 741–866, Cambridge University Press, Cambridge, United Kingdom and New York, NY, USA, 2013.
- Forster, P., Ramaswamy, V., Artaxo, P., Berntsen, T., Betts, R., Fahey, D. W., Haywood, J., Lean, J. L., Lowe, D. C., Myhre, G., Nganga, J., Prinn, R., Raga, G., Schulz, M., and Van Dorland, R.: Changes in atmospheric constituents and in radiative forcing, in: *Climate Change 2007: The Physical Science Basis. Contribution of Working Group I to the Fourth Assessment Report of the Intergovernmental Panel on Climate Change*, edited by Solomon, S., Qin, D., Manning, M., Chen, Z., Marquis, M., Averyt, K., Tignor, M., and Miller, H., chap. 2, pp. 131–234, Cambridge University Press, Cambridge, United Kingdom and New York, NY, USA, 2007.
- Fortuin, J. P. F. and Kelder, H.: An ozone climatology based on ozonesonde and satellite measurements, *J. Geophys. Res.*, 31, 31,709–31,734, 1998.
- Frame, T. H. A. and Gray, L. J.: The 11-yr solar cycle in ERA-40 data: an update to 2008, *J. Climate*, 23, 2213–2222, doi:10.1175/2009JCLI3150.1, 2010.
- Fröhlich, C.: Solar Irradiance Variability Since 1978, *Space Science Reviews*, 125, 53–65, doi:10.1007/s11214-006-9046-5, 2006.
- Fröhlich, C.: Evidence of a long-term trend in total solar irradiance, *Astronomy & Astrophysics*, 501, L27–L30, 2009.
- Gao, C., Robock, A., and Ammann, C.: Volcanic forcing of climate over the past 1500 years: An improved ice core-based index for climate models, *J. Geophys. Res.*, 113, D23 111, doi:10.1029/2008JD010239, 2008.
- Gerber, E. P., Butler, A., Calvo, N., Charlton-Perez, A., Giorgetta, M., Manzini, E., Perlwitz, J., Polvani, L. M., Sassi, F., Scaife, A. A., Shaw, T. A., Son, S.-W., and Watanabe, S.: Assessing and understanding the impact of stratospheric dynamics and variability on the earth system, *Bull. Amer. Meteor. Soc.*, 93, 845–859, doi:10.1175/bAms-d-11-00145.1, 2012.

- Gillett, N. P.: Detection of volcanic influence on global precipitation, *Geophys. Res. Lett.*, 31, 2–5, doi:10.1029/2004GL020044, 2004.
- Gillett, N. P. and Thompson, D. W. J.: Simulation of recent southern hemisphere climate change., *Science*, 302, 273–5, doi:10.1126/science.1087440, 2003.
- Giorgetta, M. A., Jungclaus, J., Reick, C. H., Legutke, S., Bader, J., Böttinger, M., Brovkin, V., Crueger, T., Esch, M., Fieg, K., Glushak, K., Gayler, V., Haak, H., Hollweg, H.-D., Ilyina, T., Kinne, S., Kornbluh, L., Matei, D., Mauritsen, T., Mikolajewicz, U., Mueller, W., Notz, D., Pithan, F., Raddatz, T., Rast, S., Redler, R., Roeckner, E., Schmidt, H., Schnur, R., Segschneider, J., Six, K. D., Stockhause, M., Timmreck, C., Wegner, J., Widmann, H., Wieners, K.-H., Claussen, M., Marotzke, J., and Stevens, B.: Climate and carbon cycle changes from 1850 to 2100 in MPI-ESM simulations for the Coupled Model Intercomparison Project phase 5, *Journal of Advances in Modeling Earth Systems*, 5, 572–597, doi:10.1002/jame.20038, 2013.
- Glueck, M. F. and Stockton, C. W.: Reconstructions of the North Atlantic Oscillation, *International Journal of Climatology*, 21, 1453–1465, 2001.
- González-Rouco, J. F., Beltrami, H., Zorita, E., and von Storch, H.: Simulation and inversion of borehole temperature profiles in surrogate climates: Spatial distribution and surface coupling, *Geophys. Res. Lett.*, 33, L01 703, doi:10.1029/2005GL024693, 2006.
- Graf, H. F., Kirchner, I., Robock, A., and Schult, I.: Pinatubo eruption winter climate effects: Model versus observations, *Climate Dyn.*, 92, 81–93, 1993.
- Gray, L. J., Rumbold, S. T., and Shine, K. P.: Stratospheric temperature and radiative forcing response to 11-year solar cycle changes in irradiance and ozone, *J. Atmos. Sci.*, 66, 2402–2417, doi:10.1175/2009JAS2866.1, 2009.
- Gray, L. J., Beer, J., Geller, M., Haigh, J. D., Lockwood, M., Matthes, K., Cubasch, U., Fleitmann, D., Harrison, G., Hood, L., Luterbacher, J., Meehl, G. A., Shindell, D. T., Geel, B. V., and White, W.: Solar influences on climate, *Rev. Geophys.*, 48, 1–53, doi:10.1029/2009RG000282, 2010.
- Guiot, J., Corona, C., and members, E.: Growing season temperatures in Europe and climate forcings over the past 1400 years., *PloS one*, 5, e9972, doi:10.1371/journal.pone.0009972, 2010.
- Haigh, J. D.: The role of stratospheric ozone in modulating the solar radiative forcing of climate, *Nature*, 370, 544–546, 1994.
- Haigh, J. D.: The impact of solar variability on climate, *Science*, 272, 981–984, 1996.
- Haigh, J. D.: The effects of solar variability on the Earth’s climate, *Philosophical Transactions of the Royal Society A: Mathematical, Physical and Engineering Sciences*, 361, 95–111, doi:10.1098/rsta.2002.1111, 2003.
- Haigh, J. D.: The sun and the earth’s climate, *Living Reviews in Solar Physics*, 4, 1–64, doi:10.12942/lrsp-2007-2, 2007.
- Haigh, J. D., Blackburn, M., and Day, R.: The response of tropospheric circulation to perturbations in lower-stratospheric temperature, *J. Climate*, 18, 3672–3685, 2005.
- Hammer, C. U., Clausen, H. B., and Dansgaard, W.: Greenland ice sheet evidence of post-glacial volcanism and its climatic impact, *Nature*, 288, 230–235, doi:10.1038/288230a0, 1980.
- Hansen, J., Ruedy, R., Sato, M., Lo, K., Met Office, and Hadley Center: Global surface temperature change, *Rev. Geophys.*, 48, 1–29, doi:10.1029/2010RG000345, 2010.
- Hartmann, D., Tank, A. K., Rusticucci, M., Alexander, L., Brönnimann, S., Charabi, Y., Dentener, F., Dlugokencky, E., Easterling, D., Kaplan, A., Soden, B., Thorne, P., Wild, M., and Zhai, P.: Observations: atmosphere and surface, in: *Climate Change 2007: The Physical Science Basis. Contribution of Working Group I to the Fourth Assessment Report of the Intergovernmental Panel on Climate Change*, edited by Stocker, T. F., Qin, D., Plattner, G.-K., Tignor, M., Allen, S., Boschung, J., Nauels, A., Xia, Y., Bex, V., and Midgley, P., chap. 2, pp. 159–254, Cambridge University Press, Cambridge, United Kingdom and New York, NY, USA, 2013.

- Hassler, B., Bodeker, G. E., and Dameris, M.: Technical Note: A new global database of trace gases and aerosols from multiple sources of high vertical resolution measurements, *Atmos. Chem. Phys.*, 8, 5403–5421, doi:10.5194/acp-8-5403-2008, 2008.
- Hawkins, E. and Sutton, R.: The potential to narrow uncertainty in regional climate predictions, *Bull. Amer. Meteor. Soc.*, 90, 1095–1107, 2009.
- Haynes, P.: Stratospheric dynamics, *Annu. Rev. Fluid Mech.*, 37, 263–293, doi:10.1146/annurev.fluid.37.061903.175710, 2005.
- Heikkilä, U., Beer, J., and Feichter, J.: Meridional transport and deposition of atmospheric ^{10}Be , *Atmos. Chem. Phys.*, 9, 515–527, 2009.
- Heikkilä, U., Beer, J., Abreu, J. A., and Steinhilber, F.: On the atmospheric transport and deposition of the cosmogenic radionuclides (^{10}Be): A review, *Space Science Reviews*, 176, 321–332, doi:10.1007/s11214-011-9838-0, 2011.
- Held, I. M., Winton, M., Takahashi, K., Delworth, T., Zeng, F., and Vallis, G. K.: Probing the fast and slow components of global warming by returning abruptly to preindustrial forcing, *J. Climate*, 23, 2418–2427, doi:10.1175/2009JCLI3466.1, 2010.
- Herschel, W.: Observations tending to investigate the nature of the Sun, in order to find the causes or symptoms of its variable emission of light and heat; with remarks on the Use that may possibly be dawn from Solar Observations, *Philos. Trans. R. Soc. Lond.*, 91, 265–318, 1801.
- Hibler, W. D.: A dynamic thermodynamic sea ice model, *J. Phys. Oceanogr.*, 9, 815–846, 1979.
- Hobbs, P. V.: Introduction to atmospheric chemistry, Cambridge University Press, Cambridge, UK., 2000.
- Holton, J. R., Haynes, P. H., McIntyre, M. E., Douglass, A. R., Rood, R. B., and Pfister, L.: Stratosphere-troposphere exchange, *Rev. Geophys.*, 33, 403–439, 1995.
- Hu, Y. and Tung, K. K.: Possible ozone-induced long-term changes in planetary wave activity in late winter, *J. Climate*, 16, 3027–3038, 2003.
- Hurrell, J. W.: Decadal trends in the North Atlantic Oscillation: Regional temperatures and precipitation, *Science*, 269, 676–679, 1995.
- Iles, C. E., Hegerl, G. C., Schurer, A. P., and Zhang, X.: The effect of volcanic eruptions on global precipitation, *J. Geophys. Res.*, 118, 8770–8786, doi:10.1002/jgrd.50678, 2013.
- Ineson, S., Scaife, A. A., Knight, J. R., Manners, J. C., Dunstone, N. J., Gray, L. J., and Haigh, J. D.: Solar forcing of winter climate variability in the Northern Hemisphere, *Nature Geoscience*, 4, 1–5, doi:10.1038/ngeo1282, 2011.
- IPCC: Summary for policymakers, in: *Climate Change 2013: The Physical Science Basis. Contribution of Working Group I to the Fifth Assessment Report of the Intergovernmental Panel on Climate Change*, edited by Stocker, T., Qin, D., Plattner, G.-K., Tignor, M., Allen, S., Boschung, J., Nauels, A., Xia, Y., Bex, V., and Midgley, P., pp. 3–29, Cambridge University Press, Cambridge, United Kingdom and New York, NY, USA, 2013.
- Jackman, C. H., Marsh, D. R., Vitt, F. M., Garcia, R. R., Fleming, E. L., Labow, G. J., Randall, C. E., López-Puertas, M., Funke, B., von Clarmann, T., and Stiller, G. P.: Short- and medium-term atmospheric constituent effects of very large solar proton events, *Atmos. Chem. Phys.*, 8, 765–785, 2008.
- Jacob, D. J.: Introduction to atmospheric chemistry, Princeton University Press, Princeton, New Jersey, 1999.
- Jones, G. S., Lockwood, M., and Stott, P. A.: What influence will future solar activity changes over the 21st century have on projected global near-surface temperature changes?, *J. Geophys. Res.*, 117, 1–13, doi:10.1029/2011JD017013, 2012.
- Jungclaus, J. H., Keenlyside, N., Botzet, M., Haak, H., Luo, J.-J., Latif, M., Marotzke, J., Mikolajewicz, U., and Roeckner, E.: Ocean circulation and tropical variability in the coupled model ECHAM5/MPI-OM, *J. Climate*, 19, 3952–3972, doi:10.1175/JCLI3827.1, 2006.

- Jungclauss, J. H., Lorenz, S. J., Timmreck, C., Reick, C. H., Brovkin, V., Six, K., Segschneider, J., Giorgetta, M. A., Crowley, T. J., Pongratz, J., Krivova, N. A., Vieira, L. E., Solanki, S. K., Klocke, D., Botzet, M., Esch, M., Gayler, V., Haak, H., Raddatz, T. J., Roeckner, E., Schnur, R., Widmann, H., Claussen, M., Stevens, B., and Marotzke, J.: Climate and carbon-cycle variability over the last millennium, *Climate of the Past*, 6, 723–737, doi:10.5194/cp-6-723-2010, 2010.
- Kang, S. M., Polvani, L. M., Fyfe, J. C., and Sigmond, M.: Impact of polar ozone depletion on subtropical precipitation., *Science*, 332, 951–4, doi:10.1126/science.1202131, 2011.
- Kang, S. M., Polvani, L. M., Fyfe, J. C., Son, S.-W., Sigmond, M., and P. Correa, G. J.: Modeling evidence that ozone depletion has impacted extreme precipitation in the austral summer, *Geophys. Res. Lett.*, 40, 4054–4059, doi:10.1002/grl.50769, 2013.
- Karpechko, A. Y. and Gillett, N. P.: Quantitative assessment of Southern Hemisphere ozone in chemistry-climate model simulations, *Atmos. Chem. Phys.*, 10, 1385–1400, doi:10.5194/acp-10-1385-2010, 2010.
- Knudsen, M. F., Riisager, P., Donadini, F., Snowball, I., Muscheler, R., Korhonen, K., and Pesonen, L. J.: Variations in the geomagnetic dipole moment during the Holocene and the past 50 kyr, *Earth Planet. Sci. Lett.*, 272, 319–329, doi:10.1016/j.epsl.2008.04.048, 2008.
- Kodera, K.: Influence of volcanic eruptions on the troposphere through stratospheric dynamical processes in the Northern Hemisphere winter, *J. Geophys. Res.*, 99, 1273–1282, 1994.
- Kodera, K.: Solar influence on the spatial structure of the NAO during the winter 1900–1999, *Geophys. Res. Lett.*, 30, 1175, doi:10.1029/2002GL016584, 2003.
- Kodera, K. and Kuroda, Y.: Dynamical response to the solar cycle, *J. Geophys. Res.*, 107, 4749, doi:10.1029/2002JD002224, 2002.
- Kopp, G. and Lean, J. L.: A new, lower value of total solar irradiance: Evidence and climate significance, *Geophys. Res. Lett.*, 38, L01 706, doi:10.1029/2010GL045777, 2011.
- Laken, B. A., Pallé, E., Čalogović, J., and Dunne, E. M.: A cosmic ray-climate link and cloud observations, *Journal of Space Weather and Space Climate*, 2, A18, doi:10.1051/swsc/2012018, 2012.
- Lamb, H. H.: Volcanic dust in the atmosphere; with a chronology and assessment of its meteorological significance, *Philosophical Transactions of the Royal Society*, 266, 425–533, doi:10.1098/rsta.1970.0010, 1970.
- Langematz, U., Kunze, M., Krüger, K., Labitzke, K., and Roff, G. L.: Thermal and dynamical changes of the stratosphere since 1979 and their link to ozone and CO₂ changes, *J. Geophys. Res.*, 108, 4027, doi:10.1029/2002JD002069, 2003.
- Le Treut, H., Somerville, R., Cubasch, U., Ding, Y., Mauritzen, C., Mokssit, A., Peterson, T., and Prather, M.: Historical overview of climate change science, in: *Climate Change 2007: The Physical Science Basis. Contribution of Working Group I to the Fourth Assessment Report of the Intergovernmental Panel on Climate Change*, edited by Solomon, S., Qin, D., Manning, M., Chen, Z., Marquis, M., Averyt, K., Tignor, M., and Miller, H., chap. 1, pp. 94–127, Cambridge University Press, Cambridge, United Kingdom and New York, NY, USA, 2007.
- Lean, J.: Evolution of the sun’s spectral irradiance since the Maunder Minimum, *Geophys. Res. Lett.*, 27, 2425–2428, doi:10.1029/2000GL000043, 2000.
- Lehner, F., Raible, C. C., and Stocker, T. F.: Testing the robustness of a precipitation proxy-based North Atlantic Oscillation reconstruction, *Quaternary Science Reviews*, 45, 85–94, doi:10.1016/j.quascirev.2012.04.025, 2012.
- Lehner, F., Born, A., Raible, C. C., and Stocker, T. F.: Amplified inception of European Little Ice Age by sea ice-ocean-atmosphere feedbacks, *J. Climate*, 26, 7586–7602, doi:10.1175/JCLI-D-12-00690.1, 2013.
- Lockwood, M.: Solar change and climate: an update in the light of the current exceptional solar minimum, *Proceedings of the Royal Society A: Mathematical, Physical and Engineering Sciences*, 466, 303–329, doi:10.1098/rspa.2009.0519, 2010.

- Lockwood, M.: Solar influence on global and regional climates, *Surveys in Geophysics*, 33, 503–534, doi:10.1007/s10712-012-9181-3, 2012.
- Lorenz, E. N.: Deterministic nonperiodic flow, *J. Atmos. Sci.*, 20, 130–141, 1963.
- Luterbacher, J., Schmutz, C., Gyalistras, D., Xoplaki, E., and Wanner, H.: Reconstructions of monthly NAO and EU indices back to AD 1675, *Geophys. Res. Lett.*, 26, 2745–2748, doi:10.1029/1999GL900576, 1999.
- Luterbacher, J., Xoplaki, E., Dietrich, D., Rickli, R., Jacobeit, J., Beck, C., Gyalistras, D., Schmutz, C., and Wanner, H.: Reconstruction of sea level pressure fields over the Eastern North Atlantic and Europe back to 1500, *Climate Dyn.*, 18, 545–561, doi:10.1007/s00382-001-0196-6, 2002.
- Luterbacher, J., Dietrich, D., Xoplaki, E., Grosjean, M., and Wanner, H.: European seasonal and annual temperature variability, trends, and extremes since 1500., *Science*, 303, 1499–503, doi:10.1126/science.1093877, 2004.
- Mann, M. E., Zhang, Z., Rutherford, S., Bradley, R. S., Hughes, M. K., Shindell, D. T., Ammann, C. M., Faluvegi, G., and Ni, F.: Global signatures and dynamical origins of the Little Ice Age and Medieval Climate Anomaly., *Science*, 326, 1256–60, doi:10.1126/science.1177303, 2009.
- Manney, G. L., Santee, M. L., Rex, M., Livesey, N. J., Pitts, M. C., Veefkind, P., Nash, E. R., Wohltmann, I., Lehmann, R., Froidevaux, L., Poole, L. R., Schoeberl, M. R., Haffner, D. P., Davies, J., Dorokhov, V., Gernandt, H., Johnson, B., Kivi, R., Kyrö, E., Larsen, N., Levelt, P. F., Makshtas, A., McElroy, C. T., Nakajima, H., Parrondo, M. C., Tarasick, D. W., von der Gathen, P., Walker, K. A., and Zinoviev, N. S.: Unprecedented Arctic ozone loss in 2011., *Nature*, 478, 469–75, doi:10.1038/nature10556, 2011.
- Manzini, E., Giorgetta, M. A., Esch, M., Kornbluh, L., and Roeckner, E.: The influence of sea surface temperatures on the northern winter stratosphere: Ensemble simulations with the MAECHAM5 model, *J. Climate*, 19, 3863–3881, doi:10.1175/JCLI3826.1, 2006.
- Marsland, S.: The Max-Planck-Institute global ocean/sea ice model with orthogonal curvilinear coordinates, *Ocean Modelling*, 5, 91–127, doi:10.1016/S1463-5003(02)00015-X, 2003.
- Matuschek, O.: Data-Mining in den Reisetagebüchern James Silk Buckingham 1815/1816. Neu entwickelte Suchalgorithmen und effiziente Arbeitsmethoden in der Historischen Klimatologie, Ph.D. thesis, Albert-Ludwigs-Universität Freiburg, Germany, submitted, 2014.
- Mauritsen, T., Stevens, B., Roeckner, E., Crueger, T., Esch, M., Giorgetta, M., Haak, H., Jungclaus, J., Klocke, D., Matei, D., Mikolajewicz, U., Notz, D., Pincus, R., Schmidt, H., and Tomassini, L.: Tuning the climate of a global model, *Journal of Advances in Modeling Earth Systems*, 4, M00A01, doi:10.1029/2012MS000154, 2012.
- McGuffie, K. and Henderson-Sellers, A.: *A climate modelling primer*, Wiley, 2005.
- McLandress, C., Shepherd, T. G., Scinocca, J. F., Plummer, A. A., Sigmond, M., Jonsson, A. I., and Reader, M. C.: Separating the dynamical effects of climate change and ozone depletion. part II: southern hemisphere troposphere, *J. Climate*, 24, 1850–1868, doi:10.1175/2010JCLI3958.1, 2011.
- Meehl, G. A., Washington, W. M., Wigley, T. M. L., Arblaster, J. M., and Dai, A.: Solar and greenhouse gas forcing and climate response in the twentieth century, *J. Climate*, 16, 426–444, doi:10.1175/1520-0442(2003)016<0426:SAGGFA>2.0.CO;2, 2003.
- Meehl, G. A., Arblaster, J. M., Branstator, G., and van Loon, H.: A coupled air-sea response mechanism to solar forcing in the pacific region, *J. Climate*, 21, 2883–2897, doi:10.1175/2007JCLI1776.1, 2008.
- Meehl, G. A., Arblaster, J. M., Matthes, K., Sassi, F., and van Loon, H.: Amplifying the pacific climate system response to a small 11-year solar cycle forcing., *Science*, 325, 1114–1118, doi:10.1126/science.1172872, 2009.

- Meehl, G. A., Arblaster, J. M., and Marsh, D. R.: Could a future “Grand Solar Minimum” like the Maunder Minimum stop global warming?, *Geophys. Res. Lett.*, 40, 1789–1793, doi:10.1002/grl.50361, 2013.
- Mignot, J., Khodri, M., Frankignoul, C., and Servonnat, J.: Volcanic impact on the Atlantic Ocean over the last millennium, *Climate of the Past*, 7, 1439–1455, doi:10.5194/cp-7-1439-2011, 2011.
- Miller, G. H., Southon, J. R., Anderson, C., Björnsson, H., Thordarson, T., Geirsdottir, A., Zhong, Y., Larsen, D. J., Otto-Bliesner, B. L., Holland, M. M., Bailey, D. A., Rensnider, K. A., and Lehman, S. J.: Abrupt onset of the Little Ice Age triggered by volcanism and sustained by sea-ice/ocean feedbacks, *Geophys. Res. Lett.*, 39, 1–5, doi:10.1029/2011GL050168, 2012.
- Misios, S. and Schmidt, H.: The role of the oceans in shaping the tropospheric response to the 11 year solar cycle, *Geophys. Res. Lett.*, 40, 6373–6377, doi:10.1002/2013GL058439, 2013.
- Mlawer, E. J., Taubman, S. J., Brown, P. D., Iacono, M. J., and Clough, S. A.: Radiative transfer for inhomogeneous atmospheres: RRTM, validated correlated-k model for the longwave, *J. Geophys. Res.*, 102, 663–16 682, 1997.
- Molina, M. J. and Rowland, F. S.: Predicted present stratospheric abundances of chlorine species from photodissociation of carbon tetrachloride, *Geophys. Res. Lett.*, 1, 309–312, 1974.
- Muscheler, R., Joos, F., Beer, J., Müller, S. A., Vonmoos, M., and Snowball, I.: Solar activity during the last 1000yr inferred from radionuclide records, *Quaternary Science Reviews*, 26, 82–97, doi:10.1016/j.quascirev.2006.07.012, 2007.
- Muthers, S., Anet, J. G., Raible, C. C., Brönnimann, S., Rozanov, E., Arfeuille, F., Peter, T., Shapiro, A. I., Beer, J., Steinhilber, F., Brugnara, Y., and Schmutz, W.: Northern hemispheric winter warming pattern after tropical volcanic eruptions: Sensitivity to the ozone climatology, *J. Geophys. Res.*, 110, 1340–1355, doi:10.1002/2013JD020138, 2014a.
- Muthers, S., Anet, J. G., Stenke, A., Raible, C. C., Brönnimann, S., Rozanov, E., Peter, T., Arfeuille, F., Shapiro, A. I., Beer, J., Steinhilber, F., Brugnara, Y., and Schmutz, W.: The coupled atmosphere-chemistry-ocean model SOCOL-MPIOM, *Geoscientific Model Development Discussions*, 7, 3013–3084, doi:10.5194/gmdd-7-3013-2014, 2014b.
- Muthers, S., Arfeuille, F., and Raible, C. C.: Dynamical and chemical ozone perturbations after large volcanic eruptions: Role of the climate state and the strength of the eruption, *J. Geophys. Res.*, submitted, 2014c.
- Myhre, G., Shindell, D., Bréon, F.-M., Collins, W., Fuglestedt, J., Huang, J., Koch, D., Lamarque, J.-F., Lee, D., Mendoza, B., Nakajima, T., Robock, A., Stephens, G., Takemura, T., and Zhang, H.: Anthropogenic and Natural Radiative Forcing, in: *Climate Change 2013: The Physical Science Basis. Contribution of Working Group I to the Fifth Assessment Report of the Intergovernmental Panel on Climate Change*, edited by Stocker, T. F., Qin, D., Plattner, G.-K., Tignor, M., Allen, S., Boschung, J., Nauels, A., Xia, Y., Bex, V., and Midgley, P., chap. 8, pp. 659–740, Cambridge University Press, Cambridge, United Kingdom and New York, NY, USA, 2013.
- Otterå, O. H., Bentsen, M., Drange, H., and Suo, L.: External forcing as a metronome for Atlantic multidecadal variability, *Nature Geoscience*, 3, 688–694, doi:10.1038/ngeo955, 2010.
- PAGES 2k Network: Continental-scale temperature variability during the past two millennia, *Nature Geoscience*, 6, 339–346, doi:10.1038/NNGEO1797, 2013.
- Petoukhov, V., Ganopolski, A., Brovkin, V., Claussen, M., Eliseev, A., Kubatzki, C., and Rahmstorf, S.: CLIMBER-2: a climate system model of intermediate complexity. Part I: model description and performance for present climate, *Climate Dyn.*, 16, 1–17, doi:10.1007/PL00007919, 2000.
- Pfister, C., Luterbacher, J., Wanner, H., Wheeler, D., Brázdil, R., Ge, Q., Hao, Z., Moberg, A., Grab, S., and del Prieto, M.: Documentary evidence as climate proxies, White paper from the pages/clivar proxy uncertainty workshop in trieste, PAGES, 2009.

- Phipps, S. J., Rotstayn, L. D., Gordon, H. B., Roberts, J. L., Hirst, A. C., and Budd, W. F.: The CSIRO Mk3L climate system model version 1.0 – Part 2: Response to external forcings, *Geoscientific Model Development*, 5, 649–682, doi:10.5194/gmd-5-649-2012, 2012.
- Pinto, J. G. and Raible, C. C.: Past and recent changes in the North Atlantic oscillation, *Wiley Interdisciplinary Reviews: Climate Change*, 3, 79–90, doi:10.1002/wcc.150, 2012.
- Purich, A. and Son, S.-W.: Impact of Antarctic ozone depletion and recovery on southern hemisphere precipitation, evaporation, and extreme changes, *J. Climate*, 25, 3145–3154, doi:10.1175/JCLI-D-11-00383.1, 2012.
- Raible, C. C., Casty, C., Luterbacher, J., Pauling, A., Esper, J., Frank, D. C., Büntgen, U., Roesch, A. C., Tschuck, P., Wild, M., Vidale, P.-L., Schär, C., and Wanner, H.: Climate variability-observations, reconstructions, and model simulations for the Atlantic-European and Alpine region from 1500-2100 AD, *Climatic Change*, 79, 9–29, doi:10.1007/s10584-006-9061-2, 2006.
- Raible, C. C., Lehner, F., González-Rouco, J. F., and Fernández-Donado, L.: Changing correlation structures of the Northern Hemisphere atmospheric circulation from 1000 to 2100 AD, *Climate of the Past*, 10, 537–550, doi:10.5194/cp-10-537-2014, 2014.
- Randall, D. A., Wood, R. A., Bony, S., Colman, R., Fichefet, T., Fyfe, J., Kattsov, V., Pitman, A., Shukla, J., Srinivasan, J., Stouffer, R. J., Sumi, A., and Taylor, K. E.: Climate models and their evaluation, in: *Climate Change 2007: The Physical Science Basis. Contribution of Working Group I to the Fourth Assessment Report of the Intergovernmental Panel on Climate Change*, edited by Solomon, S., Qin, D., Manning, M., Chen, Z., Marquis, M., Averyt, K., M.Tignor, and Miller, H., *Climate Change 2007: The Physical Science Basis. Contribution of Working Group I to the Fourth Assessment Report of the Intergovernmental Panel on Climate Change*, chap. 8, Cambridge University Press, Cambridge, United Kingdom and New York, NY, USA, 2007.
- Randel, W. J. and Wu, F.: Cooling of the Arctic and Antarctic Polar Stratospheres due to Ozone Depletion, *J. Climate*, 12, 1467–1479, doi:10.1175/1520-0442(1999)012<1467:COTAAA>2.0.CO;2, 1999.
- Rial, J. A., Pielke, R. A., Beniston, M., Claussen, M., Canadell, J., Cox, P., Held, H., de Noblet-Ducoudré, N., Prinn, R., Reynolds, J. F., and Salas, J. D.: Nonlinearities, feedbacks and critical thresholds within the Earth’s climate system, *Climatic Change*, 65, 11–38, doi:10.1023/B:CLIM.0000037493.89489.3f, 2004.
- Rind, D.: Complexity and climate, *Science*, 284, 105–7, 1999.
- Rind, D., Shindell, D. T., Perlwitz, J., and Lerner, J.: The relative importance of solar and anthropogenic forcing of climate change between the Maunder Minimum and the present, *J. Climate*, 17, 906–929, 2004.
- Rind, D., Lean, J., Lerner, J., Lonergan, P., and Leboissitier, A.: Exploring the stratospheric/tropospheric response to solar forcing, *J. Geophys. Res.*, 113, D24 103, doi:10.1029/2008JD010114, 2008.
- Ritz, S. P., Stocker, T. F., and Joos, F.: A coupled dynamical ocean–energy balance atmosphere model for paleoclimate studies, *J. Climate*, 24, 349–375, doi:10.1175/2010JCLI3351.1, 2011.
- Robock, A.: Volcanic eruptions and climate, *Rev. Geophys.*, 38, 191–219, 2000.
- Robock, A. and Mao, J.: Winter warming from large volcanic eruptions, *Geophys. Res. Lett.*, 12, 2405–2408, 1992.
- Rodrigo, F. S., Pozo-Vázquez, D., Esteban-Parra, M. J., and Castro-Díez, Y.: A reconstruction of the winter North Atlantic Oscillation index back to A.D. 1501 using documentary data in southern Spain, *J. Geophys. Res.*, 106, 805–818, 2001.
- Roeckner, E., Bäuml, G., Bonaventura, L., Brokopf, R., Esch, M., Giorgetta, M., Hagemann, S., Kirchner, I., Kornblueh, L., Manzini, E., Rhodin, A., Schlese, U., Schulzweida, U., and Tompkins, A.: The atmospheric general circulation model ECHAM5 - Model description, MPI report 349, Max-Planck Institute for Meteorology, Hamburg, Germany, 2003.

- Rohde, R., Muller, R. A., Jacobsen, R., Muller, E., Perlmutter, S., Rosenfeld, A., Wurtele, J., Groom, D., and Wickham, C.: A new estimate of the average earth surface land temperature spanning 1753 to 2011, *Geoinformatics & Geostatistics: An Overview*, 1, 1–7, doi:10.4172/2327-4581.1000101, 2012.
- Roth, R. and Joos, F.: A reconstruction of radiocarbon production and total solar irradiance from the Holocene ^{14}C and CO_2 records: implications of data and model uncertainties, *Climate of the Past*, 9, 1879–1909, doi:10.5194/cp-9-1879-2013, 2013.
- Rottman, G.: Measurement of total and spectral solar irradiance, *Space Science Reviews*, 125, 39–51, doi:10.1007/s11214-006-9045-6, 2006.
- Roy, I.: The role of the Sun in atmosphere-ocean coupling, *International Journal of Climatology*, 34, 655–677, doi:10.1002/joc.3713, 2013.
- Rozanov, E., Schlesinger, M. E., Zubov, V., Yang, F., and Andronova, N. G.: The UIUC three-dimensional stratospheric chemical transport model: Description and evaluation of the simulated source gases and ozone, *J. Geophys. Res.*, 104, 11,755–11,781, doi:10.1029/1999JD900138, 1999.
- Rozanov, E., Schlesinger, M. E., and Zubov, V.: The University of Illinois, Urbana-Champaign three-dimensional stratosphere-troposphere general circulation model with interactive ozone photochemistry: Fifteen-year control run climatology, *J. Geophys. Res.*, 106, 27,233–27,254, doi:10.1029/2000JD000058, 2001.
- Rozanov, E., Calisto, M., Egorova, T., Peter, T., and Schmutz, W.: Influence of the precipitating energetic particles on atmospheric chemistry and climate, *Surveys in Geophysics*, 33, 483–501, doi:10.1007/s10712-012-9192-0, 2012.
- Russell, C. T., Luhmann, J. G., and Jian, L. K.: How unprecedented a solar minimum?, *Rev. Geophys.*, 48, 1–16, doi:10.1029/2009RG000316, 2010.
- Sato, M., Hansen, J. E., McCormick, M. P., and Pollack, J. B.: Stratospheric aerosol optical depths, 1850–1990, *J. Geophys. Res.*, 98, 22,987–22,994, 1993.
- Schmidt, G. A., Jungclaus, J. H., Ammann, C. M., Bard, E., Braconnot, P., Crowley, T. J., Delaygue, G., Joos, F., Krivova, N. A., Muscheler, R., Otto-Bliesner, B. L., Pongratz, J., Shindell, D. T., Solanki, S. K., Steinhilber, F., and Vieira, L. E. A.: Climate forcing reconstructions for use in PMIP simulations of the last millennium (v1.0), *Geoscientific Model Development*, 4, 33–45, doi:10.5194/gmd-5-185-2012, 2011.
- Schmidt, G. A., Jungclaus, J. H., Ammann, C. M., Bard, E., Braconnot, P., Crowley, T. J., Delaygue, G., Joos, F., Krivova, N. A., Muscheler, R., Otto-Bliesner, B. L., Pongratz, J., Shindell, D. T., Solanki, S. K., Steinhilber, F., and Vieira, L. E. A.: Climate forcing reconstructions for use in PMIP simulations of the Last Millennium (v1.1), *Geoscientific Model Development*, 5, 185–191, doi:10.5194/gmd-5-185-2012, 2012.
- Schmutz, C., Luterbacher, J., Gyalistras, D., Xoplaki, E., and Wanner, H.: Can we trust proxy-based NAO index reconstructions?, *Geophys. Res. Lett.*, 27, 1135–1138, 2000.
- Schraner, M., Rozanov, E., Schnadt Poberaj, C., Kenzelmann, P., Fischer, A. M., Zubov, V., Luo, B. P., Hoyle, C. R., Egorova, T., Fueglistaler, S., Brönnimann, S., Schmutz, W., and Peter, T.: Technical Note: Chemistry-climate model SOCOL: version 2.0 with improved transport and chemistry/microphysics schemes, *Atmos. Chem. Phys.*, 8, 5957–5974, doi:10.5194/acp-8-5957-2008, 2008.
- Schrijver, C. J., Livingston, W. C., Woods, T. N., and Mewaldt, R. A.: The minimal solar activity in 2008–2009 and its implications for long-term climate modeling, *Geophys. Res. Lett.*, 38, L06 701, doi:10.1029/2011GL046658, 2011.
- Shapiro, A. I., Schmutz, W., Rozanov, E., Schoell, M., Haberreiter, M., Shapiro, A. V., and Nyeki, S.: A new approach to the long-term reconstruction of the solar irradiance leads to large historical solar forcing, *Astronomy & Astrophysics*, 529, A67, doi:10.1051/0004-6361/201016173, 2011.

- Shepherd, T. G.: Issues in Stratosphere-troposphere Coupling., *J. Meteor. Soc. Japan*, 80, 769–792, doi:10.2151/jmsj.80.769, 2002.
- Shindell, D., Rind, D., Balachandran, N., Lean, J., and Lonergan, P.: Solar cycle variability, ozone, and climate, *Science*, 284, 305–8, 1999.
- Shindell, D., Faluvegi, G., Lacis, A., Hansen, J. and Ruedy, R., and Aguilar, E.: Role of tropospheric ozone increases in 20th-century climate change, *J. Geophys. Res.*, 111, D08302, doi:10.1029/2005JD006348, 2006.
- Shindell, D. T., Schmidt, G. A., Mann, M. E., Rind, D., and Waple, A. M.: Solar forcing of regional climate change during the Maunder Minimum., *Science*, 294, 2149–52, doi:10.1126/science.1064363, 2001.
- Shindell, D. T., Schmidt, G. A., Miller, R. L., and Mann, M. E.: Volcanic and solar forcing of climate change during the preindustrial era, *J. Climate*, 16, 4094–4107, doi:10.1175/1520-0442(2003)016<4094:VASFOC>2.0.CO;2, 2003.
- Shindell, D. T., Schmidt, G. A., Mann, M. E., and Faluvegi, G.: Dynamic winter climate response to large tropical volcanic eruptions since 1600, *J. Geophys. Res.*, 109, D05104, doi:10.1029/2003JD004151, 2004.
- Shine, K. P., Bourqui, M. S., Forster, P. M. D. F., Hare, S. H. E., Langematz, U., Braesicke, P., Grewe, V., Ponater, M., Schnadt, C., Smith, C. A., Haigh, J. D., Austin, J., Butchart, N., Shindell, D. T., Randel, W. J., Nagashima, T., Portmann, R. W., Solomon, S., Seidel, D. J., Lanzante, J., Klein, S., Ramaswamy, V., and Schwarzkopf, M. D.: A comparison of model-simulated trends in stratospheric temperatures, *Q. J. R. Meteorol. Soc.*, 129, 1565–1588, doi:10.1256/qj.02.186, 2003.
- Sigl, M., McConnell, J. R., Layman, L., Maselli, O., McGwire, K., Pasteris, D., Dahl-Jensen, D., Steffensen, J. P., Vinther, B., Edwards, R., Mulvaney, R., and Kipfstuhl, S.: A new bipolar ice core record of volcanism from WAIS Divide and NEEM and implications for climate forcing of the last 2000 years, *Journal of Geophysical Research: Atmospheres*, 118, 1151–1169, doi:10.1029/2012JD018603, 2013.
- Simmons, A. and Burridge, D.: An energy and angular-momentum conserving vertical finite-difference scheme and hybrid vertical coordinates, *Mon. Wea. Rev.*, 109, 758–766, 1981.
- Simmons, A. J., Burridge, D. M., Jarraud, M., Girard, C., and Wergen, W.: The ECMWF medium-range prediction models development of the numerical formulations and the impact of increased resolution, *Meteorol. Atmos. Phys.*, 40, 28–60, 1989.
- Solanki, S. K., Krivova, N. A., and Haigh, J. D.: Solar irradiance variability and climate, *Annual Review of Astronomy and Astrophysics*, 51, 311–351, doi:10.1146/annurev-astro-082812-141007, 2013.
- Solomon, S.: Stratospheric ozone depletion: A review of concepts and history, *Rev. Geophys.*, 37, 275, doi:10.1029/1999RG900008, 1999.
- Solomon, S., Crutzen, P. J., and Roble, R. G.: Photochemical coupling between the thermosphere and the lower atmosphere: 1. Odd nitrogen from 50 to 120 km, *J. Geophys. Res.*, 87, 7206, doi:10.1029/JC087iC09p07206, 1982.
- Son, S.-W., Gerber, E. P., Perlwitz, J., Polvani, L. M., Gillett, N. P., Seo, K.-H., Eyring, V., Shepherd, T. G., Waugh, D., Akiyoshi, H., Austin, J., Baumgaertner, A., Bekki, S., Braesicke, P., Brühl, C., Butchart, N., Chipperfield, M. P., Cugnet, D., Dameris, M., Dhomse, S., Frith, S., Garny, H., Garcia, R., Hardiman, S. C., Jöckel, P., Lamarque, J. F., Mancini, E., Marchand, M., Michou, M., Nakamura, T., Morgenstern, O., Pitari, G., Plummer, D. A., Pyle, J., Rozanov, E., Scinocca, J. F., Shibata, K., Smale, D., Teyssède, H., Tian, W., and Yamashita, Y.: Impact of stratospheric ozone on Southern Hemisphere circulation change: A multimodel assessment, *J. Geophys. Res.*, 115, D00M07, doi:10.1029/2010JD014271, 2010.
- Song, Y. and Robinson, W. A.: Dynamical mechanisms for stratospheric influences on the troposphere, *J. Atmos. Sci.*, 61, 1711–1725, doi:10.1175/1520-0469(2004)061<1711:DMFSIO>2.0.CO;2, 2004.

- Soukharev, B. E. and Hood, L. L.: Solar cycle variation of stratospheric ozone: Multiple regression analysis of long-term satellite data sets and comparisons with models, *J. Geophys. Res.*, 111, D20 314, doi:10.1029/2006JD007107, 2006.
- Spanghel, T., Cubasch, U., Raible, C. C., Schimanke, S., Körper, J., and Hofer, D.: Transient climate simulations from the Maunder Minimum to present day: Role of the stratosphere, *J. Geophys. Res.*, 115, 1–18, doi:10.1029/2009JD012358, 2010.
- SPARC: Assessment of stratospheric aerosol properties (ASAP), SPARC Report No. 4 1295, World Climate Research Programme WCRP-124,WMO/TD, edited by: Thomason, L. and Peter, T., 2006.
- Stachelin, J., Harris, N. R. P., Appenzeller, C., and Eberhard, J.: Ozone trends: A review, *Rev. Geophys.*, 39, 231, doi:10.1029/1999RG000059, 2001.
- Steinhilber, F. and Beer, J.: Prediction of solar activity for the next 500 years, *Journal of Geophysical Research: Space Physics*, 118, 1861–1867, doi:10.1002/jgra.50210, 2013.
- Steinhilber, F., Abreu, J. A., and Beer, J.: Solar modulation during the Holocene, *Astrophysics and Space Sciences Transactions*, 4, 1–6, doi:10.5194/astra-4-1-2008, 2008.
- Steinhilber, F., Beer, J., and Fröhlich, C.: Total solar irradiance during the Holocene, *Geophys. Res. Lett.*, 36, 1–5, doi:10.1029/2009GL040142, 2009.
- Steinhilber, F., Abreu, J. A., Beer, J., Brunner, I., Christl, M., Fischer, H., Heikkilä, U., Kubik, P. W., Mann, M., McCracken, K. G., Miller, H., Miyahara, H., Oerter, H., and Wilhelms, F.: 9,400 years of cosmic radiation and solar activity from ice cores and tree rings., *Proc. Natl. Acad. Sci. U. S. A.*, 109, 5967–71, doi:10.1073/pnas.1118965109, 2012.
- Stenchikov, G., Robock, A., Ramaswamy, V., Schwarzkopf, M. D., Hamilton, K., and Ramachandran, S.: Arctic Oscillation response to the 1991 Mount Pinatubo eruption: Effects of volcanic aerosols and ozone depletion, *J. Geophys. Res.*, 107, 1–16, doi:10.1029/2002JD002090, 2002.
- Stenchikov, G., Delworth, T. L., Ramaswamy, V., Stouffer, R. J., Wittenberg, A., and Zeng, F.: Volcanic signals in oceans, *J. Geophys. Res.*, 114, 1–13, doi:10.1029/2008JD011673, 2009.
- Stenke, A., Schraner, M., Rozanov, E., Egorova, T., Luo, B., and Peter, T.: The SOCOL version 3.0 chemistry–climate model: description, evaluation, and implications from an advanced transport algorithm, *Geoscientific Model Development*, 6, 1407–1427, doi:10.5194/gmd-6-1407-2013, 2013.
- Stevenson, D. S., Young, P. J., Naik, V., Lamarque, J.-F., Shindell, D. T., Voulgarakis, A., Skeie, R. B., Dalsoren, S. B., Myhre, G., Berntsen, T. K., Folberth, G. A., Rumbold, S. T., Collins, W. J., MacKenzie, I. A., Doherty, R. M., Zeng, G., van Noije, T. P. C., Strunk, A., Bergmann, D., Cameron-Smith, P., Plummer, D. A., Strode, S. A., Horowitz, L., Lee, Y. H., Szopa, S., Sudo, K., Nagashima, T., Josse, B., Cionni, I., Righi, M., Eyring, V., Conley, A., Bowman, K. W., Wild, O., and Archibald, A.: Tropospheric ozone changes, radiative forcing and attribution to emissions in the Atmospheric Chemistry and Climate Model Intercomparison Project (ACCMIP), *Atmos. Chem. Phys.*, 13, 3063–3085, doi:10.5194/acp-13-3063-2013, 2013.
- Stocker, T. F.: Introduction to climate modelling, Springer, 2011.
- Strahan, S. E., Douglass, A. R., and Newman, P. A.: The contributions of chemistry and transport to low arctic ozone in March 2011 derived from Aura MLS observations, *J. Geophys. Res.*, 118, 1563–1576, doi:10.1002/jgrd.50181, 2013.
- Svensmark, H., Bondo, T., and Svensmark, J.: Cosmic ray decreases affect atmospheric aerosols and clouds, *Geophys. Res. Lett.*, 36, L15 101, doi:10.1029/2009GL038429, 2009.
- Swingedouw, D., Terray, L., Cassou, C., Voldoire, A., Salas-Mélia, D., and Servonnat, J.: Natural forcing of climate during the last millennium: fingerprint of solar variability, *Climate Dyn.*, 36, 1349–1364, doi:10.1007/s00382-010-0803-5, 2011.
- Thompson, D. W. and Wallace, J. M.: Regional climate impacts of the Northern Hemisphere annular mode., *Science*, 293, 85–9, doi:10.1126/science.1058958, 2001.

- Thompson, D. W. J. and Solomon, S.: Interpretation of recent Southern Hemisphere climate change., *Science*, 296, 895–9, doi:10.1126/science.1069270, 2002.
- Thompson, D. W. J. and Wallace, J. M.: The Arctic Oscillation signature in the wintertime geopotential height and temperature fields, *Geophys. Res. Lett.*, 25, 1297–1300, 1998.
- Thompson, D. W. J., Baldwin, M. P., and Solomon, S.: Stratosphere - Troposphere Coupling in the Southern Hemisphere, *Journal of Atmospheric Sciences*, 62, 708–715, 2005.
- Thompson, D. W. J., Solomon, S., Kushner, P. J., England, M. H., Grise, K. M., and Karoly, D. J.: Signatures of the Antarctic ozone hole in Southern Hemisphere surface climate change, *Nature Geoscience*, 4, 741–749, doi:10.1038/ngeo1296, 2011.
- Thompson, D. W. J., Seidel, D. J., Randel, W. J., Zou, C.-Z., Butler, A. H., Mears, C., Osso, A., Long, C., and Lin, R.: The mystery of recent stratospheric temperature trends., *Nature*, 491, 692–7, doi:10.1038/nature11579, 2012.
- Tie, X. and Brasseur, G.: The response of stratospheric ozone to volcanic eruptions: Sensitivity to atmospheric chlorine loading, *Geophys. Res. Lett.*, 22, 3035–3038, 1995.
- Timmreck, C.: Modeling the climatic effects of large explosive volcanic eruptions, *Wiley Interdisciplinary Reviews: Climate Change*, 3, 545–564, doi:10.1002/wcc.192, 2012.
- Timmreck, C., Lorenz, S. J., Crowley, T. J., Kinne, S., Raddatz, T. J., Thomas, M. A., and Jungclaus, J. H.: Limited temperature response to the very large AD 1258 volcanic eruption, *Geophys. Res. Lett.*, 36, 5–9, doi:10.1029/2009GL040083, 2009.
- Timmreck, C., Graf, H.-F., Lorenz, S. J., Niemeier, U., Zanchettin, D., Matei, D., Jungclaus, J. H., and Crowley, T. J.: Aerosol size confines climate response to volcanic super-eruptions, *Geophys. Res. Lett.*, 37, 1–5, doi:10.1029/2010GL045464, 2010.
- Trenberth, K. E. and Dai, A.: Effects of Mount Pinatubo volcanic eruption on the hydrological cycle as an analog of geoengineering, *Geophys. Res. Lett.*, 34, L15702, doi:10.1029/2007GL030524, 2007.
- Trouet, V., Esper, J., Graham, N. E., Baker, A., Scourse, J. D., and Frank, D. C.: Persistent positive north Atlantic medieval climate anomaly, *Science*, 324, 78–80, 2009.
- Valcke, S.: The OASIS3 coupler: A European climate modelling community software, *Geoscientific Model Development*, 6, 373–388, doi:10.5194/gmd-6-373-2013, 2013.
- Varma, V., Prange, M., Spanghel, T., Lamy, F., Cubasch, U., and Schulz, M.: Impact of solar-induced stratospheric ozone decline on Southern Hemisphere westerlies during the Late Maunder Minimum, *Geophys. Res. Lett.*, 39, L20704, doi:10.1029/2012GL053403, 2012.
- von Hobe, M., Ulanovsky, A., Volk, C. M., Groß, J., Tilmes, S., Konopka, P., Günther, G., Werner, A., Spelten, N., Shur, G., Yushkov, V., Ravagnani, F., Schiller, C., Müller, R., and Stroh, F.: Severe ozone depletion in the cold Arctic winter 2004–05, *Geophys. Res. Lett.*, 33, L17815, doi:10.1029/2006GL026945, 2006.
- Vose, R. S., Arndt, D., Banzon, V. F., Easterling, D. R., Gleason, B., Huang, B., Kearns, E., Lawrimore, J. H., Menne, M. J., Peterson, T. C., Reynolds, R. W., Smith, T. M., Williams, C. N., and Wuertz, D. B.: NOAA’s merged land–ocean surface temperature analysis, *Bull. Amer. Meteor. Soc.*, 93, 1677–1685, doi:10.1175/BAMS-D-11-00241.1, 2012.
- Wanner, H., Brönnimann, S., Casty, C., Gyalistras, D., Luterbacher, J., Schmutz, C. and Stephenson, D. B., and Xoplaki, E.: North Atlantic Oscillation - concepts and studies, *Surveys in Geophysics*, 22, 321–381, doi:10.1023/A:1014217317898, 2001.
- Wanner, H., Beer, J., Bütikofer, J., Crowley, T. J., Cubasch, U., Flückiger, J., Goosse, H., Grosjean, M., Joos, F., Kaplan, J. O., Küttel, M., Müller, S. A., Prentice, I. C., Solomina, O., Stocker, T. F., Tarasov, P., Wagner, M., and Widmann, M.: Mid- to Late Holocene climate change: an overview, *Quaternary Science Reviews*, 27, 1791–1828, doi:10.1016/j.quascirev.2008.06.013, 2008.
- Waple, A. M., Mann, M. E., and Bradley, R. S.: Long-term patterns of solar irradiance forcing in model experiments and proxy based surface temperature reconstructions, *Climate Dyn.*, 18, 563–578, doi:10.1007/s00382-001-0199-3, 2002.

- Webb, M. J., Lambert, F. H., and Gregory, J. M.: Origins of differences in climate sensitivity, forcing and feedback in climate models, *Climate Dyn.*, 40, 677–707, doi:10.1007/s00382-012-1336-x, 2013.
- Wegmann, M., Brönnimann, S., Bhend, J., Franke, J., Folini, D., Wild, M., and Luterbacher, J.: Volcanic influence on European summer precipitation through monsoons: Possible cause for “Years Without a Summer”, *J. Climate*, doi:10.1175/JCLI-D-13-00524.1, in press., 2014.
- WMO: Scientific assessment of ozone depletion 2002, Global ozone research and monitoring project - report 47, World Meteorological Organization, Genf, 2002.
- Wofsy, S. C., McElroy, M. B., and Yung, Y. L.: The chemistry of atmospheric bromine, *Geophys. Res. Lett.*, 2, 215–218, 1975.
- Wolf, R.: Abstract of his latest results, *Mon. Not. R. Astron. Soc.*, 21, 77, 1861.
- Yoshimori, M., Stocker, T. F., Raible, C. C., and Renold, M.: Externally forced and internal variability in ensemble climate simulations of the Maunder Minimum, *J. Climate*, 18, 4253–4270, 2005.
- Yung, Y. L., Pinto, J. P., Watson, R. T., and Sander, S. P.: Atmospheric bromine and ozone perturbations in the lower stratosphere, *J. Atmos. Sci.*, 37, 339–353, 1980.
- Zanchettin, D., Timmreck, C., Bothe, O., Lorenz, S. J., Hegerl, G., Graf, H.-F., Luterbacher, J., and Jungclauss, J. H.: Delayed winter warming: a robust decadal response to strong tropical volcanic eruptions?, *Geophys. Res. Lett.*, 40, 204–209, doi:10.1029/2012GL054403, 2012.
- Zhang, R., Delworth, T. L., Sutton, R., Hodson, D. L. R., Dixon, K. W., Held, I. M., Kushnir, Y., Marshall, J., Ming, Y., Msadek, R., Robson, J., Rosati, A. J., Ting, M., and Vecchi, G. A.: Have aerosols caused the observed atlantic multidecadal variability?, *J. Atmos. Sci.*, 70, 1135–1144, doi:10.1175/JAS-D-12-0331.1, 2013.
- Zhong, Y., Miller, G. H., Otto-Bliesner, B. L., Holland, M. M., Bailey, D. A., Schneider, D. P., and Geirsdottir, A.: Centennial-scale climate change from decadal-paced explosive volcanism: a coupled sea ice-ocean mechanism, *Climate Dyn.*, 37, 2373–2387, doi:10.1007/s00382-010-0967-z, 2010.
- Zhou, J. and Tung, K.-K.: Observed tropospheric temperature response to 11-yr solar cycle and what it reveals about mechanisms, *J. Atmos. Sci.*, 70, 9–14, doi:10.1175/JAS-D-12-0214.1, 2013.
- Zorita, E., von Storch, H., Gonzalez-Rouco, F. J., Cubasch, U., Luterbacher, J., Legutke, S., Fischer-Bruns, I., and Schlese, U.: Climate evolution in the last five centuries simulated by an atmosphere-ocean model: global temperatures, the North Atlantic Oscillation and the Late Maunder Minimum, *Meteor. Z.*, 13, 271–289, doi:10.1127/0941-2948/2004/0013-0271, 2004.

Chapter 2.

The coupled atmosphere-chemistry-ocean model SOCOL–MPIOM

Stefan Muthers, Julien G. Anet, Andrea Stenke, Christoph C. Raible, Eugene Rozanov, Stefan Brönnimann, Thomas Peter, Florian Arfeuille, Alexander I. Shapiro, Jürg Beer, Friedhelm Steinhilber, Yuri Brugnara, and Werner Schmutz.

Published in *Geoscientific Model Development Discussions*, vol. 7, pp. 3013–3084, 2014.

Abstract: The newly developed atmosphere-ocean-chemistry-climate model Socol-MPIOM is presented by demonstrating the influence of the interactive chemistry module on the climate state and the variability. Therefore, we compare pre-industrial control simulations with (CHEM) and without (NOCHEM) interactive chemistry. In general, the influence of the chemistry on the mean state and the variability is small and mainly restricted to the stratosphere and mesosphere. The largest differences are found for the atmospheric dynamics in the polar regions, with slightly stronger northern and southern winter polar vortices in CHEM. The strengthening of the vortex is related to larger stratospheric temperature gradients, which are attributed to a parametrization of the absorption of ozone and oxygen in the Lyman-alpha, Schumann-Runge, Hartley, and Higgins bands. This effect is parametrized in the version with interactive chemistry only. A second reason for the temperature differences between CHEM and NOCHEM is related to diurnal variations in the ozone concentrations in the higher atmosphere, which are missing in NOCHEM. Furthermore, stratospheric water vapour concentrations differ substantially between the two experiments, but their effect on the temperatures is small. In both setups, the simulated intensity and variability of the northern polar vortex is inside the range of present day observations. Sudden stratospheric warming events are well reproduced in terms of their frequency, but the distribution amongst the winter months is too uniform.

Additionally, the performance of Socol-MPIOM under changing external forcings is assessed for the period 1600-2000 using an ensemble of simulations driven by a spectral solar forcing reconstruction. The amplitude of the reconstruction is large in comparison to other state-of-the-art reconstructions, providing an upper limit for the importance of the solar signal. In the pre-industrial period (1600-1850) the simulated surface temperature

trends are in reasonable agreement with temperature reconstructions, although the multi-decadal variability is more pronounced. This enhanced variability can be attributed to the variability in the solar forcing. The simulated temperature reductions during the Maunder Minimum are in the lowest probability range of the proxy records. During the Dalton Minimum, when also volcanic forcing is an important driver of temperature variations, the agreement is better. In the industrial period from 1850 onward SOCOL-MPIOM overestimates the temperature increase in comparison to observational data sets. Sensitivity simulations show that this overestimation can be attributed to the increasing trend in the solar forcing reconstruction that is used in this study and an additional warming induced by the simulated ozone changes.

2.1. Introduction

In recent years, the stratosphere has become more and more important for our understanding and proper simulation of climate variability and climate change (Baldwin et al., 2007; Gerber et al., 2012). While most of the CMIP3 models include only a poorly resolved stratosphere (Cordero and Forster, 2006), 14 of 39 general circulation models (GCMs) participating in CMIP5 include a 'high-top' atmosphere, with a fully resolved stratosphere (Flato et al., 2013). The importance of the vertical resolution in the stratosphere is highlighted in several studies (Gillett et al., 2002; Sigmond et al., 2004; Scaife et al., 2011; Hardiman et al., 2012).

The stratosphere interact with the troposphere and plays an important role for the climate in the troposphere, at the surface and for the oceanic circulation (e. g. Baldwin and Dunkerton, 1999; Graversen and Christiansen, 2003; Thompson et al., 2005; Reichler et al., 2012). Furthermore, surface climate is influenced by changes in the chemical composition of the stratosphere (Gillett and Thompson, 2003; Son et al., 2010; Thompson et al., 2011). The interactions between stratosphere and troposphere are most prominent in the northern and southern high latitudes during winter time. With the beginning of the polar night stratospheric temperatures start to decrease rapidly and the increasing equator-pole temperature gradient forces a strong and persistent zonal circulation. This polar vortex isolates the polar air masses and prevents the advection of warmer air towards the polar latitudes. Very strong wind anomalies in the polar vortices influence the circulation in the troposphere (Baldwin et al., 1994; Baldwin and Dunkerton, 2001; Thompson et al., 2005), a phenomena named stratosphere–troposphere coupling. Of particular relevance are unusually weak stratospheric zonal winds associated with a break down of the vortex (e.g., sudden stratospheric warmings). These disturbances are triggered by unusual wave activity propagating upward from the troposphere. Several processes were proposed to be involved in the wave propagation and to influence the stratosphere–troposphere coupling (Song and Robinson, 2004; Gerber et al., 2012), but the underlying mechanisms are still debated (Thompson et al., 2006; Gerber et al., 2012).

The winter climate at high latitudes is also closely related to the most important modes of variability, the Northern Annual Mode (NAM) in the northern Hemisphere (NH) and the Southern Annual Mode (SAM) in the southern Hemisphere (SH). These modes are found at any atmospheric level, from the stratosphere down to the surface. In the stratosphere, the NAM/SAM can be expressed by the variability of the polar vortices. At the surface the NAM is better known as the Arctic Oscillation (AO), which is basically the same phenomenon, though defined slightly differently, as the North Atlantic Oscillation (NAO) (Hurrell, 1995; Wanner et al., 2001; Pinto and Raible, 2012). The dynamical imprint of both is a North-South shift in the position of the maximum winds or jets in the troposphere. Stratosphere–troposphere coupling events connect these stratospheric and tropospheric modes of variability, hence a stronger polar vortex co-varies with a positive phase of the AO. Via the jet streams and their influence on tropospheric dynamics, the AO causally relates to, and thus is partially predictive of, weather patterns, with a negative AO index tending to be representative of high pressure in the polar region, weaker zonal winds, and greater movement of cold polar air into the mid latitudes.

These modes of variability are influenced by different external forcings, like changes in solar ultra-violet (UV) radiation (Haigh, 1994, 1996; Shindell et al., 1999; Kodera and Kuroda, 2002; Haigh et al., 2005; Labitzke, 2007; Anet et al., 2014; Gray et al., 2013),

volcanic aerosols (Graf et al., 1993; Stenchikov et al., 2002; Shindell et al., 2003; Muthers et al., 2014), or ozone variations (Haigh, 1994; Shindell et al., 1999; Gillett and Thompson, 2003; Son et al., 2010; Kang et al., 2011; Thompson et al., 2011). Furthermore, NAM and SAM may interact with other modes of variability like the QBO or ENSO (Labitzke, 1987; Giorgetta et al., 1999; Labitzke, 2007). A common feature of these studies is a top-down perspective (e.g., Meehl et al., 2009) where a perturbation changes the vertical and horizontal temperature gradient in the stratosphere and affects stratospheric dynamics. The changing stratospheric wind systems alter the vertical propagation of planetary waves and change the circulation in the troposphere (Kodera, 1994; Kodera and Kuroda, 2002).

Differently, in the bottom-up mechanism the influence of an external forcing mainly takes place at the surface, e.g., the cooling after strong volcanic eruptions or variations in the surface temperatures related to variations in the solar forcing. Changes in the circulation and the climate are then modulated from the bottom of the atmosphere. Air-sea interactions may amplify the response (Meehl et al., 2008). This, however, does not mean that the stratosphere is not involved. Stenchikov et al. (2002) found for the effect of volcanic aerosols that a change at the bottom also influences the stratospheric circulation. They found a change in the vertical component of the Eliassen-Palm flux, a vector determining the relative importance of the eddy heat and momentum fluxes for the propagation of waves, which indicates a reduction of the wave drag in the lower stratosphere. Climate model results further suggest that both, top-down and the bottom-up mechanisms, need to act together to produce a realistic response similar to the observations (Meehl et al., 2009).

The dynamics in the stratosphere interacts also with a large number of chemical processes, most important the ozone chemistry (Haigh, 1994; Shindell et al., 1999, 2001; Gillett and Thompson, 2003; Son et al., 2010; Thompson et al., 2011; Purich and Son, 2012; Varma et al., 2012). In case of the solar forcing, the variability in the UV part of the spectrum modulates the ozone production and heating rates followed by positive or negative temperature anomalies. These anomalies influence the equator-to-pole gradient, the strength of the polar vortices, and modify the Brewer-Dobson circulation (Haigh, 1994; Hu and Tung, 2003; Anet et al., 2013a). In case of volcanic aerosols, heterogeneous reactions take place on the aerosol surface, which also influence the ozone chemistry (Tie and Brasseur, 1995; Solomon et al., 1996; Anet et al., 2013a). In both cases, the response of the ozone chemistry is further modulated by the presence of ozone depleting halogens (Tie and Brasseur, 1995; Rozanov et al., 2002). The changing ozone concentrations in turn induce dynamical changes (Stenchikov et al., 2002).

Coupled climate models have been proven to be an essential tool for understanding processes and feedbacks between the different components of the climate system, e.g., between ocean and atmosphere. Chemistry transport models (CTMs) are numerical models that simulate a number of chemical species, their interactions and the influences of different atmospheric variables (temperature, shortwave and longwave flux, etc.). GCMs coupled to CTMs allow a direct consideration of chemistry-climate interactions. Most of the coupled chemistry-climate model (CCM) simulations so far were performed with prescribed sea surface temperatures (SSTs; e.g., Eyring et al., 2006) or simplified mixed-layer oceans (e.g., Stenke et al., 2013a). However, imposed SSTs can alter the stratosphere-troposphere interaction (Kirchner et al., 1999). The coupling to an interactive ocean model is therefore preferable for long-term simulations and future projections.

The purpose of this study is to present the atmosphere-ocean-chemistry-climate model (AOCCM) SOCOL-MPIOM. The atmospheric component of the model covers the atmosphere from the surface to the mesosphere (0.01 hPa) and enables the simulation of interactions between the physical and the chemical components of the climate system. In section 2.2 the model is introduced and an overview of the experiments used in this study is given. In section 2.3 the performance and the characteristic of the AOCCM SOCOL-MPIOM are evaluated using results from a pre-industrial control simulation. The effect of the atmospheric chemistry on the climate is assessed by comparing it to a simulation without interactive chemistry. Furthermore, we describe an ensemble of transient simulations for the period 1600-2000 to assess the behaviour of SOCOL-MPIOM under the influence of changing external forcings (section 2.4). Finally, we close with a discussion and a summary of the results.

2.2. Model description and experimental setup

2.2.1. Model description

The coupled model consists of the chemistry-climate model SOCOL (SOlar Climate Ozone Links), which is coupled to the ocean-sea-ice model MPIOM by the OASIS3 coupler. The CCM SOCOL version 3 (Stenke et al., 2013b) is based on the middle atmosphere model MA-ECHAM5 version 5.4.01 (Roeckner et al., 2003) and a modified version of the chemistry model MEZON (Model for Evaluation of oZONe trends, Rozanov et al. (1999, 2001); Egorova et al. (2003); Hoyle (2005); Schraner et al. (2008)).

MA-ECHAM5: This is a spectral general circulation model (GCM) based on the primitive equations with temperature, vorticity, divergence, the surface pressure, humidity, and cloud water as prognostic variables (Roeckner et al., 2003, 2006; Manzini et al., 2006). In the vertical dimension a hybrid sigma-pressure coordinate system is used.

The shortwave (SW) radiation code originates from the European Centre of Medium-Range Weather Forecasts (ECMWF) model IFS (Fouquart and Bonnel, 1980). The solar spectrum is split into six wavelength intervals, including three bands in the UV and visible ranges (185-250 nm, 250-440 nm, 440-690 nm) and three bands in the near-IR range (690-1190 nm, 1190-2380 nm, 2380-4000 nm) (Cagnazzo et al., 2007). This SW scheme considers Rayleigh scattering, scattering and absorption by aerosols and clouds, and the absorption of solar irradiance by water vapour, ozone (both varying in space and time) as well as CO₂, N₂O, CH₄, and O₂. The latter are considered as uniformly mixed gases in MA-ECHAM5, but CH₄ and N₂O can optionally also vary in time and space (as it is done in SOCOL).

The longwave (LW) radiation scheme follows the rapid radiative transfer model (RRTM) scheme (Mlawer et al., 1997), which calculates radiation fluxes and heating rates over 16 LW bands reaching from 10–3000 cm⁻¹. In the computations absorption by water vapour, CO₂, ozone, N₂O, CH₄, CFC-11, CFC-12, CFC-22, aerosols, as well as clouds are considered.

With the vertical resolution used in this study (39 levels up to 0.01 hPa), the model does not produce a Quasi-Biennial Oscillation (QBO) by itself. Therefore, a QBO nudging is applied by a linear relaxation of the zonal winds in the equatorial stratosphere (Giorgetta et al., 1999). The model assimilates the input data between 20° N to 20° S in the

horizontal and from 90 hPa up to 3 hPa in the vertical. ECHAM5 also includes a river run-off scheme (Hagemann and Duemenil, 1998; Hagemann and Duemenil-Gates, 2003) and simplified glacier calving, in the way that snow falling on ice sheets is instantaneously transferred to the next ocean grid cell.

Chemistry-climate coupling: MEZON and MA-ECHAM5 are coupled by the three dimensional temperature field and the radiative forcing of the different greenhouse gases (H_2O , O_3 , CH_4 , N_2O , and CFCs).

SOCOL: In the chemical module, 31 chemical species can react together via 140 gas-phase-, 46 photolysis-, and 16 heterogeneous reactions. The latter appear either in or on aqueous sulphuric acid aerosols as well as on three types of Polar Stratospheric Clouds (PSCs), i.e., on supercooled ternary solution (STS) droplets, water ice, or nitric acid trihydrate (NAT).

For SOCOL, the SW radiation code of MA-ECHAM5 has been modified in several aspects. In MA-ECHAM5 variations in the solar forcing are considered by variations in the total solar irradiance (TSI), the ratio of the irradiance in the six SW bands to the TSI, however, is fixed. SOCOL directly uses the spectral solar irradiance (SSI) as input for the six bands and, therefore, allows for a change in the spectral composition. As the absorption of radiation by oxygen and ozone in the Lyman-alpha, Schumann-Runge, Hartley, and Higgins bands is only partially included in MA-ECHAM5, missing heating rates are parametrized using an approach similar to Egorova et al. (2004).

The time step for the dynamical processes and physical parametrizations in the model is 15 minutes with a spectral truncation of T31. However, to reduce the high computational demand of the chemistry module, the chemical routines are called – simultaneously to the full radiative transfer calculations – every two hours. Over the two hour interval the heating rates are estimated based on the 2 hourly radiative transfer calculations and the solar angle that is calculated at every time step.

Precipitation of energetic particles into the atmosphere is simulated by different parametrizations for galactic cosmic rays (GCR), low energetic electrons (LEE) and solar energetic proton (SEP) events (Calisto et al., 2011; Rozanov et al., 2012). The routines are designed in such a way that from the known ionization rate distributions, a certain amount of N (GCR, SPE, LEE), NO (GCR, SPE, LEE) and OH (GCR, SPE) is produced.

Additionally to the interactive chemistry mode the chemistry module can be deactivated. In this case prescribed three dimensional ozone concentrations are used for the radiative transfer calculations. These ozone concentrations can origin from a model simulation with interactive chemistry. By forcing the model with ozone concentrations directly on the model grid, errors related to the vertical interpolation can be avoided. In contrast to many other models, SOCOL does not use zonally averaged ozone concentrations, as this leads to significant biases in the stratospheric climate and also affects tropospheric dynamics (Vaugh et al., 2009). Zonally averaged ozone forcing also might influence the propagation of planetary waves (Gabriel et al., 2007). In the setup without interactive chemistry the model version is nearly identical to MA-ECHAM5, except for the modification related to the SSI forcing mentioned above. Furthermore, the additional heating by absorption in the Lyman-alpha, Schumann-Runge, Hartley, and Higgins band is by default deactivated. Despite the small differences to MA-ECHAM5, these modifications lead to a significant change in the simulated climate.

MPIOM: The oceanic component consists of the ocean model MPIOM (Marsland,

2003; Jungclaus et al., 2006) including a sea-ice component. It uses an Arakawa C grid with the North Pole shifted to Greenland and the South Pole centred over Antarctica. Shifting the poles towards land surfaces avoids numerical singularities at the North Pole and allows a higher resolution in the deep water formation regions in the North Atlantic. The grid has a nominal resolution of 3° , that varies between 22 km near Greenland and 350 km in the tropical Pacific. In the vertical the grid is divided into 40 levels with decreasing resolution from the surface to the bottom. The time step of the calculations in the ocean model is 144 minutes in this setup.

Atmosphere-ocean coupling: Both components, the atmosphere and the ocean, are coupled every 24 hours using the OASIS3 coupler (Budich et al., 2010; Valcke, 2013). For each day the coupler transfers momentum, heat, and freshwater fluxes from the atmosphere to the ocean and sea surface temperatures (SST), sea ice, snow cover on sea ice, and momentum to the atmosphere. No flux correction is needed in the coupling process.

2.2.2. Experiments

To assess the influence of the interactive chemistry on the climate state a 1400 year long 1600 AD control simulation with interactive chemistry (CHEM) is compared to a simulation under the same set of boundary conditions, but without interactive chemistry (NOCHEM). Furthermore, an ensemble of transient simulations, i.e., with varying boundary conditions, covering the period 1600-2000 AD is performed. An overview of the experiments used in this study is given in Table 2.1.

Control simulations

For the control experiment, SOCOL uses a horizontal resolution of T31 (approx. $3.75^\circ \times 3.75^\circ$) and 39 vertical levels, resolving the atmosphere up to 0.01 hPa (approx. 80 km). The ocean component is branched off from the initial conditions of a transient millennium simulation with the MPI-ESM (ECHAM5-MPIOM with additional models for the land and ocean carbon cycle) for the year 1600 AD (Jungclaus et al., 2010). The atmospheric and chemistry components are initialized from scratch.

The control simulation is performed as time-slice experiment and all forcings are held constant at 1600 AD conditions (CO_2 : 276.4 ppm, CH_4 : 692.7 ppb, N_2O : 269.0 ppb), except for the volcanic aerosol forcing, where the unperturbed year 1599 is chosen. For the land-surface boundary condition the forcing from the ECHAM5 package is used, representing present day values (Hagemann, 2002). The QBO-nudging uses an idealized QBO cycle based on Brönnimann et al. (2007), to avoid an unrealistic dominance of a westerly or easterly QBO phase.

The oceanic component of SOCOL-MPIOM is initialized using restart files from the coupled system ECHAM5-MPIOM. However, when assuming a total solar irradiance (TSI) of 1367 Wm^{-2} (as in ECHAM5-MPIOM) the new SOCOL-MPIOM experiences a positive temperature drift that requires a tuning of the model. As tuning parameter the value of the TSI is chosen. To estimate the optimal tuning value for the TSI, a number of 200 year experiments with constant TSI reductions chosen between from 0 Wm^{-2} to -18 Wm^{-2} relative to the 1368 Wm^{-2} reference value is performed. All experiment are forced by constant 1600 AD boundary conditions and started from the same initial state.

Table 2.1.: Overview of the experiments used in this study. In column 'chem' the usage of the interactive chemistry module is indicated. Column 'type' denotes whether the experiment is performed as time-slice (t-slice) experiment with invariant boundary conditions or as transient (trans) simulation with time varying boundary conditions.

	length / period	chemistry	solar amplitude	type	forcings
CHEM	1400yrs	yes	const.	t-slice	const. 1600 AD
NOCHEM	222yrs	no	const.	t-slice	const. 1600 AD
2xCO2	70yrs	yes	const.	t-slice	const. 1990, except for CO ₂
2xCO2_NC	70yrs	no	const.	t-slice	const. 1990, except for CO ₂
4xCO2	150yrs	yes	const.	t-slice	const. 1990, except for CO ₂
M1	1600 – 2000	yes	medium	trans.	all
M2	1600 – 2000	yes	medium	trans.	all
L1	1600 – 2000	yes	large	trans.	all
L2	1600 – 2000	yes	large	trans.	all
SOLAR	1840 – 2000	no	medium	trans.	solar only
GHG	1840 – 2000	no	const.	trans.	GHG only
AERO	1840 – 2000	no	const.	trans.	aerosols only
OZONE	1840 – 2000	no	const.	trans.	ozone only
FULL	1840 – 2000	no	medium	trans.	all

The simulations with the smallest temperature drift is continued for another 1200 years and used as control simulation in this publication. It is forced by a solar constant of 1355 Wm^{-2} . This value is meant to represent 1600 conditions. With the solar forcing reconstruction of Shapiro et al. (2011), which is used in the transient simulations (see below), this corresponds to a TSI of 1358.7 Wm^{-2} for the year 1990. The new TSI value used for SOCOL-MPIOM therefore agrees reasonably well with the most recent TSI estimate of $1360.8 \pm 0.5 \text{ Wm}^{-2}$ (Kopp and Lean, 2011).

To assess the influence of the chemistry module on the climate state and variability a second control experiment without interactive chemistry is performed (NOCHEM). This simulation is branched off 1178 years after the start of the interactive simulation. The length of this experiment is 222 years. Both simulations are driven by the same forcings and boundary conditions, except for the forcings specific for the chemistry module, which are not considered in NOCHEM. Furthermore, ozone values need to be prescribed in NOCHEM in order to consider the effect of ozone in the radiation scheme. Here, a 4 dimensional, daily ozone climatology calculated over the simulation years 1178 to 1399 (length 222 years) of CHEM is used.

The control simulations are needed to (a) assess a potential underlying temperature drift due to the coupling of the model components, (b) as initial conditions for the transient simulations, and (c) to characterize the role of the interactive chemistry module on the climate. Due to the high computational demand of the chemistry computations and the slow adjustment time of the ocean it was not possible to perform a second control simulation for 1990 conditions, as it is usually done in model evaluation studies.

Climate sensitivity experiments

The climate sensitivity of SOCOL-MPIOM is analysed by two types of experiments (Table 2.1).

The transient climate response (TCR) is estimated using an experiment with 1 %/yr CO_2 increase until a doubling of the CO_2 concentrations is reached (Cubasch et al., 2001). The TCR is then defined by the global mean temperature change in the 20-yr period around the year of the doubling of the CO_2 concentrations.

Furthermore, we estimate the equilibrium response of the model following the approach by (Gregory et al., 2004). Therefore, the coupled model is forced by an instantaneous quadrupling of the CO_2 concentrations and the equilibrium climate sensitivity (ECS) is estimated based on a linear relationship between the TOA radiative flux and the global mean surface air temperature after a simulation length of 150 years.

Both experiments are initialized using 1990 conditions from the transient simulation M1. All other forcings are constant at 1990 level. The underlying positive temperature drift is assessed by a reference simulation without changing CO_2 concentrations. The temperature increase is then calculated relative to this experiment.

Finally, the influence on the interactive chemistry on the TCR is analysed using a second TCR experiment, where the chemistry module is disabled. The ozone climatology for this simulation is based in the simulated ozone in the 1990 reference experiment.

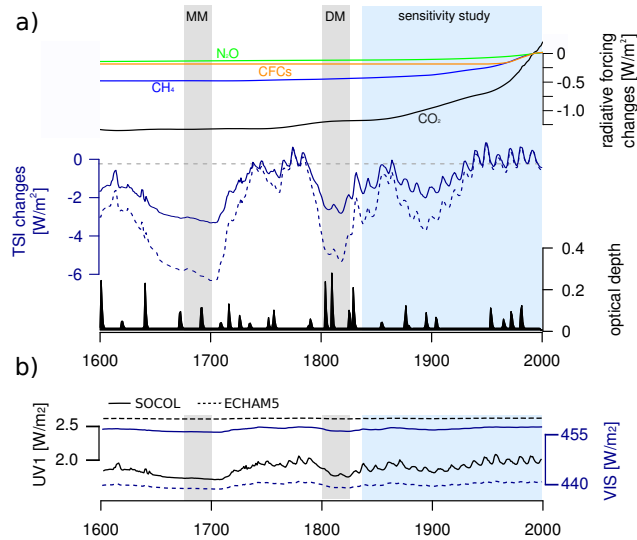


Figure 2.1.: (a) Overview of the major external forcings applied in the transient simulations. Top: Evolution of the radiative forcing from major greenhouse gases CO_2 , CH_4 , N_2O , and CFCs (calculated as in Ramaswamy et al., 2001). For CFCs the sum of CFC-11 and CFC-22 is shown as representative forcing. Values are expressed as deviations of the radiative forcing from the 1990 value. Middle: Total solar irradiance with respect to 1990. The dashed line represents the mean value of the TSI reconstruction of Shapiro et al. (2011), the solid line follows the upper envelope of the uncertainty range. Bottom: Volcanic forcing as global mean, annual mean aerosol optical depth in the visible band (Arfeuille et al., 2014). Three periods are highlighted: MM: late Maunder Minimum (1670–1699); DM: Dalton Minimum (1800–1829); and the period used in the sensitivity simulations (1840–2000). (b) Variability in the UV1 (185–250 nm) and visible (440–690 nm) spectral band (solid) in the SSI reconstruction of Shapiro et al. (2011) and (dashed) in ECHAM5 when the same TSI is applied.

Transient simulations

A set of four transient simulations for the period 1600–2000 AD is started from initial conditions of the CHEM control simulation using SOCOL-MPIOM with interactive chemistry. An overview of the external forcings is given in Figure 2.1. Greenhouse gas (GHG) forcings (CO_2 , CH_4 , and N_2O) are taken from the PMIP3 database (Etheridge et al., 1996, 1998; MacFarling-Meure, 2004; Ferretti et al., 2005; MacFarling-Meure et al., 2006). Emissions of ozone depleting substances (ODS) are based on the historical concentrations from the CMIP5 database.

For the solar forcing reconstructed spectral solar irradiance (SSI) values from Shapiro et al. (2011) are used, which are shown as total solar irradiance (TSI) in Figure 2.1. The reconstruction of Shapiro et al. (2011) is based on the solar modulation potential derived from ^{10}Be measurements in polar ice cores. In comparison to many other state-of-the-art solar forcing reconstructions, this reconstruction is characterized by a larger amplitude (Schmidt et al., 2012). The TSI difference between the Maunder Minimum (end of the 17th century) and present day is in the order of $6 \pm 3 \text{ Wm}^{-2}$. To consider larger and smaller variations, we created two SSI datasets both covering the uncertainty range of the reconstruction. The larger amplitude forcing represents the mean estimate of

6 Wm^{-2} (dashed line in Fig. 2.1), the second forcing with 3 Wm^{-2} amplitude (solid line) represents the upper boundary of the uncertainty of the SSI reconstruction. The two solar forcing scenarios will be referred to as L (large) and M (medium) in the following. Note that compared to other recent estimates a TSI difference of 3 Wm^{-2} between Maunder Minimum and present day is still considered to be large. In Steinhilber et al. (2009) for example the forcing difference between Maunder Minimum (MM) and present day is only $0.9 \pm 0.4 \text{ Wm}^{-2}$.

The SW radiation scheme in SOCOL has been modified in comparison to the original scheme distributed with ECHAM5. In the original ECHAM5 the SW spectra is divided into 6 spectral intervals and the TSI is distributed over the six spectral bands using fixed ratios. In the SW scheme of SOCOL the solar energy input can be prescribed for each band individually. This allows for a different variability in different spectral intervals. The differences in the spectral partitioning between SOCOL and ECHAM5 are pronounced, when the spectral solar reconstruction of Shapiro et al. (2011) is used (Fig. 2.1 b). In the UV region ($< 440 \text{ nm}$), considerably less energy is available in SOCOL (differences $> 6 \text{ Wm}^{-2}$ in UV2), but the multi-decadal scale variability is larger. Between the Maunder Minimum and the following period of high solar activity around 1780, the differences reach up to 6 Wm^{-2} . In the visible band (440-690 nm) a higher energy input is assumed in SOCOL, which explains the positive temperature bias in SOCOL-MPIOM compared to the ECHAM5-MPIOM that required the tuning of the model (see above). Differences in this spectral interval are in the order of 15 Wm^{-2} . Between 690 – 1190 nm and 2380 – 4000 nm, the energy input is again larger in ECHAM5 ($+5.5 \text{ Wm}^{-2}$ and $+4.5 \text{ Wm}^{-2}$, respectively), for the interval 1190 – 2380 nm larger SSI values are found in SOCOL ($+3.5 \text{ Wm}^{-2}$).

Other solar related forcings, like photolysis rates for the chemistry or the input for the parametrizations of the additional heating by oxygen or ozone absorption, are generated based on the SSI data set.

Four experiments are performed with two sharing the same solar forcing. We refer to the experiments as L1 and L2 for the large amplitude solar forcing and M1 and M2 for the medium amplitude solar forcing in the following. All other forcings are identical in the four simulations. The experiment M1 and M2 are initialized using restart files for the ocean and the atmosphere from the CHEM simulation (model year 450 and 500). To produce the initial conditions for L1 and L2 a second control simulation is performed. This experiment is identical to CHEM, with the only difference of a lower solar forcing, which is reduced by the forcing difference between the medium and the large amplitude solar forcing for the year 1600 (Fig. 2.1). From this control simulation, the restart files are also extracted for model year 450 and 500.

The stratospheric aerosols (Fig. 2.1) used in the simulations are described in Arfeuille et al. (2014). Aerosol optical properties (spectrally dependent) for the radiation scheme and surface area density information for the chemistry scheme are calculated offline using a microphysical aerosol model AER (Weisenstein et al., 1997) and stratospheric aerosol mass information from ice cores (Gao et al., 2008).

Tropospheric aerosols are based on CAM3.5 simulations with a bulk aerosol model driven by fixed SSTs and the 1850 – 2000 CMIP5 emissions (S. Bauer, personal communication, 2011). Before 1850, the aerosol concentrations are scaled by the world population except for 10 % of the presumed 1990 biomass burning aerosols which are considered

natural.

The emissions of CO and NO_x are based on the historical CMIP5 data sets which are available from 1850 onwards. Before 1850 the anthropogenic fraction is scaled linearly with world population. The biomass burning emissions are assumed to be constant over time. Emissions from shipping are projected linearly back to 1800, before 1800 the emissions are set to zero.

The lower boundary condition over land (land surface data) is kept at present day values as in the control simulation (Hagemann, 2002). For the QBO nudging, the QBO reconstruction from Brönnimann et al. (2007) is included, which is extended back in time to cover the full period 1600-2000. For this backward extension an idealized QBO cycle and annual cycle is assumed.

The cosmic ray intensity is reconstructed based on the solar modulation potential (Steinhilber et al., 2008). Available observations for solar proton events (SPE) are used for the periods 1963–2008 (Jackman et al., 2009). Before 1963 SPEs are randomized using a return-period based analysis of the last 45 yr, and weighted with the Ap index, an index of the geomagnetic activity. The NO_x influx, finally, is reconstructed based on the Ap and the Aa index, which are themselves reconstructed using sunspot numbers (Baumgaertner et al., 2009). Paleo-magnetic datasets (C. Finlay, personal communication, 2010) are applied to the model in order to take into account the geomagnetic dependency of the ionization.

In the analysis all transient simulations are detrended by subtracting the underlying positive trend estimated from the control simulation.

Sensitivity simulations

The contributions from different external forcings to the temperature increase from 1850 to 2000 is assessed by a set of sensitivity experiments (Table 2.1). In these simulations specific forcings are held either constant at pre-industrial levels or prescribed in a transient way. All simulations are initialized in the year 1840 using the atmospheric state of the transient simulation M1.

For these sensitivity experiments, the version of SOCOL-MPIOM without interactive chemistry is used. This setup allows us to use fixed ozone concentrations at pre-industrial levels or to prescribe the simulated ozone from the transient simulations as forcing. In this way the radiative effect of the simulated ozone changes can be assessed. The following forcings are considered:

- SOLAR: solar forcing with medium amplitude. In this experiment the increase in TSI since 1900 is 1.7 Wm^{-2} (TOA).
- GHG: For this experiment only the major GHGs (CO₂, CH₄, and N₂O) increase (see Fig. 2.1 a), except for CFCs.
- AERO: Only stratospheric and tropospheric aerosols change.

For these three experiments ozone concentrations are held constant at pre-industrial levels.

- OZONE: In this experiment only ozone is used as time varying forcing. The ozone concentrations used as forcing are extracted from M1, but the concentrations in the other three transient experiments are very similar.

- **FULL:** All major forcings (solar, GHGs, aerosols, ozone) are included in this simulation.

For each forcing combination a single experiment is performed. The forcing from CFCs are not considered in the sensitivity experiments.

2.2.3. Observational data sets

To evaluate the simulated climate variables different observational data sets are used throughout this study.

The stratospheric temperatures and dynamics in the control simulation are compared to the two reanalysis products ERA40 (Uppala et al., 2005) and ERA Interim (Dee et al., 2011) from the European Centre for Medium Range Weather Forecasts (ECMWF). ERA40 covers the period 1957-2002, while for ERA Interim the years 1979-2013 are considered.

The simulated temperature increase since the second half of the 19th century is compared to two global surface air temperature data sets and a reanalysis product. The Goddard Institute for Space Studies Surface Temperature analysis (GISTEMP) contains a spatial land and ocean surface temperature analysis for the period 1880-2013 (Hansen et al., 2010). The data set is solely based on instrumental records from meteorological stations, ships, buoys, and other. The data from land stations are corrected for urban heat island effects using satellite observations. SSTs are based on the NOAA data set ERSST (Smith et al., 2008). The second temperature data set is from the Climatic Research Unit at the Hadley Centre of the UK Met Office (HadCRUT4). It is also based on instrumental temperature records and covers the period 1850-2013 (Brohan et al., 2006). HadCRUT4 makes use of the SST data set HadSST3 for the conditions over oceans (Kennedy et al., 2011).

Additionally, we use the 20th century reanalysis (20CR; Compo et al., 2011). By assimilating only sea level pressure, SST and sea ice informations (HadISST; Rayner et al., 2003) as boundary conditions, 20CR generates a physically consistent, three dimensional picture of the atmosphere with high temporal resolution. 20CR contains 56 ensemble members, to consider uncertainties in the boundary conditions. The reanalysis covers the period 1871-2010.

2.3. Pre-industrial model climatology and imprint of atmospheric chemistry

In this section, the mean climate state and the most important variability patterns in a pre-industrial (1600 AD) control simulation of SOCOL-MPIOM is described and the difference between a simulation including interactive chemistry (CHEM) and a simulation without interactive chemistry (NOCHEM) is analysed.

The development of the global mean 2-m air temperature in the control simulation CHEM is shown in Figure 2.2. Despite the tuning approach described above, the simulation is still dominated by a continuous positive drift of $0.037\text{ }^{\circ}\text{C}/100\text{ yr}$, averaged over the last 500 simulation years. The temperature trend is slightly larger in the SH

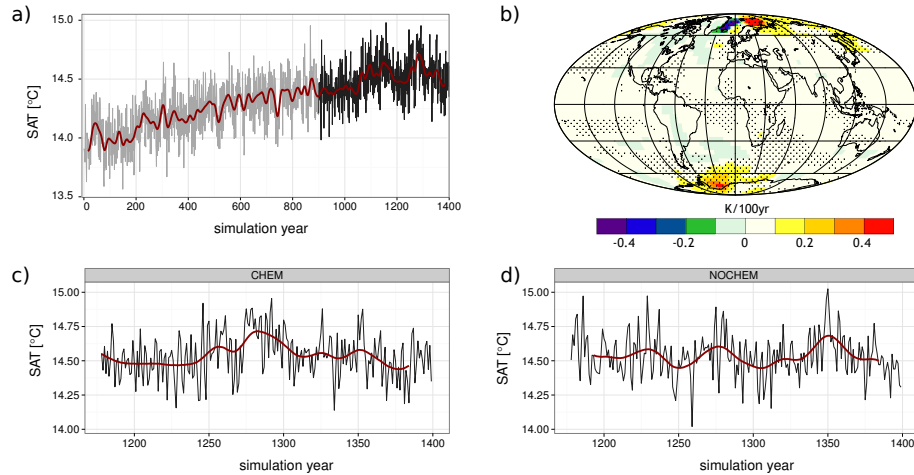


Figure 2.2.: (a) Time series of the global mean 2 m air temperature as annual mean values (black) and 31 year low pass filtered values (red) for the simulation with interactive chemistry (CHEM). The spin-up period is indicated by light grey colours, the last 500 years, which are used to calculate the trend pattern (b), are shown in black colours. (b) Linear temperature trends in K/100 yr for the last 500 years in CHEM. Regions with significant trends are stippled. (c,d) Time series of the global mean 2 m air temperature as annual mean values (black) and 31 year low pass filtered values (red) for the simulation with (CHEM) and without (NOCHEM) interactive chemistry over the common 222 year period.

($0.038^{\circ}\text{C}/100\text{yr}$) than in the NH ($0.036^{\circ}\text{C}/100\text{yr}$) and stronger over land than over the ocean.

For the last 500 years, the largest positive temperatures trends are found in the polar regions, especially in the Barents and the Weddell Seas (Fig. 2.2). Here, the overall positive drift affects the sea ice edge, which amplifies the temperature trends. Clearly, the warming of the atmosphere near the surface influences also the state of ocean. On all levels, down to the deep ocean a positive temperature trend is present, reaching, e.g., $0.05^{\circ}\text{C}/100\text{yr}$ at depth around 3500 m.

In the common 222-yr period the global mean 2-m air temperature in CHEM and NOCHEM is very similar, besides some variations related to the model's internal variability (Fig. 2.2 c and d). This confirms that the interactive chemistry does not affect the model equilibrium. Furthermore, the drift in the 2-m temperatures is no longer significant in this 222-yr period. Still, the oceanic temperatures are not in equilibrium.

With an average value of 14.45°C for CHEM the simulated global mean temperature is higher than the pre-industrial observed mean over 1850-1890 of $13.7 \pm 0.2^{\circ}\text{C}$ (Brohan et al., 2006). However, the value is similar to the global mean temperature in the MPI-ESM based on ECHAM5 and MPIOM (Fig. 4 in Mauritsen et al. (2012)). From the ongoing temperature drift it can be assumed that the model has not reached equilibrium so far. The top-of-the-atmosphere (TOA) radiation balance is still characterized by a positive imbalance of 1.6 Wm^{-2} , averaged over the last 100 years of the simulations. However, most climate models do not exactly conserve energy (Mauritsen et al., 2012). Nevertheless, compared to the MPI-ESM, which has an imbalance of approximately 1

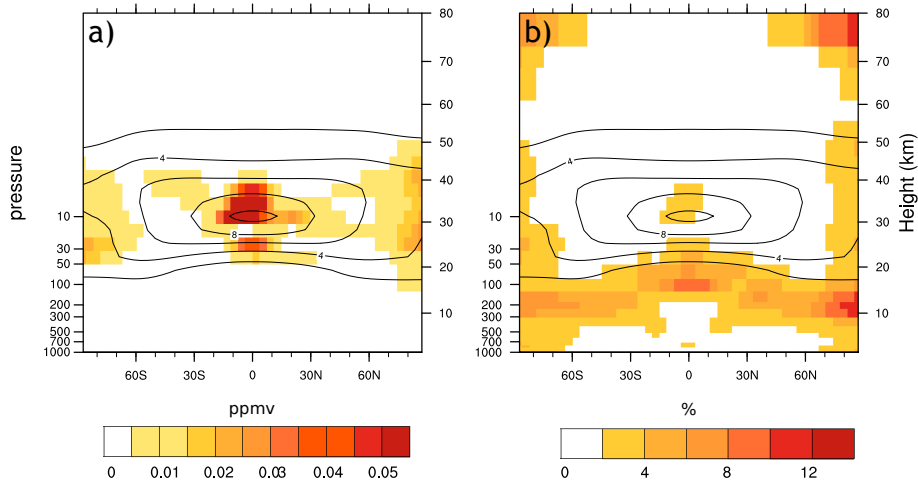


Figure 2.3.: Variability in the annual mean zonally averaged ozone mixing ratios in the CHEM simulation. (a) standard deviation (in ppmv). (b) variability expressed as standard deviation normalized by the long-term mean (given as percentages). Contours show the long term-mean ozone concentrations.

Wm^{-2} , the temperatures are likely to adjust further, even after 1400 years of simulation.

In the following the differences in the mean climate and the variability between CHEM and NOCHEM for different variables and components of the climate system is presented.

2.3.1. Stratospheric changes with interactive chemistry

Ozone variability

A detailed evaluation of the chemistry in SOCOL3 is given in Stenke et al. (2013b). Here, we focus only on the simulated variability in stratospheric ozone concentrations and their possible influence on the climate variability. The main difference between CHEM and NOCHEM is the fact that ozone concentrations vary on all time scales in CHEM, whereas NOCHEM is driven by an ozone climatology, which represents the climatological annual cycle and therefore does not contain any variability on time scales shorter than one day and longer than one year.

The time series of global mean ozone mixing ratios at different pressure altitudes reveal that variability takes place on different time-scales, from day-to-day up to the decadal scale. A pronounced and significant 2.3yr periodicity is found, which is the QBO imprint on the ozone chemistry.

In the zonal mean perspective the largest variability is found in the tropics at the altitude of the concentration maximum (Fig. 2.3). Secondary maxima occur in the lower stratosphere in both polar regions. The normalized variability (Fig. 2.3) is more pronounced in the polar stratosphere of both hemispheres compared to the tropics. Variability in the troposphere and mesosphere is in general very small and is only reflected in the normalized anomalies. The variations are more pronounced on the intra-seasonal scale (not shown), where for the NH polar stratosphere, the variability in the winter season (DJF) ozone concentrations exceeds 10 %. The variability in the vertically inte-

grated total column ozone reflects the pattern found for the zonal averages (not shown). The northern and southern polar regions are characterized by the highest interannual variability, while the variability in the North is larger than in the South. In the Arctic, variability is particularly pronounced in the boreal winter and spring season. Over Antarctica, larger variances are found mainly during austral spring.

Temperatures

The seasonal zonal mean differences in the air temperature between CHEM and NOCHEM are presented in Figure 2.4 a.

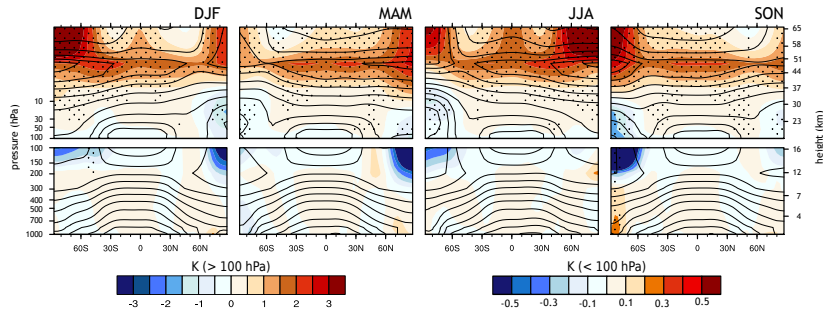
The largest temperature differences are found in the mesosphere, where CHEM is more than 3 °C warmer. These differences are most pronounced in the summer season of the corresponding hemisphere. In the upper and middle stratosphere the temperatures are significantly higher at latitudes between 30° and 50° on both hemispheres and significantly lower in polar regions. The positive differences are below 0.6 °C and do not show a clear seasonal variation. The negative differences in the lower stratosphere are most pronounced and significant during winter and spring and reach up to -1.5 °C.

The higher mesospheric and upper stratospheric temperatures in CHEM are result of different processes. In SOCOL-MPIOM with interactive chemistry a parametrization of the absorption of radiation by oxygen and ozone in the Lyman-alpha, Schumann-Runge, Hartley, and Higgins bands is included. This effect creates additional heating in the higher atmosphere, which is not included in NOCHEM. Tests show that this parametrization is responsible for a pronounced heating of the higher atmosphere, especially in summer. In the annual average the temperature is up to 7 °C warmer and the effect is visible at all latitudes in the mesosphere and upper stratosphere. Therefore, an additional negative signal in the mesosphere is needed to create the pattern shown in Figure 2.4.

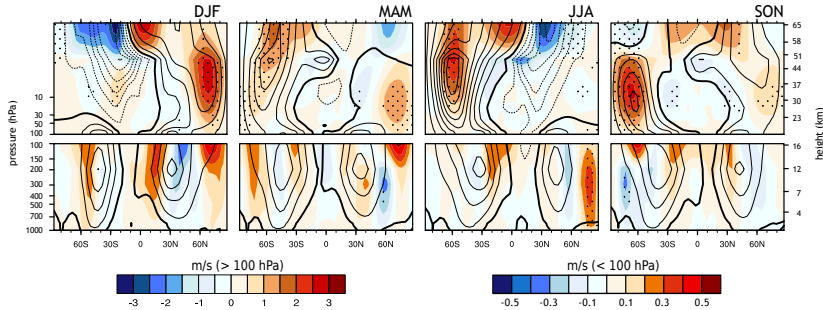
One mechanism that is responsible for colder conditions in the higher atmosphere in the case of the setup with interactive chemistry is found in the interactions between the chemical module and the SW radiation scheme. In NOCHEM ozone concentrations are prescribed as a daily climatology, whereas ozone in CHEM varies from time step to time step. In the mesosphere ozone undergoes a pronounced diurnal cycle. During daytime ozone is destroyed by UV radiation and in the night the transport of ozone enriched air from lower levels leads to an increase in the ozone concentrations. Differences between night and day reach up to 15 %. Consequently, the highest model levels in CHEM are colder during daytime, but this cooling can not be compensated at night. The diurnal cycle of the ozone concentrations in the mesosphere has a cooling effect of around 5 °C, which is largest at 30 °N and 30 °S.

Additional differences between CHEM and NOCHEM are found in the water vapour concentrations (not shown). In the NOCHEM configuration the only source of water vapour in the stratosphere and mesosphere is the transport from the troposphere. With interactive chemistry water vapour is also produced by the oxidation of CH₄. Large differences in the specific humidity between NOCHEM and CHEM are found in the summer hemisphere and at altitudes above 40 km, where the values differ by up to 37 %. The higher water vapour mixing ratios in CHEM lead to a cooling of the higher atmosphere between 60 °S and 60 °N. In the annual mean the maximum anomalies are in the order of 1 °C. Contrary to Maycock et al. (2011) who reported a maximum cooling

a) temperature differences



b) zonal wind differences



c) variance ratios

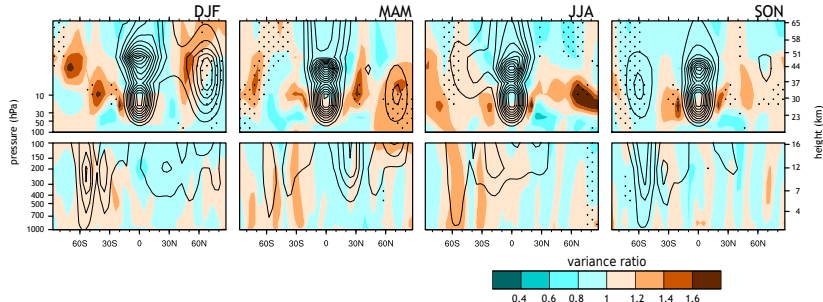


Figure 2.4.: Zonal and seasonal mean anomalies between CHEM and NOCHEM, i.e., CHEM minus NOCHEM for (a) temperatures, (b) the zonal wind component, and (c) the variance ratio of the zonal mean wind component between CHEM and NOCHEM, i.e., $\text{variance}(\text{CHEM}) / \text{variance}(\text{NOCHEM})$. Atmospheric levels above (top) and below (bottom) 100 hPa are displayed separately to improve readability in the lower atmosphere. Contours: seasonal means in CHEM with contours (a) from 230 K to 300 K by 10 K and (b) -50 m/s to 50 m/s by 10 m/s. In (c) the average seasonal variance in CHEM is shown, with contours from 0 m²/s² to 140 m²/s² by 25 m²/s² for levels above 100 hPa and 0 m²/s² to 15 m²/s² by 3 m²/s² for levels below 100 hPa. Stippling: significant differences between the ensembles. In case of the seasonal mean comparison (a, b) a Student's t-test is used. The variance comparison is based on a F-Test. Test results with $p \leq 0.05$ are stippled. Differences are calculated over the common 222 year period.

Table 2.2.: Climatological indices for the winter (DJF) zonal wind component at 50 hPa in different latitudes, similar to Driscoll et al. (2012). Climatological indices for CHEM and NOCHEM are calculated over the common 222 year period. Reanalysis values are based on ERA Interim for the period 1979 – 2013 (Dee et al., 2011) and ERA 40 for the years 1957 – 2002 (Uppala et al., 2005). Values given denote the average zonal wind speed in the given latitude range at 50 hPa in m/s; the standard deviation is given in brackets.

	30°S–30°N	55°N–65°N
CHEM	-2.4 (3.6)	23.1 (7.7)
NOCHEM	-2.4 (3.5)	22.5 (7.8)
ERA Interim	-3.7 (5.1)	19.0 (8.6)
ERA 40	-3.8 (5.1)	19.1 (8.1)

in the lower stratosphere after a uniform increase of the stratospheric water vapour, the cooling effect in SOCOL-MPIOM is strongest in the upper stratosphere and mesosphere. This is probably related to the fact that the water vapour difference between CHEM and NOCHEM are not uniformly distributed and reach the largest differences in the higher stratosphere.

Further tests for the parametrization of GCR, LEE, and SEP events show that these parametrizations does not substantially affect the atmospheric temperatures.

Dynamics

The differences in the zonal wind component reflect the changes in the meridional temperature gradients (Fig. 2.4) b. Both polar vortices are significantly strengthened during winter and spring in the case of the simulation with interactive chemistry. With this vortex intensification, the colder conditions in CHEM in the SH and NH polar stratosphere can be understood: A stronger vortex isolates the air masses over the poles and prevents the meridional transport of warmer air into the vortex centre. Both differences, the temperature and the zonal wind speed, are larger in the SH. In the summer hemisphere, the changed temperature gradient forces a strengthening of the easterly circulation at mesospheric levels.

A comparison between model results and observations for the zonal wind component at 50 hPa in the boreal winter season is given in Table 2.2. Similar to Driscoll et al. (2012), we average over the tropical latitudes (30°S–30°N) and the northern mid latitudes (55°N–65°N) and compare to against the reanalysis products ERA40 and ERA Interim, covering the period 1957-2002 and 1979-2013, respectively.

In the tropical latitudes the average wind conditions and the standard deviation are lower compared to the values in ERA Interim. However, SOCOL-MPIOM agrees much better with ERA Interim than the CMIP5 models evaluated by Driscoll et al. (2012), which can be attributed to the QBO nudging implemented in the model. No significant difference is found between CHEM and NOCHEM for the tropical indices. For the northern polar night jet the difference between CHEM and NOCHEM becomes slightly larger, illustrated by stronger zonal wind in winter for CHEM. The differences are not very large

Table 2.3.: Average number of SSW events per winter (NDJFM) following the definition of Charlton and Polvani (2007). SSW events for CHEM and NOCHEM are calculated over the common 222 year period. For comparison the reanalysis products ERA 40 (1957–2002) and ERA Interim (1979–2013) are used.

	Nov	Dec	Jan	Feb	Mar	Σ
CHEM	0.12	0.07	0.07	0.14	0.23	0.63
NOCHEM	0.10	0.07	0.10	0.19	0.21	0.67
ERA40	0.02	0.09	0.24	0.16	0.13	0.64
ERA Interim	0.00	0.12	0.18	0.26	0.21	0.76

(0.6 m/s), but statistically significant. The variability in the daily mean zonal wind component does not differ significantly between CHEM and NOCHEM. Compared to ERA Interim SOCOL-MPIOM simulates higher zonal winds with a slightly lower standard deviation. Still, the agreement is better than in most CMIP5 models evaluated by Driscoll et al. (2012). In particular this agreement is notable, since earlier studies suggested that the underestimation of stratosphere–troposphere coupling events after tropical volcanic eruptions may be related to a too strong and too stable northern polar vortex in many GCMs (Stenchikov et al., 2006; Driscoll et al., 2012). Although the different climate states, pre-industrial control vs. late 20th century, might bias the comparison there is confidence that SOCOL-MPIOM simulates wind conditions in the tropical and northern high latitudes reasonably well. Furthermore, the comparison between CHEM and NOCHEM reveals an influence of interactive ozone chemistry on the mean intensity of the winter northern polar vortex.

The stability of the northern polar vortex is closely related to sudden stratospheric warmings (SSW). Major SSWs are stratospheric extreme events, in which the westerly flow during winter time is reversed and a strong warming in the polar stratosphere can be observed. SSW events in the NH are associated with a 'break down' of the polar vortex and are consequently also reflected in the NAM. Via stratosphere–troposphere interactions, SSW events influence the storm-track activity (Thompson and Wallace, 2001; Breiteig, 2008) and the increase of blocking situations (Woollings et al., 2010). Here we assess the ability of SOCOL-MPIOM in simulating of SSWs and possible influences of the interactive chemistry on the frequency of SSWs. Again, we use the two reanalysis products from the ECMWF and compare them to the values from the two pre-industrial control simulations. SSW events are based on the definition of Charlton and Polvani (2007). The central date of an event is defined as the day during the months November to March when the zonal mean wind component at 60°N and 10 hPa changes from westerly to easterly direction. The following 20 days after the onset of an event are excluded from the analysis to avoid double counting single events. Final warming events at the end of the winter season are excluded by an additional constraint demanding that the last events need to be followed by at least 10 days with westward wind conditions before the end of April.

The total number of SSW events per winter is similar to ERA 40 and ERA Interim (Table 2.3). During the winter months SOCOL-MPIOM simulates a too uniform dis-

tribution of SSWs. In the reanalysis a clear maximum is found in January (ERA 40) or February (ERA Interim), whereas both experiments simulate a minimum of events in January. Note that the difference between ERA 40 and ERA Interim is due to the different periods, in the common period 1979-2002 the difference is negligible. With interactive chemistry less SSW events are simulated, which may be related to the stronger polar vortex in CHEM.

Note that this more realistic simulation of SSWs is a major improvement to earlier versions of SOCOL (Fischer et al., 2008) and is attributed to a better representation of the stratospheric temperatures in the polar regions in winter and spring (Stenke et al., 2013b).

In the NOCHEM simulation, the ozone forcing is implemented in terms of a four dimensional ozone climatology, representing the average annual cycle at each grid point. Any interannual variability in the ozone mixing ratios is excluded by this approach. This may affect different physical variables of the atmosphere and reduce their variability on interannual time scales.

Changes in the interannual variability of the zonal mean temperatures and zonal winds are described in the following. Therefore, the ratio of the two variances, i.e. $\frac{\text{var}(\text{CHEM})}{\text{var}(\text{NOCHEM})}$ is calculated. A ratio of 1 corresponds to no change, values < 1 (> 1) to a reduction (increase) of the variance with interactive chemistry. Results for the seasonal averages are shown in Figure 2.4. The highest variability in the zonal wind is found in the tropical stratosphere for all seasons (contours). This pattern is related to the QBO. Secondary maxima of the variability are found in the NH during DJF and MAM, related to the winter polar vortex. In the SH the variability of the polar vortex is lower, i.e., the vortex is more stable in the winter months. Still, a second maxima is found for austral spring in the vortex region. In the NH, the variability in the winter vortex is enhanced in the southern part of the vortex and reduced in the centre of the vortex with interactive chemistry. A slightly lower variability in the centre may be related to the overall stronger vortex and is also reflected in the lower number of SSW events. The increasing variability in the mid-latitudes could be related to the chemistry, however, the differences are marginally significant. A significant increase in the variability in the northern polar vortex is found for the boreal spring season. In the SH, the low variability in the winter polar vortex is slightly (albeit significantly) higher in winter, but reduced in the following spring season.

In summary, the largest differences between the simulation with and without interactive chemistry are only indirectly related to the chemistry. With interactive chemistry the absorption of oxygen and ozone in different wavelength bands leads to enhanced heating rates in the upper atmosphere. This warming is compensated by interactions between the diurnal cycle of mesospheric ozone and the SW radiation scheme. Furthermore, the stratospheric water vapour concentrations are considerably lower, since an important source of water vapour (CH_4 oxidation) is not considered in the model. These differences affect the temperature distribution, the wind field and the polar vortices. However, the overall differences in the stratospheric climate are small.

2.3.2. Tropospheric and surface changes

In the troposphere, significant temperature differences are only found during the austral spring season in the southern high latitudes below 250 hPa (Fig. 2.4). The warming is

related to differences in the cloud cover between CHEM and NOCHEM. During austral winter and spring significantly more clouds are formed in CHEM, with differences up to 20 % in the vertical integrated total cloud cover. The additional clouds are mainly limited to areas southward of 60°S and altitudes between 250 and 100 hPa, covering the lower stratosphere and upper troposphere. These clouds are a consequence of the higher stratospheric water vapour concentration due to the oxidation of CH₄ in the chemistry module. Under the cold conditions of the polar night, the available water vapour condenses to ice clouds, which absorb and reflect a fraction of the outgoing longwave radiation and warm the air column below. The clouds are formed during the winter season and reach their largest coverage in August. Similarly, the radiation balance changes in time and the temperature anomaly peaks in August. The tropospheric temperature anomaly is therefore still weak and not significant during austral winter, but has a clear and significant impact on the temperatures in austral spring.

A similar effect is found in the NH for the boreal winter. However, here the effect is smaller, since the cooling in the polar stratosphere is smaller over the Arctic than over Antarctica and less clouds are formed.

Differences in the tropospheric zonal mean wind reveal a more heterogeneous pattern. In the SH, the reduced meridional temperature gradient in spring causes a shift of the westerlies to the equator, with a significant reduction in the South and (insignificant) increases in the North. However, during austral summer and autumn the westerly circulation is stronger in the South (sign. in MAM). In the NH, a significant weakening of the westerlies at high latitudes is also found for MAM together with a strengthening in summer.

At the surface the differences between CHEM and NOCHEM are smaller and only a few significant changes are found (Fig. 2.5). In the Barents Sea, higher temperatures in CHEM are present during the entire year and related to less sea ice (Fig. 2.5). The variability in the sea ice cover in the Barents Sea is in general very large. The sea level pressure or wind patterns reveal no consistent changes that may help to explain the differences. Differences between CHEM and NOCHEM in this region are therefore probably related to internal processes in the ocean that modulate the inflow of warm Atlantic water into the Barents Sea basin and, consequently, the sea ice cover and the surface temperatures.

In the SH high latitudes, the higher temperatures in CHEM during austral spring is obviously related to the cloud cover differences as explained above. In the Southern Ocean, between Australia and Antarctica a cooling is present during the entire year.

In the North Atlantic sea level pressure (SLP) significantly increases in CHEM compared to NOCHEM (Fig. 2.5). In the North Pacific a significant reduction of the SLP is found for MAM and a significant increase for the SON season. No significant changes are found for the SLP field in the SH, except for austral spring, which is related to the temperature differences between CHEM and NOCHEM.

Besides changes in the mean climate, the missing interannual variability in the ozone concentration may also influence the variability at the surface. However, the surface temperatures do not show a systematic and significant change in the variability for any season (not shown).

The variance ratio between CHEM and NOCHEM of the SLP field is shown in Figure 2.6. In the NH, the centres of action that modulate weather and climate during the

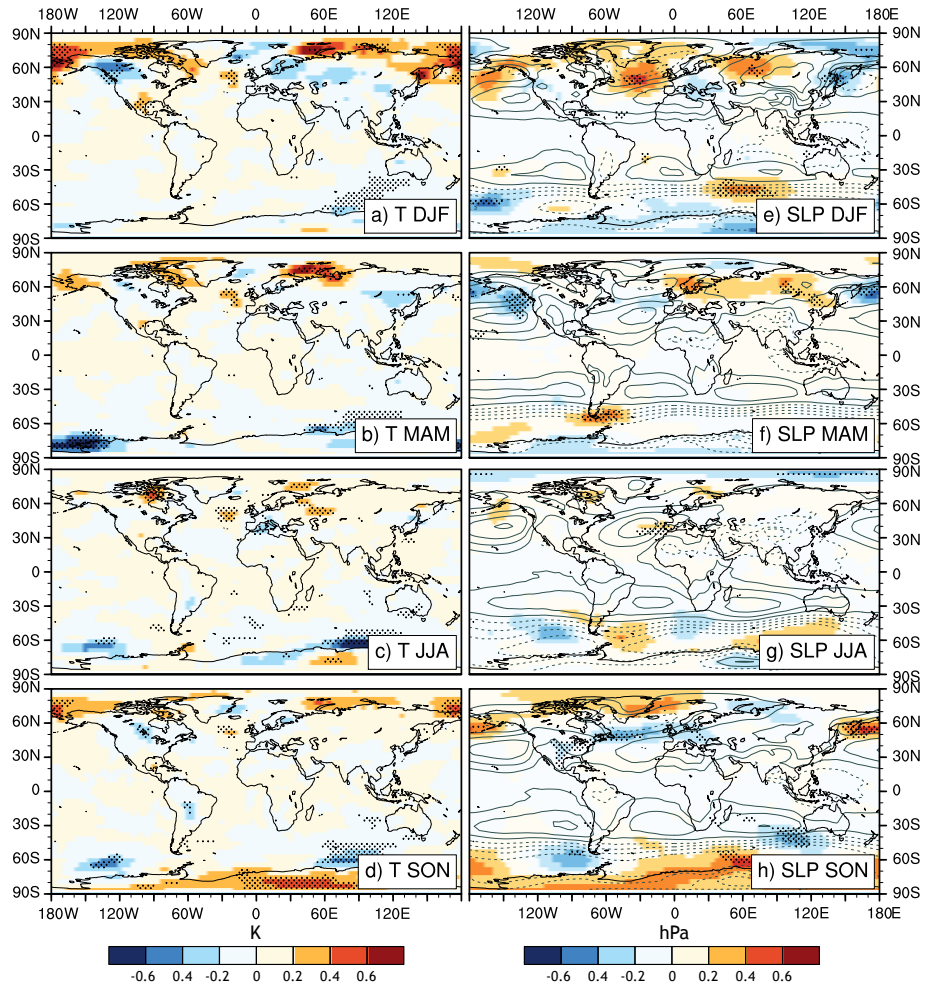


Figure 2.5.: Differences in the seasonal mean 2 m temperature (left) and sea level pressure (right) between the CHEM and NOCHEM control simulation. Seasons are displayed from top to bottom (DJF: a, e; MAM: b, f; JJA: c, g; SON: d, h). Gray contours in the sea level pressure panels display the seasonal average field in CHEM. The significance of the anomalies is indicated by stipplings for $p \leq 0.05$ (Student's t-test).

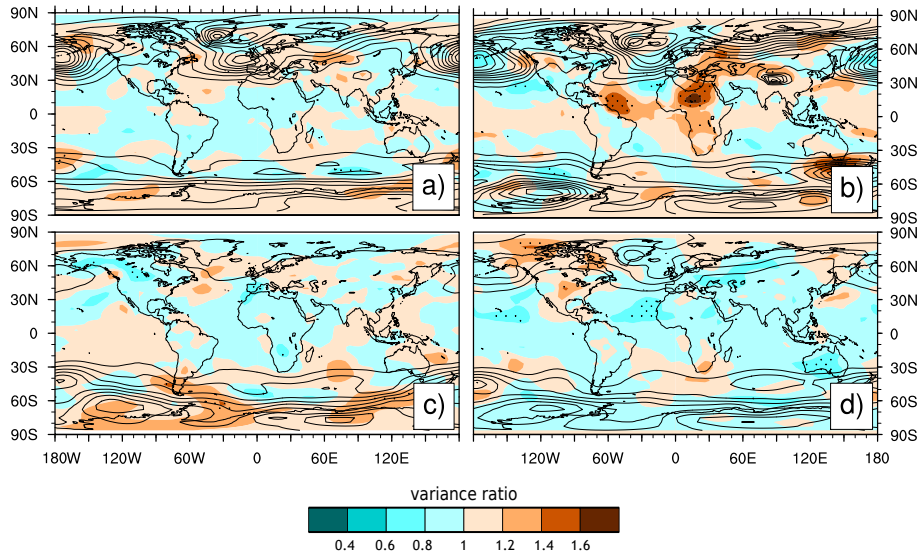


Figure 2.6.: Variance ratio (i.e. $\text{variance}(\text{CHEM}) / \text{variance}(\text{NOCHEM})$) for the seasonal mean sea level pressure with (a) DJF, (b) MAM, (c) JJA, and (d) SON. Stippling: significant differences between the ensembles based on a F-Test. Test results with $p \leq 0.05$ are stippled. Contours: seasonal variance in CHEM. Differences are calculated over the common 222 year period.

winter months are the North Atlantic (Iceland low and Azores high) and the Aleutian low. No significant influence of the interactive chemistry in these highly variable regions is found. During the other seasons, some significant changes are detected, but mainly in regions with an overall low variability (e.g., in the tropics). The reasons for these changes are unclear. In the SH mid- and high latitudes the variability is increased in all seasons except autumn, however, the regions with significant increases change from season to season.

For the ocean no significant differences between CHEM and NOCHEM are found, besides the above mentioned sea ice cover anomalies in the Barents Sea (not shown). The ocean is therefore not affected by the interactive atmospheric chemistry.

In summary, the influence of the interactive chemistry in the troposphere is regionally and seasonally limited. The largest difference between CHEM and NOCHEM, the change in winter and spring climate over Antarctica, is related to the differences in stratospheric water vapour concentrations between the two experiments. Significant and consistent influences of the chemistry on the variability are rare.

2.3.3. Climate sensitivity of SOCOL-MPIOM

The climate sensitivity is the temperature response after a perturbation in the radiative forcing. Knowledge about the climate sensitivity of a model is crucial for the interpretation of transient climate simulations past and future climates. Several methods can be applied to estimate the climate sensitivity of a model. We focus here on two approaches, the transient climate response (TCR) and the equilibrium climate sensitivity (ECS).

In Figure 2.7 both measures are compared to the TCR and ECS values of the CMIP5

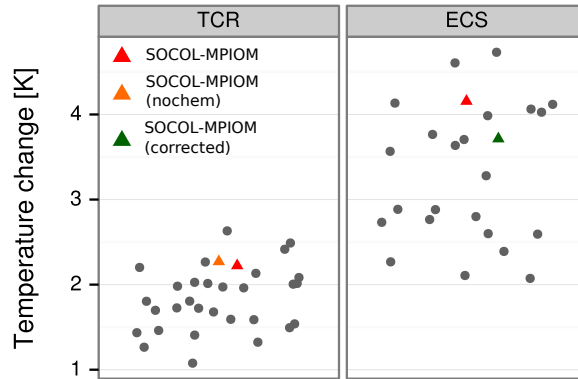


Figure 2.7.: Comparison of the Transient Climate Response (TCR, left) and the Equilibrium Climate Sensitivity (ECS, right) for a doubling of CO_2 for the CMIP5 (grey dots, Flato et al., 2013) and SOCOL-MPIOM (triangles). The ECS is determined by two different approaches. The first estimate (red triangle) considers only the top-of-the-atmosphere (TOA) radiative flux and the global mean temperature (Gregory et al., 2004). For the second estimate (green triangle), the first estimate is corrected by the deep ocean heat uptake, following Li et al. (2012).

ensemble. With 2.2 K the TCR of SOCOL-MPIOM is in the range of the higher sensitivities of the CMIP5 ensemble. For the configuration without interactive chemistry, which is forced by a perpetual 1990 ozone climatology a second double CO_2 simulation lead to the slightly larger TCR of 2.3 K. Hence, the interactive chemistry module has only minor influences on the TCR of SOCOL-MPIOM. The ECS has been estimated from the CO_2 quadrupling experiments (Andrews et al., 2012). With 4.2 K it is also among the models with the high climate sensitivity. Still, the estimate is within the sensitivity range from 1.5 to 4.5 K (Stocker et al., 2013).

In comparison to the MPI-ESM based on ECHAM5-MPIOM, the TCR is the same but the ECS is considerably higher. For the IPCC AR4 Randall et al. (2007) reported a TCR of 2.2 K and an ECS of 3.4 K, for a configuration with higher spatial resolution (T63L39 in the atmosphere and approx. $1.5^\circ \times 1.5^\circ$ in the ocean). For a configuration with the same spatial resolution in the atmosphere and the ocean, but a lower vertical resolution in the atmosphere, Li et al. (2012) reported an ECS of 3.7 K. They also showed that the approach by Gregory et al. (2004) might lead to an overestimation of the ECS in the order of 10 % and proposed an improved methodology that takes the tendency of the deep-ocean heat uptake (ocean below 1500 m) into account. At the end of the 150 year experiment, the heat uptake is clearly positive and the correction proposed by Li et al. (2012) results in a lower value of 3.7 K, which corresponds better with the estimate of Li et al. (2012). Still, the value is in the upper range of the CMIP5 ensemble.

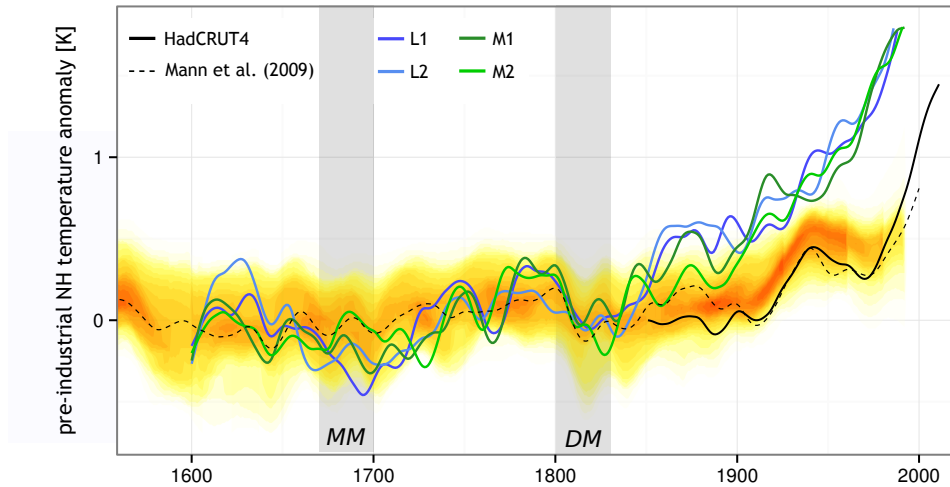


Figure 2.8.: NH average 2-m temperatures for the four transient simulations (coloured lines) in comparison to the probability range (yellow/ref shading) of different NH temperature reconstructions (Jansen et al., 2007). The ensemble members L1 and L2 correspond to the large amplitude solar forcing, M1 and M1 were forced by the moderate TSI amplitude. Furthermore, the NH averaged pre-industrial temperature anomaly in the Mann et al. (2009) reconstruction, which is used for the spatial comparison, and in HadCRUT4 is shown. Reconstructions and simulations are given as anomalies to the pre-industrial period 1600–1850. This allows for a direct comparison of the variability in the pre-industrial period despite the strong temperature trend from 1850 on. HadCRUT4 values are displayed relative to the value for the year 1850. All time series are decadal smoothed with a cubic-smoothing spline. Grey bars indicate the 30-yr periods covering the MM and the DM, which are used to calculate the temperature anomalies.

2.4. Transient climate simulations

In this section we present results from an ensemble of transient climate simulations performed with the AOCCM SOCOL-MPIOM for the periods 1600-2000. Three periods will be analysed in detail focusing on the surface air temperature (SAT): the early pre-industrial period with the two pronounced solar minima, namely the late Maunder Minimum (MM, 1670–1699) and the Dalton Minimum (DM, 1800–1829), and the industrial period (1850-2000), which is highly influenced by anthropogenic emissions of GHGs.

2.4.1. Temperature variability in the pre-industrial period

The NH mean temperature in the four transient simulations is compared to proxy reconstructions in Figure 2.8. The shading represent the probability range of the NH temperature variations based on multiple proxies (Jansen et al., 2007). Values are expressed as anomalies from the mean over the pre-industrial period 1600-1850. First the temperature variability in the pre-industrial period is assessed.

The simulations show both agreement and disagreement for certain periods. For the entire pre-industrial period, the simulations exhibit pronounced multi-decadal scale temperature variations. On a decadal scales, the influence of volcanic eruptions on these

Table 2.4.: NH temperature differences [K] for the late Maunder Minimum (1679–1699) relative to the two reference periods 1600–1629 and 1770–1799 and for the Dalton Minimum (1800–1829) relative to the period 1770–1799. "Reconstructions" refers to the temperature anomaly of the median of the reconstructed NH temperature anomalies in Jansen et al. (2007).

	1670/1699	1670/1699	1800/1829
	1600/1629	1770/1799	1770/1799
M1	-0.24	-0.48	-0.15
M2	-0.03	-0.35	-0.30
L1	-0.34	-0.54	-0.18
L2	-0.40	-0.36	-0.13
reconstructions	0.03	-0.15	-0.08

variations is large. In the 17th century, the first signal common in all simulations is a temperature increase from the year 1600 onwards, which is related to the recovery after the volcanic eruption in the first simulation year (1600, Huaynaputina). Also the eruption in the year 1641 (Parker) is clearly visible in the simulations and the reconstructions. From 1650 onwards the negative trend in the solar forcing, leading into the MM, becomes visible. The lowest MM values are reached approximately around the year 1700, but the variability between the simulations is large. Although the large solar forcing differences (up to 3 Wm^{-2}) are not visible for the lowest values of the MM, the effect of the solar forcing becomes apparent when the temperatures between the beginning and the end of the 17th century is compared (Table 2.4). For the first three versus the last three decades of the 17th century, the NH mean temperature is reduced by -0.34 K and -0.40 K in L1 and L2, respectively, and by -0.24 K and -0.03 K for M1 and M2, respectively. Contrary to the simulations, the MM is barely visible in the reconstruction as the so called Little Ice Age starts before the 17th century. Using a different approach, but a similar set of temperature proxies for the NH, Frank et al. (2010) identified the period 1601–1630 as the coldest 30 years of the last millennium. Consequently, no additional cooling can be found towards the end of the 17th century and the temperature differences between 1600–1629 and 1670–1699 is +0.03 K.

It should be mentioned that the temperature variations in the MM may also be influenced by the artificially stable 1600 AD conditions from the control run, which are used to initialize the transient simulations. This may result in an unrealistic climate state at the beginning of the 17th century that complicates the comparison with the reconstructions.

With the end of the MM the NH mean temperatures start to increase again, following the increasing trend in the radiative forcing from the sun. This increase is again larger compared to the reconstructions and suspended for multiple years by several volcanic eruptions. The most prominent example is the temperature reductions after the Katla eruption on Iceland (1755) and the eruption of Makian in Indonesia (1761), which cause a pronounced NH cooling for several years, although their total aerosol mass is relatively

small (Gao et al., 2008). For the post MM temperature increase, the differences between the two solar forcings are not very pronounced (Table 2.4) and for both solar forcings the temperature amplitudes are overestimated by a factor of 2 or larger, in comparison to the reconstructions.

From 1800 onwards, the solar energy input decreases again with the onset of the DM. This period is clearly dominated by the two volcanic eruptions 1809 (unknown) and 1815 (Tambora) as well as the eruption pair 1831 and 1835 (Babuyan Claro and Cosiguina). For the DM the differences in the two solar forcing reconstructions (up to 2.5 Wm^{-2}) are not reflected in the NH averaged temperatures and the agreement with the reconstructions is better.

The internal variability is an important factor that complicates the identification of the fingerprints of external forcings in the climate system. For climate models, the technique of ensemble simulations allows to extract the forcing signal. To reliably exclude any signal of internal variability, the number of simulations has to be sufficiently large. An ensemble size of 2 is clearly too small to get robust estimates of the signals caused by external forcings. Still, we average over each ensemble in the following to increase the signal-to-noise ratio. Using the two ensembles, L and M, we compare the spatial patterns for the MM and the DM against the patterns found in reconstructions. As reference period, which should represent an undisturbed pre-industrial situation relative to the two solar minima, the period 1770–1799 is selected. During these 30 years the solar irradiance values are very similar in both forcing datasets and also comparable to present day values (Fig. 2.1). Furthermore, no large volcanic eruption took place. For the solar minima, we select a 30-yr window roughly around the lowest TSI values, i.e. the period 1670–1699 for the late MM and the period 1800–1829 for the DM. Anomalies for these periods are compared to the spatial multi-proxy based temperature reconstructions of Mann et al. (2009).

The reconstructed temperatures during the MM are stronger reduced in the NH than in the SH, with the lowest temperatures over the North American continent and over northern Europe (Fig. 2.9 e). Weak positive anomalies are also found, but they are not significant. Similar to the hemispheric mean time series, the cooling signal during the MM is more pronounced in both ensembles (Fig. 2.9 a, b). The simulated MM temperature anomalies are almost everywhere negative and significant. For the L-forcing, the anomalies are slightly more pronounced than for the M-forcing, but the difference is small, which agrees with the findings for the hemispheric means (Table 2.4).

For the DM, the reconstructed temperature pattern is similar to the MM, with a larger cooling in the NH and the largest anomalies in North America and Scandinavia (Fig. 2.9 f). Overall the cooling is weaker than during the MM. The simulated patterns are less homogeneous and the differences between the two ensembles are larger (Fig. 2.9 c, d). Nevertheless, both ensembles resemble the cold anomalies of the reconstruction. Large areas of cold anomalies are found in the tropics and over the Barents Sea, where sea ice increases (not shown). Despite the cold anomalies, significant warmer conditions are found in the Labrador Sea (M-forcing) or the North Atlantic (L-forcing), which are not present in the reconstructions and may be related to internal variability of the ocean circulation or a response of the Atlantic meridional overturning to the volcanic forcing (e.g. Mignot et al., 2011). Overall the agreement to the reconstructions is better for the DM than for the MM, although for both periods the simulated temperature anomalies are more pronounced.

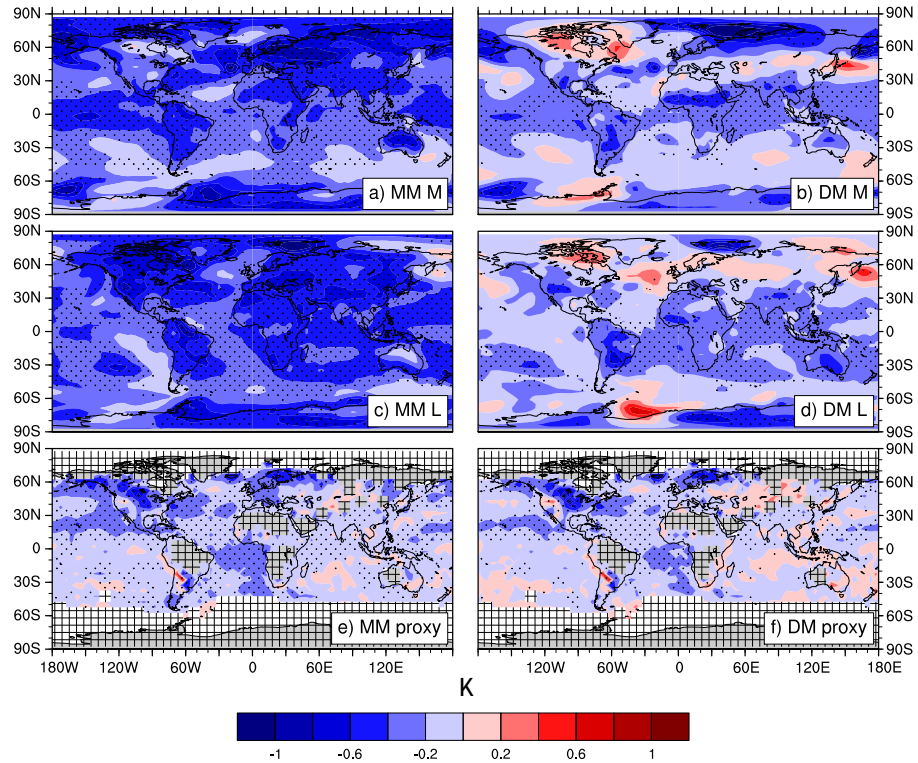


Figure 2.9.: Temperature differences for the Maunder Minimum (1670–1699, left, a,c,e) and the Dalton Minimum (1800–1829, right, b,d,f) with respect to the common reference period (1770–1799) for the ensemble average with medium solar amplitude (top, a,c), large solar amplitude (middle, b,d) and the spatial reconstruction of Mann et al. (2009) (bottom, e,f). Stippling: significant differences (Student’s t-test, $p \leq 0.05$).

Note that for the NH hemispheric average (Fig. 2.8) the centennial variations in Mann et al. (2009) are not very pronounced and represent mainly the median of Jansen et al. (2007).

Whereas the agreement during the DM is rather good, the MM temperature reductions are in the lowest probability range of the reconstructions. During the DM, temperature reductions are dominated by several volcanic eruptions, but the solar forcing reduction is less strong and shorter compared to the MM. Therefore, the influence of the solar variability is probably more pronounced during the MM and better separated from volcanic signals, than in the DM. For L1 and L2 the solar signal is obvious in both members during the MM. For M1 and M2 one member simulates nearly no cooling during the MM, despite a forcing reduction of up to 3 Wm^{-2} for several decades. This indicates that the internal variability of the climate system might compensate even large variations in the external forcing.

The relative contributions of the solar and the volcanic forcing for the temperature variations during the DM is difficult to extract from the transient experiments. However, using SOCOL-MPIOM Anet et al. (2013a, 2014) showed that the temperature reduction in the DM is mainly related to the variability in the visible part of the solar spectrum

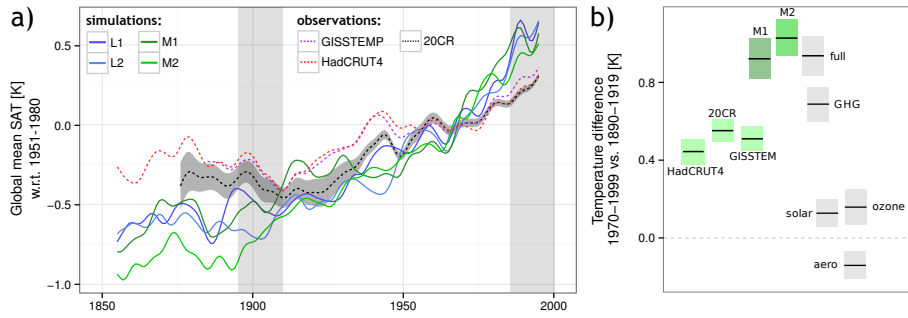


Figure 2.10.: (a) Global mean, annually averaged surface air temperature in the transient simulations and different observation based data sets. All time series are filtered by an 11 year low pass filter. For 20CR the ensemble spread (ensemble standard deviation) is indicated by the shaded area. All data sets are given as anomalies w.r.t. the period 1951 – 1980. (b) Average global mean temperature increase for the period 1970–1999 relative to 1890–1919 (highlighted by the grey regions in a). M1 and M2 refer to the two transient simulations with medium solar forcing amplitude. Bars indicate the average temperature difference between the two periods, gray boxes represent the 95% confidence intervals.

and volcanic eruptions. The UV variability is not important for the surface climate. The volcanic forcing cools the climate mainly in the tropics and is larger in the SH than in the NH, which is related to the asymmetric distribution of the aerosol cloud of the Tambora eruption.

2.4.2. Temperature trends after 1850

A significant anthropogenic influence on the global mean temperature starts at the latest with the beginning of the industrialization, i.e., approximately since the mid of the 19th century. Moreover, a sufficient number of instrumental based weather observations are available since the mid 19th century so that it is possible to derive global mean surface temperatures (Brohan et al., 2006; Hansen et al., 2010) or to apply them in data assimilation projects (Compo et al., 2011). For a climate model, the ability to reproduce these observed temperature trends is crucial. Therefore, the simulated temperature development since 1850 in the four transient simulations with SOCOL-MPIOM is described in the following.

Transient simulations

In the following the simulated surface air temperatures are compared to the observational data sets GISTEM and HadCRUT4 and to the 20th century reanalysis (20CR).

The global mean surface air temperature (SAT) increase is very similar in the two instrumental records and in the reanalysis (Fig. 2.10 a). Before 1900 no positive trend is visible in the global mean SAT. In all records, the temperature increase of the 20th century is not continuous, but rather divided in two periods. The first increase is found between 1910 until 1940. This period is known as the early 20th century warming (Brönnimann, 2009). In 20CR this increase starts at the same time, but is slightly weaker.

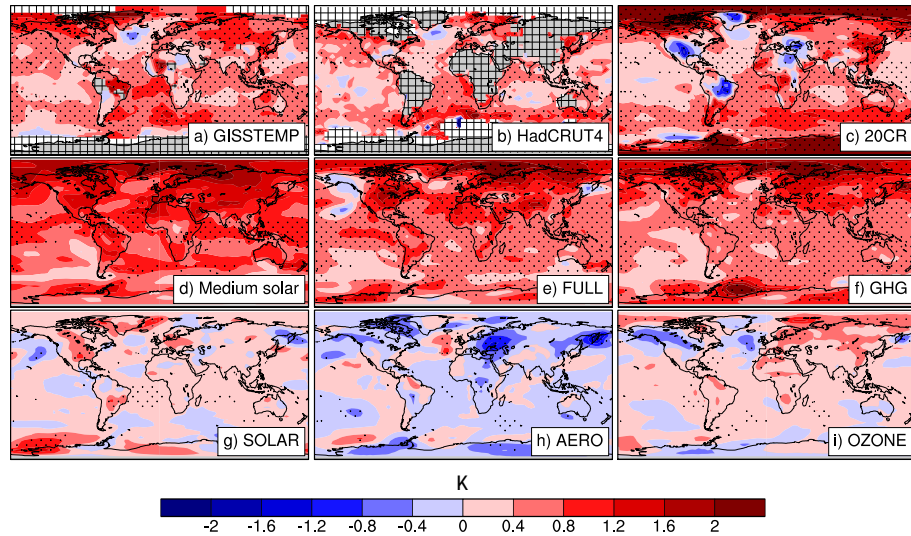


Figure 2.11.: Surface air temperature difference [K] between the two 30-yr periods 1890-1919 and 1970-1999 for different data sets and simulations. Top: observational data sets (a) GISSTEMP, (b) HadCRUT4, (c) 20CR. Middle and bottom: model experiments (d) medium solar - ensemble average (e) full forcing sensitivity run, (f) GHG only, (g) solar only, (h) aerosols only, and (i) ozone only. Stippling: significant differences using a Students t-test ($p \leq 0.05$) and taking auto-correlation into account. For (a) GISSTEMP and (b) HadCRUT4 missing values are indicated by the cross pattern.

After 1940 the global mean temperature rise is reduced or even suspended for about two decades. Finally, from 1960 onwards a clearly positive temperature trend is found in all data sets. In the instrumental records the temperature increase in the first half of the 20th century and the cold period around 1950 are more pronounced than in 20CR.

The simulated mean SAT increase since 1850 is much stronger in all transient simulations than in the observations. From around 1900 onwards temperatures increase more or less linear, with a slight acceleration after 1960. The surface temperature trends are very similar in all four experiments. In particular, no substantial difference between model results obtained with medium and large amplitude solar forcing is found, although the difference in the increase in the TSI values during the 20th century is up to 1.7 Wm^{-2} (TOA). However, in the ocean heat uptake, the difference between the two forcings is clearly visible. Furthermore, stronger increases in the outgoing longwave radiation in the L simulations partly compensate the forcing difference. To reduce complexity, we concentrate on the medium solar forcing amplitude simulations in the following.

The pattern of the temperature changes might help to identify differences to the observed records. Furthermore, regions with pronounced temperature increase that may be associated with positive feedbacks can be identified. Therefore, we compare the temperature difference between a 30-yr period at the beginning (1890-1919) and at the end of the 20th century (1970-1999). The results are however not sensitive to the exact choice of the periods and a trend pattern analysis also leads to similar results.

A comparison of the pattern of the SAT increase in the 20th century is given in Figure 2.11. In the observations significant positive temperature changes can be found over

the entire globe, interrupted by regions without any changes or significant temperature reductions. Over the oceans a warming is obvious almost everywhere. The largest temperature increases are found in the Southern Ocean at mid latitudes, reaching around 2 K/100yr. In general differences between the records are small over the ocean. This is to some degree expected, since, e.g., 20CR used the same SST records (HadSST) as HadCRUT4 as lower boundary condition. Over the continent, the pattern is spatially more heterogeneous, but regions with significant positive temperature increases are found on all continents. In 20CR regions with temperature reductions are more pronounced than in the other two records.

In comparison to HadCRUT4 and GISTEMP the changes in the southern and in particular in the northern polar region are much stronger in 20CR. For 20CR it is known that the Arctic temperature field suffers from a large, time-varying bias (Brönnimann et al., 2012) and an incorrect sea-ice distribution (Compo et al., 2011). However, also HadCRUT4 and GISTEMP are affected by a very low spatial and temporal coverage of instrumental based observations in these regions. These caveats should be considered when comparing trend estimates for the NH and SH polar regions.

In the simulations the strong signal in the global mean temperature is also apparent in the spatial pattern. The warming is too strong in many regions, and spatially very uniform. In the northern polar region, some signals of polar amplification can be found. However, the differences in the global average are related to a strong and uniform warming over the entire globe and not to an overestimated polar amplification.

The spatially uniform warming may be related to a specific forcing like GHG or solar. The TCR of 2.2 K suggests a stronger temperature increase due to the anthropogenic GHG emissions in the 20th century. Contrary, results from Anet et al. (2013b) showed that the model response to the future GHG increase (RCP 4.5) is comparable to other CMIP5 models. In their experiments the temperature increase at the end of the 21st century (1.96 ± 0.12 K) is well in the range of the CMIP5 ensemble (1.8 ± 0.5 K, e.g., Knutti and Sedláček (2012)). Therefore, other forcings may contribute to the trend in the 20th century and amplify it.

Sensitivity to separated external forcings

The role of different forcings for the temperature trends since 1850 is evaluated using a number of sensitivity simulations where one external forcing or a combination of forcings is applied and the remaining forcings are held constant at pre-industrial levels (Table 2.1).

In doing so, the major GHGs, the solar activity, stratospheric and tropospheric aerosols and simulated ozone changes are investigated. In the troposphere, ozone concentration in general increased (Stevenson et al., 2013), whereas they are reduced by the emission of ozone depleting halogens in the stratosphere (Stachelin et al., 2001). Both changes have different effects on the radiation balance.

The contributions of the different forcings to the temperature trends is assessed by comparing the differences in the global mean temperatures between the two 30-yr periods defined above (1890-1919 and 1970-1999). The results are again not very sensitive to the exact choice of these periods.

In the full forcing experiment the mean temperature increase agrees well with the in-

creases found in the two transient simulations (Fig. 2.10 b). This gives us confidence, that the setup of the sensitivity experiments is able to reproduce the temperature behaviour, when all major forcings are considered. The major part of the temperature increase simulated by all forcings is explained by the GHG forcing (73 %). The solar forcing (13 %) and the ozone trends (16 %) also contribute to the warming. The only negative signal (-15 %) is related to stratospheric and tropospheric aerosols. All individual forcings (solar, ozone, GHG, aerosols) add up to only 87 % of the full forcing experiment, suggesting that additional positive feedbacks are involved in the case of the full forcing experiment (e.g., sea ice albedo feedback).

To analyse the spatial structure of the global mean temperature differences, we compare again the difference pattern between the two 30-yr periods (Fig. 2.11). The warming is globally very uniform with some hints for polar amplifications in the northern high latitudes. This full forcing pattern is very similar to the changes of the GHG experiment, except for an overall larger trend. As in the global analysis, the GHG forcing dominates the full-forcing trend almost everywhere. The other three forcings display a much larger spatial heterogeneity and temperature changes are comparably small. The solar forcing, which, on global average, leads to a warming of approximately 0.13 K, has slightly significant contributions, e.g., over northern America, Greenland and Europa. Over Europe and North America the contributions from the solar forcing are clearly visible in the full forcing experiment. Further significant temperature increases are found in the tropical Atlantic and Indian Ocean. The aerosol forcing, which combines the influence of tropospheric and stratospheric aerosols, leads to significant negative temperature changes in the tropical continental areas of the SH and over a large region covering Russia and East Asia. Furthermore, a significant positive influence is found for the North Atlantic. Finally, the simulation forced by transient ozone changes reveals a significant and pronounced positive temperature increase in the NH high latitudes, which peaks over the Barents Sea. In the SH high latitudes, no comparable signal is found. Overall, several regions of significant positive temperature increases are associated with the ozone forcing.

The solar forcing used in the experiments accounts for an increase in the net radiative forcing (RF) of 0.28 Wm^{-2} (global average assuming a global mean albedo of 0.7), between the periods defined above. In the historical CMIP5 simulations the corresponding forcing difference is only 0.09 Wm^{-2} (Lean, 2000; Wang et al., 2005). For the same periods, the RF from tropospheric ozone changes is estimated to be $0.4 \pm 0.2 \text{ Wm}^{-2}$ (Myhre et al., 2013). The positive RF from tropospheric ozone is further compensated to some extent by the negative forcing from stratospheric ozone depletion, estimated to be around $-0.05 \pm 0.1 \text{ Wm}^{-2}$ (Myhre et al., 2013). The combined RF from CO_2 , CH_4 , and N_2O (Ramaswamy et al., 2001), is 1.20 Wm^{-2} between 1989–1919 and 1970–1999.

Based on the RF and the temperature response ΔT we estimate a transient sensitivity parameter α [K/Wm^{-2}], with $\alpha = \Delta T/\text{RF}$, for the three forcings. Values of α are estimated as 0.46 ± 0.25 , 0.46 ± 0.25 and $0.58 \pm 0.08 \text{ K/Wm}^{-2}$ for the solar, ozone (net RF: 0.30 Wm^{-2}), and GHG experiment, respectively. The confidence interval is based on the 95% confidence interval for the temperature response ΔT only. Note that the estimate is associated with further uncertainties related to the RF, in particular for ozone, and that ΔT is extracted from a single simulation. The analysis, thus, shows that the temperature response associated with the different forcings is consistent and the resulting signal is a combination of the climate sensitivity of SOCOL-MPIOM, the large solar forcing and the inclusion of the additional RF from the ozone chemistry.

2.5. Discussion and Conclusions

This paper presents the coupled atmosphere-chemistry-ocean model SOCOL-MPIOM. The model is described using results from a number of simulations without changes in the external forcings (control simulations) and with transient external forcings for the period 1600-2000 AD.

Without changing external forcings the influence of the interactive chemistry module on the mean climate state and its variability is small and mainly confined to the stratosphere and mesosphere. The largest differences in the temperatures in the middle atmosphere are associated with several processes. First, the parametrization of the absorption in the Lyman-alpha, Schumann-Runge, Hartley, and Higgins bands is responsible for a warmer mesosphere and higher stratosphere in the simulation with interactive chemistry. This parametrization is disabled in the configuration without interactive chemistry, but will be implemented in future version. Second, interactions between the diurnal variation in the mesospheric ozone concentrations and the radiation scheme lead to a cooling, partly compensating the aforementioned warming. Furthermore, stratospheric water vapour concentrations are higher with interactive chemistry due to the additional water vapour produced by the oxidation of methane in the chemistry module. Future version of the model configuration should therefore implement a parametrization of this process, e.g., similar to the approach in ECHAM 6 (Schmidt et al., 2013).

In the transient simulations for the period 1600-2000 the spectral solar forcing reconstructions of Shapiro et al. (2011) is tested and the simulations are compared to temperature reconstructions. To consider the uncertainty in the solar forcing, two different solar forcing data sets with large amplitude (corresponding to the mean forcing provided by Shapiro et al. (2011)) and a medium amplitude (upper uncertainty envelope) are used. Both amplitudes are substantially larger than previous state-of-the-art solar forcing reconstructions. For the MM, the temperature response is in general larger than the signal found in reconstructions, whereas the agreement between proxies and simulations for the DM is better. The larger differences between reconstructions and model results in the MM may be related either to the MM being still affected by the model spin-up period or to the large amplitude of the solar forcing, with considerably larger variations than all other recent solar forcing reconstructions. During the DM, the period of reduced solar activity is shorter than during the MM and the solar effect is weaker. Instead, the volcanic forcing is the dominant driver for the surface temperature change.

The temperature variations in the transient simulations are always subject to internal variability and the influence of the solar forcing is therefore not directly visible in the hemispheric averages or the global mean for every solar minima. Likewise, the differences between the medium and the large amplitude solar forcing are not always obvious. However, when the difference in the NH temperature between the simulations with medium and large solar forcing is calculated for all solar minima and maxima, the influence of the solar forcing becomes visible. Between 1600 and 2000, the sun went through three grand solar minima (MM, DM, and Gleisberg minima) and four periods of higher solar activity. The temperature change for each of these periods, i.e., the temperature change from a solar minima to the following maxima or a maxima to the following minima, is significantly influenced by the TSI, except for the temperature reduction into the DM and the increase after the Gleisberg minimum. In these two cases strong other forcings, large volcanic eruption in the DM and the GHG increase after the Gleisberg minimum,

dominate over the solar forcing. Averaged and normalized over all periods the simulated NH temperature change resulting from a change in the TSI is 0.06 K/Wm^{-2} . When the two periods mentioned above are excluded, the response increases to 0.11 K/Wm^{-2} .

With a transient climate response (TCR) of 2.2 K and an equilibrium climate sensitivity (ECS) of 3.7 K the sensitivity of SOCOL-MPIOM is on the higher side of the CMIP5 ensemble, but comparable to the related ECHAM5-MPIOM. The high sensitivity may also be influenced by the warm climate state used for the CO_2 perturbation experiments. The experiments are initialized using restart files for the year 1990 from the transient simulations. These transient runs are affected by a persistent positive temperature drift from the control simulation and an overestimation of the 20th century temperature increase. The climate state at the beginning of the CS experiments is therefore clearly too warm. Although the ECS is commonly assumed to be independent of the climate state, Meraner et al. (2013) showed that the climate state indeed has an influence on the ECS. In warmer climates, the ECS increases due to a stronger water vapour feedback.

The influence of the interactive chemistry on the TCR is very small but negative ($\sim -0.1 \text{ K}$). This is in agreement with results from Dietmüller et al. (2014). With the ECHAM/MESSy Atmospheric Chemistry (EMAC) model they found a reduction of the climate sensitivity parameter by 3.4% with interactive chemistry in the case of a (instantaneous) double CO_2 scenario. The reduction is explained by negative feedbacks introduced by the ozone chemistry with influences on the stratospheric water vapour. However, contrary to Dietmüller et al. (2014) who explained the feedback by reduction of the ozone concentrations in the lower tropical stratosphere of up to 20%, the reductions in our experiments is much smaller ($< 1 \%$).

In the industrial period, the climate sensitivity of the model in combination with the solar and the forcing from the ozone changes results in an overestimation of the temperature trends up to a factor of 2. Contrary to the solar forcing proposed for CMIP5 (Lean, 2000; Wang et al., 2005) and many other TSI reconstructions, the forcing of Shapiro et al. (2011) used in the transient simulations shows a strong increase in the radiative forcing from the sun in the first half of the 20th century. This increase is not within the confidence interval for the TSI changes presented in the last IPCC report (Myhre et al., 2013).

An additional positive signal comes from the simulated increase in the tropospheric ozone concentrations that also contribute to the global mean temperature trend. Estimates for the changes in global tropospheric ozone since pre-industrial times are rare and largely based on model simulations (Myhre et al., 2013). In comparison to other models the simulated tropospheric global ozone increase is stronger in this study. While SOCOL-MPIOM simulates increases in the order of 15 DU between the beginning and the end of the 20th century, Shindell et al. (2006) estimated an increase of around 10 DU. In a multi-model study with 17 different chemistry-climate models, Stevenson et al. (2013) found an increase of 8.4 DU between the 1850th and 2000th. Consequently, the effect on the temperature trends is larger, being 0.16 K in this study and $\sim 0.10 \text{ K}$ in the simulation with the GISS model II (Shindell et al., 2006). However, the chemistry in the GISS model II is limited to levels below 150 hPa and parts of the tropical upper troposphere are not included. This may result in an underestimation of the effect by 20%, as discussed by the authors (Shindell et al., 2006).

When only the radiative forcing from GHGs and the negative contributions from the

aerosols are considered, the simulated warming would agree reasonably well with the observations. With the additional forcings used here, either the climate sensitivity of SOCOL-MPIOM would need to be lower or possible missing negative forcings would need to be included to match the observed temperature trends.

Despite the lack of a full understanding of the strong transient climate response and equilibrium climate sensitivity of the new model, with the coupling of SOCOL-MPIOM a novel atmosphere-chemistry-ocean model has been developed that allows the inclusion of chemistry-climate feedbacks in long-term simulations for the past and the future. Furthermore, with a configuration that allows the deactivation of the chemistry scheme the influence of the chemistry-climate feedbacks in the climate can be assessed. Earlier studies with SOCOL-MPIOM highlighted the relevance of the atmospheric chemistry in climate model simulations (Anet et al., 2013a, 2014, 2013b; Muthers et al., 2014). Under conditions without a change in the external forcings, the influence of the interactive chemistry on the climate state is small. Future work will concentrate on the role of chemistry-climate feedbacks under changing external forcings.

acknowledgements The authors thank the Max-Planck Institute for Meteorology in Hamburg, Germany, in particular Johann Jungclaus and Helmuth Haak, for providing the restart files from the Millennium Simulations and the technical support. This work has been supported by the Swiss National Science Foundation under grant CRSI122-130642 (FUPSOL), CRSII2-147659 (FUPSOL II) and under grant CRSI22-130642 21 (FuMES), as well as by the CCES project MAIOLICA-2. ER and WS would like to acknowledge the support of the project by State Secretariat for Education, Research and Innovation (SERI) of Swiss Confederation under the grant C11.01124 (project SOVAC). ECMWF ERA-40 data used in this study have been obtained from the ECMWF Data Server. This paper profited from discussions during the PAGES/FUPSOL Workshop in 2012.

Bibliography

- Andrews, T., Gregory, J. M., Webb, M. J., and Taylor, K. E.: Forcing, feedbacks and climate sensitivity in CMIP5 coupled atmosphere-ocean climate models, *Geophys. Res. Lett.*, 39, L09 712, doi:10.1029/2012GL051607, 2012.
- Anet, J. G., Muthers, S., Rozanov, E., Raible, C. C., Peter, T., Stenke, A., Shapiro, A. I., Beer, J., Steinhilber, F., Brönnimann, S., Arfeuille, F., Brugnara, Y., and Schmutz, W. K.: Forcing of stratospheric chemistry and dynamics during the Dalton Minimum, *Atmos. Chem. Phys.*, 13, 10 951–10 967, doi:10.5194/acp-13-10951-2013, 2013a.
- Anet, J. G., Rozanov, E. V., Muthers, S., Peter, T., Brönnimann, S., Arfeuille, F., Beer, J., Shapiro, A. I., Raible, C. C., Steinhilber, F., and Schmutz, W. K.: Impact of a potential 21st century “grand solar minimum” on surface temperatures and stratospheric ozone, *Geophys. Res. Lett.*, 40, 4420–4425, doi:10.1002/grl.50806, 2013b.
- Anet, J. G., Muthers, S., Rozanov, E. V., Raible, C. C., Stenke, A., Shapiro, A. I., Brönnimann, S., Arfeuille, F., Brugnara, Y., Beer, J., Steinhilber, F., Schmutz, W., and Peter, T.: Impact of solar vs. volcanic activity variations on tropospheric temperatures and precipitation during the Dalton Minimum, *Climate of the Past*, 10, 921–938, doi:10.5194/cp-10-921-2014, 2014.
- Arfeuille, F., Weisenstein, D., Mack, H., Rozanov, E., Peter, T., and Brönnimann, S.: Volcanic forcing for climate modeling: a new microphysics-based data set covering years 1600–present, *Climate of the Past*, 10, 359–375, doi:10.5194/cp-10-359-2014, 2014.
- Baldwin, M. P. and Dunkerton, T. J.: Propagation of the Arctic Oscillation from the stratosphere to the troposphere, *J. Geophys. Res.*, 104, 30 937–30 946, doi:10.1029/1999JD900445, 1999.
- Baldwin, M. P. and Dunkerton, T. J.: Stratospheric harbingers of anomalous weather regimes., *Science*, 294, 581–4, doi:10.1126/science.1063315, 2001.
- Baldwin, M. P., Cheng, X., and Dunkerton, T. J.: Observed correlations between winter-mean tropospheric and stratospheric circulation anomalies, *Geophys. Res. Lett.*, 21, 1141–1144, 1994.
- Baldwin, M. P., Dameris, M., and Shepherd, T. G.: How will the stratosphere affect climate change?, *Science*, 316, 1576–1577, 2007.
- Baumgaertner, A. J. G., Jöckel, P., and Brühl, C.: Energetic particle precipitation in ECHAM5/MESy1 - Part 1: Downward transport of upper atmospheric NO_x produced by low energy electrons, *Atmos. Chem. Phys.*, 9, 2729–2740, doi:10.5194/acp-9-2729-2009, 2009.
- Breiteig, T.: Extra-tropical synoptic cyclones and downward propagating anomalies in the Northern Annular Mode, *Geophys. Res. Lett.*, 35, L07 809, doi:10.1029/2007GL032972, 2008.
- Brohan, P., Kennedy, J. J., Harris, I., Tett, S. F. B., and Jones, P. D.: Uncertainty estimates in regional and global observed temperature changes: A new data set from 1850, *J. Geophys. Res.*, 111, D12 106, doi:10.1029/2005JD006548, 2006.
- Brönnimann, S.: Early twentieth-century warming, *Nature Geoscience*, 2, 735–736, doi:10.1038/ngeo670, 2009.
- Brönnimann, S., Annis, J. L., Vogler, C., and Jones, P. D.: Reconstructing the Quasi-Biennial Oscillation back to the early 1900s, *Geophys. Res. Lett.*, 34, L22 805, doi:10.1029/2007GL031354, 2007.
- Brönnimann, S., Grant, A. N., Compo, G. P., Ewen, T., Griesser, T., Fischer, A. M., Schraner, M., and Stickler, A.: A multi-data set comparison of the vertical structure of temperature variability and change over the Arctic during the past 100 years, *Climate Dyn.*, 39, 1577–1598, doi:10.1007/s00382-012-1291-6, 2012.
- Budich, R., Gioletta, M., Jungclaus, J., Redler, R., and Reick, C.: The MPI-M Millennium Earth System Model: An assembling guide for the COSMOS configuration, MPI report, Max-Planck Institute for Meteorology, Hamburg, Germany, 2010.

- Cagnazzo, C., Manzini, E., Giorgetta, M. A., Forster, P. M. D. F., and Morcrette, J. J.: Impact of an improved shortwave radiation scheme in the MAECHAM5 General Circulation Model, *Atmos. Chem. Phys.*, 7, 2503–2515, doi:10.5194/acp-7-2503-2007, 2007.
- Calisto, M., Usoskin, I., Rozanov, E., and Peter, T.: Influence of galactic cosmic rays on atmospheric composition and dynamics, *Atmos. Chem. Phys.*, 11, 4547–4556, doi:10.5194/acp-11-4547-2011, 2011.
- Charlton, A. J. and Polvani, L. M.: A new look at stratospheric sudden warmings. Part I: Climatology and modeling benchmarks, *J. Climate*, 20, 449–470, 2007.
- Compo, G. P., Whitaker, J. S., Sardeshmukh, P. D., Matsui, N., Allan, R. J., Yin, X., Gleason, B. E., Vose, R. S., Rutledge, G., Bessemoulin, P., Brönnimann, S., Brunet, M., Crouthamel, R. I., Grant, A. N., Groisman, P. Y., Jones, P. D., Kruk, M. C., Kruger, A. C., Marshall, G. J., Maugeri, M., Mok, H. Y., Nordli, O., Ross, T. F., Trigo, R. M., Wang, X. L., Woodruff, S. D., and Worley, S. J.: The Twentieth Century Reanalysis project, *Quart. J. Roy. Meteor. Soc.*, 137, 1–28, doi:10.1002/qj.776, 2011.
- Cordero, E. C. and Forster, P. M. D. F.: Stratospheric variability and trends in models used for the IPCC AR4, *Atmos. Chem. Phys.*, 6, 5369–5380, 2006.
- Cubasch, U., Meehl, G., Boer, G., Stouffer, R., Dix, M., Noda, A., Senior, C., Raper, S., Yap, K., Abe-Ouchi, A., Brinkop, S., Claussen, M., Collins, M., Evans, J., Fischer-Bruns, I., Flato, G., Fyfe, J., Ganopolski, A., Gregory, J., Hu, Z.-Z., Joos, F., Knutson, T., Knutti, R., Landsea, C., Mearns, L., Milly, C., Mitchell, J., Nozawa, T., Paeth, H., Räisänen, J., Sausen, R., Smith, S., Stocker, T., Timmermann, A., Ulbrich, U., Weaver, A., Wegner, J., Whetton, P., Wigley, T., Winton, M., and Zwiers, F.: Projections of future climate change, in: *Climate Change 2001: The Scientific Basis*, pp. 525–582, Cambridge University Press, 2001.
- Dee, D. P., Uppala, S. M., Simmons, A. J., Berrisford, P., Poli, P., Kobayashi, S., Andrae, U., Balmaseda, M. A., Balsamo, G., Bauer, P., Bechtold, P., Beljaars, A. C. M., van de Berg, L., Bidlot, J., Bormann, N., Delsol, C., Dragani, R., Fuentes, M., Geer, A. J., Haimberger, L., Healy, S. B., Hersbach, H., Hólm, E. V., Isaksen, L., Kållberg, P., Köhler, M., Matricardi, M., McNally, A. P., Monge-Sanz, B. M., Morcrette, J.-J., Park, B.-K., Peubey, C., de Rosnay, P., Tavolato, C., Thépaut, J.-N., and Vitart, F.: The ERA-Interim reanalysis: Configuration and performance of the data assimilation system, *Quart. J. Roy. Meteor. Soc.*, 137, 553–597, doi:10.1002/qj.828, 2011.
- Dietmüller, S., Ponater, M., and Sausen, R.: Interactive ozone induces a negative feedback in CO₂ driven climate change simulations, *J. Geophys. Res.*, 119, 1796–1805, doi:10.1002/2013JD020575, 2014.
- Driscoll, S., Bozzo, A., Gray, L. J., Robock, A., and Stenchikov, G.: Coupled Model Inter-comparison Project 5 (CMIP5) simulations of climate following volcanic eruptions, *J. Geophys. Res.*, 117, D17 105, doi:10.1029/2012JD017607, 2012.
- Egorova, T., Rozanov, E., Zubov, V., and Karol, I. L.: Model for investigating ozone trends (MEZON), *Izvestiya, Atmospheric and Oceanic Physics*, 39, 277–292, 2003.
- Egorova, T., Rozanov, E., Manzini, E., Schmutz, W., and Peter, T.: Chemical and dynamical response to the 11-year variability of the solar irradiance simulated with a chemistry-climate model, *Geophys. Res. Lett.*, 31, 6225–6230, doi:10.1029/2003GL019294, 2004.
- Etheridge, D., Steele, L., Langenfelds, R., Francey, R., Barnola, J., and Morgan, V.: Natural and anthropogenic changes in atmospheric CO₂ over the last 1000 years from air in Antarctic ice and firn, *J. Geophys. Res.*, 101, 4115–4128, doi:10.1029/95JD03410, 1996.
- Etheridge, D. M., Steele, L. P., Francey, R. J., and Langenfelds, R. L.: Atmospheric methane between 1000 A.D. and present: Evidence of anthropogenic emissions and climatic variability, *J. Geophys. Res.*, 103, 15 979–15 993, doi:10.1029/98JD00923, 1998.
- Eyring, V., Butchart, N., Waugh, D. W., Akiyoshi, H., Austin, J., Bekki, S., Bodeker, G. E., Boville, B. A., Brühl, C., Chipperfield, M. P., Cordero, E., Dameris, M., Deushi, M., Fioletov, V. E., Frith, S. M., Garcia, R. R., Gettelman, A., Giorgetta, M. A., Grewe, V., Jourdain,

- L., Kinnison, D. E., Mancini, E., Manzini, E., Marchand, M., Marsh, D. R., Nagashima, T., Newman, P. A., Nielsen, J. E., Pawson, S., Pitari, G., Plummer, D. A., Rozanov, E., Schraner, M., Shepherd, T. G., Shibata, K., Stolarski, R. S., Struthers, H., Tian, W., and Yoshiki, M.: Assessment of temperature, trace species, and ozone in chemistry-climate model simulations of the recent past, *J. Geophys. Res.*, 111, D22 308, doi:10.1029/2006JD007327, 2006.
- Ferretti, D. F., Miller, J. B., White, J. W. C., Etheridge, D. M., Lassey, K. R., Lowe, D. C., Meure, C. M. M. F., Dreier, M. F., Trudinger, C. M., Van Ommen, T. D., and Langenfelds, R. L.: Unexpected changes to the global methane budget over the past 2000 years, *Science*, 309, 1714–1717, doi:10.1126/science.1115193, 2005.
- Fischer, A. M., Schraner, M., Rozanov, E., Kenzelmann, P., Schnadt Poberaj, C., Brunner, D., Lustenberger, A., Luo, B. P., Bodeker, G. E., Egorova, T., Schmutz, W., Peter, T., Brönnimann, S., and Onnimann: Interannual-to-decadal variability of the stratosphere during the 20th century: ensemble simulations with a chemistry-climate model, *Atmos. Chem. Phys.*, 8, 7755–7777, 2008.
- Flato, G., Marotzke, J., Abiodun, B., Braconnot, P., Chou, S., Collins, W., Cox, P., Driouech, F., Emori, S., Eyring, V., Forest, C., Gleckler, P., Guilyardi, E., Jakob, C., Kattsov, V., Reason, C., and Rummukainen, M.: Evaluation of climate models, in: *Climate Change 2013: The Physical Science Basis. Contribution of Working Group I to the Fifth Assessment Report of the Intergovernmental Panel on Climate Change*, edited by Stocker, T., Qin, D., Plattner, G.-K., Tignor, M., Allen, S., Boschung, J., Nauels, A., Xia, Y., Bex, V., and Midgley, P., chap. 6, pp. 741–866, Cambridge University Press, Cambridge, United Kingdom and New York, NY, USA, 2013.
- Fouquart, Y. and Bonnel, B.: Computations of solar heating of the Earth’s atmosphere: A new parameterization, *Beitr. Phys. Atmos.*, 53, 35–62, 1980.
- Frank, D. C., Esper, J., Raible, C. C., Büntgen, U., Trouet, V., Stocker, B., and Joos, F.: Ensemble reconstruction constraints on the global carbon cycle sensitivity to climate., *Nature*, 463, 527–30, doi:10.1038/nature08769, 2010.
- Gabriel, A., Peters, D., Kirchner, I., and Graf, H.-F.: Effect of zonally asymmetric ozone on stratospheric temperature and planetary wave propagation, *Geophys. Res. Lett.*, 34, L06 807, doi:10.1029/2006GL028998, 2007.
- Gao, C., Robock, A., and Ammann, C.: Volcanic forcing of climate over the past 1500 years: An improved ice core-based index for climate models, *J. Geophys. Res.*, 113, D23 111, doi:10.1029/2008JD010239, 2008.
- Gerber, E. P., Butler, A., Calvo, N., Charlton-Perez, A., Giorgetta, M., Manzini, E., Perlwitz, J., Polvani, L. M., Sassi, F., Scaife, A. A., Shaw, T. A., Son, S.-W., and Watanabe, S.: Assessing and understanding the impact of stratospheric dynamics and variability on the earth system, *Bull. Amer. Meteor. Soc.*, 93, 845–859, doi:10.1175/bAms-d-11-00145.1, 2012.
- Gillett, N. P. and Thompson, D. W. J.: Simulation of recent southern hemisphere climate change., *Science*, 302, 273–5, doi:10.1126/science.1087440, 2003.
- Gillett, N. P., Allen, M. R., McDonald, R. E., Senior, C. A., Shindell, D. T., and Schmidt, G. A.: How linear is the Arctic Oscillation response to greenhouse gases?, *J. Geophys. Res.*, 107, 1–7, doi:10.1029/2001JD000589, 2002.
- Giorgetta, M. A., Bengtsson, L., and Arpe, K.: An investigation of QBO signals in the east Asian and Indian monsoon in GCM experiments, *Climate Dyn.*, 15, 435–450, doi:10.1007/s003820050292, 1999.
- Graf, H. F., Kirchner, I., Robock, A., and Schult, I.: Pinatubo eruption winter climate effects: Model versus observations, *Climate Dyn.*, 92, 81–93, 1993.
- Graversen, R. G. and Christiansen, B.: Downward propagation from the stratosphere to the troposphere: A comparison of the two hemispheres, *J. Geophys. Res.*, 108, 1–10, doi:10.1029/2003JD004077, 2003.

- Gray, L. J., Scaife, A. A., Mitchell, D. M., Osprey, S., Ineson, S., Hardiman, S. C., Butchart, N., Knight, J., Sutton, R., and Kodera, K.: A lagged response to the 11-year solar cycle in observed winter Atlantic/European weather patterns, *J. Geophys. Res.*, 24, 13,405–13,420, doi:10.1002/2013JD020062, 2013.
- Gregory, J. M., Ingram, W. J., Palmer, M. A., Jones, G. S., Stott, P. A., Thorbe, R. B., Lowe, J. A., Johns, T. C., and Williams, K. D.: A new method for diagnosing radiative forcing and climate sensitivity, *Geophys. Res. Lett.*, 31, L03 205, doi:10.1029/2003GL018747, 2004.
- Hagemann, S.: An improved land surface parameter dataset for global and regional climate models, MPI report 336, Max-Planck Institut fuer Meteorologie, Hamburg, Germany, 2002.
- Hagemann, S. and Duemenil, L.: A parameterisation of the lateral waterflow for the global scale, *Clim. Dyn.*, 14, 17–31, 1998.
- Hagemann, S. and Duemenil-Gates, L.: Improving a subgrid runoff parameterisation scheme for climate models by the use of high resolution data derived from satellite observations, *Clim. Dyn.*, 21, 349–359, 2003.
- Haigh, J. D.: The role of stratospheric ozone in modulating the solar radiative forcing of climate, *Nature*, 370, 544–546, 1994.
- Haigh, J. D.: The impact of solar variability on climate, *Science*, 272, 981–984, 1996.
- Haigh, J. D., Blackburn, M., and Day, R.: The response of tropospheric circulation to perturbations in lower-stratospheric temperature, *J. Climate*, 18, 3672–3685, 2005.
- Hansen, J., Ruedy, R., Sato, M., Lo, K., Met Office, and Hadley Center: Global surface temperature change, *Rev. Geophys.*, 48, 1–29, doi:10.1029/2010RG000345, 2010.
- Hardiman, S. C., Butchart, N., Hinton, T. J., Osprey, S. M., and Gray, L. J.: The effect of a well-resolved stratosphere on surface climate: Differences between CMIP5 simulations with high and low top versions of the Met Office Climate Model, *J. Climate*, 25, 7083–7099, doi:10.1175/JCLI-D-11-00579.1, 2012.
- Hoyle, C. R.: Three dimensional chemical transport model study of ozone and related gases 1960–2000, Ph.D. thesis, Eidgenössische Technische Hochschule, Zürich, Switzerland, 2005.
- Hu, Y. and Tung, K. K.: Possible ozone-induced long-term changes in planetary wave activity in late winter, *J. Climate*, 16, 3027–3038, 2003.
- Hurrell, J. W.: Decadal trends in the North Atlantic Oscillation: Regional temperatures and precipitation, *Science*, 269, 676–679, 1995.
- Jackman, C. H., Marsh, D. R., Vitt, F. M., Garcia, R. R., Randall, C. E., Fleming, E. L., and Frith, S. M.: Long-term middle atmospheric influence of very large solar proton events, *Journal of Geophysical Research: Atmospheres*, 114, 304, doi:10.1029/2008JD011415, 2009.
- Jansen, E., Overpeck, J., Briffa, K. R., Duplessy, J.-C., Joos, F., Masson-Delmotte, V., Olago, D., Otto-Bliesner, B., Peltier, W., Rahmstorf, S., Ramesh, R., Raynaud, D., Rind, D., Solomina, O., Villalba, R., Zhang, D., Trenberth, K. E., Jones, P. D., Ambenje, P., Bojariu, R., Easterling, D., Tank, A. K., Parker, D., Rahimzadeh, F., Renwick, J. A., Rusticucci, M., Soden, B., and Zhai, P.: Palaeoclimate, in: *Climate Change 2007: The Physical Science Basis. Contribution of Working Group I to the Fourth Assessment Report of the Intergovernmental Panel on Climate Change*, edited by Solomon, S., Qin, D., Manning, M., Chen, Z., Marquis, M., Averyt, K. B., Tignor, M., and Miller, H. L., *Climate Change 2007: The Physical Science Basis. Contribution of Working Group I to the Fourth Assessment Report of the Intergovernmental Panel on Climate Change.*, chap. 6, pp. 434–497, Cambridge University Press, Cambridge, United Kingdom and New York, NY, USA, 2007.
- Jungclaus, J. H., Keenlyside, N., Botzet, M., Haak, H., Luo, J.-J., Latif, M., Marotzke, J., Mikolajewicz, U., and Roeckner, E.: Ocean circulation and tropical variability in the coupled model ECHAM5/MPI-OM, *J. Climate*, 19, 3952–3972, doi:10.1175/JCLI3827.1, 2006.
- Jungclaus, J. H., Lorenz, S. J., Timmreck, C., Reick, C. H., Brovkin, V., Six, K., Segschneider, J., Giorgetta, M. A., Crowley, T. J., Pongratz, J., Krivova, N. A., Vieira, L. E., Solanki, S. K.,

- Klocke, D., Botzet, M., Esch, M., Gayler, V., Haak, H., Raddatz, T. J., Roeckner, E., Schnur, R., Widmann, H., Claussen, M., Stevens, B., and Marotzke, J.: Climate and carbon-cycle variability over the last millennium, *Climate of the Past*, 6, 723–737, doi:10.5194/cp-6-723-2010, 2010.
- Kang, S. M., Polvani, L. M., Fyfe, J. C., and Sigmond, M.: Impact of polar ozone depletion on subtropical precipitation., *Science*, 332, 951–4, doi:10.1126/science.1202131, 2011.
- Kennedy, J. J., Rayner, N. A., Smith, R. O., Parker, D. E., and Saunby, M.: Reassessing biases and other uncertainties in sea surface temperature observations measured in situ since 1850: 2. Biases and homogenization, *J. Geophys. Res.*, 116, D14 104, doi:10.1029/2010JD015220, 2011.
- Kirchner, I., Stenchikov, G. L., Graf, H.-F., Robock, A., and Antuña, J. C.: Climate model simulation of winter warming and summer cooling following the 1991 Mount Pinatubo volcanic eruption, *J. Geophys. Res.*, 104, 19 039–19 055, doi:10.1029/1999JD900213, 1999.
- Knutti, R. and Sedláček, J.: Robustness and uncertainties in the new CMIP5 climate model projections, *Nat. Clim. Chang.*, 3, 369–373, doi:10.1038/nclimate1716, 2012.
- Kodera, K.: Influence of volcanic eruptions on the troposphere through stratospheric dynamical processes in the Northern Hemisphere winter, *J. Geophys. Res.*, 99, 1273–1282, 1994.
- Kodera, K. and Kuroda, Y.: Dynamical response to the solar cycle, *J. Geophys. Res.*, 107, 4749, doi:10.1029/2002JD002224, 2002.
- Kopp, G. and Lean, J. L.: A new, lower value of total solar irradiance: Evidence and climate significance, *Geophys. Res. Lett.*, 38, L01 706, doi:10.1029/2010GL045777, 2011.
- Labitzke, K.: Sunspots, the QBO, and the stratospheric temperature in the north polar region, *Geophys. Res. Lett.*, 14, 535–537, 1987.
- Labitzke, K.: Solar variation and stratospheric response, *Space Science Reviews*, 125, 247–260, doi:10.1007/s11214-006-9061-6, 2007.
- Lean, J.: Evolution of the sun’s spectral irradiance since the Maunder Minimum, *Geophys. Res. Lett.*, 27, 2425–2428, doi:10.1029/2000GL000043, 2000.
- Li, C., Storch, J.-S., and Marotzke, J.: Deep-ocean heat uptake and equilibrium climate response, *Climate Dyn.*, 40, 1071–1086, doi:10.1007/s00382-012-1350-z, 2012.
- MacFarling-Meure, C., Etheridge, D., Trudinger, C., Steele, P., Langenfelds, R., Van Ommen, T., Smith, A., and Elkins, J.: Law Dome CO₂, CH₄ and N₂O ice core records extended to 2000 years BP, *Geophys. Res. Lett.*, 33, L14 810, doi:10.1029/2006GL026152, 2006.
- MacFarling-Meure, C. M. F.: The natural and anthropogenic variations of carbon dioxide, methane and nitrous oxide during the Holocene from ice core analysis, Ph.D. thesis, University of Melbourne, 2004.
- Mann, M. E., Zhang, Z., Rutherford, S., Bradley, R. S., Hughes, M. K., Shindell, D. T., Ammann, C. M., Faluvegi, G., and Ni, F.: Global signatures and dynamical origins of the Little Ice Age and Medieval Climate Anomaly., *Science*, 326, 1256–60, doi:10.1126/science.1177303, 2009.
- Manzini, E., Giorgetta, M. A., Esch, M., Kornbluh, L., and Roeckner, E.: The influence of sea surface temperatures on the northern winter stratosphere: Ensemble simulations with the MAECHAM5 model, *J. Climate*, 19, 3863–3881, doi:10.1175/JCLI3826.1, 2006.
- Marsland, S.: The Max-Planck-Institute global ocean/sea ice model with orthogonal curvilinear coordinates, *Ocean Modelling*, 5, 91–127, doi:10.1016/S1463-5003(02)00015-X, 2003.
- Mauritsen, T., Stevens, B., Roeckner, E., Crueger, T., Esch, M., Giorgetta, M., Haak, H., Jungclaus, J., Klocke, D., Matei, D., Mikolajewicz, U., Notz, D., Pincus, R., Schmidt, H., and Tomassini, L.: Tuning the climate of a global model, *Journal of Advances in Modeling Earth Systems*, 4, M00A01, doi:10.1029/2012MS000154, 2012.
- Maycock, A. C., Shine, K. P., and Joshi, M. M.: The temperature response to stratospheric water vapour changes, *Quart. J. Roy. Meteor. Soc.*, 137, 1070–1082, doi:10.1002/qj.822, 2011.

- Meehl, G. A., Arblaster, J. M., Branstator, G., and van Loon, H.: A coupled air-sea response mechanism to solar forcing in the pacific region, *J. Climate*, 21, 2883–2897, doi:10.1175/2007JCLI1776.1, 2008.
- Meehl, G. A., Arblaster, J. M., Matthes, K., Sassi, F., and van Loon, H.: Amplifying the pacific climate system response to a small 11-year solar cycle forcing., *Science*, 325, 1114–1118, doi:10.1126/science.1172872, 2009.
- Meraner, K., Mauritsen, T., and Voigt, A.: Robust increase in equilibrium climate sensitivity under global warming, *Geophys. Res. Lett.*, 40, 5944–5948, doi:10.1002/2013GL058118, 2013.
- Mignot, J., Khodri, M., Frankignoul, C., and Servonnat, J.: Volcanic impact on the Atlantic Ocean over the last millennium, *Climate of the Past*, 7, 1439–1455, doi:10.5194/cp-7-1439-2011, 2011.
- Mlawer, E. J., Taubman, S. J., Brown, P. D., Iacono, M. J., and Clough, S. A.: Radiative transfer for inhomogeneous atmospheres: RRTM, validated correlated-k model for the longwave, *J. Geophys. Res.*, 102, 663–16 682, 1997.
- Muthers, S., Anet, J. G., Raible, C. C., Brönnimann, S., Rozanov, E., Arfeuille, F., Peter, T., Shapiro, A. I., Beer, J., Steinhilber, F., Brugnara, Y., and Schmutz, W.: Northern hemispheric winter warming pattern after tropical volcanic eruptions: Sensitivity to the ozone climatology, *J. Geophys. Res.*, 110, 1340–1355, doi:10.1002/2013JD020138, 2014.
- Myhre, G., Shindell, D., Bréon, F.-M., Collins, W., Fuglestedt, J., Huang, J., Koch, D., Lamarque, J.-F., Lee, D., Mendoza, B., Nakajima, T., Robock, A., Stephens, G., Takemura, T., and Zhang, H.: Anthropogenic and Natural Radiative Forcing, in: *Climate Change 2013: The Physical Science Basis. Contribution of Working Group I to the Fifth Assessment Report of the Intergovernmental Panel on Climate Change*, edited by Stocker, T. F., Qin, D., Plattner, G.-K., Tignor, M., Allen, S., Boschung, J., Nauels, A., Xia, Y., Bex, V., and Midgley, P., chap. 8, pp. 659–740, Cambridge University Press, Cambridge, United Kingdom and New York, NY, USA, 2013.
- Pinto, J. G. and Raible, C. C.: Past and recent changes in the North Atlantic oscillation, *Wiley Interdisciplinary Reviews: Climate Change*, 3, 79–90, doi:10.1002/wcc.150, 2012.
- Purich, A. and Son, S.-W.: Impact of Antarctic ozone depletion and recovery on southern hemisphere precipitation, evaporation, and extreme changes, *J. Climate*, 25, 3145–3154, doi:10.1175/JCLI-D-11-00383.1, 2012.
- Ramaswamy, V., Boucher, O., Haigh, J., Hauglustine, D. ., Haywood, J., Myhre, G., Nakajima, T., Shi, G. Y., and Solomon, S.: Radiative forcing of climate change, in: *IPCC Third Assessment Report: Climate Change 2001*, edited by Houghton, J., Ding, Y., Griggs, D., Noguer, M., van der Linden, P., Dai, X., Maskell, K., and Johnson, C., chap. 6, pp. 350–416, Cambridge University Press, Cambridge, United Kingdom and New York, NY, USA, 2001.
- Randall, D. A., Wood, R. A., Bony, S., Colman, R., Fichefet, T., Fyfe, J., Kattsov, V., Pitman, A., Shukla, J., Srinivasan, J., Stouffer, R. J., Sumi, A., and Taylor, K. E.: Climate models and their evaluation, in: *Climate Change 2007: The Physical Science Basis. Contribution of Working Group I to the Fourth Assessment Report of the Intergovernmental Panel on Climate Change*, edited by Solomon, S., Qin, D., Manning, M., Chen, Z., Marquis, M., Averyt, K., M.Tignor, and Miller, H., *Climate Change 2007: The Physical Science Basis. Contribution of Working Group I to the Fourth Assessment Report of the Intergovernmental Panel on Climate Change*, chap. 8, Cambridge University Press, Cambridge, United Kingdom and New York, NY, USA, 2007.
- Rayner, N. A., Parker, D. E., Horton, E. B., Folland, C. K., Alexander, L. V., Rowell, D. P., Kent, E. C., and Kaplan, A.: Global analyses of sea surface temperature, sea ice, and night marine air temperature since the late nineteenth century, *J. Geophys. Res.*, 108, 4407, doi:10.1029/2002JD002670, 2003.
- Reichler, T., Kim, J., Manzini, E., and Kröger, J.: A stratospheric connection to Atlantic climate variability, *Nature Geoscience*, 5, 1–5, doi:10.1038/ngeo1586, 2012.

Roeckner, E., Bäuml, G., Bonaventura, L., Brokopf, R., Esch, M., Giorgetta, M., Hagemann, S., Kirchner, I., Kornblüeh, L., Manzini, E., Rhodin, A., Schlese, U., Schulzweida, U., and Tompkins, A.: The atmospheric general circulation model ECHAM5 - Model description, MPI report 349, Max-Planck Institute for Meteorology, Hamburg, Germany, 2003.

Roeckner, E., Brokopf, R., Esch, M., Giorgetta, M., Hagemann, S., Kornblüeh, L., Manzini, E., Schlese, U., and Schulzweida, U.: Sensitivity of simulated climate to horizontal and vertical resolution in the ECHAM5 atmosphere model., *J. Climate*, 19, 3771–3791, 2006.

Roazanov, E., Schlesinger, M. E., Zubov, V., Yang, F., and Andronova, N. G.: The UIUC three-dimensional stratospheric chemical transport model: Description and evaluation of the simulated source gases and ozone, *J. Geophys. Res.*, 104, 11,755–11,781, doi:10.1029/1999JD900138, 1999.

Roazanov, E., Schlesinger, M. E., and Zubov, V.: The University of Illinois, Urbana-Champaign three-dimensional stratosphere-troposphere general circulation model with interactive ozone photochemistry: Fifteen-year control run climatology, *J. Geophys. Res.*, 106, 27,233–27,254, doi:10.1029/2000JD000058, 2001.

Roazanov, E., Calisto, M., Egorova, T., Peter, T., and Schmutz, W.: Influence of the precipitating energetic particles on atmospheric chemistry and climate, *Surveys in Geophysics*, 33, 483–501, doi:10.1007/s10712-012-9192-0, 2012.

Roazanov, E. V., Schlesinger, M. E., Andronova, N. G., Yang, F., Malyshev, S. L., Zubov, V. A., Egorova, T. A., and Li, B.: Climate/chemistry effects of the Pinatubo volcanic eruption simulated by the UIUC stratosphere/troposphere GCM with interactive photochemistry, *J. Geophys. Res.*, 107(D21), 4594, doi:10.1029/2001JD000974, 2002.

Scaife, A. A., Spanghel, T., Fereday, D. R., Cubasch, U., Langematz, U., Akiyoshi, H., Bekki, S., Braesicke, P., Butchart, N., Chipperfield, M. P., Gettelman, A., Hardiman, S. C., Michou, M., Roazanov, E., and Shepherd, T. G.: Climate change projections and stratosphere–troposphere interaction, *Climate Dyn.*, 38, 2089–2097, doi:10.1007/s00382-011-1080-7, 2011.

Schmidt, G. A., Jungclaus, J. H., Ammann, C. M., Bard, E., Braconnot, P., Crowley, T. J., Delaygue, G., Joos, F., Krivova, N. A., Muscheler, R., Otto-Bliesner, B. L., Pongratz, J., Shindell, D. T., Solanki, S. K., Steinhilber, F., and Vieira, L. E. A.: Climate forcing reconstructions for use in PMIP simulations of the Last Millennium (v1.1), *Geoscientific Model Development*, 5, 185–191, doi:10.5194/gmd-5-185-2012, 2012.

Schmidt, H., Rast, S., Bunzel, F., Esch, M., Giorgetta, M., Kinne, S., Krismer, T., Stenchikov, G., Timmreck, C., Tomassini, L., and Walz, M.: Response of the middle atmosphere to anthropogenic and natural forcings in the CMIP5 simulations with the Max Planck Institute Earth system model, *Journal of Advances in Modeling Earth Systems*, 5, 98–116, doi:10.1002/jame.20014, 2013.

Schraner, M., Roazanov, E., Schnadt Poberaj, C., Kenzelmann, P., Fischer, A. M., Zubov, V., Luo, B. P., Hoyle, C. R., Egorova, T., Fueglistaler, S., Brönnimann, S., Schmutz, W., and Peter, T.: Technical Note: Chemistry-climate model SOCOL: version 2.0 with improved transport and chemistry/microphysics schemes, *Atmos. Chem. Phys.*, 8, 5957–5974, doi:10.5194/acp-8-5957-2008, 2008.

Shapiro, A. I., Schmutz, W., Roazanov, E., Schoell, M., Haberreiter, M., Shapiro, A. V., and Nyeki, S.: A new approach to the long-term reconstruction of the solar irradiance leads to large historical solar forcing, *Astronomy & Astrophysics*, 529, A67, doi:10.1051/0004-6361/201016173, 2011.

Shindell, D., Rind, D., Balachandran, N., Lean, J., and Lonergan, P.: Solar cycle variability, ozone, and climate, *Science*, 284, 305–8, 1999.

Shindell, D., Faluvegi, G., Lacis, A., Hansen, J. and Ruedy, R., and Aguilar, E.: Role of tropospheric ozone increases in 20th-century climate change, *J. Geophys. Res.*, 111, D08 302, doi:10.1029/2005JD006348, 2006.

- Shindell, D. T., Schmidt, G. A., Mann, M. E., Rind, D., and Waple, A. M.: Solar forcing of regional climate change during the Maunder Minimum., *Science*, 294, 2149–52, doi:10.1126/science.1064363, 2001.
- Shindell, D. T., Schmidt, G. A., Miller, R. L., and Mann, M. E.: Volcanic and solar forcing of climate change during the preindustrial era, *J. Climate*, 16, 4094–4107, doi:10.1175/1520-0442(2003)016<4094:VASFOC>2.0.CO;2, 2003.
- Sigmond, M., Siegmund, P. C., Manzini, E., and Kelder, H.: A simulation of the separate climate effects of middle-atmospheric and tropospheric CO₂ doubling, *J. Climate*, 17, 2352–2367, 2004.
- Smith, T. M., Reynolds, R. W., Peterson, T. C., and Lawrimore, J.: Improvements to NOAA’s historical merged land–ocean surface temperature analysis (1880–2006), *J. Climate*, 21, 2283–2296, doi:10.1175/2007JCLI2100.1, 2008.
- Solomon, S., Portmann, R. W., Garcia, R. R., Thomason, L. W., Poole, L. R., McCormick, M. P., and Cly, C.: The role of aerosol variations in anthropogenic ozone depletion at northern midlatitudes, *J. Geophys. Res.*, 101, 6713–6727, 1996.
- Son, S.-W., Gerber, E. P., Perlwitz, J., Polvani, L. M., Gillett, N. P., Seo, K.-H., Eyring, V., Shepherd, T. G., Waugh, D., Akiyoshi, H., Austin, J., Baumgaertner, A., Bekki, S., Braesicke, P., Brühl, C., Butchart, N., Chipperfield, M. P., Cugnet, D., Dameris, M., Dhomse, S., Frith, S., Garny, H., Garcia, R., Hardiman, S. C., Jöckel, P., Lamarque, J. F., Mancini, E., Marchand, M., Michou, M., Nakamura, T., Morgenstern, O., Pitari, G., Plummer, D. A., Pyle, J., Rozanov, E., Scinocca, J. F., Shibata, K., Smale, D., Teyssède, H., Tian, W., and Yamashita, Y.: Impact of stratospheric ozone on Southern Hemisphere circulation change: A multimodel assessment, *J. Geophys. Res.*, 115, D00M07, doi:10.1029/2010JD014271, 2010.
- Song, Y. and Robinson, W. A.: Dynamical mechanisms for stratospheric influences on the troposphere, *J. Atmos. Sci.*, 61, 1711–1725, doi:10.1175/1520-0469(2004)061<1711:DMFSIO>2.0.CO;2, 2004.
- Stachelin, J., Harris, N. R. P., Appenzeller, C., and Eberhard, J.: Ozone trends: A review, *Rev. Geophys.*, 39, 231, doi:10.1029/1999RG000059, 2001.
- Steinhilber, F., Abreu, J. A., and Beer, J.: Solar modulation during the Holocene, *Astrophysics and Space Sciences Transactions*, 4, 1–6, doi:10.5194/astra-4-1-2008, 2008.
- Steinhilber, F., Beer, J., and Fröhlich, C.: Total solar irradiance during the Holocene, *Geophys. Res. Lett.*, 36, 1–5, doi:10.1029/2009GL040142, 2009.
- Stenchikov, G., Robock, A., Ramaswamy, V., Schwarzkopf, M. D., Hamilton, K., and Ramachandran, S.: Arctic Oscillation response to the 1991 Mount Pinatubo eruption: Effects of volcanic aerosols and ozone depletion, *J. Geophys. Res.*, 107, 1–16, doi:10.1029/2002JD002090, 2002.
- Stenchikov, G., Hamilton, K., Stouffer, R. J., Robock, A., Ramaswamy, V., Santer, B., and Graf, H.-F.: Arctic Oscillation response to volcanic eruptions in the IPCC AR4 climate models, *J. Geophys. Res.*, 111, 1–17, doi:10.1029/2005JD006286, 2006.
- Stenke, A., Hoyle, C. R., Luo, B., Rozanov, E., Gröbner, J., Maag, L., Brönnimann, S., and Peter, T.: Climate and chemistry effects of a regional scale nuclear conflict, *Atmos. Chem. Phys.*, 13, 9713–9729, doi:10.5194/acp-13-9713-2013, 2013a.
- Stenke, A., Schraner, M., Rozanov, E., Egorova, T., Luo, B., and Peter, T.: The SOCOL version 3.0 chemistry–climate model: description, evaluation, and implications from an advanced transport algorithm, *Geoscientific Model Development*, 6, 1407–1427, doi:10.5194/gmd-6-1407-2013, 2013b.
- Stevenson, D. S., Young, P. J., Naik, V., Lamarque, J.-F., Shindell, D. T., Voulgarakis, A., Skeie, R. B., Dalsoren, S. B., Myhre, G., Berntsen, T. K., Folberth, G. A., Rumbold, S. T., Collins, W. J., MacKenzie, I. A., Doherty, R. M., Zeng, G., van Noije, T. P. C., Strunk, A., Bergmann, D., Cameron-Smith, P., Plummer, D. A., Strode, S. A., Horowitz, L., Lee, Y. H., Szopa, S., Sudo, K., Nagashima, T., Josse, B., Cionni, I., Righi, M., Eyring, V., Conley, A.,

- Bowman, K. W., Wild, O., and Archibald, A.: Tropospheric ozone changes, radiative forcing and attribution to emissions in the Atmospheric Chemistry and Climate Model Intercomparison Project (ACCMIP), *Atmos. Chem. Phys.*, 13, 3063–3085, doi:10.5194/acp-13-3063-2013, 2013.
- Stocker, T., Qin, D., Plattner, G.-K., Alexander, L., Allen, S., Bindoff, N., Bréon, F.-M., Church, J., Cubasch, U., Emori, S., Forster, P., Friedlingstein, P., Gillett, N., Gregory, J., Hartmann, D., Jansen, E., Kirtman, B., Knutti, R., Kumar, K. K., Lemke, P., Marotzke, J., Masson-Delmotte, V., Meehl, G., Mokhov, I., Piao, S., Ramaswamy, V., Randall, D., Rhein, M., Rojas, M., Sabine, C., Shindell, D., Talley, L., Vaughan, D., and Xie, S.-P.: Technical Summary, in: *Climate change 2013: The physical science basis. Contribution of working group I to the fifth assessment report of the Intergovernmental Panel on Climate Change*, edited by Stocker, T., Qin, D., Plattner, G.-K., Tignor, M., Allen, S., Boschung, J., Nauels, A., Xia, Y., Bex, V., and Midgley, P., pp. 33–115, Cambridge University Press, Cambridge, United Kingdom and New York, NY, USA, 2013.
- Thompson, D. W. and Wallace, J. M.: Regional climate impacts of the Northern Hemisphere annular mode., *Science*, 293, 85–9, doi:10.1126/science.1058958, 2001.
- Thompson, D. W. J., Baldwin, M. P., and Solomon, S.: Stratosphere - Troposphere Coupling in the Southern Hemisphere, *Journal of Atmospheric Sciences*, 62, 708–715, 2005.
- Thompson, D. W. J., Furtado, J. C., and Shepherd, T. G.: On the tropospheric response to anomalous stratospheric wave drag and radiative heating, *J. Atmos. Sci.*, 63, 2616–2629, 2006.
- Thompson, D. W. J., Solomon, S., Kushner, P. J., England, M. H., Grise, K. M., and Karoly, D. J.: Signatures of the Antarctic ozone hole in Southern Hemisphere surface climate change, *Nature Geoscience*, 4, 741–749, doi:10.1038/ngeo1296, 2011.
- Tie, X. and Brasseur, G.: The response of stratospheric ozone to volcanic eruptions: Sensitivity to atmospheric chlorine loading, *Geophys. Res. Lett.*, 22, 3035–3038, 1995.
- Uppala, S. M., Kållberg, P. W., Simmons, A. J., Andrae, U., Bechtold, V. D. C., Fiorino, M., Gibson, J. K., Haseler, J., Hernandez, A., Kelly, G. A., Li, X., Onogi, K., Saarinen, S., Sokka, N., Allan, R. P., Andersson, E., Arpe, K., Balmaseda, M. A., Beljaars, A. C. M., Berg, L. V. D., Bidlot, J., Bormann, N., Caires, S., Chevallier, F., Dethof, A., Dragosavac, M., Fisher, M., Fuentes, M., Hagemann, S., Hólm, E., Hoskins, B. J., Isaksen, I., Janssen, P. A. E. M., Jenne, R., McNally, A. P., Mahfouf, J.-F., Morcrette, J.-J., Rayner, N. A., Saunders, R. W., Simon, P., Sterl, A., Trenberth, K. E., Untch, A., Vasiljevic, D., Viterbo, P., and Woollen, J.: The ERA-40 re-analysis, *Quart. J. Roy. Meteor. Soc.*, 131, 2961–3012, doi:10.1256/qj.04.176, 2005.
- Valcke, S.: The OASIS3 coupler: A European climate modelling community software, *Geoscientific Model Development*, 6, 373–388, doi:10.5194/gmd-6-373-2013, 2013.
- Varma, V., Prange, M., Spanghel, T., Lamy, F., Cubasch, U., and Schulz, M.: Impact of solar-induced stratospheric ozone decline on Southern Hemisphere westerlies during the Late Maunder Minimum, *Geophys. Res. Lett.*, 39, L20 704, doi:10.1029/2012GL053403, 2012.
- Wang, Y.-M., Lean, J. L., and Sheeley, Jr., N. R.: Modeling the sun’s magnetic field and irradiance since 1713, *The Astrophysical Journal*, 625, 522–538, doi:10.1086/429689, 2005.
- Wanner, H., Brönnimann, S., Casty, C., Gyalistras, D., Luterbacher, J., Schmutz, C. and Stephenson, D. B., and Xoplaki, E.: North Atlantic Oscillation - concepts and studies, *Surveys in Geophysics*, 22, 321–381, doi:10.1023/A:1014217317898, 2001.
- Waugh, D. W., Oman, L., Newman, P. A., Stolarski, R. S., Pawson, S., Nielsen, J. E., and Perlwitz, J.: Effect of zonal asymmetries in stratospheric ozone on simulated Southern Hemisphere climate trends, *Geophys. Res. Lett.*, 36, L18 701, doi:10.1029/2009GL040419, 2009.
- Weisenstein, D., Yue, G., Ko, M., Sze, N., Rodriguez, J., and Scott, C.: A two-dimensional model of sulfur species and aerosols, *J. Geophys. Res.*, 102, 13 019–13 035, 1997.
- Woollings, T., Charlton-Perez, A., Ineson, S., Marshall, A. G., and Masato, G.: Associations between stratospheric variability and tropospheric blocking, *J. Geophys. Res.*, 115, D06 108, doi:10.1029/2009JD012742, 2010.

Chapter 3.

Northern hemispheric winter warming pattern after tropical volcanic eruptions: Sensitivity to the ozone climatology

Stefan Muthers, Julien G. Anet, Christoph C. Raible, Stefan Brönnimann, Eugene Rozanov, Florian Arfeuille, Thomas Peter, Alexander I. Shapiro, Jürg Beer, Friedhelm Steinhilber, Yuri Brugnara, and Werner Schmutz.

Published in *Journal of Geophysical Research*, vol. 119, 3, pp. 1340–1355, 2014.

RESEARCH ARTICLE

10.1002/2013JD020138

Key Points:

- Dynamic response to volcanic eruption depends on the ozone concentrations
- Stronger ozone gradients strengthen the dynamic response
- Resulting winter warming pattern is highly significant

Supporting Information:

- Readme
- Figure S1
- Figure S2
- Figure S3
- Figure S4

Correspondence to:

S. Muthers,
muthers@climate.unibe.ch

Citation:

Muthers, S., J. G. Anet, C. C. Raible, S. Brönnimann, E. Rozanov, F. Arfeuille, T. Peter, A. I. Shapiro, J. Beer, F. Steinhilber, Y. Brugnara, and W. Schmutz (2014), Northern hemispheric winter warming pattern after tropical volcanic eruptions: Sensitivity to the ozone climatology, *J. Geophys. Res. Atmos.*, 119, doi:10.1002/2013JD020138.

Received 8 MAY 2013

Accepted 14 JAN 2014

Accepted article online 18 JAN 2014

Northern hemispheric winter warming pattern after tropical volcanic eruptions: Sensitivity to the ozone climatology

S. Muthers^{1,2}, J. G. Anet³, C. C. Raible^{1,2}, S. Brönnimann^{2,4}, E. Rozanov^{3,5}, F. Arfeuille^{2,4}, T. Peter³, A. I. Shapiro⁵, J. Beer⁶, F. Steinhilber⁶, Y. Brugnara^{2,4}, and W. Schmutz⁵

¹Climate and Environmental Physics, University of Bern, Bern, Switzerland, ²Oeschger Centre for Climate Change Research, University of Bern, Bern, Switzerland, ³Institute for Atmospheric and Climate Science, ETH, Zurich, Switzerland, ⁴Institute of Geography, University of Bern, Bern, Switzerland, ⁵Physikalisch-Meteorologisches Observatorium Davos and World Radiation Center, Davos, Switzerland, ⁶Swiss Federal Institute of Aquatic Science and Technology, Dübendorf, Switzerland

Abstract An important key for the understanding of the dynamic response to large tropical volcanic eruptions is the warming of the tropical lower stratosphere and the concomitant intensification of the polar vortices. Although this mechanism is reproduced by most general circulation models today, most models still fail in producing an appropriate winter warming pattern in the Northern Hemisphere. In this study ensemble sensitivity experiments were carried out with a coupled atmosphere-ocean model to assess the influence of different ozone climatologies on the atmospheric dynamics and in particular on the northern hemispheric winter warming. The ensemble experiments were perturbed by a single Tambora-like eruption. Larger meridional gradients in the lower stratospheric ozone favor the coupling of zonal wind anomalies between the stratosphere and the troposphere after the eruption. The associated sea level pressure, temperature, and precipitation patterns are more pronounced and the northern hemispheric winter warming is highly significant. Conversely, weaker meridional ozone gradients lead to a weaker response of the winter warming and the associated patterns. The differences in the number of stratosphere-troposphere coupling events between the ensembles experiments indicate a nonlinear response behavior of the dynamics with respect to the ozone and the volcanic forcing.

1. Introduction

Large tropical volcanic eruptions are a major factor in natural climate change [Robock, 2000; Cole-Dai, 2010; Timmreck, 2012]. The direct radiative effect of an eruption leads to a cooling at the surface. At the same time, dynamic effects can cause positive temperature anomalies on the regional scale, e.g., in the Northern Hemisphere where a winter warming pattern has been identified at high latitudes after several historical eruptions [e.g., Robock and Mao, 1992; Stenchikov et al., 2002; Shindell et al., 2004; Fischer et al., 2007; Christiansen, 2008; Zanchettin et al., 2012]. After the eruption of Mount Pinatubo in 1991 climate model simulations indicated that the winter warming following the eruption is related to stratospheric dynamics [Graf et al., 1993]. The aerosol loading in the lower stratosphere increases the reflection of short-wave radiation back to space and the absorption of near-infrared and long-wave radiation. For tropical and subtropical volcanic eruptions a large fraction of the aerosol is advected into the tropical pipe, so that its long-wave absorption leads to a warming of the tropical stratosphere, which strengthens the meridional temperature gradient and accelerates the polar night jet [Kodera, 1994]. These wind anomalies penetrate downward into the troposphere and intensify the westerlies [Graf et al., 1993]. Therefore, the radiative forcing of the volcanic eruption can induce a positive phase of the Arctic Oscillation (AO) or the North Atlantic Oscillation (NAO), which is held responsible for the higher winter temperature in the northern high latitudes [Robock, 2000; Shindell et al., 2004].

A number of mechanisms was proposed to explain the propagation of wind anomalies from the stratosphere to the troposphere or vice versa [Shepherd, 2002; Song and Robinson, 2004]. However, none of them is yet fully understood [Thompson et al., 2006; Gerber et al., 2012]. Alternatively, several studies described the interaction between stratosphere and troposphere in a statistical way using empirical orthogonal function analysis or correlations techniques [e.g., Baldwin et al., 1994; Baldwin and Dunkerton, 2001; Thompson et al., 2005]. These authors defined stratosphere-troposphere couplings by coupled modes of variability between the stratosphere and the troposphere. For the Northern Hemisphere this coupled mode

consists of the stratospheric polar vortex and the NAO or AO. Independent of the underlying mechanisms, stratosphere-troposphere coupling is known to be the key to understanding the winter warming pattern that follows large volcanic eruptions.

The state of the stratosphere has significantly changed in the past few decades. In particular, its composition has changed due to increased anthropogenic emissions of greenhouse gases, aerosol, and ozone-depleting substances [Solomon, 1999; Baldwin *et al.*, 2007]. The temperature changes, resulting from this change in composition, alter the stratospheric dynamics [Gillett *et al.*, 2002; Gillett and Thompson, 2003; Thompson *et al.*, 2011] and might influence the response of the circulation to volcanic eruption, though the magnitude of the temperature changes is still under discussion [Thompson *et al.*, 2012].

Moreover, the dynamic response of the atmosphere to a strong volcanic eruption also depends on the direct effects of the eruption products on the stratospheric chemistry. In modern times, i.e., in the presence of ozone-depleting halogens, sulfate aerosols act as a component to facilitate heterogeneous reactions, which deactivate nitrogen oxides (NO_x), but in turn activate halogens, leading to a significant reduction of the ozone concentrations [Solomon, 1999; Rozanov *et al.*, 2002]. In preindustrial times with low halogen loading in the stratosphere, the ozone mixing ratios increase after powerful volcanic eruptions, due to heterogeneous deactivation reactions of NO_x on the sulfate aerosol surfaces, slowing down the NO_x -driven ozone destruction cycles [Tie and Brasseur, 1995; Solomon *et al.*, 1996].

For the Pinatubo eruption Stenchikov *et al.* [2002] simulated the impact of the ozone depletion on the temperatures and the dynamics using the SKYHI model forced by observed ozone anomalies. They estimated the cooling to be in the order of 1 K in the tropics and more than 6 K in the northern polar stratosphere. The high-latitude cooling increases the meridional temperature gradient and produces a positive phase of the AO.

The ability of general circulation models (GCMs) to simulate the dynamically induced winter warming in the Northern Hemisphere was evaluated in several studies [Stenchikov *et al.*, 2006; Miller *et al.*, 2006; Driscoll *et al.*, 2012]. For the Intergovernmental Panel on Climate Change Fourth Assessment Report (IPCC AR4) models, Stenchikov *et al.* [2006] revealed that some of the models tend to simulate positive AO phases, but the amplitude was in general too weak compared to observations. Furthermore, models may underestimate the stratospheric-troposphere coupling [Miller *et al.*, 2006]. For the Coupled Model Intercomparison Project Phase 5 (CMIP5) [Taylor *et al.*, 2012], Driscoll *et al.* [2012] repeated the evaluation of Stenchikov *et al.* [2006]. Despite improvements in spatial resolution and representation of the aerosol forcing, none of the 13 evaluated CMIP5 models was able to simulate a sufficiently strong dynamic response.

None of these evaluated CMIP3 and CMIP5 models included an interactive ozone chemistry module. To consider the radiative forcing of ozone in the radiation scheme ozone values are either prescribed in a constant or in a time-dependent way. Half of the IPCC AR4 models were forced by constant ozone climatologies [Miller *et al.*, 2006; Son *et al.*, 2010]. Depending on the climatology used the state of the stratosphere could differ and may influence the response to tropical eruptions.

The aim of this study is to analyze the role of different ozone climatologies in the dynamic response to tropical volcanic eruptions using a coupled atmosphere-ocean model simulation without interactive chemistry. In section 2 the setup of the simulations and the ozone climatologies are described; section 3 presents the results. In section 4 the results and the climatologies are discussed and compared to proxy data and other ozone data sets.

2. Model and Experiment Design

Our basic approach is to examine the dynamic response to tropical volcanic eruptions using two different background ozone climatologies applied to the coupled atmosphere-ocean model SOCOL3-MPIOM (Max Planck Institute ocean model).

SOCOL3 (SOlar Climate Ozone Links, Stenke *et al.* [2013]) consists of the atmosphere model MA-ECHAM (middle atmosphere configuration) version 5.4.01 [Roeckner *et al.*, 2003] coupled to a modified version of the chemistry module MEZON (ModEl for investigation of the oZONe trends). In this study the interactive chemistry module is disabled as we focus on the role of background ozone level on the dynamic atmospheric response to large tropical eruptions. Still, SOCOL3 without interactive chemistry differs from the original

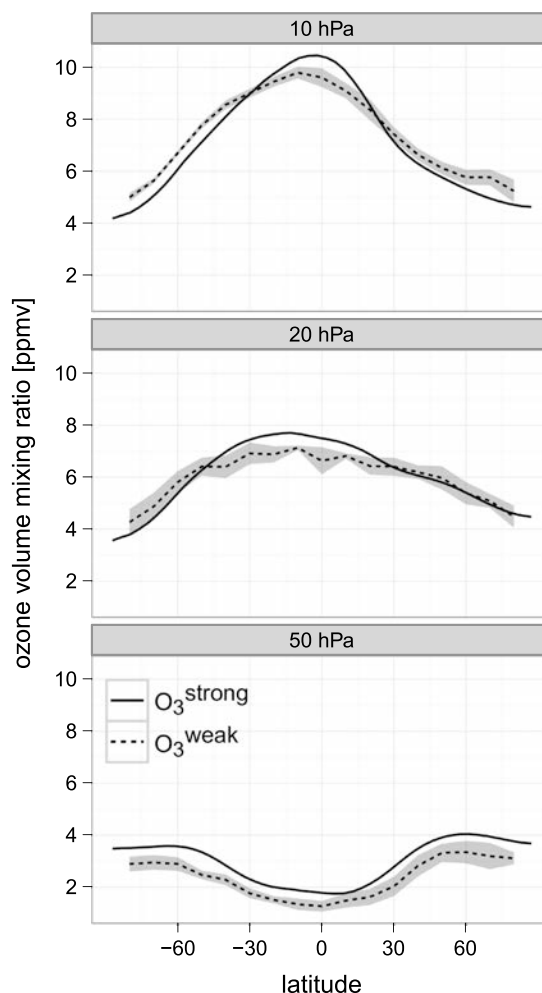


Figure 1. Mean winter season (December–January–February (DJF)) ozone mixing ratios in ppmv at 10, 20, and 50 hPa pressure altitudes of the two ozone climatologies used in this study. Dashed curve: climatology with weaker meridional gradient (O_3^{weak}) from Fortuin and Kelder [1998]. Shading: one standard deviation. Solid curve: climatology with stronger meridional gradient (O_3^{strong}) extracted from a 800 year long preindustrial control simulation with the interactive chemistry–climate model SOCOL3-MPIOM.

MA-ECHAM in several aspects (e.g., spectral solar irradiance forcing). For the experiments, a model resolution of T31 in the atmosphere (approximately $3.75^\circ \times 3.75^\circ$) and 39 vertical levels up to 0.01 hPa (80 km) is used.

The ocean model MPIOM (Max Planck Institute ocean model [Marshall, 2003; Jungclaus et al., 2006]) is used in a nominal resolution of 3° , but with the North Pole shifted toward Greenland, to reach higher resolution in the North Atlantic and in the deepwater formation regions. Both components are coupled using the OASIS3 coupler [Budich et al., 2010; Valcke, 2013].

Ozone Climatologies. Different states of the stratosphere are represented by two ozone climatologies, which are characterized by different meridional ozone gradients in the middle stratosphere. The first climatology is from Fortuin and Kelder [1998] and is based on observational data for the period 1980–1991. It is distributed with the ECHAM5 package and therefore used widely in ECHAM5 simulations [e.g., Jungclaus et al., 2010]. The second climatology was extracted from a 800 year long preindustrial control simulation for 1600 A.D. conditions with the interactive chemistry–climate model SOCOL3-MPIOM by averaging over the last 400 simulation years assuming a nearly steady state. Both climatologies are zonally averaged and interpolated to

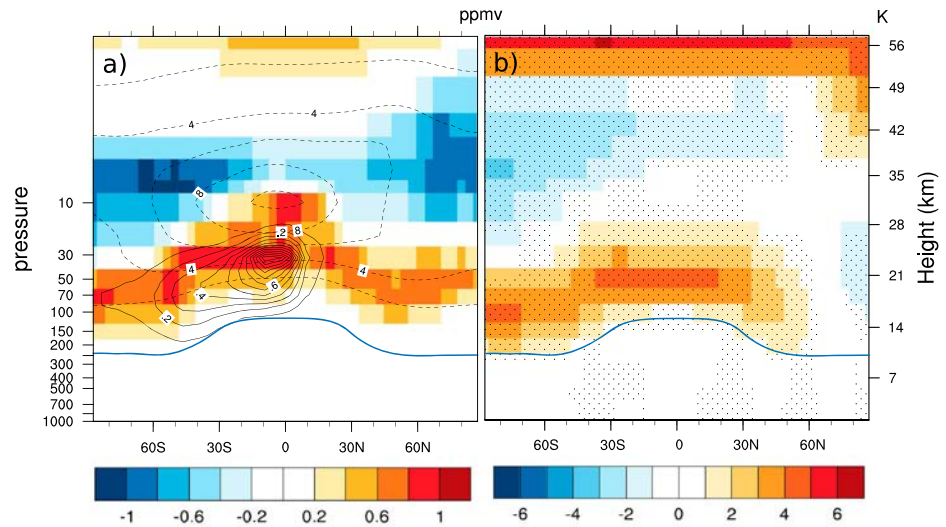


Figure 2. (a) Colored: Zonal mean seasonal mean (DJF) differences in the ozone volume mixing ratios (ppmv) between the two climatologies ($O_3^{strong} - O_3^{weak}$). Solid contours: volcanic aerosol forcing in terms of cumulative extinctions (from 0 to 1.5 km^{-1}) in the visible band of the model (440–690 nm) during the first year after the eruption. Dashed contours: mean DJF ozone volume mixing ratios (from 0 to 14 ppmv) in O_3^{strong} . (b) Resulting zonal average DJF temperature differences in K between the two control ensembles ($CTRL.O_3^{strong} - CTRL.O_3^{weak}$). Stippling: significant differences (Student's t test $p < 0.05$). Thick blue curve: DJF mean approximate tropopause height.

the same pressure levels. In Figure 1 the climatologies are compared for different levels in the stratosphere, and in Figure 2 a in terms of zonal mean anomalies. A general feature of ozone distributions (Figure 1) is that the meridional gradient is positive at low altitudes (i.e., more ozone toward the poles), but negative at high altitudes (i.e., more ozone toward the equator). This is caused by the enhanced ozone production in the tropical upper stratosphere relative to the midlatitude and higher latitude. The climatology of Fortuin and Kelder [1998] shows lower values below 30 hPa. Differences reach 20 % in the lower stratosphere, which is partly due to the fact that the Fortuin and Kelder [1998] climatology reflects the impact of industrial ozone-depleting species. Conversely, at altitudes above the 30 hPa level this climatology shows up to 10 % higher values of ozone, possibly due to the lower solar UV irradiance for the year 1600 climatology. For comparison the standard deviation of the Fortuin and Kelder [1998] climatology is shown as shading in Figure 1. At the three selected levels the difference between the two data sets are for most latitudes in the order of two standard deviations. For the dynamics in the stratosphere the meridional distribution of ozone is more important than its absolute value due to the thermal wind relationship. For the meridional gradient the largest differences between the two climatologies are found at the levels with the highest absolute mixing ratios, i.e., 1.3 ppmv between tropics and northern high latitudes around 10 hPa (Figure 1). Here the gradient is considerably weaker in the Fortuin and Kelder [1998] climatology. We therefore distinguish the two climatologies in terms of their meridional ozone gradient in the middle stratosphere and refer to them as O_3^{weak} (climatology of Fortuin and Kelder [1998]) and O_3^{strong} (model climatology).

Ensemble simulations. Two control ensemble experiments are performed forced by O_3^{strong} and O_3^{weak} , respectively. These two experiments $CTRL.O_3^{strong}$ and $CTRL.O_3^{weak}$ are used as reference. Except for the different ozone climatologies both control ensembles are driven with identical greenhouse gas and solar forcing, representing 1600 A.D. conditions.

Additionally, two sets of ensemble simulations are performed, with a tropical volcanic eruptions applied in the third year after the start of the simulations. Again, we use the strong gradient ozone climatology ($VOLC.O_3^{strong}$) and the weak gradient climatology ($VOLC.O_3^{weak}$). The simulation length of each ensemble member is 18 years. The ensemble names and configurations are summarized in Table 1.

For each set, 15 ensemble members are carried out using different initial conditions from a long-term control simulation. The restart files for the ocean, atmosphere, and the coupler were selected in 10 year steps,

Table 1. Overview of the Ensemble Simulations^a

Label	O ₃ Climatology	Volcanic Eruption
CTRL.O ₃ ^{strong}	O ₃ ^{strong}	No
VOLC.O ₃ ^{strong}	O ₃ ^{strong}	Yes
CTRL.O ₃ ^{weak}	O ₃ ^{weak}	No
VOLC.O ₃ ^{weak}	O ₃ ^{weak}	Yes

^aLabel: name used in this manuscript, O₃ climatology: ozone forcing, and indicator whether the members are perturbed by a volcanic eruption. Ensemble size is 15 for all ensembles, and each member ran for 18 years.

covering the period of year 500 to 640 in the long-term control. The large ensemble size increases the signal-to-noise ratio for the winter warming pattern [Shindell *et al.*, 2004] and allows to average out influences of El Niño–Southern Oscillation on the dynamic response to the eruption [Shindell *et al.*, 2004; Zhang *et al.*, 2012].

In the following the results from the perturbed ensemble sets are presented as anomalies to the unperturbed mean of the corresponding control ensemble. The mean of each control ensemble was calculated by averaging over all available simulation

years, i.e., 15 experiments × 18 years. As statistical test for the comparison we use an unpaired, two-sided Student's *t* test [von Storch and Zwiers, 2000]. The degree of freedom defined in the test is 28 when comparing two perturbed ensembles (15 + 15 – 2) and 283 when comparing a perturbed ensemble and its corresponding control (15 × 18 + 15 – 2). The high number of degrees of freedom is possible due to the very low autocorrelation in the year-to-year DJF values.

Volcanic Forcing. The eruption used in the perturbed ensemble sets is the Tambora eruption that took place in April 1815 in Indonesia and led to the “year without a summer” [Stothers, 1984; Auchmann *et al.*, 2012]. The volcanic aerosol loading data set was prepared offline using the Atmospheric and Environmental Research Inc. model AER [Arfeuille *et al.*, 2013a]. As the transport of the aerosols in the stratosphere is directed mainly toward the winter hemisphere, the majority of aerosols is spread toward the Southern Hemisphere (compare to Figure 6 in Arfeuille *et al.* [2013a]). The cumulative extinction in the visible band (440–690 nm) for the first year of the eruption is shown as solid contours in Figure 2a. Figure 3 (left) displays the monthly mean aerosol optical depth in the visible band.

For the lower boundary over land, the land surface data of the ECHAM5 package is used [Hagemann, 2002]. In the highest levels of the equatorial stratosphere, the zonal winds are forced by data sets of the quasi-biennial oscillation (QBO). Here a backward extended version of the reconstruction of Brönnimann *et al.* [2007] was used for nudging the model. The QBO was in a westerly phase at the beginning of the eruption and shifted to an easterly phase in the following winter season. The QBO forcing is the same in the control and in the perturbed simulations, meaning that the QBO phase in the third year of each simulations is identical. However, climatological values for the control ensemble simulations are calculated using all available simulation years. In this case the influence of the QBO is averaged out.

Finally, we note that neither the ozone concentrations nor the volcanic aerosols are transported or else affected by the model but are prescribed according to the climatological or aerosol record data.

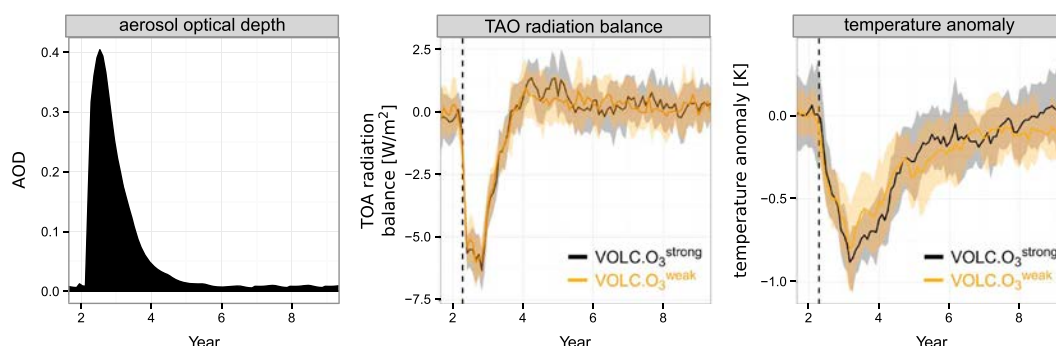


Figure 3. (left) Changes in the monthly mean optical depth at 550 nm caused by the volcanic eruption. (middle) Globally averaged monthly mean top-of-the-atmosphere (TOA) radiation balance anomalies relative to the average annual cycle in the corresponding control ensemble. (right) Monthly mean global mean temperature anomalies. Shading: ensemble standard deviation. Vertical dashed line: start of the eruption.

3. Results From the Sensitivity Experiments

3.1. Global Scale

We focus first on the global scale, where a surface cooling that follows the eruption is found in both perturbed ensemble simulations (VOLC.O₃^{strong} and VOLC.O₃^{weak}, compare Figure 3). The cooling is largest 1 year after the eruption with a reduction of the global average annual mean temperature of -0.75 K in VOLC.O₃^{strong} and -0.63 K in VOLC.O₃^{weak}, respectively. The differences between the ensemble mean VOLC.O₃^{strong} anomalies and the ensemble mean VOLC.O₃^{weak} anomalies are significant with $p = 0.037$ (Student's t test). The cooling is larger in the Southern Hemisphere due to the larger amount of aerosols in the southern stratosphere. Globally, the cooling is statistically significant for 6 years in VOLC.O₃^{strong} and for 7 years in VOLC.O₃^{weak} ($p < 0.05$, Student's t test). In terms of the top-of-the-atmosphere radiative forcing (Figure 3, middle) VOLC.O₃^{weak} experiences a maximum reduction of -6.0 W/m², whereas the reduction is slightly but insignificantly larger in VOLC.O₃^{strong} (-6.3 W/m²).

3.2. Regional Scale

The response for the northern hemispheric winter warming is shown in Figure 4 for the 2 m temperature, for the 500 hPa geopotential height, and for precipitation. In both ensemble experiments a temperature dipole with warming over northern and eastern Europe and cooling over southern Europe and the Middle East is identified. However, the warming of near-surface air over Scandinavia (2.7 K versus 1.0 K, area average between 10°E–30°E and 55°N–70°N, gray box in Figure 4) is considerably stronger and its significance higher in VOLC.O₃^{strong} than in VOLC.O₃^{weak}. Further temperature anomalies in VOLC.O₃^{strong} are a warming over eastern North-America and a cold anomaly over western Greenland and in the Labrador Sea. In VOLC.O₃^{weak} these cold anomalies are much weaker or missing.

The anomalies for both perturbed ensemble experiments are expressed relative to their corresponding control ensemble and the differences found between the two anomalies are therefore not related to differences between the control ensembles. The differences between the two control ensembles are shown in Figure S1a in the supporting information for the 2 m temperatures in winter (DJF, supporting information). In the two perturbed ensemble experiments the warming in northern Europe is related to an anomalously high 500 hPa geopotential height in the Atlantic basin located between 35°N and 55°N and low geopotential height west of Iceland, similar to a positive phase of the NAO. This pattern intensifies advection of warm Atlantic air masses toward Scandinavia. Similar to the temperature, the 500 hPa geopotential anomalies are largely significant over the Atlantic basin in VOLC.O₃^{strong}, but almost insignificant in VOLC.O₃^{weak}. The pattern of the sea level pressure anomalies are very similar illustrating the barotropic structure (Figure S2 in the supporting information). The differences in the sea level pressure between the two control ensemble experiment is shown in Figure S1b for the boreal winter season (DJF, supporting information). Clearly, the positive NAO-type pattern also shifts the storm track at the eastern boundary of the Atlantic basin toward the north and results in higher precipitation in northern Europe and less precipitation in southern Europe [Hurrell, 1995; Raible et al., 2004; Fischer et al., 2007; Pinto and Raible, 2012]. The precipitation anomalies are again highly significant in VOLC.O₃^{strong}, whereas they are insignificant in the VOLC.O₃^{weak} simulations.

3.3. Zonal Wind Changes

A possible explanation for this difference in the tropospheric dynamic lies in the behavior of the polar vortex and the stratosphere-troposphere coupling identified in the two ensemble experiments. An index for the strength of the polar vortex and the downward propagation of anomalies is the zonal mean zonal wind at 60°N [Christiansen, 2001, 2005] in the following named \bar{u}_{60} . Figure 5a displays the time series of \bar{u}_{60} at 10 hPa following the eruption. For comparison the mean annual cycle in the two control ensembles is shown as dashed lines. In the perturbed ensemble experiments an intensification of the wind speed starts a few months after the eruption. This intensification increases in winter and reaches its maximum in mid-February for VOLC.O₃^{weak} and by the end of February for VOLC.O₃^{strong}. Additionally, the vortex is significantly weakened in the VOLC.O₃^{weak} experiment by the end of December, whereas the vortex in VOLC.O₃^{strong} remains very strong throughout the winter. Moreover, the polar vortex is significantly stronger in VOLC.O₃^{strong} from February on ($p \leq 0.05$, Student's t test) than in the VOLC.O₃^{weak} experiment. The increase of the vortex speed relative to the respective control ensemble are comparable. This indicates that the additional intensification caused by the volcanic eruption is comparable for both ozone climatologies.

We also find a clear difference in the vortex intensities between the control ensembles (dashed lines in Figure 5a). In January, when the vortex index reaches its maximum, zonal winds are about 5 m/s ($\sim 15\%$)

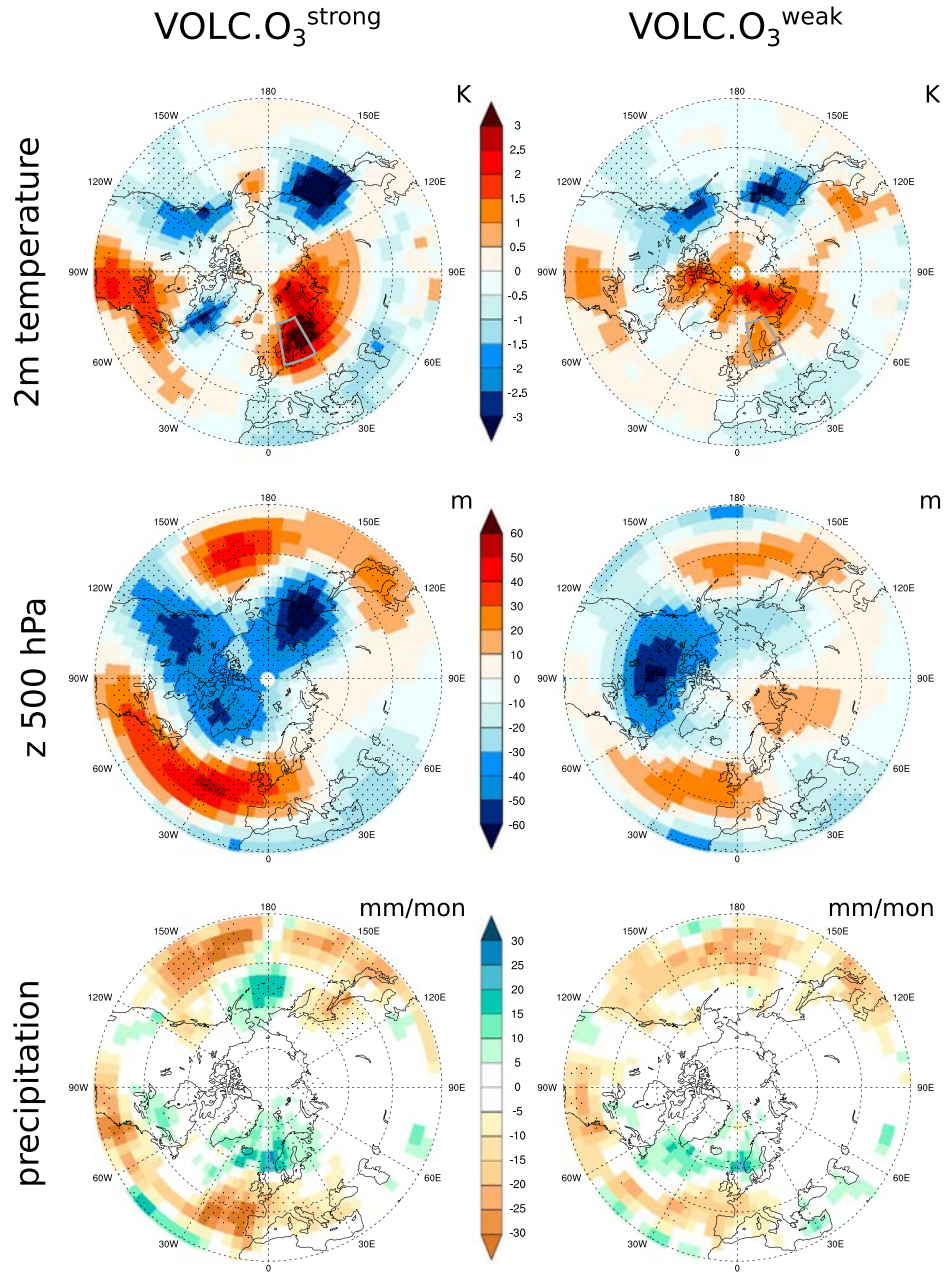


Figure 4. Ensemble mean anomalies for (top) the 2 m temperature, (middle) 500 hPa geopotential height, and (bottom) precipitation in the winter (DJF) following the eruption for the strong ozone gradient climatology (VOLC.O₃^{strong}, left) and the weak gradient climatology (VOLC.O₃^{weak}, right). Anomalies are expressed in terms of anomalies to the DJF mean in the corresponding control (CTRL.O₃^{strong} and CTRL.O₃^{weak}). Significant differences ($p \leq 0.05$, Student's t test) are indicated by stippling. Gray boxes in the temperature plots indicate the Scandinavian region used to calculate temperature anomalies.

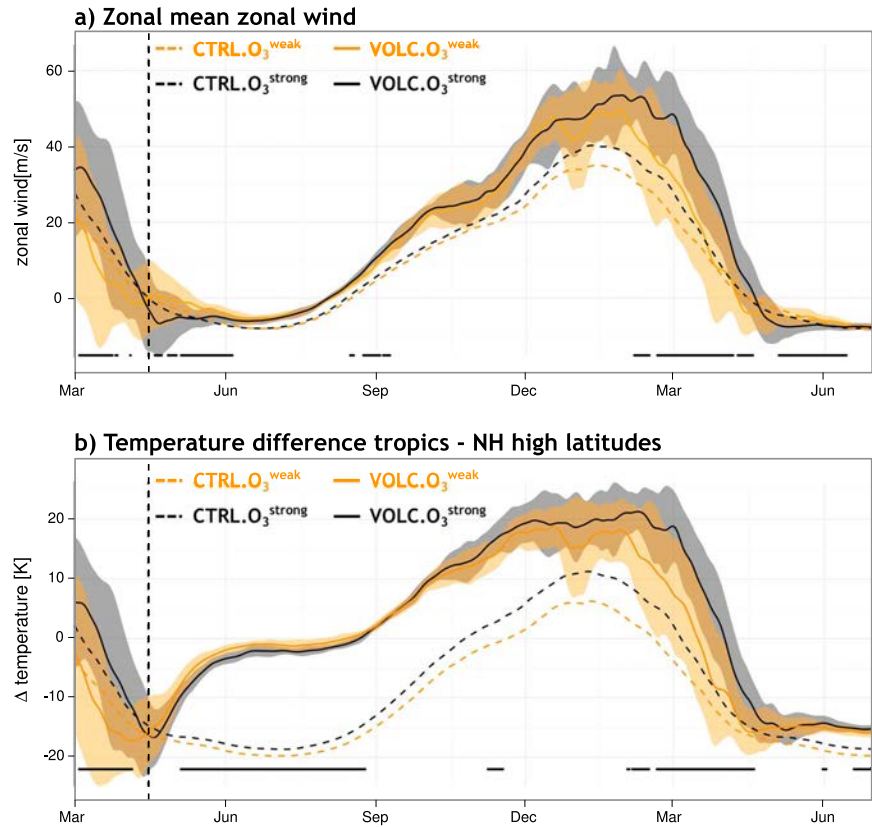


Figure 5. (a) Time series of the daily zonal mean zonal wind at 60°N (\bar{u}_{60}) and 10 hPa in m/s for VOLC.O₃^{strong} (solid black) and VOLC.O₃^{weak} (solid orange). (b) Daily zonal mean stratospheric temperature difference in K at 40 hPa between the tropics and the northern high latitudes (i.e., 20°S–20°N mean minus 70°N–90°N mean). Solid lines: ensemble mean. Shaded areas: ensemble standard deviation. Dashed lines: mean annual cycle in the control ensembles (black: CTRL.O₃^{strong}, orange: CTRL.O₃^{weak}). Vertical dashed line: start of the eruption. Dots at the bottom: significant differences between the two perturbed ensembles (Student’s *t* test with $p \leq 0.05$). All time series are smoothed by a 11 day low-pass filter.

stronger in the simulation with larger ozone gradients in the middle stratosphere (VOLC.O₃^{strong}). Besides some weeks in April, the two control ensembles differ significantly ($p \leq 0.05$, Student’s *t* test) during the entire year (not shown). In the winter season both control ensemble experiments lie within the uncertainty range (one standard deviation) of the daily average \bar{u}_{60} derived from ERA Interim (average 1979–2013, see supporting information Figure S3) [Dee et al., 2011].

The different vortex intensities are explained by the differences in the ozone climatologies. In the O₃^{strong} climatology higher ozone concentrations are found in the lower and middle stratosphere, with larger anomalies in the tropical stratosphere than in the polar region (Figure 2a). Higher ozone values in the tropics lead to a more efficient UV absorption and thus to higher temperatures in the tropical lower stratosphere in the strong ozone gradient case. Since the temperature anomalies at the poles are smaller due to less insolation, the net effect is an increase of the temperature gradient between tropics and the northern high latitudes in the lower and middle stratosphere (Figure 2b). In both ensembles the intensity of the polar vortex is closely related to this temperature difference. In the stratosphere the correlation between \bar{u}_{60} and the meridional temperature difference between the tropics and high latitudes exceeds 0.95 at all levels between 10 hPa and 100 hPa. Consequently, the stratospheric temperature differences between the two control ensemble experiments are the driver for the differences in the vortex intensities [Andrews et al., 1987].

In the perturbed ensemble experiment the stratospheric temperatures are also affected by the volcanic aerosol, whose highest concentrations are in the regions where the two ozone climatologies differ the

most (solid contours in Figure 2a). In these layers the volcanic aerosols are responsible for an increase of the absorption of near-infrared and infrared radiation, which leads to anomalous high temperatures, and alter the lower stratospheric temperature gradient between the tropics and the poles. For all ensembles, the temporal development of the temperature difference at 40 hPa is shown in Figure 5b. The 40 hPa level is selected, since the highest correlation coefficients ($r > 0.98$) between the temperature difference and the vortex index in the control ensembles are found at this altitude. However, the results at stratospheric levels above and below are comparable to the results at 40 hPa. The dashed lines in Figure 5b represent the mean annual cycle of the temperature gradients in the two control ensembles. The differences between the two cycles resemble the differences between the ozone climatologies. Relative to the control ensembles the temperature differences in VOLC.O₃^{strong} and VOLC.O₃^{weak} starts to increase immediately after the eruption and reaches its maximum in winter. In summer, intensifications are very similar (although with slightly higher wind speeds in VOLC.O₃^{weak}). From November to April, higher temperature differences are found in the ensemble with larger meridional ozone gradients (VOLC.O₃^{strong}). The meridional temperature profile for the perturbed and unperturbed DJF temperatures at 40 hPa is shown in Figure S4.

3.4. Stratosphere-Troposphere Coupling

In order to influence climate at the surface, stratospheric zonal wind anomalies have to propagate vertically through the tropopause. To illustrate the dynamic coupling between the stratosphere and the troposphere we show Hovmöller diagrams of both perturbed ensemble $\bar{u}60$ means relative to the corresponding control (Figure 6). The pattern is similar in both ensemble experiments. An intensification of the zonal mean zonal wind starts in the upper stratosphere about 2 months after the beginning of the eruption. In the following months the signal propagates downward into the lower stratosphere. However, the magnitude of anomalies in the lower stratosphere and the troposphere differs between the ensemble experiments showing higher anomalies in later winter in VOLC.O₃^{strong}. During the winter season, several pulses of downward propagating positive signals from the stratosphere to the troposphere are visible in the VOLC.O₃^{strong} ensemble average, whereas much fewer events are found in VOLC.O₃^{weak}. In the next step we show that these events, visible in the ensemble mean, are related to a larger number of stratosphere-troposphere couplings in the VOLC.O₃^{strong} ensemble.

3.5. Robustness Tests

The ensemble mean $\bar{u}60$ gives only hint on the coupling between the stratosphere and the troposphere, as information on the single events is partly lost by the averaging procedure. Furthermore, it could happen that a single ensemble member dominates the anomaly pattern shown in Figure 4 or 6. Therefore, we analyze the temperature anomalies and the stratosphere-troposphere couplings in detail.

For the Scandinavian surface temperature anomalies clear differences are found between the two ensemble experiments. The histogram for the posteruption DJF temperature anomalies averaged over northern Europe (10°E–30°E and 55°N–70°N, gray box in Figure 4) reveals that the majority of ensemble members in VOLC.O₃^{strong} are warmer than the average anomaly in VOLC.O₃^{weak} (Figure 7a). Therefore, the temperature anomalies shown in Figure 4 are not just dominated by one or two extreme members.

The same applies to the number of stratosphere-troposphere couplings. As a measure for the characterization of days with coupling events or anomalously high zonal winds in the troposphere and lower stratosphere, $\bar{u}60$ is averaged over the levels 1000 to 100 hPa. This measure does not directly consider the conditions at higher atmospheric levels. However, a composite over events with the index value exceeding a certain threshold (e.g., one standard deviation σ) reveals that anomalously high wind speeds in the lower levels are preceded by anomalously high wind conditions at higher levels in the stratosphere by up to 30 days (Figure 7b). This behavior is found in both control simulations, and also when higher thresholds are used. Applied to the posteruption winter of the perturbed simulations 123 days with anomalously high winds in the troposphere are found in the members of VOLC.O₃^{strong}, whereas only 57 days show stratosphere-troposphere couplings in the VOLC.O₃^{weak} simulations (using a threshold of $2 \cdot \sigma_{\text{CTRL.O}_3^{\text{strong}}}$). This result is again independent of the threshold applied as the comparison for threshold between 0.5 and 3.0 σ shows (Figure 7c). Finally, using a jackknife resampling test [von Storch and Zwiers, 2000] we test whether these results are dominated by a single extreme member. The number of days with a wind speed index $\geq 2 \cdot \sigma_{\text{CTRL.O}_3^{\text{strong}}}$ were calculated for all possible combinations, where one member was excluded from the statistics. The histogram of the results (Figure 7d) show that in any case, the two perturbed ensembles differ notably and reveal the robustness of the results.

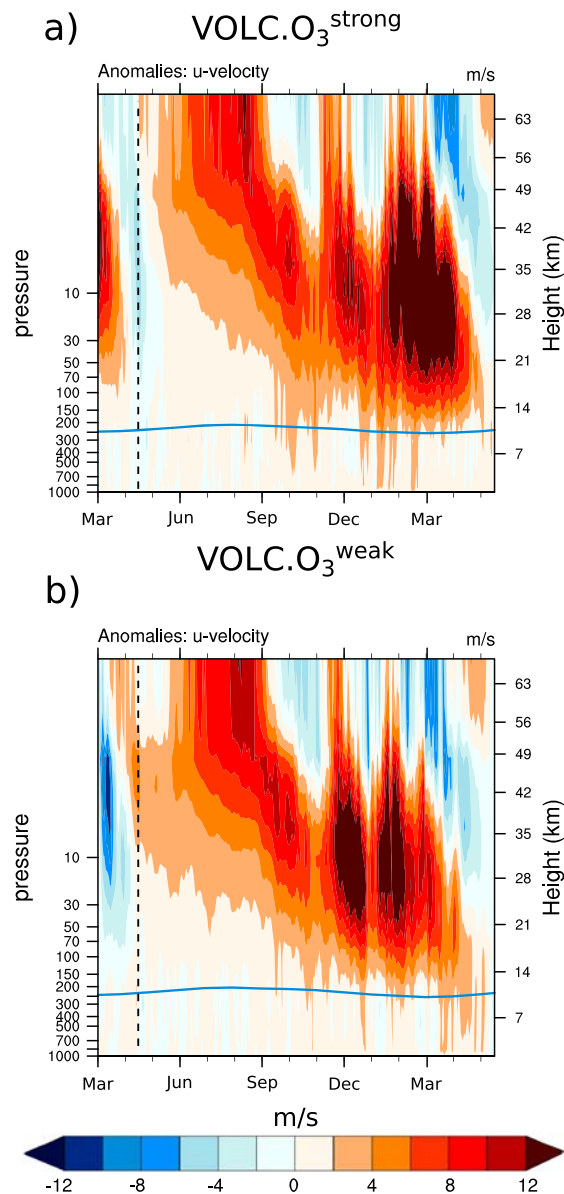


Figure 6. Ensemble mean daily zonal mean zonal wind anomalies in m/s at 60°N (\bar{u}_{60}) as a function of height and time, for (a) VOLC.O₃^{strong} and (b) VOLC.O₃^{weak}. The start of the eruption is indicated by the vertical dashed line. Anomalies are expressed relative to the corresponding ensemble mean. The thick blue line denotes the approximate tropopause height.

3.6. Nonlinearity

Finally, we address whether the impact of the two perturbations, the ozone climatology and the volcanic eruption, can be linearly superimposed. Again we use the mean tropospheric wind index defined above, but instead of anomalies with respect to the corresponding control ensemble sets, we consider the absolute values of the ensemble simulations. The effect of the ozone climatology is assessed using the control ensembles. The stronger gradient climatology leads to an intensification of the winter zonal winds of around 0.55 m/s in the mean value as well as in the higher percentiles. The effect of the eruption on the zonal wind extracted from the difference between CTRL.O₃^{weak} and VOLC.O₃^{weak} is 1.6 m/s for the mean and 5.2 m/s for

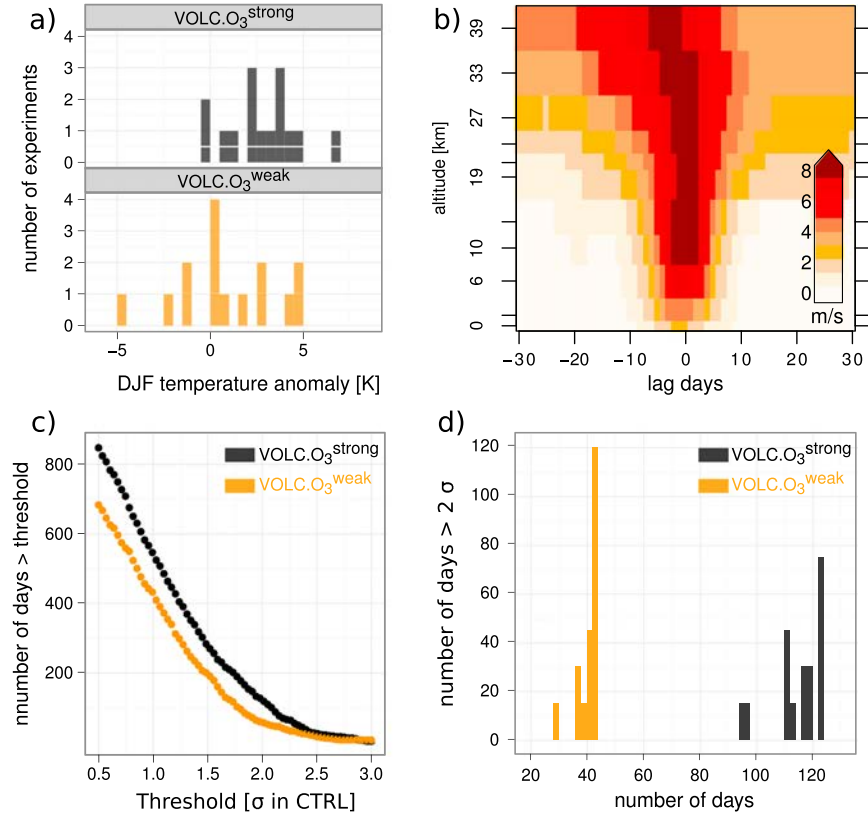


Figure 7. (a) Histogram for the post eruption northern Europe DJF temperature anomaly in the ensemble member. The temperature anomaly was averaged over the region 10°E–30°E and 55°N–70°N (binwidth of the histogram: 0.5 K). (b) Composite of the time-height development of anomalies in the zonal mean zonal wind at 60°N (\bar{u}_{60}) in m/s for events with anomalously high mean tropospheric wind speed. An event is defined as a day (for multiday events the central day was chosen), where the mean \bar{u}_{60} between 1000 and 100 hPa exceeds one standard deviation ($\sigma = 2.85$ m/s). The composite shows the temporal development for the 30 days before and after the exceeding of the threshold for CTRL.O₃^{strong} (based on 460 events). (c) Number of days in the posteruption winter season where the mean \bar{u}_{60} between 1000 and 100 hPa exceeds a given threshold (expressed as standard deviation in CTRL.O₃^{strong}, reaching from 0.5 to 3), for VOLC.O₃^{strong} and VOLC.O₃^{weak}, respectively. (d) Histogram (binwidth: 2 days) of the number of days with \bar{u}_{60} between 1000 and 100 hPa > $2 \cdot \sigma$ using a leave-one-out jackknife test for both perturbed ensembles.

the 95th percentile. Assuming a linear superposition of both effects, the combined effect should result in an intensification of around 2.15 m/s for the mean value and 5.75 m/s for the 95th percentile. However, between CTRL.O₃^{weak} and VOLC.O₃^{strong} differences of 2.6 m/s for the mean value and 6.4 m/s for the 95th percentile are found, which indicates some nonlinear, amplifying coupling between the ozone differences and the volcanic signal.

4. Comparison With Data

When comparing the European winter warming pattern from both ensembles to the climate signals in reconstructions, the VOLC.O₃^{strong} ensemble is in better agreement. Fischer *et al.* [2007] reconstructed the average winter temperature, pressure, and precipitation response after 15 major volcanic eruptions based on multiproxy reconstructions for Europe. They found a clear and significant positive phase of the NAO with the corresponding temperature and precipitation pattern [Fischer *et al.*, 2007, Figure 2]. Also the absolute values of the anomalies compare very well. However, given that the Tambora eruption simulated here is the strongest eruption of the last several hundred years and the Fischer *et al.* [2007] composite represents the average over 15 large volcanic eruptions a direct comparison of the absolute anomalies is difficult. Yet the high significance of the anomalies gives us confidence that the model response is robust compared to what we expect from the reconstructions.

It should be noted that the setup used in this study does not simulate the interactive response of the chemistry to the tropical eruption. With interactive ozone chemistry the response may be different due to positive or negative feedbacks. In the preindustrial case, without ozone-depleting substances (ODS) ozone values are expected to increase in the extratropical lower stratosphere, due to the deactivation of NO_x via heterogeneous reactions on the surface of the volcanic aerosols [Tie and Brasseur, 1995; Solomon *et al.*, 1996; Anet *et al.*, 2013]. This effect may reduce the meridional ozone gradient and weaken the dynamic response.

With ODS in the stratosphere, ozone values are reduced in the extratropical lower stratosphere by the activation of chlorine and the resulting ozone destruction [Tie and Brasseur, 1995; Kinne *et al.*, 1992; Rozanov *et al.*, 2002]. In this case the eruption might increase the meridional ozone gradient and amplify the dynamic effects. Furthermore, the cooling of the polar stratosphere that accompanies the vortex intensification can increase the number of polar stratospheric clouds, further reduce ozone, and create a positive feedback.

The ozone climatologies used in this sensitivity study originate from two different sources. The weak gradient climatology is based on observational data for the late 20th century. The second climatology with stronger meridional gradients was extracted from a preindustrial control simulation with interactive chemistry. Although each climatology represents a distinct state of the stratosphere (preindustrial without ozone depletion versus present day with ozone depletion), a direct interpretation of the results in terms of a shift from preindustrial to present day is not possible due to the different data sources and biases (see Stenke *et al.* [2013] for an evaluation of the chemistry climate model).

Nevertheless, the two climatologies are compared to existing transient data sets to estimate how the forcings used in this sensitivity study compare to ozone changes in the past and to the uncertainties between different ozone reconstructions. The knowledge of the preindustrial (1600 A.D. in this study) ozone values is of course limited and based only on model results. However, since the emission of ozone-depleting substances is a phenomena of the late 20th century, we safely assume that ozone values of the early 20th century are comparable to preindustrial values [Brönnimann *et al.*, 2003].

In the last years, a few data sets of transient ozone concentrations were developed. For the CMIP5 simulations, Cionni *et al.* [2011] created ozone forcing from 1850 onward based on model results and observations Stratosphere-troposphere Processes And their Role in Climate (SPARC). Due to the approach they used, the variability in the early decades of the record is rather low. Therefore, we also compare to a newer ozone reconstruction of Brönnimann *et al.* [2013] that starts in 1900 and show realistic interannual variability (HISTOZ 1.0). The latter reconstruction is based on SOCOL (version 2) simulations [Fischer *et al.*, 2008], augmented by historical total ozone observations from the 1920s to 1970s. From 1979 it is supplemented with an observation-based ozone data set [Hassler *et al.*, 2008].

Two periods were selected for the comparison. An early period from 1900 to 1919 represents the undisturbed situation, i.e., without the attendance of ODS in the atmosphere, and a later period ranging from 1970 to 1989 (roughly the period of Fortuin and Kelder [1998]) that includes the effect of ozone depletion. All values are averaged over the winter season (DJF). With ODS the climatology of Fortuin and Kelder [1998] compares very well with the SPARC record, which is expected since this climatology is one of the data sources used to compile the SPARC climatology. Substantial differences between HISTOZ (which for the majority of the period consists of the [Hassler *et al.*, 2008] observation data set) and SPARC are found for the meridional gradient, with HISTOZ showing stronger gradients at 10 and 20 hPa and weaker gradients at 50 hPa (Figure 8, left). Without ODS the deviations between the different data sets become larger. Again HISTOZ (which in this period is based on SOCOL simulations only, see Fischer *et al.* [2008]) is characterized by larger meridional ozone differences at 10 and 20 hPa and weaker differences at 50 hPa (Figure 8, middle).

The important comparison is the change in the ozone profile caused by ODS (Figure 8, right). Here we find substantial differences to SPARC and HISTOZ, which confirms our statement that the results should not be interpreted as a shift from preindustrial to present day. At 10 and 20 hPa we find a clear ozone reduction in the tropics in our climatology whereas the two transient records show either a weak reduction (HISTOZ) or slight increase (SPARC) in the tropics and a clear decrease of the ozone values in the northern high latitudes. The effect of ozone depletion on the meridional ozone gradient is therefore much stronger (compared to HISTOZ) or even the opposite (SPARC). At 50 hPa a general ozone reduction with the attendance of ODS is found on nearly all latitudes in all data sets. However, the reductions are between 2 and 4 times higher in the climatologies used in this study.

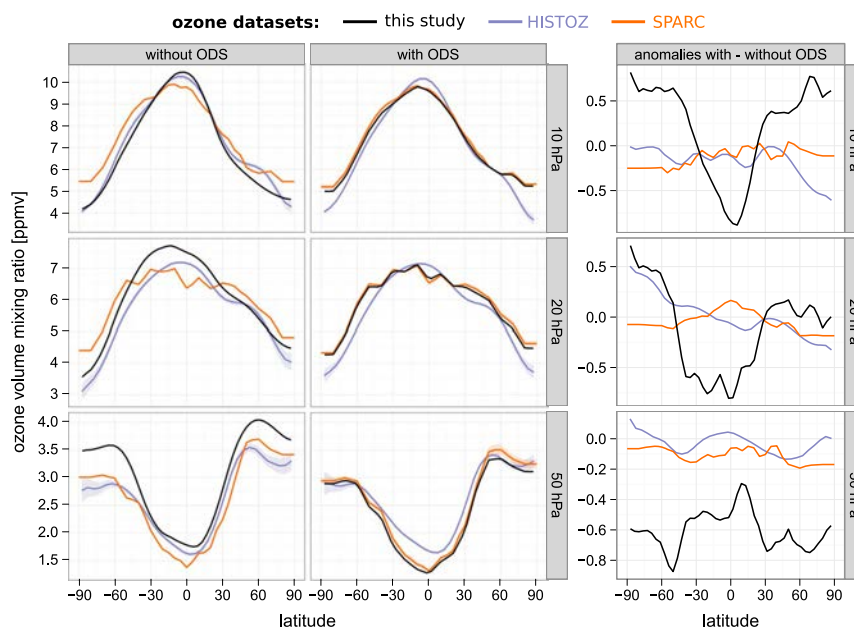


Figure 8. Comparison between the DJF ozone volume mixing ratios (ppmv) in the climatologies used in this study to the HISTOZ 1.0 [Brönnimann et al., 2013] and the SPARC data set [Cionni et al., 2011]. (left) Mean ozone profile for periods without ODS (average 1900–1919). (middle) Profile for periods with the attendance of ODS (average 1970–1989). (right) Change in the ozone mixing ratios between the two periods. Meridional profiles are shown for the 10, 20, and 50 hPa altitudes. Shading indicates one standard deviation in the corresponding record. Please note the different axis scaling.

5. Discussion and Conclusions

In ensemble sensitivity simulations forced with two different ozone climatologies, we found a strong difference in the coupling of positive wind speed anomalies after large volcanic eruptions from the stratosphere to the troposphere. These differences are related to the different background states of the stratosphere linked to the two ozone climatologies. The two ozone climatologies mainly differ in the meridional ozone gradients between high and low latitudes. With a larger ozone gradient the northern winter polar vortex is around 15% stronger, and the volcanic eruption causes an additional intensification of the vortex. Although the volcanic intensification is roughly of similar strength in the weak gradient ensemble ($\text{VOLC.O}_3^{\text{weak}}$), the combined net effect is larger in $\text{VOLC.O}_3^{\text{strong}}$ and results in a higher number of stratosphere-troposphere coupling events which lead to higher and more extended temperature anomalies in northern Europe.

This analysis is subjected to a number of caveats and limitations which we discuss in the following:

1. The volcanic forcing by Arfeuille et al. [2013a] that is used in this study to implement the impact of the Tambora eruptions disagrees in some aspects with earlier volcanic forcing reconstructions. In particular the high asymmetry, with the majority of aerosols spread into the Southern Hemisphere, is discussed. An explanation for this asymmetry is already given by the authors. Tambora erupted in April 1815, corresponding to the fall season of the Southern Hemisphere. In the following weeks and months the aerosol accumulated in the tropical stratosphere and was slowly transported toward higher latitudes. In the stratosphere the transport is mainly directed toward the winter hemisphere [Holton et al., 1995], which explains the larger accumulation of aerosols in the Southern Hemisphere. This is also in agreement with transport assumptions made by [Ammann et al., 2003] for their volcanic forcing. A similar, although less pronounced asymmetry, can be found in the forcing of Crowley et al. [2008]. Moreover, as shown in Arfeuille et al. [2013b], the methodology used succeeds in reproducing the very asymmetric aerosol cloud of the Agung 1963 eruption, which has a similar timing and location compared to the Tambora 1815 eruption (i.e., March, 8°S) and a similar asymmetric hemispheric partitioning [Stothers, 2001]. Another caveat related to the volcanic forcing is that the forcing was calculated offline and therefore does not react to the

different dynamics related to the different ozone climatologies. However, this approach is chosen in most of the GCMs today.

2. The simulated heating in the tropical stratosphere forced by the volcanic aerosols is probably overestimated, a feature that is common to many GCMs [Lanzante and Free, 2008; Driscoll et al., 2012]. A part of the overestimation may be related to the fact that the chosen setup does not simulate the ozone chemistry interactively and therefore the cooling effect caused by tropical ozone depletion is not included [Kirchner et al., 1999; Stenchikov et al., 2002].
3. This study does not consider the effect of different QBO phases on the results, instead all ensembles are nudged toward the same, easterly QBO phase in the winter after the eruption. Since the northern high-latitude geopotential height in the stratosphere is known to be in general higher during easterly phases of the QBO [Holton and Tan, 1980, 1982], the vortex intensification may be even stronger when the QBO is in a westerly phase [Stenchikov et al., 2004; Thomas et al., 2009a]. In which way, this affects the anomalies at the surface needs to be assessed in future work.

In the IPCC AR4, several models used a constant ozone climatology [Miller et al., 2006; Son et al., 2010] and it was found that the winter warming pattern is in general too weak compared with observations [Miller et al., 2006; Stenchikov et al., 2006]. Beginning with CMIP5 a prescribed time-dependent ozone forcing, which considers changes in the atmospheric ozone composition is recommended, but the models still fail in reproducing an appropriate winter warming response [Driscoll et al., 2012].

A part this failure may be related to the fact that the effect of ozone depletion, as observed after Pinatubo, are still not considered in the forcing [Cionni et al., 2011]. The polar ozone depletion might strengthen the positive AO phase [Stenchikov et al., 2002]. However, even with prescribed ozone anomalies models still fail in producing a significant winter warming pattern, even in larger ensembles [Thomas et al., 2009b]. Furthermore, winter warming patterns have also been found for eruptions that were not influenced by the effect of ozone-depleting substances, i.e., eruption before 1970.

The results presented here show that the state of the stratosphere, especially the polar vortex, is an important prerequisite for a decent simulation of the dynamic response to eruptions and that the meridional ozone gradient strongly influences the state of the polar vortex.

The differences between existing ozone records for the past and the uncertainties in chemistry-climate model-based ozone projections for the future [Eyring et al., 2007; Karpechko and Gillett, 2010] are large. We show that the decision for a particular ozone data set might significantly influence the dynamic response to tropical volcanic eruptions in a nonlinear way. Analyzing the mechanisms involved in the stratosphere-troposphere coupling was out of scope of this sensitivity study. However, understanding which processes are dominant (compare Gerber et al. [2012]) is necessary for a thorough evaluation of the role of ozone gradients. Furthermore, the evidence presented here needs to be evaluated in other GCMs without interactive ozone chemistry and with other volcanic eruptions. Future work will also assess the question how the findings change with interactive ozone chemistry.

Acknowledgments

The authors thank the three anonymous reviewers for their fruitful comments. Moreover, we would like to thank Greg Bodeker (Bodeker Scientific) and Birgit Hassler (NOAA) for providing the combined vertical ozone profile database through the British Atmospheric Data Centre (BADC). This project is supported by the Swiss National Science Foundation under the grant CRS1122-130642 (FUPSOL). This paper profited from discussions during the PAGES/FUSOL Workshop in 2012.

References

- Ammann, C. M., G. A. Meehl, W. M. Washington, and C. S. Zender (2003), A monthly and latitudinally varying volcanic forcing dataset in simulations of 20th century climate, *Geophys. Res. Lett.*, *30*(12), 1–4, doi:10.1029/2003GL016875.
- Andrews, D. G., J. R. Holton, and C. B. Leovy (1987), *Middle Atmosphere Dynamics*, 489 p., Academic Press, London.
- Anet, J. G., et al. (2013), Forcing of stratospheric chemistry and dynamics during the Dalton Minimum, *Atmos. Chem. Phys.*, *13*, 10,951–10,967, doi:10.5194/acp-13-10951-2013.
- Arfeuille, F., D. Weisenstein, H. Mack, E. Rozanov, T. Peter, and S. Brönnimann (2013a), Volcanic forcing for climate modeling: A new microphysics-based dataset covering years 1600–present, *Clim. Past Discuss.*, *9*, 967–1012, doi:10.5194/cpd-9-967-2013.
- Arfeuille, F., B. P. Luo, P. Heckendorn, D. Weisenstein, J. X. Sheng, E. Rozanov, M. Schraner, S. Brönnimann, L. W. Thomason, and T. Peter (2013b), Modeling the stratospheric warming following the Mt. Pinatubo eruption: Uncertainties in aerosol extinctions, *Atmos. Chem. Phys.*, *13*, 11,221–11,234, doi:10.5194/acp-13-11221-2013.
- Auchmann, R., S. Brönnimann, L. Breda, M. Bühler, R. Spadin, and A. Stickler (2012), Extreme climate, not extreme weather: The summer of 1816 in Geneva, Switzerland, *Clim. Past*, *8*, 325–335, doi:10.5194/cp-8-325-2012.
- Baldwin, M. P., and T. J. Dunkerton (2001), Stratospheric harbingers of anomalous weather regimes, *Science*, *294*(5542), 581–4, doi:10.1126/science.063315.
- Baldwin, M. P., X. Cheng, and T. J. Dunkerton (1994), Observed correlations between winter-mean tropospheric and stratospheric circulation anomalies, *Geophys. Res. Lett.*, *21*(12), 1141–1144.
- Baldwin, M. P., M. Dameris, and T. G. Shepherd (2007), How will the stratosphere affect climate change?, *Science*, *316*, 1576–1577.
- Brönnimann, S., J. Staehelin, S. F. G. Farmer, J. C. Cain, T. Svendby, and T. Svenøe (2003), Total ozone observations prior to the IGY. I: A history, *Q. J. Roy. Meteorol. Soc.*, *129*(593), 2797–2817, doi:10.1256/qj.02.118.

- Brönnimann, S., J. L. Annis, C. Vogler, and P. D. Jones (2007), Reconstructing the quasi-biennial oscillation back to the early 1900s, *Geophys. Res. Lett.*, *34*, L22805, doi:10.1029/2007GL031354.
- Brönnimann, S., J. Bhend, J. Franke, S. Flückiger, A. M. Fischer, R. Bleisch, G. Bodeker, B. Hassler, E. Rozanov, and M. Schraner (2013), A global historical ozone data set and prominent features of stratospheric variability prior to 1979, *Atmos. Chem. Phys.*, *13*, 9623–9639, doi:10.5194/acp-13-9623-2013.
- Budich, R., M. Gioretta, J. Jungclaus, R. Redler, and C. Reick (2010), The MPI-M Millennium Earth System Model: An assembling guide for the COSMOS configuration, *MPI report*, Max-Planck Institute for Meteorology, Hamburg, Germany.
- Christiansen, B. (2001), Downward propagation of zonal mean zonal wind anomalies from the stratosphere to the troposphere: Model and reanalysis, *J. Geophys. Res.*, *106*(D21), 27,307–27,322, doi:10.1029/2000JD000214.
- Christiansen, B. (2005), Downward propagation and statistical forecast of the near-surface weather, *J. Geophys. Res.*, *110*, D14104, doi:10.1029/2004JD005431.
- Christiansen, B. (2008), Volcanic eruptions, large-scale modes in the Northern Hemisphere, and the El Niño–Southern Oscillation, *J. Climate*, *21*, 910–922, doi:10.1175/2007JCLI1657.1.
- Cionni, I., V. Eyring, J. F. Lamarque, W. J. Randel, D. S. Stevenson, F. Wu, G. E. Bodeker, T. G. Shepherd, D. T. Shindell, and D. W. Waugh (2011), Ozone database in support of CMIP5 simulations: Results and corresponding radiative forcing, *Atmos. Chem. Phys.*, *11*, 11,267–11,292, doi:10.5194/acp-11-11267-2011.
- Cole-Dai, J. (2010), Volcanoes and climate, *WIREs Clim. Change*, *1*, 824–839, doi:10.1002/wcc.76.
- Crowley, T., G. Zielinski, B. Vinther, R. Udisti, K. Kreutz, J. Cole-Dai, and E. Castellano (2008), Volcanism and the little ice age, *PAGES News*, *16*, 22–23.
- Dee, D. P., et al. (2011), The ERA-Interim reanalysis: Configuration and performance of the data assimilation system, *Q. J. Roy. Meteorol. Soc.*, *137*, 553–597, doi:10.1002/qj.828.
- Driscoll, S., A. Bozzo, L. J. Gray, A. Robock, and G. Stenchikov (2012), Coupled Model Intercomparison Project 5 (CMIP5) simulations of climate following volcanic eruptions, *J. Geophys. Res.*, *117*, D17105, doi:10.1029/2012JD017607.
- Eyring, V., et al. (2007), Multimodel projections of stratospheric ozone in the 21st century, *J. Geophys. Res.*, *112*, D16303, doi:10.1029/2006JD008332.
- Fischer, A. M., et al. (2008), Interannual-to-decadal variability of the stratosphere during the 20th century: Ensemble simulations with a chemistry-climate model, *Atmos. Chem. Phys.*, *8*, 7755–7777, doi:10.5194/acp-8-7755-2008.
- Fischer, E. M., J. Luterbacher, E. Zorita, S. F. B. Tett, C. Casty, and H. Wanner (2007), European climate response to tropical volcanic eruptions over the last half millennium, *Geophys. Res. Lett.*, *34*, 1–6, doi:10.1029/2006GL027992.
- Fortuin, J. P. F., and H. Kelder (1998), An ozone climatology based on ozonesonde and satellite measurements, *J. Geophys. Res.*, *103*, 31,709–31,734, doi:10.1029/1998JD200008.
- Gerber, E. P., et al. (2012), Assessing and understanding the impact of stratospheric dynamics and variability on the Earth system, *Bull. Am. Meteorol. Soc.*, *93*, 845–859, doi:10.1175/bams-d-11-00145.1.
- Gillett, N. P., and D. W. J. Thompson (2003), Simulation of recent Southern Hemisphere climate change, *Science*, *302*(5643), 273–275, doi:10.1126/science.1.087440.
- Gillett, N. P., M. R. Allen, R. E. Mcdonald, C. A. Senior, D. T. Shindell, and G. A. Schmidt (2002), How linear is the Arctic Oscillation response to greenhouse gases?, *J. Geophys. Res.*, *107*, 1–7, doi:10.1029/2001JD000589.
- Graf, H. F., I. Kirchner, A. Robock, and I. Schult (1993), Pinatubo eruption winter climate effects: Model versus observations, *Clim. Dynam.*, *92*, 81–93.
- Hagemann, S. (2002), An improved land surface parameter dataset for global and regional climate models, *MPI report 336*, Max-Planck Institut fuer Meteorologie, Hamburg, Germany.
- Hassler, B., G. E. Bodeker, and M. Dameris (2008), Technical note: A new global database of trace gases and aerosols from multiple sources of high vertical resolution measurements, *Atmos. Chem. Phys.*, *8*, 5403–5421, doi:10.5194/acp-8-5403-2008.
- Hurrell, J. W. (1995), Decadal trends in the North Atlantic Oscillation: Regional temperatures and precipitation, *Science*, *269*, 676–679.
- Holton, J. R., and H.-C. Tan (1980), The influence of the equatorial-biennial oscillation on the global circulation at 50 mb, *J. Atmos. Sci.*, *37*, 2200–2208.
- Holton, J. R., and H.-C. Tan (1982), The quasi-biennial Northern Hemisphere Oscillation in the lower stratosphere, *J. Meteorol. Soc. Jpn.*, *60*(1), 140–148.
- Holton, J. R., P. H. Haynes, M. E. McIntyre, A. R. Douglass, R. B. Rood, and L. Pfister (1995), Stratosphere–troposphere exchange, *Rev. Geophys.*, *33*(4), 403–439.
- Jungclaus, J. H., N. Keenlyside, M. Botzet, H. Haak, J.-J. Luo, M. Latif, J. Marotzke, U. Mikolajewicz, and E. Roeckner (2006), Ocean circulation and tropical variability in the coupled model ECHAM5/MPI-OM, *J. Climate*, *19*, 3952–3972, doi:10.1175/JCLI3827.1.
- Jungclaus, J. H., et al. (2010), Climate and carbon-cycle variability over the last millennium, *Clim. Past*, *6*, 723–737, doi:10.5194/cp-6-723-2010.
- Karpechko, A. Y., and N. P. Gillett (2010), Quantitative assessment of Southern Hemisphere ozone in chemistry-climate model simulations, *Atmos. Chem. Phys.*, *10*, 1385–1400.
- Kinne, S., O. B. Toon, and M. J. Prather (1992), Buffering of stratospheric circulation by changing amounts of tropical ozone a Pinatubo case study, *Geophys. Res. Lett.*, *19*(19), 1927–1930.
- Kirchner, I., G. L. Stenchikov, H.-F. Graf, A. Robock, and J. C. Antuña (1999), Climate model simulation of winter warming and summer cooling following the 1991 Mount Pinatubo volcanic eruption, *J. Geophys. Res.*, *104*(D16), 19,039–19,055, doi:10.1029/1999JD900213.
- Kodera, K. (1994), Influence of volcanic eruptions on the troposphere through stratospheric dynamical processes in the Northern Hemisphere winter, *J. Geophys. Res.*, *99*(D1), 1273–1282.
- Lanzante, J. R., and M. Free (2008), Comparison of radiosonde and GCM vertical temperature trend profiles: Effects of dataset choice and data homogenization, *J. Climate*, *21*, 5417–5435, doi:10.1175/2008JCLI2287.1.
- Marsland, S. (2003), The Max-Planck-Institute global ocean/sea ice model with orthogonal curvilinear coordinates, *Ocean Model.*, *5*(2), 91–127, doi:10.1016/S1463-5003(02)00015-X.
- Miller, R. L., G. A. Schmidt, and D. T. Shindell (2006), Forced annular variations in the 20th century Intergovernmental Panel on Climate Change Fourth Assessment Report models, *J. Geophys. Res.*, *111*, 1–17, doi:10.1029/2005JD006323.
- Pinto, J. G., and C. C. Raible (2012), Past and recent changes in the North Atlantic Oscillation, *WIREs Clim. Change*, *3*, 79–90, doi:10.1002/wcc.150.
- Raible, C. C., U. Luksch, and K. Fraedrich (2004), Precipitation and Northern Hemisphere regimes, *Atmos. Sci. Lett.*, *5*, 43–55, doi:10.1016/j.atmosclet.2003.12.001.
- Robock, A. (2000), Volcanic eruptions and climate, *Rev. Geophys.*, *38*, 191–219.

- Robock, A., and J. Mao (1992), Winter warming from large volcanic eruptions, *Geophys. Res. Lett.*, *12*, 2405–2408.
- Roeckner, E., et al. (2003), The atmospheric general circulation model ECHAM5 - Model description, *MPI report 349*, Max-Planck Institute for Meteorology, Hamburg, Germany.
- Roazanov, E. V., M. E. Schlesinger, N. G. Andronova, F. Yang, S. L. Malyshev, V. A. Zubov, T. A. Egorova, and B. Li (2002), Climate/chemistry effects of the Pinatubo volcanic eruption simulated by the UIUC stratosphere/troposphere GCM with interactive photochemistry, *J. Geophys. Res.*, *107*(D21), 4594, doi:10.1029/2001JD000974.
- Shepherd, T. G. (2002), Issues in stratosphere-troposphere coupling, *J. Meteorol. Soc. Jpn.*, *80*(4B), 769–792, doi:10.2151/jmsj.80.769.
- Shindell, D. T., G. A. Schmidt, M. E. Mann, and G. Faluvegi (2004), Dynamic winter climate response to large tropical volcanic eruptions since 1600, *J. Geophys. Res.*, *109*, D05104, doi:10.1029/2003JD004151.
- Solomon, S. (1999), Stratospheric ozone depletion: A review of concepts and history, *Rev. Geophys.*, *37*(3), 275–316, doi:10.1029/1999RG000008.
- Solomon, S., R. W. Portmann, R. R. Garcia, L. W. Thomason, L. R. Poole, M. P. McCormick, and C. Cly (1996), The role of aerosol variations in anthropogenic ozone depletion at northern midlatitudes, *J. Geophys. Res.*, *101*(95), 6713–6727.
- Son, S.-W., et al. (2010), Impact of stratospheric ozone on Southern Hemisphere circulation change: A multimodel assessment, *J. Geophys. Res.*, *115*, D00M07, doi:10.1029/2010JD014271.
- Song, Y., and W. A. Robinson (2004), Dynamical mechanisms for stratospheric influences on the troposphere, *J. Atmos. Sci.*, *61*, 1711–1725, doi:10.1175/1520-0469(2004)061<1711:DMFSIO>2.0.CO;2.
- Stenchikov, G., A. Robock, V. Ramaswamy, M. D. Schwarzkopf, K. Hamilton, and S. Ramachandran (2002), Arctic Oscillation response to the 1991 Mount Pinatubo eruption: Effects of volcanic aerosols and ozone depletion, *J. Geophys. Res.*, *107*(D24), 1–16, doi:10.1029/2002JD002090.
- Stenchikov, G., K. Hamilton, A. Robock, V. Ramaswamy, and M. D. Schwarzkopf (2004), Arctic Oscillation response to the 1991 Pinatubo eruption in the SKYHI general circulation model with a realistic quasi-biennial oscillation, *J. Geophys. Res.*, *109*, D03112, doi:10.1029/2003JD003699.
- Stenchikov, G., K. Hamilton, R. J. Stouffer, A. Robock, V. Ramaswamy, B. Santer, and H.-F. Graf (2006), Arctic Oscillation response to volcanic eruptions in the IPCC AR4 climate models, *J. Geophys. Res.*, *111*, 1–17, doi:10.1029/2005JD006286.
- Stenke, A., M. Schraner, E. Roazanov, T. Egorova, B. Luo, and T. Peter (2013), The SOCOL version 3.0 chemistry-climate model: Description, evaluation, and implications from an advanced transport algorithm, *Geosci. Model Dev.*, *6*, 1407–1427, doi:10.5194/gmd-6-1407-2013.
- Stothers, R. B. (1984), The great Tambora eruption in 1815 and its aftermath, *Science*, *224*(4654), 1191–1198.
- Stothers, R. B. (2001), Major optical depth perturbations to the stratosphere from volcanic eruptions: Stellar extinction period, 1961–1978, *J. Geophys. Res.*, *106*(D3), 2993–3003, doi:10.1029/2000JD900652.
- Taylor, K. E., R. J. Stouffer, and G. A. Meehl (2012), An overview of CMIP5 and the experiment design, *Bull. Am. Meteorol. Soc.*, *93*, 485–498, doi:10.1175/BAMS-D-11-00094.1.
- Thomas, M. A., M. A. Giorgetta, C. Timmreck, H.-F. Graf, and G. Stenchikov (2009a), Simulation of the climate impact of Mt. Pinatubo eruption using ECHAM5—Part 2: Sensitivity to the phase of the QBO, *Atmos. Chem. Phys.*, *9*, 3001–3009, doi:10.5194/acp-9-3001-2009.
- Thomas, M. A., C. Timmreck, M. a. Giorgetta, H.-F. Graf, and G. Stenchikov (2009b), Simulation of the climate impact of Mt. Pinatubo eruption using ECHAM5—Part 1: Sensitivity to the modes of atmospheric circulation and boundary conditions, *Atmos. Chem. Phys.*, *9*, 757–769, doi:10.5194/acp-9-757-2009.
- Thompson, D. W. J., M. P. Baldwin, and S. Solomon (2005), Stratosphere-troposphere coupling in the Southern Hemisphere, *J. Atmos. Sci.*, *62*, 708–715.
- Thompson, D. W. J., J. C. Furtado, and T. G. Shepherd (2006), On the tropospheric response to anomalous stratospheric wave drag and radiative heating, *J. Atmos. Sci.*, *63*, 2616–2629.
- Thompson, D. W. J., S. Solomon, P. J. Kushner, M. H. England, K. M. Grise, and D. J. Karoly (2011), Signatures of the Antarctic ozone hole in Southern Hemisphere surface climate change, *Nat. Geosci.*, *4*, 741–749, doi:10.1038/ngeo1296.
- Thompson, D. W. J., D. J. Seidel, W. J. Randel, C.-Z. Zou, A. H. Butler, C. Mears, A. Osso, C. Long, and R. Lin (2012), The mystery of recent stratospheric temperature trends, *Nature*, *491*, 692–697, doi:10.1038/nature11579.
- Tie, X., and G. Brasseur (1995), The response of stratospheric ozone to volcanic eruptions: Sensitivity to atmospheric chlorine loading, *Geophys. Res. Lett.*, *22*(22), 3035–3038.
- Timmreck, C. (2012), Modeling the climatic effects of large explosive volcanic eruptions, *WIREs Clim. Change*, *3*, 545–564, doi:10.1002/wcc.192.
- Valcke, S. (2013), The OASIS3 coupler: A European climate modelling community software, *Geosci. Model Dev.*, *6*, 373–388, doi:10.5194/gmd-6-373-2013.
- von Storch, H., and F. W. Zwiers (2000), *Statistical Analysis in Climate Research*, 484 p., Cambridge Univ. Press, Cambridge.
- Zanchettin, D., C. Timmreck, O. Bothe, S. J. Lorenz, G. Hegerl, H.-F. Graf, J. Luterbacher, and J. H. Jungclaus (2012), Delayed winter warming: A robust decadal response to strong tropical volcanic eruptions?, *Geophys. Res. Lett.*, *40*, 204–209, doi:10.1029/2012GL054403.
- Zhang, D., R. Blender, and K. Fraedrich (2012), Volcanoes and ENSO in millennium simulations: Global impacts and regional reconstructions in East Asia, *Theor. Appl. Climatol.*, *111*, 437–454, doi:10.1007/s00704-012-0670-6.

Supplementary material

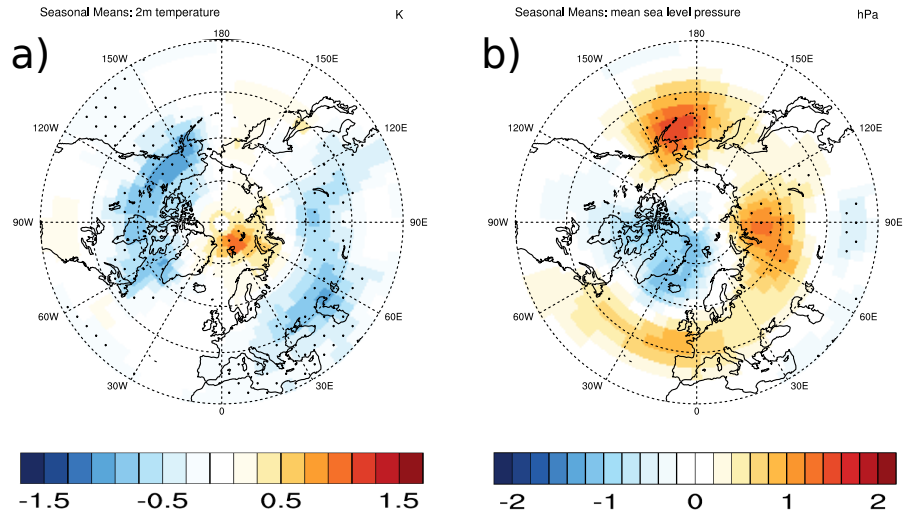


Figure S1.: Difference for the DJF 2m air temperature (a) and the sea level pressure (b) between CTRL.O₃^{strong} and CTRL.O₃^{weak}. Significant differences ($p < 0.05$, Students t-test) are stippled between the two control ensembles.

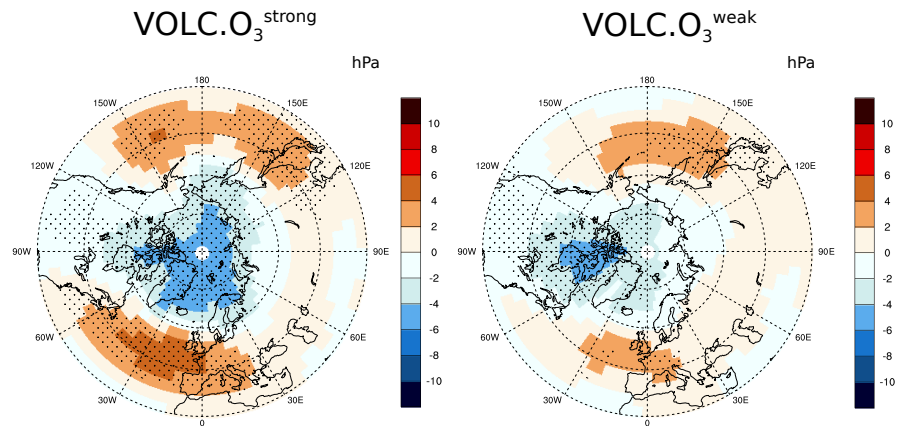


Figure S2.: Similar to Figure 4 but for the ensemble mean DJF sea level pressure (SLP) anomaly relative to the corresponding control. Significant differences ($p < 0.05$, Students t-test) are indicated by stippling.

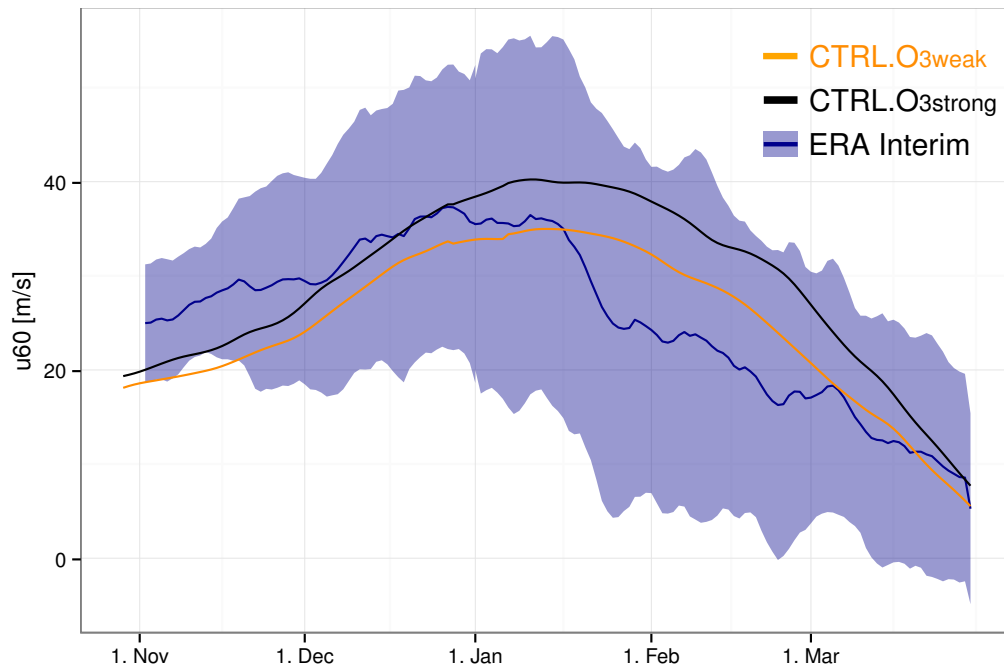


Figure S3.: Comparison of the daily climatological mean ERA Interim (average 1979-2013) November to March u60 index (zonal mean wind at 60°N and 10 hPa) to the two control ensembles CTRL.O₃^{strong} and CTRL.O₃^{weak}. The shading indicates the standard deviation of ERA Interim (Dee et al. 2011).

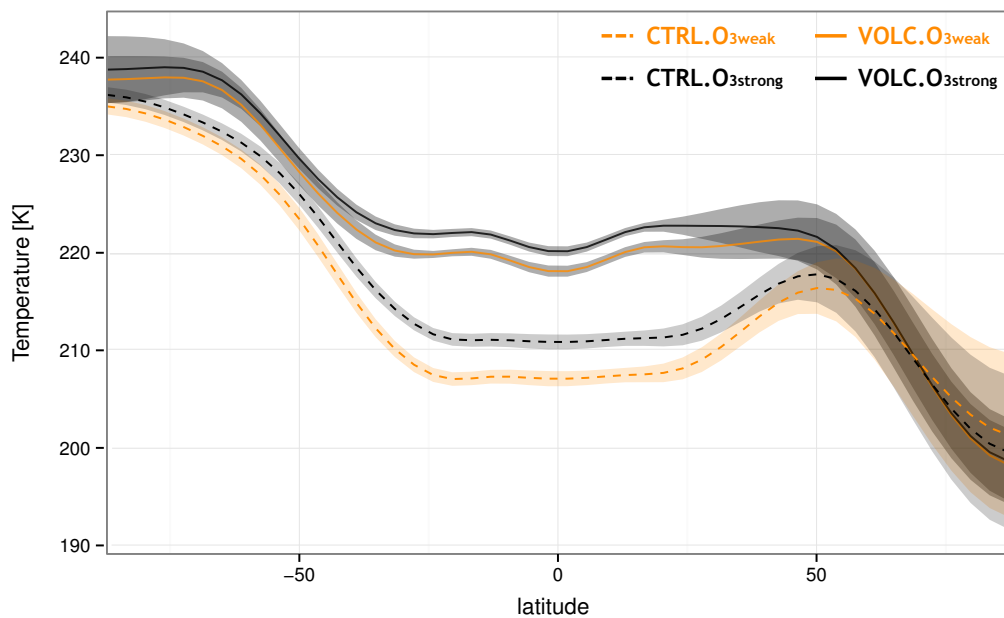


Figure S4.: Zonal mean DJF temperature profile at 40 hPa for the control ensemble mean (dashed lines) and the perturbed simulations (solid lines). The control ensemble mean is based on all available simulations years, the values for the perturbed ensemble average displays the zonal mean temperature in the first winter after the eruptions.

Chapter 4.

Dynamical and chemical ozone perturbations after large volcanic eruptions: Role of the climate state and the strength of the eruption

Stefan Muthers, Florian Arfeuille, and Christoph C. Raible

In review for the *Journal of Geophysical Research*.

Abstract: The response of stratospheric ozone to large tropical volcanic eruptions and its influence on the dynamical perturbation is analyzed in ensemble simulations with the coupled atmosphere-ocean-chemistry-climate model SOCOL-MPIOM. Following an eruption, ozone concentrations are modified by dynamic processes (DYN), resulting from the heating in the lower tropical stratosphere, and chemical reactions (HET) on the aerosol surfaces. In idealized experiments, the relative importance of these processes is assessed for different eruption strengths and for present day and preindustrial climate states, separately. The model's ability in reproducing the climate response is evaluated using the Mt Pinatubo eruption of 1991. DYN processes result in instantaneous ozone changes in the tropics and mid latitudes and are almost independent of the climate state. Furthermore, the dynamical changes in the high latitudes are dominated by DYN mechanisms. However, the model underestimates the coupling to the tropospheric circulation in comparison to observations. With increasing eruption strength, the ozone anomalies intensify and last longer. The temperature and in particular the dynamic response however, does not scale linearly with the forcing. HET processes are almost completely limited to present day climate conditions, revealing a slowly developing global ozone reduction, which persists for several years. In the polar stratosphere of both hemisphere the depletion is further amplified. With increased eruption strength the amplitude and the duration of the ozone depletion increases. HET ozone changes significantly weaken the northern polar vortex during winter and strengthen it in spring, without significant effects on the tropospheric circulation.

4.1. Introduction

Tropical volcanic eruptions, which are strong enough to inject aerosols and gases into the stratosphere, can perturb the physical and the chemical components of the climate system for several years and longer (Robock, 2000; Cole-Dai, 2010; Timmreck, 2012). Among the large number of eruption products, the sulfur dioxide (SO_2) has probably the strongest climate impact. In the stratosphere SO_2 is converted into sulfuric acid ($\text{H}_2\text{SO}_4 + \text{H}_2\text{O}$) aerosols that (a) reflect in the visible part of the solar spectrum, (b) absorb terrestrial and solar infrared radiation, and (c) provide surface for a large number of chemical reactions that alter the chemical composition of the stratosphere (Forster et al., 2007). The effect of the aerosols on the short wave radiation transfer is an increase of the optical depth of the atmosphere and results in a cooling of the troposphere and at the surface. The absorption of long wave radiation by the aerosols increases heating rates in the aerosol cloud, which lead to pronounced warming in these regions. The perturbed vertical and meridional temperature gradients affect the stratospheric circulation and by interaction between the stratosphere and the troposphere even the climate at the surface. A prominent example for this mechanism is the winter warming pattern in the Northern Hemisphere (NH) that has been observed after several large tropical volcanic eruptions (Robock and Mao, 1992; Stenchikov et al., 2002; Shindell et al., 2004; Fischer et al., 2007; Christiansen, 2008; Zanchettin et al., 2012). Anomalous positive surface temperatures over Eurasia are related to a positive phase of the Arctic Oscillation, which is forced by the coupling of the stratospheric polar vortex and the tropospheric circulation (Graf et al., 1993; Kodera, 1994).

The effect of the volcanic eruption on the stratospheric ozone chemistry can be further separated into (a) the effect of the changing temperature on the reaction rates, (b) the heterogeneous chemistry on the sulfuric acid aerosols, (c) the effect of the temperature changes and the aerosols on the polar stratospheric clouds (PSC), (d) the changes induced by the dynamical changes in the stratosphere, and (e) changes in the photolysis rates. The temperature change and the reactions on the heterogeneous aerosol surfaces mainly take place in the aerosol cloud. In particular, the heterogeneous conversion of nitrogen oxides (N_2O_5) into nitric acid (HNO_3) is of importance. This reaction effectively slows down the NO_x cycle of catalytic ozone destruction with the effect of increasing ozone concentrations in the middle stratosphere, where the NO_x cycle dominates the depletion (Tie and Brasseur, 1995; Solomon et al., 1996). In the lower stratosphere, where the Cl_x and HO_x cycles are more important the net-effect is a reduction of the ozone abundance, since the slow-down of the NO_x cycle and heterogeneous reactions intensify the Cl_x and HO_x cycles (Tie and Brasseur, 1995; Solomon et al., 1996). In the polar regions, the effect of the eruption on the PSCs is expected to intensify the ozone depletion. Firstly, with a stronger polar vortex the air temperature inside the vortex is reduced and better isolated against the mid latitudes and more PSCs can be formed. Secondly, the presence of H_2SO_4 in the polar stratosphere facilitates the formation of an additional type of PSC, which further increases the surfaces for heterogeneous reactions on PSCs.

The effect of the volcanic eruption on stratospheric ozone can therefore be roughly divided into two processes. The first process involves increased heating rates by the aerosols mainly in the tropical lower stratosphere. This leads to pronounced changes in the dynamics, which change the meridional and vertical distribution of ozone. The second process includes a large number of heterogeneous chemical reactions on the aerosol

surface, which change the chemical composition of the stratosphere and strengthen or weaken different catalytic cycles of ozone destruction.

The net effect of the chemical response further depends on the background composition of the atmosphere. The slow-down of the NO_x cycle and heterogeneous reactions are expected to intensify the chlorine cycle of ozone destruction, but chlorine levels have undergone serious changes in the last decades (Solomon, 1999). With ozone depleting halogens in the atmosphere the net effect of the eruption on the global ozone abundance is a reduction (Tie and Brasseur, 1995; Rozanov et al., 2002; Austin et al., 2013). For low halogen loadings however, the chemical reactions are expected to increase ozone globally (Tie and Brasseur, 1995; Anet et al., 2013; Austin et al., 2013). The changes in the stratospheric water vapor concentrations associated with the tropical stratospheric warming however, can accelerate the HO_x cycle and reduce ozone even in the case of reduced halogen concentrations (Heckendorn et al., 2009).

The best observed eruption is the one of Mt Pinatubo in June 1991 in the Philippines. The formation of the cloud, the dynamical changes and the effect on the chemical composition of the atmosphere has been observed by numerous satellite instruments and balloon, lidar, airborne and ground-based measurements (Bluth and Doiron, 1992; Labitzke and McCormick, 1992; McCormick, 1992; Stowe et al., 1992; Thomason, 1992; Gleason et al., 1993; Minnis et al., 1993; Hofmann et al., 1994; Randel and Wu, 1995; Antun et al., 2002). Still, some uncertainties remain in the first months after the eruption, in particular for the aerosol forcing (Arfeuille et al., 2013). The uncertainty in the sulfur emitted ranges from 7 to up to 13 Mt S (Bluth and Doiron, 1992; Guo et al., 2004; SPARC, 2006). In the stratosphere the SO_2 was converted to aerosols and distributed by the stratospheric circulation. Globally, the near surface air temperature was reduced by approximately 0.5°C as a consequence of the reduced incoming short-wave radiation (Soden et al., 2002). In the aerosol cloud, temperature increased by around 2-3 K mainly due to increased absorption in the infrared (Labitzke and McCormick, 1992). Ozone observations indicate a general reduction of the total column ozone abundance in the order 5-10%, interrupted by periods with positive anomalies, in particular in the southern hemisphere (SH). (Randel and Wu, 1995).

From the observations it is difficult to understand, which processes are responsible for the ozone changes and how these changes affect the dynamics. The attribution of the ozone changes after the Mt Pinatubo eruption has been assessed by several authors showing that the reduction of the total column ozone is mainly a result of the chemical effect of the aerosols (Pitari and Rizi, 1993; Al-Saadi et al., 2001; Shindell et al., 2003; Telford et al., 2009; Aquila et al., 2013). In the tropics total column ozone is reduced after the eruption, which is a combined signal of reduction in the lower stratosphere and increasing ozone concentrations above. Rozanov et al. (2002) attributed the reduction in the lower stratosphere to a mix of the dynamic effect and heterogeneous chemical reactions. The former reduces ozone by enhanced up-welling of ozone poor air and the latter is responsible for an increase in the ozone depletion by active chlorine. Above 18 hPa the chemical process of the NO_x deactivation dominates, which leads to positive ozone anomalies. The differences in the ozone response between the northern hemisphere (NH) and the SH, with a reduction in the NH but increasing concentrations in the SH, has been attributed to dynamical processes induced by the aerosol heating in combination with the Quasi-Biennial-Oscillation (Aquila et al., 2013). The ozone changes in the NH on the other hand are primarily caused by the heterogeneous chemical reaction effects

(Pitari and Rizi, 1993; Aquila et al., 2013). At high latitudes, several studies attribute the changes to the effect of heterogeneous reactions (Portmann et al., 1996; Solomon et al., 1996; Rosenfield et al., 1997; Telford et al., 2009; Pitari et al., 2014).

The stratospheric dynamic perturbation after a volcanic eruptions originates mainly from the aerosol heating in the tropical lower stratosphere. Changes in the ozone concentrations however, can also affect heating rates and therefore modulate the dynamic response to the eruption (Muthers et al., 2014a). Using observed ozone anomalies for the Mt Pinatubo eruption, Stenchikov et al. (2002) found a strengthening of the Arctic Oscillation (AO) in late winter and early spring after eruption, which is explained by the cooling effect of the pronounced ozone depletion in the polar stratosphere. Similar results were found by Shindell et al. (2003) who compared the Mt Pinatubo eruption in simulations with and without ozone changes. For a different climate state (Mt Tambora, 1815), without anthropogenic chlorine in the stratosphere, they found a very small influence of the ozone changes on the dynamical perturbation.

The purpose of this study is to deepen our understanding of the processes which drive the ozone changes after a strong tropical volcanic eruption and how these changes modulate the atmospheric dynamics in the stratosphere and troposphere. Moreover, the sensitivity of the processes on the eruption strength and the climate state is investigated. Therefore, we use a set of sensitivity simulations performed by the atmosphere-ocean-chemistry-climate model SOCOL-MPIOM. To evaluate the dynamic response this study focuses mainly on the NH and in particular on the winter season when the winter warming pattern takes place.

The paper is structured as follows: Section 4.2 introduces the coupled atmosphere-chemistry-ocean circulation model and the setup of the experiments. In Section 4.3 the model results for the 1991 Mt Pinatubo eruption are evaluated. In Section 4.4 the response of the underlying dynamic and chemical processes after a strong volcanic eruption is analyzed and the sensitivity to the eruption strength and climate state is addressed in Section 4.5. Finally, we discuss the results and present conclusive remarks in Section 4.6.

4.2. Model and experiments

4.2.1. Model

We use the coupled atmosphere-ocean-chemistry-climate model (AOCCM) SOCOL-MPIOM (Muthers et al., 2014b) consisting of the atmospheric component SOCOL version 3 coupled to the ocean-sea ice module MPIOM. SOCOL (Schraner et al., 2008; Stenke et al., 2013) is a spectral chemistry-climate consisting of the physical component MA-ECHAM5 (Roeckner et al., 2003; Manzini et al., 2006), which is coupled to the chemistry module MEZON (Roazanov et al., 1999; Egorova et al., 2003). The chemistry module uses temperature fields from ECHAM5 and calculates the tendency of 41 gas species, taking into account 200 gas-phase, 16 heterogeneous, and 35 photolytical reactions. Heterogeneous reactions are parametrised following Carslaw et al. (1995) and can take place in/on aqueous sulfuric acid aerosols and on three types of polar stratospheric clouds.

In the short-wave scheme of SOCOL the solar forcing is divided into six spectral intervals. The scheme considers Rayleigh scattering, scattering on aerosols and clouds,

and the absorption of solar irradiance in UV-induced photolysis reactions, e.g., by O_3 and O_2 and 44 other species. In the near-infrared intervals absorption by water vapor, CO_2 , N_2O , CH_4 , and O_3 is implemented. Furthermore, a parametrization for the absorption of radiation by O_2 and O_3 in the Lyman-alpha, Schumann-Runge, Hartley and Higgins bands is implemented following an approach similar to Egorova et al. (2004). The long-wave scheme considers frequencies from 10-3000 cm^{-1} for the absorption by water vapor, CO_2 , O_3 , N_2O , CH_4 , CFC-11, CFC-12, CFC-22, aerosols, and clouds. The interactive chemistry module of SOCOL can optionally be disabled. In this case three dimensional time dependent ozone data needs to be applied as forcing.

The horizontal resolution of SOCOL is T31, which corresponds to approximately $3.75^\circ \times 3.75^\circ$. In the vertical, 39 model levels are used with the highest level at 0.01 hPa (80 km). With this vertical resolution the model is not able to produce a Quasi-Biennial Oscillation (QBO) by itself, therefore a QBO nudging is applied (Giorgetta et al., 1999).

The atmosphere-chemistry model SOCOL is coupled to the ocean model MPIOM with sea ice module (Marshall, 2003; Junglauss et al., 2006). Here we use MPIOM in a nominal resolution of 3° , with the poles shifted to Greenland and Antarctica to avoid numerical singularities at the poles. This setup allows for a high resolution in the deep water formation region of the North Atlantic. MPIOM and SOCOL are coupled by the OASIS3 coupler (Budich et al., 2010; Valcke, 2013).

4.2.2. Experiments

In this study, several ensemble sensitivity experiments for different processes, eruption strengths, and climate states are used.

Aerosol forcing: The eruption selected for this sensitivity study is the tropical eruption of Mt Pinatubo that took place in June 1991. The aerosol forcing for the Pinatubo eruption was calculated offline using the micro-physical aerosol model AER (Weisenstein et al., 1997) following Arfeuille et al. (2013). Different eruption intensities are implemented by simulating eruptions of $1\times$, $2\times$, and $4\times$ the strength of the Mt Pinatubo eruption. The eruptions are all set to June 15th 1991, with 15, 30 and 60 Mt of SO_2 injected in the aerosol micro-physical model AER. Actual post-Pinatubo wind fields are used for each experiment in the AER model. SW extinction coefficients and surface area density (SAD) for the different forcings are depicted in Fig. 4.1. The aerosol coagulation process depends on the SO_2 concentration and hence particles tend to be larger as we inject more SO_2 . The increase in total SAD is hence not proportional to the increase in SO_2 mass injected between the $1\times$, $2\times$ and $4\times$ Pinatubo simulations. Conversely, the total stratospheric warming depends on the aerosol absorption in the infrared and varies more or less linearly with the SO_2 mass injected. However, increase in for instance the sedimentation rates with larger aerosols further modifies the relationship between the stratospheric warming and the initial sulfur mass released. Note, the forcing produced by the AER model is known to lead to biases in the heating rates in the tropical stratosphere (Heckendorn et al., 2009), which can be reduced using satellite based aerosol forcing (Arfeuille et al., 2013). However, here idealized simulations for eruptions larger than the observed Pinatubo are performed. For these the AER model allows the production of a consistent aerosol forcing data set taking micro-physical processes in the aerosol cloud into account. A detailed discussion of the forcing used for $1\times$ Pinatubo and a comparison

4. Dynamical and chemical ozone perturbations after large volcanic eruptions: Role of the climate state and the strength of the eruption

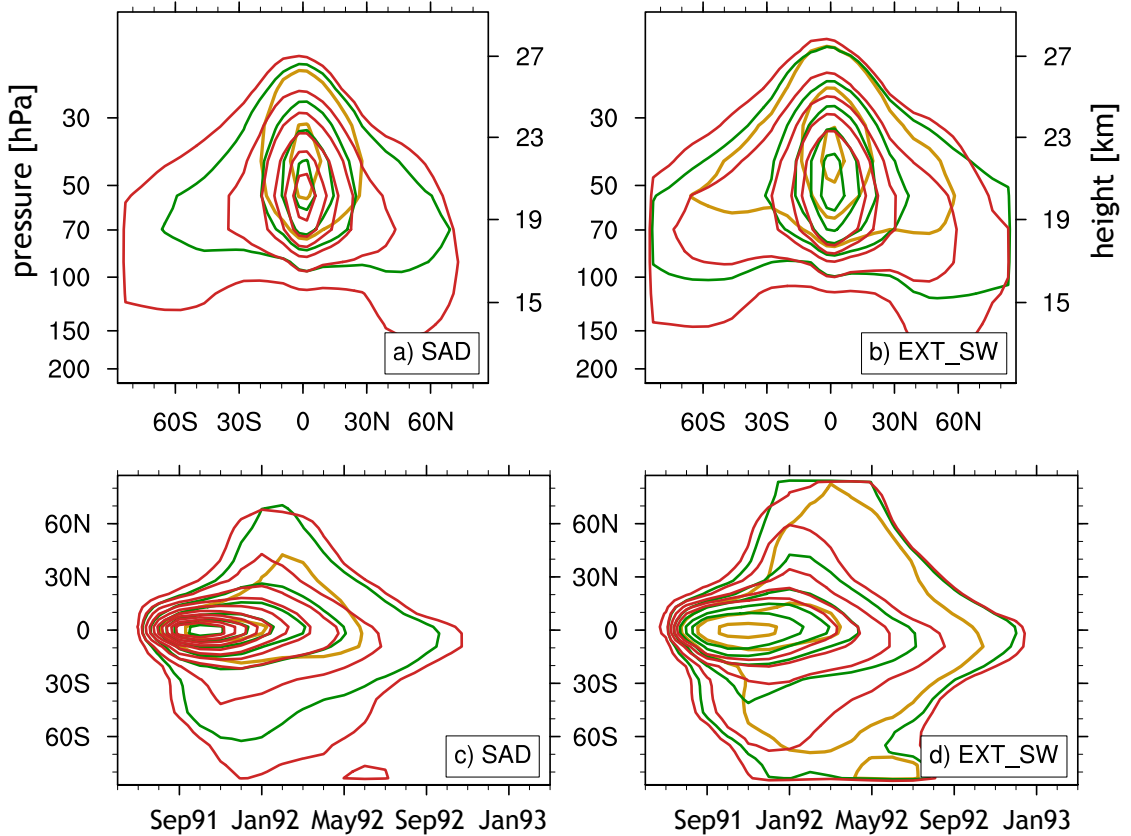


Figure 4.1.: Volcanic forcing used in the simulations for $1\times$ (orange), $2\times$ (green), and $4\times$ (red) Mt Pinatubo. (a) DJF mean surface area density (SAD) for the first winter after the eruption. Contours from 0 to 120 by $20 \mu\text{m}^2/\text{cm}^3$. (b) DJF mean for the extinction in the visible (440-690 nm) with contours from 0 to 0.05 by 0.01 km^{-1} . (c) Hovmöller diagram of the monthly mean SAD forcing at 50 hPa with contours from 0 to 200 by 20 by $20 \mu\text{m}^2/\text{cm}^3$. (d) as (c) but for the extinction in the visible with contours from 0 to 0.05 by 0.01 km^{-1} .

with other forcing data sets is given in Arfeuille et al. (2013), AER method.

Climate state: To assess the role of the climate state on the response, the eruptions either occur under present day conditions (early 1990th with high loads of ozone depleting substances in the atmosphere) or preindustrial conditions (early 19th century, low concentrations of ozone depleting halogens).

The response of the ozone chemistry to the eruption is a combination of different effects. Ensemble sensitivity experiments are performed to separate the effects for the three eruption strengths and the two climate states.

- A first set of ensemble experiments simulates the combined effect of the tropical stratospheric warming and the heterogeneous reactions on the aerosol surfaces. The volcanic forcing applied therefore includes optical properties, i.e., extinction rates for the short- and long-wave bands, as well as SAD. These experiments are labeled $1\times\text{PIN}$, $2\times\text{PIN}$, and $4\times\text{PIN}$ for the present day climate state and $\text{PI}1\times\text{PIN}$, $\text{PI}2\times\text{PIN}$, $\text{PI}4\times\text{PIN}$ for the preindustrial climate state.
- The warming effect of the aerosols is simulated in the DYN ensemble experiments.

In this case the effect is implemented by forcing the model with extinction rates for the short- and long-wave bands only. The SAD of the aerosols are set to background values without volcanic influence. Note, that although these simulations do not include the effect of heterogeneous reactions taking place on the surface of the aerosols, the experiments still use the interactive chemistry component of SOCOL, which allows the chemistry to react to the changing radiation fluxes and temperatures.

- The effect of heterogeneous chemical reactions on the aerosol surfaces are implemented in the HET experiments. Here, the model is forced with the SAD only, while the short- and long-wave parameters are set to background values.
- Finally, a set of experiments simulates the dynamical effect of the ozone changes found in the fully forced ensemble experiments, e.g. $1\times$ PIN. In this case, a configuration of SOCOL-MPIOM without interactive chemistry is forced by ensemble mean ozone mixing ratios from the full forced simulations. These ensemble simulations are named O3.

The results for the different sensitivity ensemble experiments are compared to an ensemble of control simulations. These simulations are not perturbed by a volcanic eruption. Instead, the stratospheric aerosol forcing represents background concentrations. Since the difference in the response is compared for a preindustrial and present day atmosphere, an ensemble of control experiments is performed for each climate state.

Each ensemble consists of 8 members to reduce the influence of internal variability on the results (Zanchettin et al., 2013), e.g., different El-Niño Southern Oscillation (ENSO) states (Zhang et al., 2012; Frölicher et al., 2013). The simulations length of each member is 8 years, with two years of spin-up and the eruption implemented in the third year of each simulation. Restart files are taken from an ensemble of transient simulations for the period 1600-2000 (Muthers et al., 2014b). The ensemble sensitivity experiments share the same restart files, meaning that member 1 of the full forcing simulations is initialized by the same climate state as member 1 from the DYN, HET, and O3 ensembles. For the present day climate state, initial conditions for the ocean and the atmosphere are carefully selected between the years 1987 and 1990, to represent different ENSO states. For the preindustrial restart files from the beginning of the 19th century (1811-1814) are used as initial conditions.

The QBO data used in the nudging is based on (Brönnimann et al., 2007). The QBO phases in the present day and the preindustrial climate state are almost identical, with a easterly phase at the beginning of the eruption and a shift to a westerly phase in summer of the second year. Concentration of greenhouse gases and aerosol depleting substances represent the conditions of the preindustrial and present day climate state, respectively (Etheridge et al., 1996, 1998; Ferretti et al., 2005; MacFarling-Meure et al., 2006).

4.2.3. Observations

The response of the physical climate system to the Mt Pinatubo eruption is compared to the ERA Interim analysis (Dee et al., 2011) from the European Centre for Medium Range Weather Forecast (ECMWF). The ozone anomalies are compared to the column ozone record of Bodeker et al. (2005) and for the vertical profile to the Binary DataBase of Profiles (Hassler et al., 2008, BDBP). To calculate anomalies for different parameters

4. Dynamical and chemical ozone perturbations after large volcanic eruptions: Role of the climate state and the strength of the eruption

Table 4.1.: Overview of the ensemble experiments used in this study. Eruption strength refers to the aerosol amount used in the generation of the volcanic forcing. 1× refers to the aerosol mass of the 1991 Mt Pinatubo eruption, 2× and 4× represents a doubling or quadrupling of the Pinatubo aerosol mass. Climate state: PD: 1990th conditions with ozone depleting substances. PI: preindustrial atmosphere with low concentrations of ozone depleting substances. Volcanic forcing: SAD: surface area density or the aerosols. OP: optical properties, i.e., extinction rates for different spectral intervals. bg conditions: SAD and optical properties without volcanic perturbation. For each ensemble, 8 simulations are performed.

Ensemble	Strength	Climate state	Volcanic forcing	Ozone
[1,2,4]xPIN	1x,2x,4x	PD	SAD and OP	interactive
[1,2,4]xPIN_HET	1x,2x,4x	PD	SAD only	interactive
[1,2,4]xPIN_DYN	1x,2x,4x	PD	OP only	interactive
[1,2,4]xPIN_OZONE	1x,2x,4x	PD	bg conditions	prescribed
PI_[1,2,4]xPIN	1x,2x,4x	PI	SAD and OP	interactive
PI_[1,2,4]xPIN_HET	1x,2x,4x	PI	SAD only	interactive
PI_[1,2,4]xPIN_DYN	1x,2x,4x	PI	OP only	interactive
PI_[1,2,4]xPIN_OZONE	1x,2x,4x	PI	bg conditions	prescribed
CTRL	–	PD	bg conditions	interactive
PI_CTRL	–	PI	bg conditions	interactive

after the eruption, the period 1986-1990 is used as references period.

4.3. Evaluation of the model

The model’s ability to reproduce the response of the stratospheric and tropospheric climate system due to volcanic aerosols is evaluated using the case of the Mt Pinatubo eruption in 1991. Therefore, we compare the climate response simulated by SOCOL-MPIOM to different observational data sets and reanalysis products. The observed response resembling a single realization of the climate system is compared to an ensemble of simulations. The influence of internal climate variations is therefore larger in the observations. As shown by Zanchettin et al. (2013) the state of the climate system substantially modulates the response of the near surface atmosphere and the ocean to a volcanic perturbation. Furthermore, in the simulations the impact of the QBO on stratospheric temperatures, dynamics, and ozone concentrations is removed by the comparison to an ensemble of control simulations, which are nudged to the same QBO data set. For the observations, the impact of the QBO is not entirely removed by the comparison of the Pinatubo case with the reference period 1986-1990.

4.3.1. Global mean temperature response

In the ensemble experiment for the present day 1× Pinatubo eruption a significant reduction of the global mean surface air temperatures is found (Fig. 4.2 a). For almost

three years anomalies below -0.3°C are simulated. In ERA Interim the global mean surface temperature is reduced by up to 0.33°C in August 1992. However, this value is very sensitive to the reference period and still affected by ENSO. When this influence is removed from the data the cooling is even larger (Soden et al., 2002). The simulated cooling is caused by a decline of the top-of-the-atmosphere (TOA) radiative flux, which reduces by up to -3.8 W/m^2 (October 1991, Fig. 4.2 b).

4.3.2. Stratospheric response

As already shown for an earlier version of SOCOL and for several volcanic forcing data sets (Arfeuille et al., 2013) SOCOL overestimates the warming in the tropical stratosphere. This overestimation is also found in the transient $1\times$ Pinatubo ensemble (Fig. 4.2 c). In ERA Interim the maximum temperature anomaly in the tropical stratosphere at 50 hPa after the eruption is 2.5°C for September 1991, relative to the reference period. In the SOCOL-MPIOM ensemble, the month with the highest temperature anomaly is November 1991 with a temperature increase of 8.7°C in the ensemble average. The overestimated warming is a feature common to many state-of-the-art climate models. In the multi-model ensemble average for 13 CMIP5 models (model selection as in Driscoll et al., 2012) the majority of models overestimate the warming in the tropical stratosphere (black line in Fig. 4.2). Furthermore, the range between the GCMs is large. Although SOCOL-MPIOM is at the higher end of the CMIP5 models, it is still within the model range. Furthermore, in the sensitive region of the tropical tropopause (100 hPa, Fig. 4.2 d), where H_2O transport to the stratosphere and hence HO_x chemistry highly depend on the temperature, the agreement between ERA Interim and SOCOL is better than in most CMIP5 models.

The dynamical changes induced by the stratospheric warming as well as different chemical reactions on the surface of the aerosols also affect the ozone concentrations. Column ozone anomalies for the ensemble mean (Fig. 4.3 d) reveal a similar pattern as it is identified in the observations (Fig. 4.3 a, Bodeker et al., 2005). After the eruption negative anomalies are found in the tropics and positive anomalies in the mid latitudes. The magnitude of both is stronger in SOCOL-MPIOM than in the observations. In particular the positive column ozone anomaly in the NH mid-latitudes is weaker in the Bodeker et al. (2005) data set. This may be related to the QBO effect, which is not fully removed in the observations (Aquila et al., 2013) or to an overestimation of dynamical effects related to the amplified warming in the tropical stratosphere. In the polar regions pronounced negative anomalies occur in the two winters following the eruption. For the first winter SOCOL-MPIOM and observations are comparable, given that the observations are affected by extrapolation and missing values in the high latitudes. In the second winter a pronounced and long lasting signal ozone depletion is found in the NH polar regions, which is reduced in the model simulations compared to the observations. In the SH high latitudes the ensemble average indicates persistent negative anomalies between austral winter 1992 and 1993 which is not observed.

In the zonally averaged vertical profiles of ozone mixing ratios for the NH winter and spring season, larger differences between the observations (Binary DataBase of Profiles BDBP, Hassler et al., 2008) and the simulations are found (Fig. 4.4). Both records agree on a reduction of the ozone mixing ratios in the first winter after the eruption in the tropical stratosphere at altitudes between 50 hPa and 10 hPa and increasing

4. Dynamical and chemical ozone perturbations after large volcanic eruptions: Role of the climate state and the strength of the eruption

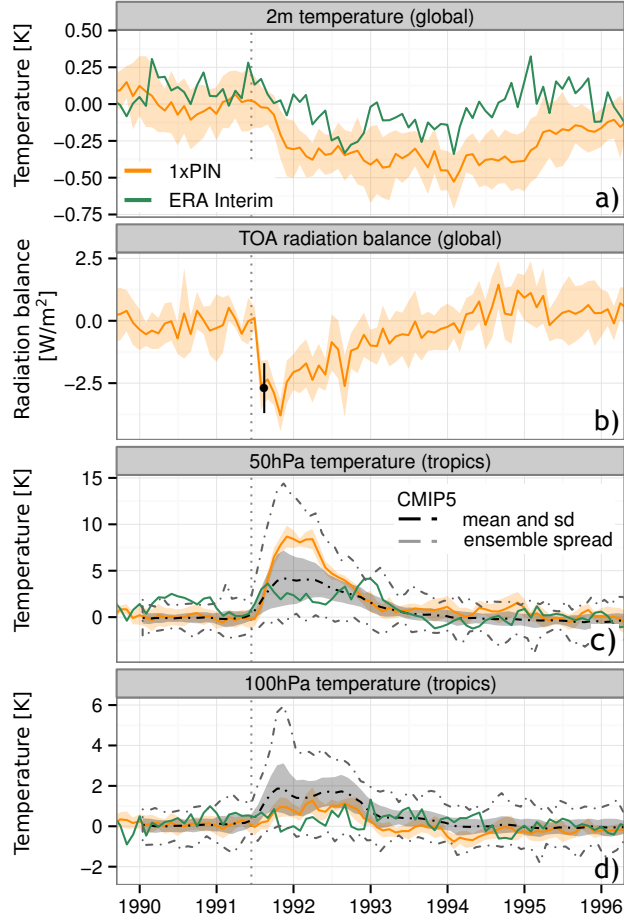


Figure 4.2.: (a): Global mean temperature anomalies following the eruption of Mt Pinatubo in the ensemble experiments (orange) with the shading indicating the ensemble standard deviation and in ERA Interim (green). (b): Top-of-the-atmosphere (TOA) radiation balance in the ensemble experiments. The error bar represents the lower estimate for the TAO radiation balance for Aug./Sept. 1991 from ERBE (NASA Earth Radiation Budget) satellite data (Minnis et al., 1993). (c): Tropical zonal mean temperature anomalies at 50 hPa averaged between 20°S and 20°N. The orange line represents the present day 1× Pinatubo ensemble average (PD1xPIN) in comparison to the ERA Interim anomalies (green) and the multi-model ensemble anomalies for 13 CMIP5 models (black). The shading corresponds to the ensemble standard deviation, the dashed gray lines around the CMIP5 ensemble average indicated the minimum and maximum anomalies. For CMIP5 13 model ensembles as in Driscoll et al. (2012) are considered. (d) as (c) but for 100 hPa. All panels: Anomalies for the present day 1× Pinatubo are calculated relative to the control ensemble average, for CMIP5 and ERA Interim the years 1986-1990 are used as reference period. The vertical dashed gray line represents the start of the eruption.

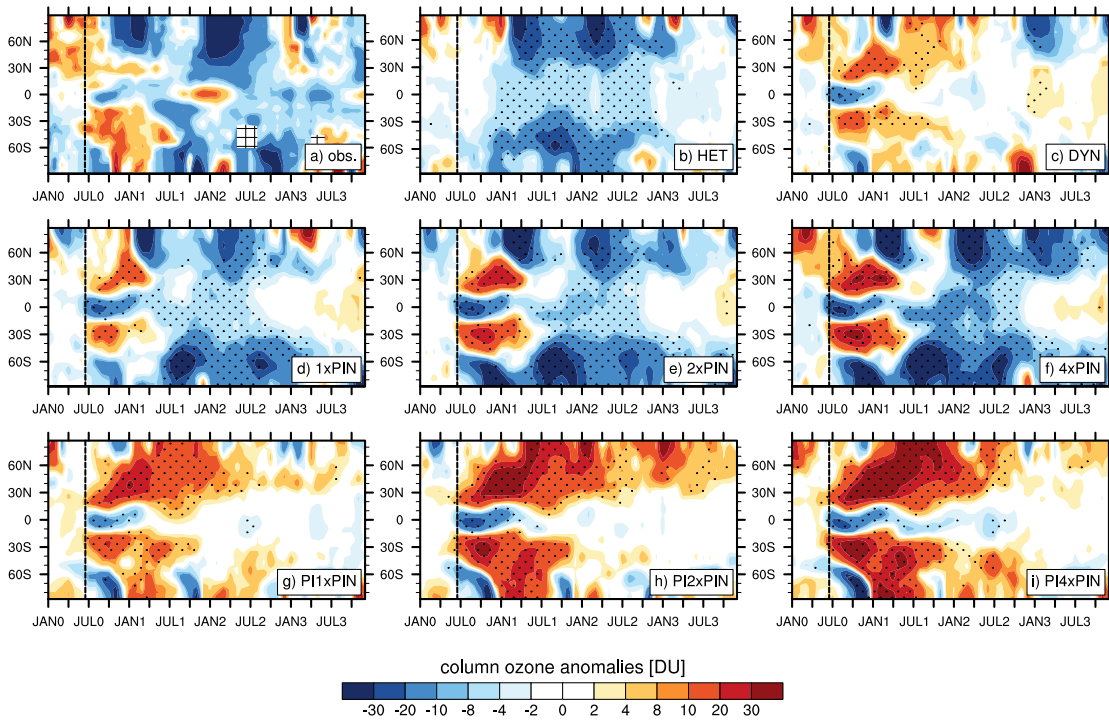


Figure 4.3.: Zonal average monthly mean total columns ozone anomalies [DU] between January 1991 (year 0) and December 1994 (year 3) in different data sets. (a) observational anomalies (Bodeker et al., 2005), (b) anomalies due to the effect of heterogeneous chemical reactions (HET) for the present day $1\times$ Pinatubo, (c) anomalies related to the warming effect of the aerosols (DYN), (d-f) full forcing effect for the (d) $1\times$, (e) $2\times$, and (f) $4\times$ Pinatubo in a present day atmosphere. (g-i) full forcing effect for the (g) $1\times$, (h) $2\times$, and (i) $4\times$ Pinatubo in a preindustrial atmosphere. Anomalies for the observations are calculated relative to the reference period 1986-1990. Hatching in the observation panel indicates missing values. The simulated anomalies are calculated relative to the corresponding control ensemble average and the stippling in the simulation panels indicates significant differences to the control (Student's t -test $p \leq 0.05$). The beginning of the eruption is depicted by the vertical dashed line.

concentrations above. Both changes are again stronger in SOCOL-MPIOM than in the observations. In the mid-latitudes of the NH positive ozone anomalies are found in both data sets, whereas only positive ozone anomalies are observed at northern polar latitudes but not simulated. In the first spring after the eruption the tropical anomalies slightly weaken in the simulations and the observations. Furthermore, SOCOL simulates a pronounced reduction of ozone in the lower polar stratosphere of the NH, which is not found in the observations. In the second winter and spring significant ozone reductions are found in the lower stratosphere for all latitudes, a pattern that agrees reasonably well with the observed anomalies.

The expected dynamic response of the stratosphere is the intensification of the winter vortex and the downward propagation of these anomalies into the troposphere. In the simulation a slight, but insignificant strengthening of the stratospheric northern polar vortex is found for the first winter after the eruption (Fig. 4.5). Furthermore, the tropospheric westerlies are significantly reduced in both hemispheres. In the following

4. Dynamical and chemical ozone perturbations after large volcanic eruptions: Role of the climate state and the strength of the eruption

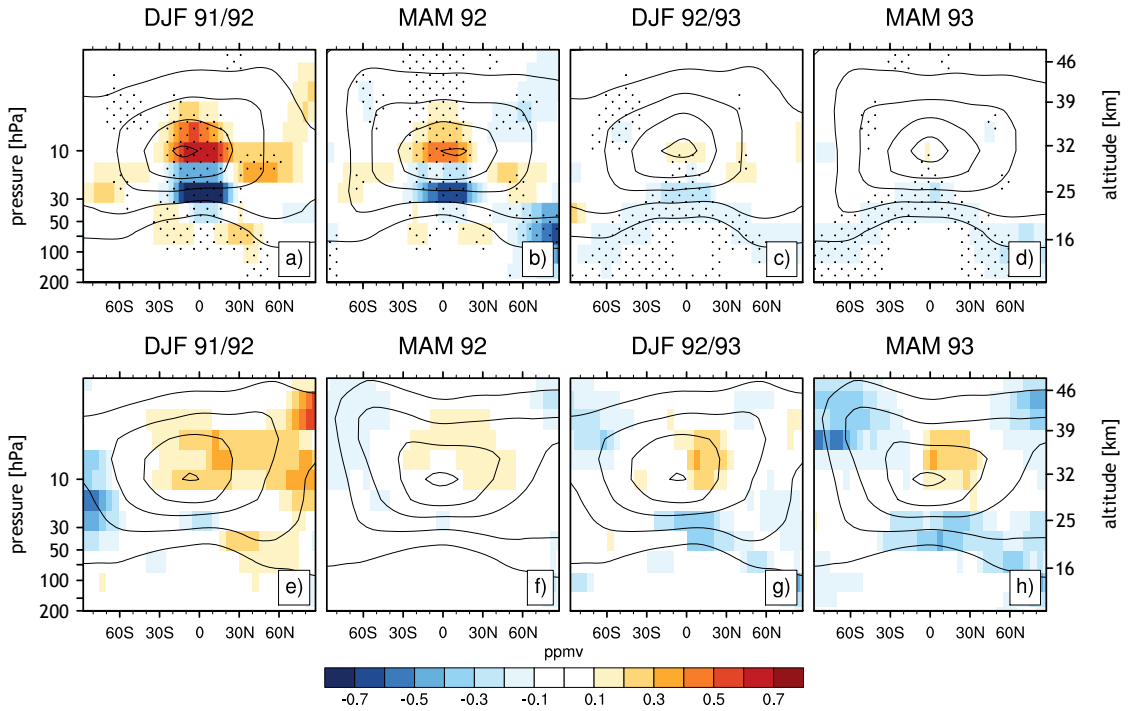


Figure 4.4.: Stratospheric seasonal mean, zonal mean ozone anomalies in ppm (a-d) for the present day $1\times$ Pinatubo ensemble average relative to the control ensemble mean and (e-h) for the BDBP observational data set (Hassler et al., 2008) relative to the average of the period 1986-1990. Shown are the DJF and MAM values for the first and the second winter after the eruption.

spring the intensification of the zonal circulation in the polar stratosphere persists. In ERA Interim negative anomalies are found in the upper stratospheric part of the polar vortex region and positive anomalies in the lower stratosphere and troposphere. The dipole pattern in the anomalies is related to the weakening of the vortex in the mid of winter, which propagates down in the following weeks and reaches the troposphere in April. This behavior is not found in the ensemble average of the present day $1\times$ Pinatubo ensemble, but at least one member simulated a comparable vortex weakening. In the second winter and spring after the eruption the simulated zonal wind in the polar stratosphere does not differ from the background state. In the reanalysis however, the polar vortex is intensified and the signal extends down to the troposphere and the surface during winter. Note the remaining QBO effect visible in the tropical anomalies in ERA Interim may also affect the comparison of the polar vortex intensities, which is also modulated by the QBO (Holton and Tan, 1980; Labitzke, 1987; Thomas et al., 2009).

4.3.3. Tropospheric response

The positive zonal wind anomalies in the lower stratosphere found in the reanalysis are clearly connected to positive anomalies in the troposphere (Fig. 4.5). This coupling of anomalies between stratosphere and troposphere is not visible in the ensemble mean. However, some ensemble members show a coupling behavior similar to the reanalysis. In the ensemble mean the tropospheric anomalies are in general weaker in the simulations.

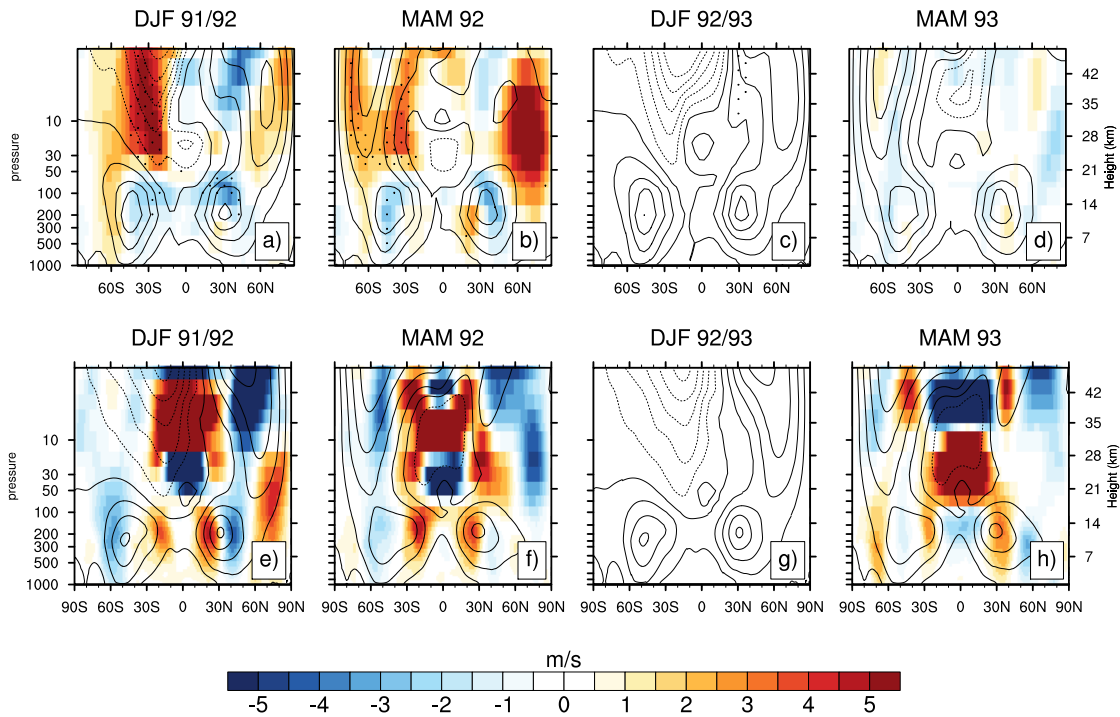


Figure 4.5.: Seasonal mean, zonal mean wind anomalies in m/s for (a-d) the present day $1 \times$ Pinatubo ensemble mean relative to the control ensemble mean and (e-h) for ERA Interim (Dee et al., 2011) relative to the mean of the period 1986/1990. Shown are the DJF and MAM values for the first and the second winter after the eruption. Stippling in the ensemble mean panels indicates significant anomalies (Student's t -test $p \leq 0.05$), contours denote the climatological zonal winds for the corresponding season.

In the second winter after the eruption no significant anomalies are visible in the ensemble average, but the vortex is clearly intensified in the reanalysis, with positive anomalies reaching down to the surface.

The differences in the dynamic response of the NH polar vortex affect also the tropospheric pressure systems. The idealized response to the volcanic eruption is a positive phase of the AO which leads to the NH winter warming pattern (Robock, 2000; Christiansen, 2008; Zanchettin et al., 2012). In the observations, a NAO-like anomaly pattern is found for the first and the second winter season after the eruption, although the anomalies are shifted towards the North (Fig. 4.6 e). In the average of the present day $1 \times$ Pinatubo ensemble simulations a comparable, but weaker response is found for the first post eruption winter (Fig. 4.6 a). In the second winter no positive NAO-like anomaly is visible in the ensemble mean (Fig. 4.6 c), but a clear and pronounced positive NAO situation is found in the reanalysis (Fig. 4.6 g). This agrees well with the stratospheric and tropospheric wind anomalies described above. Pronounced winter warmings are found in northern Europe for both post eruption winters in ERA Interim (not shown), in agreement with the pressure anomalies. In the model simulations a weak winter warming is simulated in the first winter and spring, but the anomalies are not significant. In the second winter no positive anomalies are found.

In summary, the models reproduces the thermal and chemical response to the eruption,

4. Dynamical and chemical ozone perturbations after large volcanic eruptions: Role of the climate state and the strength of the eruption

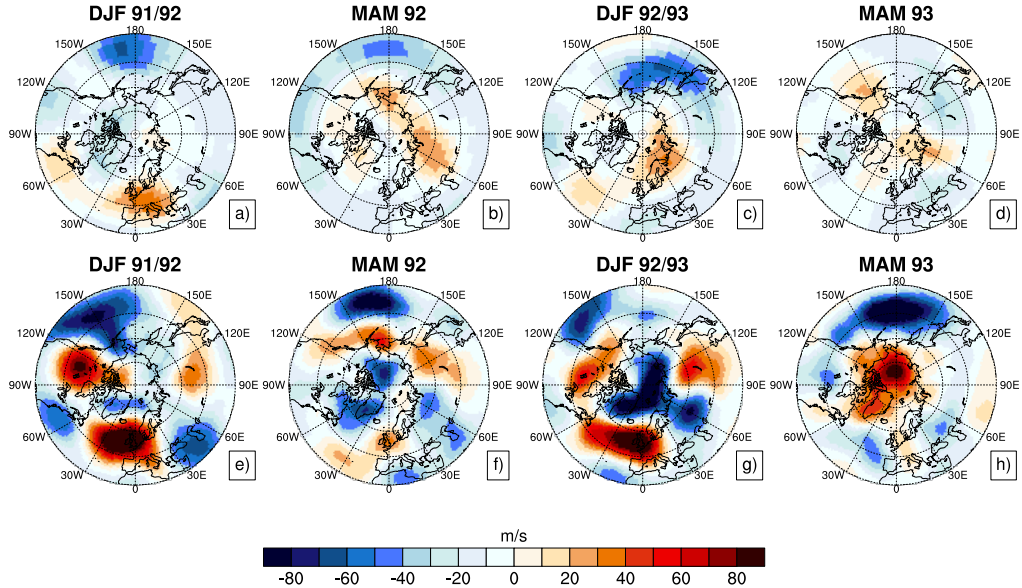


Figure 4.6.: Seasonal mean, 500 hPa geopotential height anomalies in m for (a-d) the present day $1\times$ Pinatubo ensemble mean relative to the control ensemble mean and (e-h) for ERA Interim (Dee et al., 2011) relative to the average of the period 1986-1990. Shown are the DJF and MAM values for the first and the second winter after the eruption. Stippling indicates significant anomalies (Student's t-test $p \leq 0.05$).

although the amplitudes are overestimated. For the dynamic response, in particular the response of the northern polar vortex, differences are found in timing of the positive vortex anomalies (first vs. second winter after the eruption), but in general the model is able to simulate the intensification of the polar vortex after the eruption. Furthermore, the differences in the vortex response are difficult to assess, given the large variability in the northern polar vortex. The tropospheric response in the model simulations is weaker than the response in the reanalysis, although a weak positive NAO like phase and a slight winter warming pattern is identified in the ensemble average and in several ensemble member. Nevertheless, the weak response hints at deficiencies in the dynamical coupling of the stratosphere and the troposphere.

4.4. Underlying mechanisms of response behavior

In the ensemble simulations, the strongest effect of the volcanic eruption on the dynamics is found for the first winter after the eruption. For the following analysis, which addresses the role of chemical and dynamic effect and how the response is modulated by the climate state, we therefore focus mainly on the first winter (DJF) after the eruption. Furthermore, since the sensitivity experiments are idealized experiments, which differ from the real Mt Pinatubo case presented above (e.g, in their climate state), we change the date definition and use year 0 for the year when the eruption starts (1991) and year 1 for the first year after the eruption (1992).

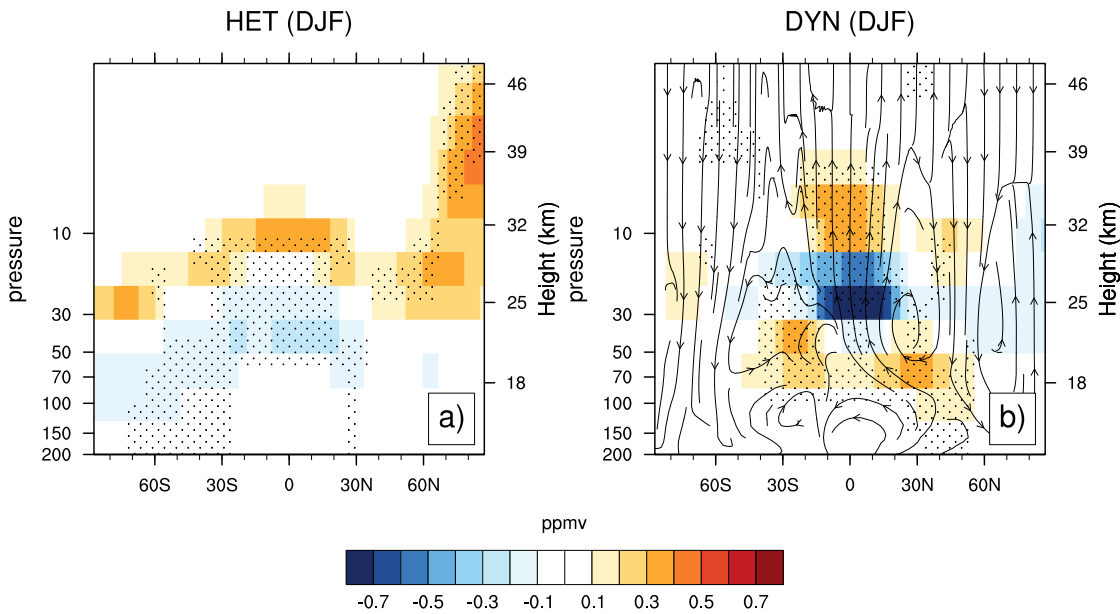


Figure 4.7.: Similar to Figure 4.4, but only for the first winter (DJF) after the eruption and for (a) the present day $1\times$ Pinatubo HET and (b) the present day $1\times$ Pinatubo DYN ensemble simulations. The streamlines in (b) show the residual circulation anomalies. Stippling indicates significant anomalies (Student's t -test $p \leq 0.05$).

4.4.1. Dynamic effect vs. heterogeneous reactions

The dynamical effect dominated by the aerosol induced warming in the lower tropical stratosphere (DYN) and the effect of heterogeneous chemical reactions on the aerosol surfaces (HET) are analyzed for the case of the present day $1\times$ Pinatubo eruption in the following.

The ozone response shows a clear difference between the two ensemble simulations when comparing to the control ensemble simulations (Fig. 4.3 b and c). IN HET the largest influence on the column ozone is found in the high latitudes of each hemisphere with pronounced ozone depletion that reaches maximum values in the spring seasons of the corresponding hemisphere (Fig. 4.3 b). Furthermore, reduced ozone values are found in tropical and mid latitudes. The general response to the chemical effect is a reduction of the ozone amount. The reduction of column ozone slowly develops for several months before it becomes significant for almost 2 years. The zonally averaged height profiles for the first winter after the eruption (Fig. 4.7 a) reveal that the chemical effect also leads to positive anomalies, in particular in the upper stratosphere. However, these anomalies are present only in the first winter after the eruption and are to some extent compensated by negative anomalies in the lower stratosphere. Furthermore, the positive anomalies disappear about one year after the eruption, whereas the negative values remain significant for more than two years.

The aerosol effect on the dynamics (DYN) on the other side has the largest impacts in the tropics and mid latitudes (Fig. 4.3 c). Here, the dynamical changes caused by the heating of the lower tropical stratosphere lead to a transport of air masses and consequently to a shift in the ozone concentrations. In a narrow band around the equator, the lifting of ozone reduced air from the lower stratosphere to higher levels causes a

4. Dynamical and chemical ozone perturbations after large volcanic eruptions: Role of the climate state and the strength of the eruption

reduction of the column ozone values at 30 hPa and increasing concentrations above (Fig. 4.7 b)

The decomposition experiments DYN and HET are also suitable to identify the underlying chemical reactions that result in the ozone changes. In HET, an important heterogeneous reaction on the H_2SO_4 aerosols involves the conversion of nitrogen oxides into nitric acid (HNO_3). Both, nitrogen oxides and nitric acid are reservoir molecules of the NO_x cycle, with nitric acid having a longer residence time than nitrogen oxide. This reaction therefore, effectively slows down the NO_x cycle of ozone destruction, which is most effective in the middle atmosphere and explains the positive anomalies above 30 hPa in HET (Fig. 4.7 a). In lower levels the HO_x and ClO_x cycle is more important. By a reduction of the NO_x concentrations the reaction also slows down the deactivation of chlorine, which dominates ozone destruction in the lower atmosphere. Furthermore, conversion stops, when all N_2O_5 is consumed. In the lower stratosphere (< 30 hPa) a negative N_2O_5 anomaly slowly develops after in the months after the beginning of the eruption. In the first winter after the eruption N_2O_5 in the lower stratosphere is reduced by more than 80% at all latitudes and this anomaly persists for more than one year. This effect is responsible for the reduction of the ozone concentrations in the lower stratosphere in the DJF season (Fig. 4.7 a) and is also the dominant effect for the general reduction of the column ozone values (Fig. 4.3 b). In the NH and SH polar stratosphere in late winter and spring the heterogeneous reactions on the aerosol surfaces and on PSCs strongly increase the chlorine concentrations in the lower stratosphere and explain the pronounced ozone reductions.

In the DYN experiments reduced ozone column abundances are found at tropical latitudes and increasing concentrations in the mid to high latitudes (Fig. 4.3 c). In the tropics, the reduced column ozone values are related to pronounced ozone reductions at 30 hPa, which are partly compensated by positive ozone anomalies above and below (Fig. 4.7 b). This equatorial anomaly pattern is very similar for all post-eruption seasons and remains significant until the end of the first year after the eruption. The circulation changes in the stratosphere that are responsible for the ozone anomalies are detected in the residual mean circulation anomaly (Andrews et al., 1987), which are depicted by streamlines in Figure 4.7 b. Ozone reductions in the tropics are caused by the uplifting of air from the lower to the middle stratosphere forced by the aerosol heating in the lower stratosphere. This vertical transport of ozone changes the vertical ozone profile and replaces ozone enhanced air at 30 hPa by ozone depleted air from lower levels. Air with enriched ozone from 30 hPa further increases ozone concentrations at 10 hPa and above. The upward motion in the tropics is balanced by descending air masses in the mid latitudes. Since these air masses originate from tropical latitudes they transport ozone enriched air into the lower stratosphere of the mid latitudes and create positive ozone anomalies. This meridional transport is visible in the positive column ozone anomalies, which first occur in subtropical latitudes and reach the high latitudes several months later. A fraction of the descending ozone is recirculated into the tropical lowermost stratosphere and explains the positive ozone anomalies at 70 hPa. The DYN effect leads also to an amplification of polar ozone depletion during a few months after the end of the winter season. This is related to the stronger and colder polar vortex (see below), which intensifies the chlorine activation on PSCs in a present day atmosphere. However, the polar ozone depletion in the DYN experiments is much weaker than the signal found in the HET ensemble experiments.

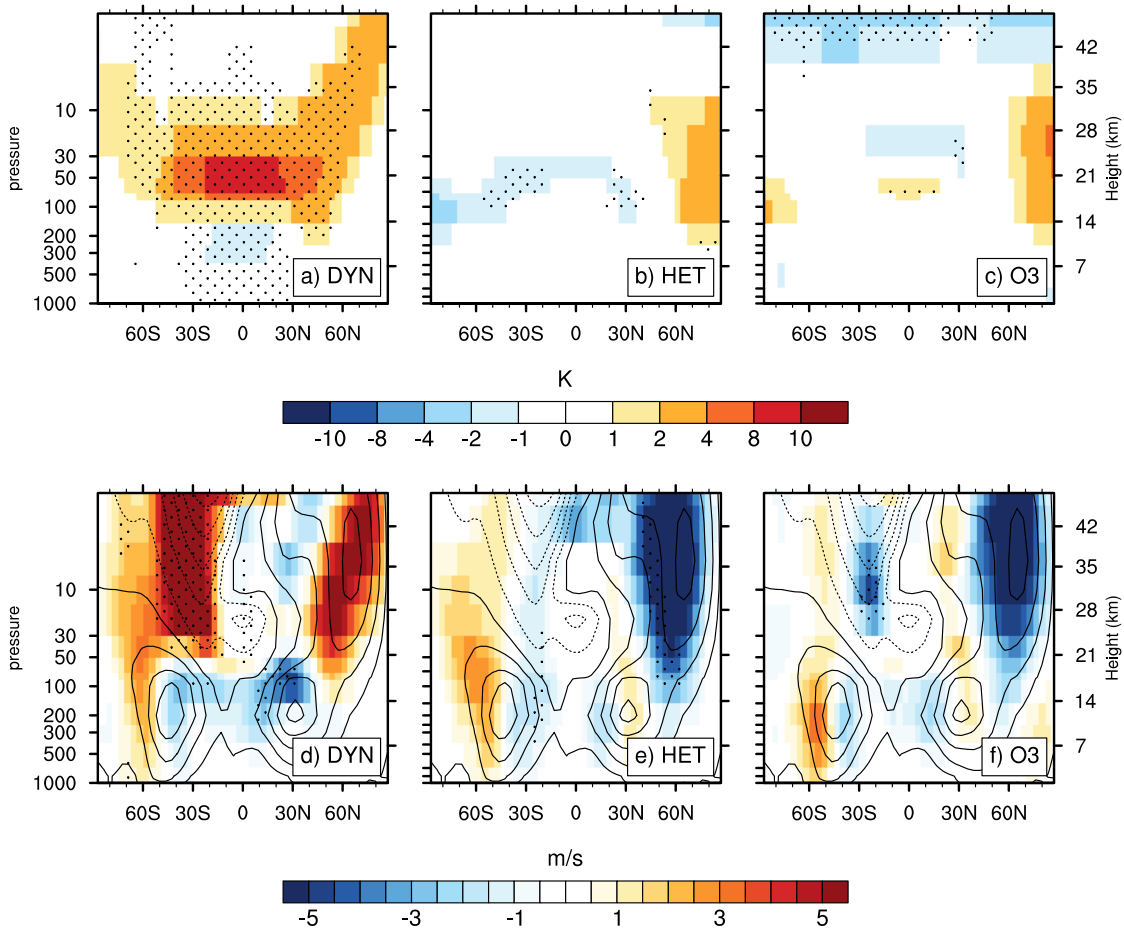


Figure 4.8.: (a-c) DJF temperature anomalies for the post eruption winter in the present day 1x Pinatubo ensemble experiments for (a) DYN, (b) HET, and (c) O3. (d-f) DJF anomalies for the zonal mean wind component for (a) DYN, (b) HET, and (c) O3. Stippling in the ensemble average panels indicates significant anomalies (Student's t-test $p \leq 0.05$), contours in the zonal wind panels indicate the climatological conditions in the control ensemble average.

For the combined effect on the ozone concentrations found in the present day 1x Pinatubo ensemble, the DYN mechanism is dominant in the tropical and mid latitudes for the first year after the eruption. In the polar latitudes the HET mechanism dominates. Furthermore, the heterogeneous chemical reactions are also responsible for a global reduction of the column ozone values in the second and third year after the eruption.

The major effect for the temperature response after the eruption is the DYN effect (Fig. 4.8 a). The chemical effect of the aerosols has a small but significant influence in a narrow band around the equator, with cooling at 50 hPa (Fig. 4.8 b). This is related to the changing ozone concentrations and corresponding UV absorption. Furthermore, in the NH winter polar stratosphere a weak, but only weakly significant warming, related to a slightly weaker polar vortex is found (see below).

In comparison to the heating of the lower stratosphere by the volcanic aerosols (DYN) the temperature anomalies caused by the ozone changes in HET are small. Still, a clear impact on the dynamics is obvious, which substantially differs from the aerosol effect

4. Dynamical and chemical ozone perturbations after large volcanic eruptions: Role of the climate state and the strength of the eruption

simulated in DYN (Fig. 4.8 d). In DYN, the warming of the aerosols strengthens the northern polar vortex in boreal winter with larger anomalies than found in the full forcing ensembles. Consequently, a negative response is needed, which is found by the significant weakening of the stratospheric zonal circulation in the HET ensemble experiments (Fig. 4.8 e).

In the troposphere, the DYN experiments simulate a significant weakening of the subtropical jets in both hemispheres. This weakening is related to the larger cooling in the tropical latitudes and consequently a weakening of the meridional temperature gradient in the troposphere. The anomalies in the tropospheric pressure systems are dominated by the warming effect of the aerosols as well. The anomalies in the 500 hPa geopotential height are very similar to the PD1xPIN response for the DYN ensemble average (not shown). For the HET ensemble simulations no significant anomalies in the tropospheric pressure systems are found.

4.4.2. Dynamic response of the combined ozone changes

As shown above, the ozone response after a tropical volcanic eruption is influenced by chemical reactions and dynamical changes due to the warming effect of the aerosols. The later is the dominant process for the dynamic response after the eruption. However, this dynamic response in turn changes the ozone concentrations by transports of ozone from one region to another, which again might affect the dynamics. Therefore, the net effect of the ozone changes might have a larger influence on the dynamics, compared to the response found in the HET sensitivity ensemble experiments. This combined effect is assessed by the O3 ensemble experiments, where the ozone concentrations from the reference ensemble (Fig. 4.3 d and 4.4 a-d) are used to force the configuration of SOCOL-MPIOM without interactive chemistry.

The influence of the combined ozone changes in O3 on the temperatures in the stratosphere is weak (Fig. 4.8 c). In the tropical stratosphere, the temperature anomalies roughly resemble the ozone anomalies. Further a cooling in the higher stratosphere and lower mesosphere during austral summer in the SH is found, which is an effect of the configuration of SOCOL-MPIOM without interactive chemistry (Muthers et al., 2014b). A second anomaly in the SH is related to differences in the PSCs between the control (interactive chemistry) and the O3 ensemble. However, the differences have nearly no impact on the stratospheric dynamics and the tropospheric circulation (Muthers et al., 2014b). Without interactive chemistry the zonal circulation in the NH winter polar stratosphere slightly weakens by approximately 1.5 m/s. In the ensemble experiment forced by the simulated ozone changes the northern polar vortex weakens on average by more than 6 m/s in winter (Fig. 4.8 f). Similar to the ensemble sensitivity experiment for the chemical effect of the volcanic aerosols the combined effect therefore also contributes to a weakening of the polar vortex. In the spring season (MAM, not shown), the zonal wind in the polar vortex region however, is stronger with anomalies in the order of 3 m/s. This intensification is marginally significant ($p \leq 0.1$).

4.5. Influence of the climate state and the eruption strength

How ozone changes after an eruption further depends on the strength of the eruption. Moreover, the climate state, in particular the amount of ozone depleting halogens in the stratosphere is expected to modulate the response. These two effects are analyzed using eruptions of $1\times$, $2\times$, and $4\times$ the size of Mt Pinatubo eruption and by the comparison of the response in a late 20th century to an early 19th century climate state. Here, we present the results for both effects, first for the ozone changes and in the following for the temperature and dynamical changes.

4.5.1. Ozone changes

Under present day conditions a stronger eruption enhances the anomalies found in the total column ozone values (Fig. 4.3 d-f). With the $2\times$ and $4\times$ Pinatubo forcing the positive anomalies in the mid latitudes are stronger, but in any case they disappear about one year after the eruption. The negative anomalies in the tropics and in particular the ozone depletion in the polar regions are amplified and last longer. In the second and third year after the eruption, negative anomalies are found for all latitudes. In case of the $4\times$ Pinatubo (Fig. 4.3 f) eruption persistent strong ozone depletion is found in the SH high latitudes for more than 2 years even during austral summer.

The simulated ozone anomalies dramatically change with the climate state. Under preindustrial conditions, i.e, an atmosphere with low concentrations of ozone depleting halogens, the negative anomalies in the winter polar stratosphere completely disappear and the positive anomalies extend from subtropical latitudes to the poles (Fig. 4.3 g-i). The dynamical-induced negative anomaly near the equator is found in the preindustrial atmosphere as well, but these negative anomalies disappear after several months and are not replaced by wide spread negative anomalies as it has been the case for the present day simulations. With stronger eruptions, the ozone anomalies are larger and last longer.

The zonal mean ozone mixing ratios for the present day climate state behave qualitatively similar as the results shown in Fig. 4.4 with larger anomalies for stronger eruptions (not shown). For $2\times$ and $4\times$ Pinatubo, the negative ozone anomaly in the polar stratosphere in the first year after the eruption become statistically significant. Under preindustrial conditions, positive anomalies are found at all altitudes, except for the narrow band with negative anomalies around the equator.

In all cases the positive anomalies in the mid latitudes and the negative anomalies at the equator are related to the DYN effect of the aerosols. Negative anomalies at high latitudes for DYN are found in the present day climate only. However, even for the $4\times$ Pinatubo eruption the negative anomalies are replaced by abrupt ozone increases in spring and summer, which extend from the subtropics to the poles. Besides the difference in winter, the response of the ozone concentrations in the DYN experiment is very similar for the two climate states, with positive anomalies being more pronounced under preindustrial than under present day conditions.

The strongest differences between the climate states are found for the HET effect of the aerosols. Under preindustrial conditions the chemical effect is very small with some positive anomalies in the mid-latitudes for a few months after the eruption. In the present day atmosphere strong signals of ozone depletion are found for all latitudes up to three years after the eruption as shown above for the $1\times$ Pinatubo ensemble experiments.

4. Dynamical and chemical ozone perturbations after large volcanic eruptions: Role of the climate state and the strength of the eruption

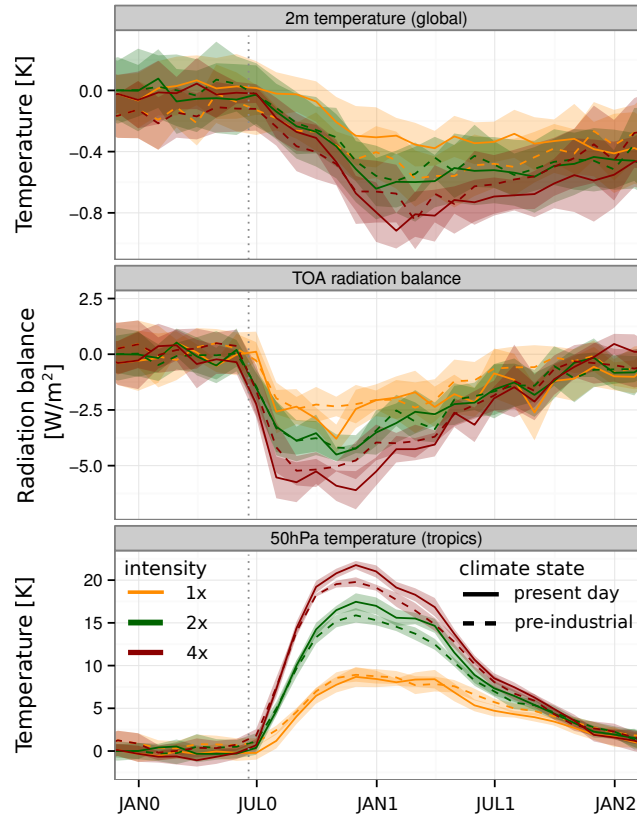


Figure 4.9.: Similar to Fig. 4.2 (a-c) but for the 1 \times , 2 \times , and 4 \times Pinatubo eruption strength and the present day and preindustrial climate state.

With increasing eruption strength, the magnitude of the anomalies becomes larger, but the duration of the significant anomalies remains similar.

4.5.2. Temperature and dynamic changes

The physical response of the climate system in terms of the reduction of the surface air temperature reveals a clear difference between the three eruption strengths (Fig. 4.9), but no significant differences between the climate states. Furthermore, the temperature reduction does not scale linearly with the forcing, which is expected given the thermal inertia of the ocean. Similarly, the reduction of the TOA radiation balance increases with eruption strength, but the climate state does not affect this reduction (Fig. 4.9).

With rising aerosol mass the temperature anomaly in the lower stratosphere increases as well (Fig. 4.9). From 1 \times to 2 \times Pinatubo the temperature increase is almost linear, but for 4 \times Pinatubo saturation effects occur. For the 1x Pinatubo no difference in the temperature anomalies is found between the two climate states. With increasing eruption strength, the lower stratospheric warming in the tropics becomes larger under present day than under preindustrial conditions.

The contrasting differences in the heterogeneous chemical reactions between preindustrial and present day are not responsible for this difference in the temperature increase. As shown in Fig. 4.7 a for the present day 1x Pinatubo HET experiments, the chemical

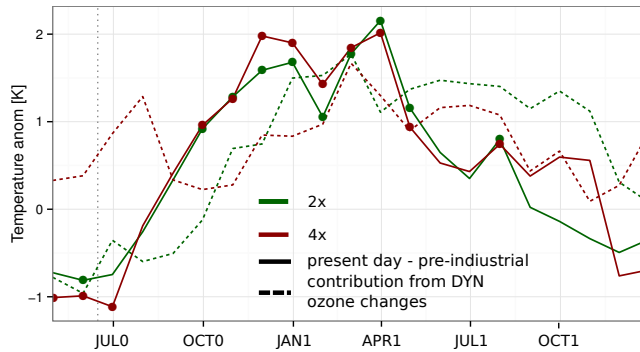


Figure 4.10.: Solid lines: Tropical lower stratospheric (50 hPa) temperature differences between present day and preindustrial in the full forcing ensemble experiments for the $2\times$ and $4\times$ Mt Pinatubo eruptions. Dots indicate significant differences between the two climate states. Dashed lines: Differences in the estimated temperature changes due to the thermal and dynamical effects on the ozone chemistry (DYN) between present day to preindustrial. The temperature effect of the dynamical and thermal ozone changes is estimated by the differences in the temperature anomalies between the O3 and HET ensemble experiments.

response in the present day atmosphere results in reduced ozone concentrations in the lower and middle tropical stratosphere, which induces a slight cooling (Fig. 4.8 b). With stronger eruptions the negative ozone and temperature anomalies are enhanced. For $2\times$ Pinatubo HET, e.g., the ozone changes cool the lower tropical stratosphere by almost 2°C during the first winter season after the eruption. In the preindustrial atmosphere ozone reductions are simulated in the lower tropical stratosphere as well, but the anomalies are weaker for all eruption strengths and the effect on the temperature is smaller (e.g., $< 1^\circ\text{C}$ in PI2xPIN_HET).

Instead, the reason for the temperature difference is found in the DYN simulations. Figure 4.10 shows the time series of the temperature differences between present day and preindustrial for the tropical lower stratosphere (solid lines). The comparison is made for the $2\times$ and the $4\times$ Pinatubo eruption and reveals again a stronger warming in the present day climate without any pronounced differences between the two eruption strengths. Furthermore, the temperature effect of the ozone changes due to dynamical processes ($\Delta T_{O_3_{dyn}}$) is assessed, by the temperature differences between O3 and HET (i.e., $\Delta T_{O_3} - \Delta T_{HET}$). The difference of this effect between present day and preindustrial is shown as dashed line in Figure 4.10 and shows a very similar behavior in terms of the timing and the amplitude of the anomalies. Furthermore, the spatial structure of the differences between the two anomalies nicely resembles the temperature differences between the present Pinatubo and the preindustrial Pinatubo full forcing ensembles, for the $2\times$ and $4\times$ forcing (not shown).

The cause for different ozone changes in DYN between present day and preindustrial is found in the residual circulation anomalies. After the eruption a redistribution of the ozone concentrations is induced by the circulation changes in the stratosphere with lifting in the tropics and descending in the mid latitudes. Some of the ozone enriched air from subtropical and mid latitudes is recirculated into the tropical lower stratosphere, as depicted by the residual circulation anomalies for the $1\times$ Pinatubo DYN experiments in the present day atmosphere (Fig. 4.7 d). In the present day climate ozone concentrations

4. Dynamical and chemical ozone perturbations after large volcanic eruptions: Role of the climate state and the strength of the eruption

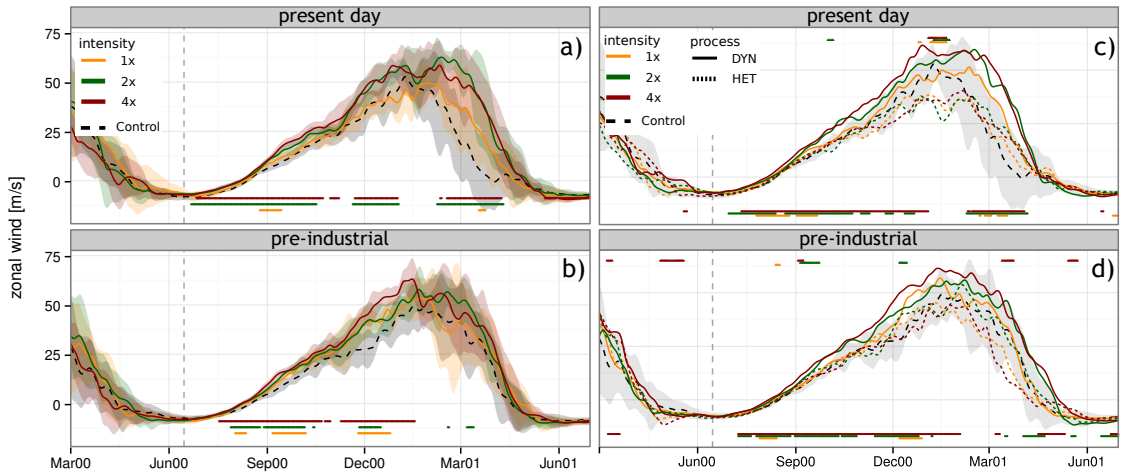


Figure 4.11.: Vortex intensity: Zonal mean zonal wind at 60°N and 10 hPa in (a) a present day and (b) preindustrial climate state for eruptions with $1\times$, $2\times$, and $4\times$ the size of Mt Pinatubo. (c,d) Vortex index for the HET and DYN sensitivity experiments for (c) present day and (d) preindustrial. For comparison, the climatological cycle of the control ensemble is shown as dashed lines. Shading indicates the standard deviation in the ensembles. Days with wind speed significant different from the control (Student's t-test, $p \leq 0.05$) are indicated by dots in the bottom of each panel (a,b). In (c) and (d) dots at the bottom indicate significant differences for the DYN ensemble experiments, whereas the days with significant anomalies in HET are indicated at the top of each panel. All values are smoothed by a 5 day low pass. The start of the eruption is depicted by the vertical dashed line.

are reduced by more than 10 % in the lower tropical stratosphere, while the reduction in the center of the ozone layer and at subtropical latitudes is lower. The net effect of the circulation anomalies is therefore that the positive ozone anomalies in the lower tropical stratosphere are larger in the present day climate than in the preindustrial climate state. Ozone as absorber in the NIR consequently increases the heating in the lower tropical stratosphere.

The difference in the temperature response between the two climate states is not reflected in the dynamics of the polar vortex, expressed by \bar{u}_{60} the zonal mean zonal wind component at 60°N (Christiansen, 2001, 2005). For both climate states the vortex is significantly stronger during the winter season in case of the $2\times$ and the $4\times$ Pinatubo eruption (Fig. 4.11 a and b). Under preindustrial conditions, the $1\times$ Pinatubo also leads to a significant strengthening of the vortex in early winter. The difference between the eruption strengths is however not always visible in the vortex intensity. For the second winter after the eruption no significant differences in the vortex intensity can be found for any climate state or eruption strength (not shown). The vortex intensification is again mainly related to the DYN mechanism (Fig. 4.11 c and d). In the HET sensitivity experiments no influence is found under preindustrial conditions. The present day vortex is significantly weaker in all HET ensembles at the turn of the year, during the vortex maxima. In late winter the vortex is stronger, but the intensification is not significant. No difference is found between the eruption strengths for the HET mechanism.

The largest differences in the vortex intensities are found between the two control ensemble simulations. Whereas the vortex does not differ substantially between the two

climate states in the early winter season, the weakening of the vortex in later winter occurs earlier in the present day ensemble simulations. This is related to the colder tropical stratosphere in the present day ensembles, where the positive temperature gradient in the middle stratosphere changes earlier to negative values. Compared to the differences between the control ensembles, the behavior of the vortex for the different eruption strengths is very comparable between the climate state.

In the troposphere the pressure pattern resemble the differences in the vortex intensities (not shown). For the present day climate a stronger and highly significant NAO-like pattern is simulated for the $2\times$ and $4\times$ volcanic forcing, with larger anomalies for the $2\times$ forcing due to the stronger polar vortex in late winter. In the preindustrial atmosphere the anomalies are in general weaker, similar to the vortex anomalies relative to the preindustrial control experiments. In case of the preindustrial $1\times$ Pinatubo no anomalies are found in the 500 hPa geopotential, but for the $2\times$ and $4\times$ eruption, significant anomalies similar to Figure 4.6 a are found.

For the winter warming pattern, none of the 6 ensembles resembles a similar response as found in ERA Interim. Even in case of the $4\times$ Pinatubo forcing the response is weaker than in the reanalysis in preindustrial and in present day. Nevertheless, positive anomalies in northern Scandinavia are found in several of the ensemble experiments with stronger warming pattern for increasing eruption strengths. In general, the response of the surface temperatures is more pronounced in the present day ensembles than in the preindustrial simulations, similar to the vortex anomalies. However, only in one case, in the present day $2\times$ Pinatubo, where the largest pressure anomalies are found, the positive temperature anomaly in northern Europe is highly statistically significant.

4.6. Discussion and Conclusions

This study addresses the role of ozone on the dynamic response after a tropical volcanic eruptions, the underlying mechanisms for the ozone changes, and the influence of the climate state and the eruption strengths. In agreement with previous studies (e.g., Rosenfield et al., 1997; Rozanov et al., 2002) we find that the response in the tropics is a combination of dynamical processes (DYN), caused by the warming effect of the aerosols, and heterogeneous reactions on the aerosol surfaces (HET). The DYN effect is typically very fast and weakens about one year after the eruption. In our simulations it is the dominant process for the tropical ozone changes with influences on the mid latitudes and is almost independent of the climate state. Larger eruptions strengthen the dynamic effect.

A caveat of this study is the overestimated warming in the tropical stratosphere, which probably also leads to an overestimation of the dynamical effect and the resulting ozone changes. This needs to be considered, when interpreting the results of the DYN experiments. Arfeuille et al. (2013) discussed possible reasons for this and concluded that it is unlikely due to an error in the forcing for most models. Here, it is likely a combination of both a SOCOL related and volcanic forcing related overestimations. Indeed, the forcing being derived from an aerosol model, it does not include satellite observations. It hence present in some regions larger biases in the altitude/latitude/size distribution of the aerosols. For comparison, we also perform two simulations forced by realistic satellite based aerosol concentrations for the Mt Pinatubo eruption (SAGE_4 λ in Ar-

4. Dynamical and chemical ozone perturbations after large volcanic eruptions: Role of the climate state and the strength of the eruption

feuille et al., 2013). In these simulations (not shown) the stratospheric warming is still overestimated (maximum temperature anomalies to Control: 6.6°C), although less pronounced. However, the focus of our study is on processes that govern the ozone response and their influences on the dynamic perturbation in the stratosphere for different climate states and eruptions larger than any eruption observed by satellites. Therefore, the AER model is used here, which allows the consistent generation of idealized forcings and takes micro-physical processes, e.g. aerosol coagulation, into account. Furthermore, we would like to emphasize that the temperature anomaly at 50 hPa is a very specific parameter. At other levels, in particular in the sensitive tropical tropopause region (100 hPa) the response in SOCOL is improved in comparison to other GCMs. Another caveat is that we have no coupling between aerosol transport and dynamical response. The increase in aerosol absorption, which changes the stratospheric dynamics does not influence the aerosol distribution. Here the same, Pinatubo $1\times$ -influenced, transport is used.

The response in the HET ensemble simulations clearly differs between the two climate states considered, in a preindustrial atmosphere the chemical effect is very weak, whereas it is pronounced and globally visible under present day conditions. This effect has also been simulated earlier, using simpler models (e.g., Tie and Brasseur, 1995; Shindell et al., 2003). In a present day atmosphere heterogeneous reactions have the highest influence in the high latitudes in particular during winter and spring. In general, the HET changes are slower than the changes due to DYN processes, but the influence lasts longer. In a decomposition experiment analyzing the HET effect of the Mt Pinatubo eruption under present day conditions, significant influences on the global mean column ozone abundance occur first about sixth months after the eruption, but remain significant for more than two years, whereas the dynamical effect significantly affects the column ozone abundance for approximately one year. The eruption intensity mainly modulates the amplitude and the duration of the ozone depletion due to chemical processes in the polar stratosphere, leading to stronger and more persistent negative ozone anomalies for larger eruptions.

The expected dynamical response to the eruption is an intensification of the polar vortices and in particular for the NH a downward propagation of the anomalies to the troposphere, which supports positive phases of the NAO or AO. Although the model simulates a realistic intensification of the northern polar vortex, the downward propagation into the troposphere is too weak, as the comparison to observations for the 1991 Mt Pinatubo eruption shows. For the moment it is unclear why the stratosphere-troposphere coupling is underestimated. Anet et al. (2014) performed simulations for the Dalton Minimum with SOCOL-MPIOM and assessed the role of different forcings for the tropospheric climate. They also found an underestimation of the top-down mechanism for the volcanic and the UV forcing and suggested model deficits in the wave generation or propagation.

The intensification of the northern polar vortex is primarily driven by the DYN mechanism. Heterogeneous reactions considered in HET, however, lead to a slight but significant weakening of the vortex in mid winter and a (insignificant) strengthening in late winter in a present day atmosphere. The weakening is related to positive (negative) ozone anomalies in the northern polar (tropical) stratosphere in the first winter that dampen the meridional temperature gradient. This effect is large enough to be visible in the full forcing ensembles, in particular for larger eruption sizes, but limited to a few weeks in mid winter. Still, either due to deficits in the stratosphere-troposphere coupling or due to low signal-to-noise ratio the dynamic imprint of the chemical effect is not visible in

the tropospheric anomalies. The general findings for the dynamic effect of the ozone changes due to heterogeneous reactions, however, are in agreement with an earlier study by Stenchikov et al. (2002) and Shindell et al. (2003) who reported a weakening of the positive AO phase in winter and a strengthening in late winter. This effect is not found for the preindustrial climate state (Shindell et al., 2003).

We conclude that the DYN effect of the aerosols in the tropical stratosphere is the dominant effect for the dynamical perturbations and finally also for the winter warming pattern in the NH, even if the overestimation of the response is taken into account. For present day, a small weakening of this mechanism is found due to heterogeneous chemical reactions. However, this response is probably dominated by the different concentrations of ozone depleting substances and is therefore expected to disappear with the recovery of stratospheric ozone concentrations in the 21th century (Austin and Wilson, 2006; Eyring et al., 2007; Austin et al., 2010). This study did not address the relative importance of the ozone changes and the GHG concentrations for the differences between the present day and the preindustrial climate state. Also the season during which the eruption occurs (e.g., Mignot et al., 2011) and the QBO phase (e.g., Thomas et al., 2009) may modulate the dynamic response of the climate system. These questions remain open and need to be addressed in follow-up studies.

acknowledgements: We would like to thank Greg Bodeker of Bodeker Scientific for providing the combined total column ozone database. Furthermore, we express our thank to Urs Beyerle (ETH Zurich) for providing the CMIP5 data used in Fig. 4.2. This work has been supported by the Swiss National Science Foundation under grant CRSI122-130642 (FUPSOL) and CRSII2-147659 (FUPSOL II). This paper profited from discussions during the PAGES/FUPSOL Workshop in 2012. The data from the ensemble simulations conducted for this study are available upon request.

Bibliography

- Al-Saadi, J. A., Pierce, R. B., Fairlie, T. D., Kleb, K. M., Eckman, R. S., Grose, W. L., Natarajan, M., and Olson, J. R.: Response of middle atmosphere chemistry and dynamics to volcanically elevated sulfate aerosol: Three-dimensional coupled model simulations, *J. Geophys. Res.*, 106, 27,255–27,275, doi:10.1029/2000JD000185, 2001.
- Andrews, D. G., Holton, J. R., and Leovy, C. B.: *Middle atmosphere dynamics*, Academic, 1987.
- Anet, J. G., Muthers, S., Rozanov, E., Raible, C. C., Peter, T., Stenke, A., Shapiro, A. I., Beer, J., Steinhilber, F., Brönnimann, S., Arfeuille, F., Brugnara, Y., and Schmutz, W. K.: Forcing of stratospheric chemistry and dynamics during the Dalton Minimum, *Atmos. Chem. Phys.*, 13, 10 951–10 967, doi:10.5194/acp-13-10951-2013, 2013.
- Anet, J. G., Muthers, S., Rozanov, E. V., Raible, C. C., Stenke, A., Shapiro, A. I., Brönnimann, S., Arfeuille, F., Brugnara, Y., Beer, J., Steinhilber, F., Schmutz, W., and Peter, T.: Impact of solar vs. volcanic activity variations on tropospheric temperatures and precipitation during the Dalton Minimum, *Climate of the Past*, 10, 921–938, doi:10.5194/cp-10-921-2014, 2014.
- Antun, J. C., Robock, A., Stenchikov, G. L., and Thomason, L. W.: Lidar validation of SAGE II aerosol measurements after the 1991 Mount Pinatubo eruption, *J. Geophys. Res.*, 107, 1–12, 2002.
- Aquila, V., Oman, L. D., Stolarski, R., Douglass, A. R., and Newman, P. A.: The response of ozone and nitrogen dioxide to the eruption of Mt. Pinatubo at southern and northern midlatitudes, *J. Atmos. Sci.*, 70, 894–900, doi:10.1175/JAS-D-12-0143.1, 2013.
- Arfeuille, F., Luo, B. P., Heckendorn, P., Weisenstein, D., Sheng, J. X., Rozanov, E., Schraner, M., Brönnimann, S., Thomason, L. W., and Peter, T.: Modeling the stratospheric warming following the Mt. Pinatubo eruption: uncertainties in aerosol extinctions, *Atmos. Chem. Phys.*, 13, 11 221–11 234, doi:10.5194/acp-13-11221-2013, 2013.
- Austin, J. and Wilson, R. J.: Ensemble simulations of the decline and recovery of stratospheric ozone, *J. Geophys. Res.*, 111, D16 314, doi:10.1029/2005JD006907, 2006.
- Austin, J., Scinocca, J., Plummer, D., Oman, L., Waugh, D., Akiyoshi, H., Bekki, S., Braesicke, P., Butchart, N., Chipperfield, M., Cugnet, D., Dameris, M., Dhomse, S., Eyring, V., Frith, S., Garcia, R. R., Garny, H., Gettelman, A., Hardiman, S. C., Kinnison, D., Lamarque, J. F., Mancini, E., Marchand, M., Michou, M., Morgenstern, O., Nakamura, T., Pawson, S., Pitari, G., Pyle, J., Rozanov, E., Shepherd, T. G., Shibata, K., Teyssède, H., Wilson, R. J., and Yamashita, Y.: Decline and recovery of total column ozone using a multimodel time series analysis, *J. Geophys. Res.*, 115, D00M10, doi:10.1029/2010JD013857, 2010.
- Austin, J., Horowitz, L. W., Schwarzkopf, M. D., Wilson, R. J., and Levy, H.: Stratospheric ozone and temperature simulated from the preindustrial era to the present day, *J. Climate*, 26, 3528–3543, doi:10.1175/JCLI-D-12-00162.1, 2013.
- Bluth, G. and Doiron, S.: Global tracking of the SO₂ clouds from the June, 1991 Mount Pinatubo eruptions, *Geophys. Res. Lett.*, 19, 151–154, 1992.
- Bodeker, G. E., Shiona, H., and Eskes, H.: Indicators of Antarctic ozone depletion, *Atmos. Chem. Phys.*, 5, 2603–2615, 2005.
- Brönnimann, S., Annis, J. L., Vogler, C., and Jones, P. D.: Reconstructing the Quasi-Biennial Oscillation back to the early 1900s, *Geophys. Res. Lett.*, 34, L22 805, doi:10.1029/2007GL031354, 2007.
- Budich, R., Gioletta, M., Jungclaus, J., Redler, R., and Reick, C.: *The MPI-M Millennium Earth System Model: An assembling guide for the COSMOS configuration*, MPI report, Max-Planck Institute for Meteorology, Hamburg, Germany, 2010.
- Carslaw, K. S., Luo, B., and Peter, T.: An analytic expression for the composition of aqueous aerosols including gas phase removal of HNO₃-H₂SO₄ stratospheric aerosols including gas phase removal of HNO₃, *Geophys. Res. Lett.*, 22, 1877–1880, 1995.

- Christiansen, B.: Downward propagation of zonal mean zonal wind anomalies from the stratosphere to the troposphere: Model and reanalysis, *J. Geophys. Res.*, 106, 27 307, doi:10.1029/2000JD000214, 2001.
- Christiansen, B.: Downward propagation and statistical forecast of the near-surface weather, *J. Geophys. Res.*, 110, D14 104, doi:10.1029/2004JD005431, 2005.
- Christiansen, B.: Volcanic eruptions, large-scale modes in the northern hemisphere, and the El Niño–Southern oscillation, *J. Climate*, 21, 910–922, doi:10.1175/2007JCLI1657.1, 2008.
- Cole-Dai, J.: Volcanoes and climate, *Wiley Interdisciplinary Reviews: Climate Change*, 1, 824–839, doi:10.1002/wcc.76, 2010.
- Dee, D. P., Uppala, S. M., Simmons, A. J., Berrisford, P., Poli, P., Kobayashi, S., Andrae, U., Balmaseda, M. A., Balsamo, G., Bauer, P., Bechtold, P., Beljaars, A. C. M., van de Berg, L., Bidlot, J., Bormann, N., Delsol, C., Dragani, R., Fuentes, M., Geer, A. J., Haimberger, L., Healy, S. B., Hersbach, H., Hólm, E. V., Isaksen, I., Kållberg, P., Köhler, M., Matricardi, M., McNally, A. P., Monge-Sanz, B. M., Morcrette, J.-J., Park, B.-K., Peubey, C., de Rosnay, P., Tavolato, C., Thépaut, J.-N., and Vitart, F.: The ERA-Interim reanalysis: Configuration and performance of the data assimilation system, *Quart. J. Roy. Meteor. Soc.*, 137, 553–597, doi:10.1002/qj.828, 2011.
- Driscoll, S., Bozzo, A., Gray, L. J., Robock, A., and Stenchikov, G.: Coupled Model Inter-comparison Project 5 (CMIP5) simulations of climate following volcanic eruptions, *J. Geophys. Res.*, 117, D17 105, doi:10.1029/2012JD017607, 2012.
- Egorova, T., Rozanov, E., Zubov, V., and Karol, I. L.: Model for investigating ozone trends (MEZON), *Izvestiya, Atmospheric and Oceanic Physics*, 39, 277–292, 2003.
- Egorova, T., Rozanov, E., Manzini, E., Schmutz, W., and Peter, T.: Chemical and dynamical response to the 11-year variability of the solar irradiance simulated with a chemistry-climate model, *Geophys. Res. Lett.*, 31, 6225–6230, doi:10.1029/2003GL019294, 2004.
- Etheridge, D., Steele, L., Langenfelds, R., Francey, R., Barnola, J., and Morgan, V.: Natural and anthropogenic changes in atmospheric CO₂ over the last 1000 years from air in Antarctic ice and firn, *J. Geophys. Res.*, 101, 4115–4128, doi:10.1029/95JD03410, 1996.
- Etheridge, D. M., Steele, L. P., Francey, R. J., and Langenfelds, R. L.: Atmospheric methane between 1000 A.D. and present: Evidence of anthropogenic emissions and climatic variability, *J. Geophys. Res.*, 103, 15 979–15 993, doi:10.1029/98JD00923, 1998.
- Eyring, V., Waugh, D. W., Bodeker, G. E., Cordero, E., Akiyoshi, H., Austin, J., Beagley, S. R., Boville, B. A., Braesicke, P., Brühl, C., Butchart, N., Chipperfield, M. P., Dameris, M., Deckert, R., Deushi, M., Frith, S. M., Garcia, R. R., Gettelman, A., Giorgetta, M. A., Kinnison, D. E., Mancini, E., Manzini, E., Marsh, D. R., Matthes, S., Nagashima, T., Newman, P. A., Nielsen, J. E., Pawson, S., Pitari, G., Plummer, D. A., Rozanov, E., Schraner, M., Scinocca, J. F., Semeniuk, K., Shepherd, T. G., Shibata, K., Steil, B., Stolarski, R. S., Tian, W., and Yoshiki, M.: Multimodel projections of stratospheric ozone in the 21st century, *J. Geophys. Res.*, 112, D16 303, doi:10.1029/2006JD008332, 2007.
- Ferretti, D. F., Miller, J. B., White, J. W. C., Etheridge, D. M., Lassey, K. R., Lowe, D. C., Meure, C. M. M. F., Dreier, M. F., Trudinger, C. M., Van Ommen, T. D., and Langenfelds, R. L.: Unexpected changes to the global methane budget over the past 2000 years, *Science*, 309, 1714–1717, doi:10.1126/science.1115193, 2005.
- Fischer, E. M., Luterbacher, J., Zorita, E., Tett, S. F. B., Casty, C., and Wanner, H.: European climate response to tropical volcanic eruptions over the last half millennium, *Geophys. Res. Lett.*, 34, 1–6, doi:10.1029/2006GL027992, 2007.
- Forster, P., Ramaswamy, V., Artaxo, P., Berntsen, T., Betts, R., Fahey, D. W., Haywood, J., Lean, J. L., Lowe, D. C., Myhre, G., Nganga, J., Prinn, R., Raga, G., Schulz, M., and Van Dorland, R.: Changes in atmospheric constituents and in radiative forcing, in: *Climate Change 2007: The Physical Science Basis. Contribution of Working Group I to the Fourth Assessment Report of the Intergovernmental Panel on Climate Change*, edited by Solomon, S.,

- Qin, D., Manning, M., Chen, Z., Marquis, M., Averyt, K., M.Tignor, and Miller, H., chap. 2, pp. 131–234, Cambridge University Press, Cambridge, United Kingdom and New York, NY, USA, 2007.
- Frölicher, T. L., Joos, F., Raible, C. C., and Sarmiento, J. L.: Atmospheric CO₂ response to volcanic eruptions: The role of ENSO, season, and variability, *Global Biogeochem. Cycles*, 27, 239–251, doi:10.1002/gbc.20028, 2013.
- Giorgetta, M. A., Bengtsson, L., and Arpe, K.: An investigation of QBO signals in the east Asian and Indian monsoon in GCM experiments, *Climate Dyn.*, 15, 435–450, doi:10.1007/s003820050292, 1999.
- Gleason, J. F., Bhartia, P. K., Herman, J. R., McPeters, R., Newman, P., Stolarski, R. S., Flynn, L., Labow, G., Larko, D., Seftor, C., Wellemeyer, C., Komhyr, W. D., Miller, A. J., and Planet, W.: Record low global ozone in 1992, *Science*, 260, 523–526, doi:10.1126/science.260.5107.523, 1993.
- Graf, H. F., Kirchner, I., Robock, A., and Schult, I.: Pinatubo eruption winter climate effects: Model versus observations, *Climate Dyn.*, 92, 81–93, 1993.
- Guo, S., Rose, W. I., Bluth, G. J. S., and Watson, I. M.: Particles in the great Pinatubo volcanic cloud of June 1991: The role of ice, *Geochemistry, Geophysics, Geosystems*, 5, 1–35, doi:10.1029/2003GC000655, 2004.
- Hassler, B., Bodeker, G. E., and Dameris, M.: Technical Note: A new global database of trace gases and aerosols from multiple sources of high vertical resolution measurements, *Atmos. Chem. Phys.*, 8, 5403–5421, doi:10.5194/acp-8-5403-2008, 2008.
- Heckendorn, P., Weisenstein, D., Fueglistaler, S., Luo, B. P., Rozanov, E., Schraner, M., Thomason, L. W., and Peter, T.: The impact of geoengineering aerosols on stratospheric temperature and ozone, *Environmental Research Letters*, 4, 045108, doi:10.1088/1748-9326/4/4/045108, 2009.
- Hofmann, D. J., Oltmans, S. J., Komhyr, W. D., Harris, J. M., Lathrop, J. A., Langford, A. O., Deshler, T., Johnson, B. J., Torres, A., and Matthews, W. A.: Ozone loss in the lower stratosphere over the United States in 1992-1993: Evidence for heterogeneous chemistry on the Pinatubo aerosol, *Geophys. Res. Lett.*, 21, 65–68, doi:10.1029/93GL02526, 1994.
- Holton, J. R. and Tan, H.-C.: The influence of the equatorial-biennial oscillation on the global circulation at 50 mb, *J. Atmos. Sci.*, 37, 2200–2208, 1980.
- Jungclaus, J. H., Keenlyside, N., Botzet, M., Haak, H., Luo, J.-J., Latif, M., Marotzke, J., Mikolajewicz, U., and Roeckner, E.: Ocean circulation and tropical variability in the coupled model ECHAM5/MPI-OM, *J. Climate*, 19, 3952–3972, doi:10.1175/JCLI3827.1, 2006.
- Kodera, K.: Influence of volcanic eruptions on the troposphere through stratospheric dynamical processes in the Northern Hemisphere winter, *J. Geophys. Res.*, 99, 1273–1282, 1994.
- Labitzke, K.: Sunspots, the QBO, and the stratospheric temperature in the north polar region, *Geophys. Res. Lett.*, 14, 535–537, 1987.
- Labitzke, K. and McCormick, M. P.: Stratospheric temperature increases due to Pinatubo aerosols, *Geophys. Res. Lett.*, 19, 207–210, 1992.
- MacFarling-Meure, C., Etheridge, D., Trudinger, C., Steele, P., Langenfelds, R., Van Ommen, T., Smith, A., and Elkins, J.: Law Dome CO₂, CH₄ and N₂O ice core records extended to 2000 years BP, *Geophys. Res. Lett.*, 33, L14810, doi:10.1029/2006GL026152, 2006.
- Manzini, E., Giorgetta, M. A., Esch, M., Kornbluh, L., and Roeckner, E.: The influence of sea surface temperatures on the northern winter stratosphere: Ensemble simulations with the MAECHAM5 model, *J. Climate*, 19, 3863–3881, doi:10.1175/JCLI3826.1, 2006.
- Marsland, S.: The Max-Planck-Institute global ocean/sea ice model with orthogonal curvilinear coordinates, *Ocean Modelling*, 5, 91–127, doi:10.1016/S1463-5003(02)00015-X, 2003.
- McCormick, M. P.: Initial assessment of the stratospheric and climatic impact of the 1991 Mount Pinatubo eruption: Prologue, *Geophys. Res. Lett.*, 19, 149, 1992.

- Mignot, J., Khodri, M., Frankignoul, C., and Servonnat, J.: Volcanic impact on the Atlantic Ocean over the last millennium, *Climate of the Past*, 7, 1439–1455, doi:10.5194/cp-7-1439-2011, 2011.
- Minnis, P., Harrison, E. F., Stowe, L. L., Gibson, G. G., Denn, F. M., Doelling, D. R., and Smith, W. L.: Radiative climate forcing by the Mount Pinatubo eruption, *Science*, 259, 1411–1415, doi:10.1126/science.259.5100.1411, 1993.
- Muthers, S., Anet, J. G., Raible, C. C., Brönnimann, S., Rozanov, E., Arfeuille, F., Peter, T., Shapiro, A. I., Beer, J., Steinhilber, F., Brugnara, Y., and Schmutz, W.: Northern hemispheric winter warming pattern after tropical volcanic eruptions: Sensitivity to the ozone climatology, *J. Geophys. Res.*, 110, 1340–1355, doi:10.1002/2013JD020138, 2014a.
- Muthers, S., Anet, J. G., Stenke, A., Raible, C. C., Brönnimann, S., Rozanov, E., Peter, T., Arfeuille, F., Shapiro, A. I., Beer, J., Steinhilber, F., Brugnara, Y., and Schmutz, W.: The coupled atmosphere-chemistry-ocean model SOCOL-MPIOM, *Geoscientific Model Development Discussions*, 7, 3013–3084, doi:10.5194/gmdd-7-3013-2014, 2014b.
- Pitari, G. and Rizi, V.: An estimate of the chemical and radiative perturbation of stratospheric ozone following the eruption of Mt. Pinatubo, *J. Atmos. Sci.*, 50, 3260–3276, 1993.
- Pitari, G., Aquila, V., Kravitz, B., Robock, A., Watanabe, S., Cionni, I., De Luca, N., Di Genova, G., Mancini, E., and Tilmes, S.: Stratospheric ozone response to sulfate geoengineering: Results from the Geoengineering Model Intercomparison Project (GeoMIP), *J. Geophys. Res.*, 119, 2629–2653, doi:10.1002/2013JD020566, 2014.
- Portmann, R. W., Solomon, S., Garcia, R. R., Thomason, L. W., Poole, L. R., and McCormick, M. P.: Role of aerosol variations in anthropogenic ozone depletion in the polar regions paper, *J. Geophys. Res.*, 101, 22,991–23,006, doi:10.1029/96JD02608, 1996.
- Randel, W. J. and Wu, F.: Ozone and temperature changes in the stratosphere following the eruption of Mount Pinatubo, *J. Geophys. Res.*, 100, 16,753–16,764, 1995.
- Robock, A.: Volcanic eruptions and climate, *Rev. Geophys.*, 38, 191–219, 2000.
- Robock, A. and Mao, J.: Winter warming from large volcanic eruptions, *Geophys. Res. Lett.*, 12, 2405–2408, 1992.
- Roeckner, E., Bäuml, G., Bonaventura, L., Brokopf, R., Esch, M., Giorgetta, M., Hagemann, S., Kirchner, I., Kornblüeh, L., Manzini, E., Rhodin, A., Schlese, U., Schulzweida, U., and Tompkins, A.: The atmospheric general circulation model ECHAM5 - Model description, MPI report 349, Max-Planck Institute for Meteorology, Hamburg, Germany, 2003.
- Rosenfield, J. E., Considine, D. C., Meade, P. E., Bacmeister, J. T., Jackman, C. H., and Schoeberl, M. R.: Stratospheric effects of Mount Pinatubo aerosol studied with a coupled two-dimensional model, *J. Geophys. Res.*, 102, 3649–3670, doi:10.1029/96JD03820, 1997.
- Rozanov, E., Schlesinger, M. E., Zubov, V., Yang, F., and Andronova, N. G.: The UIUC three-dimensional stratospheric chemical transport model: Description and evaluation of the simulated source gases and ozone, *J. Geophys. Res.*, 104, 11,755–11,781, doi:10.1029/1999JD900138, 1999.
- Rozanov, E. V., Schlesinger, M. E., Andronova, N. G., Yang, F., Malyshev, S. L., Zubov, V. A., Egorova, T. A., and Li, B.: Climate/chemistry effects of the Pinatubo volcanic eruption simulated by the UIUC stratosphere/troposphere GCM with interactive photochemistry, *J. Geophys. Res.*, 107(D21), 4594, doi:10.1029/2001JD000974, 2002.
- Schraner, M., Rozanov, E., Schnadt Poberaj, C., Kenzelmann, P., Fischer, A. M., Zubov, V., Luo, B. P., Hoyle, C. R., Egorova, T., Fueglistaler, S., Brönnimann, S., Schmutz, W., and Peter, T.: Technical Note: Chemistry-climate model SOCOL: version 2.0 with improved transport and chemistry/microphysics schemes, *Atmos. Chem. Phys.*, 8, 5957–5974, doi:10.5194/acp-8-5957-2008, 2008.
- Shindell, D. T., Schmidt, G. A., Miller, R. L., and Mann, M. E.: Volcanic and solar forcing of climate change during the preindustrial era, *J. Climate*, 16, 4094–4107, doi:10.1175/1520-0442(2003)016<4094:VASFOC>2.0.CO;2, 2003.

- Shindell, D. T., Schmidt, G. A., Mann, M. E., and Faluvegi, G.: Dynamic winter climate response to large tropical volcanic eruptions since 1600, *J. Geophys. Res.*, 109, D05 104, doi:10.1029/2003JD004151, 2004.
- Soden, B. J., Wetherald, R. T., Stenchikov, G. L., and Robock, A.: Global cooling after the eruption of Mount Pinatubo: A test of climate feedback by water vapor., *Science*, 296, 727–30, doi:10.1126/science.296.5568.727, 2002.
- Solomon, S.: Stratospheric ozone depletion: A review of concepts and history, *Rev. Geophys.*, 37, 275, doi:10.1029/1999RG900008, 1999.
- Solomon, S., Portmann, R. W., Garcia, R. R., Thomason, L. W., Poole, L. R., McCormick, M. P., and Cly, C.: The role of aerosol variations in anthropogenic ozone depletion at northern midlatitudes, *J. Geophys. Res.*, 101, 6713–6727, 1996.
- SPARC: Assessment of stratospheric aerosol properties (ASAP), SPARC Report No. 4 1295, World Climate Research Programme WCRP-124,WMO/TD, edited by: Thomason, L. and Peter, T., 2006.
- Stenchikov, G., Robock, A., Ramaswamy, V., Schwarzkopf, M. D., Hamilton, K., and Ramachandran, S.: Arctic Oscillation response to the 1991 Mount Pinatubo eruption: Effects of volcanic aerosols and ozone depletion, *J. Geophys. Res.*, 107, 1–16, doi:10.1029/2002JD002090, 2002.
- Stenke, A., Schraner, M., Rozanov, E., Egorova, T., Luo, B., and Peter, T.: The SOCOL version 3.0 chemistry–climate model: description, evaluation, and implications from an advanced transport algorithm, *Geoscientific Model Development*, 6, 1407–1427, doi:10.5194/gmd-6-1407-2013, 2013.
- Stowe, L. L., Carey, R. M., and Pellegrino, P. P.: Monitoring the Mt. Pinatubo aerosol layer with NOAA/11 AVHRR data, *Geophys. Res. Lett.*, 19, 159–162, 1992.
- Telford, P., Braesicke, P., Morgenstern, O., and Pyle, J.: Reassessment of causes of ozone column variability following the eruption of Mount Pinatubo using a nudged CCM, *Atmos. Chem. Phys.*, 9, 4251–4260, doi:10.5194/acp-9-4251-2009, 2009.
- Thomas, M. A., Giorgetta, M. A., Timmreck, C., Graf, H.-F., and Stenchikov, G.: Simulation of the climate impact of Mt. Pinatubo eruption using ECHAM5 – Part 2: Sensitivity to the phase of the QBO, *Atmos. Chem. Phys.*, 9, 3001–3009, doi:10.5194/acp-9-3001-2009, 2009.
- Thomason, L. W.: Observations of a new SAGE II aerosol extinction mode following the eruption of Mt. Pinatubo, *Geophys. Res. Lett.*, 19, 279–2182, 1992.
- Tie, X. and Brasseur, G.: The response of stratospheric ozone to volcanic eruptions: Sensitivity to atmospheric chlorine loading, *Geophys. Res. Lett.*, 22, 3035–3038, 1995.
- Timmreck, C.: Modeling the climatic effects of large explosive volcanic eruptions, *Wiley Interdisciplinary Reviews: Climate Change*, 3, 545–564, doi:10.1002/wcc.192, 2012.
- Valcke, S.: The OASIS3 coupler: A European climate modelling community software, *Geoscientific Model Development*, 6, 373–388, doi:10.5194/gmd-6-373-2013, 2013.
- Weisenstein, D., Yue, G., Ko, M., Sze, N., Rodriguez, J., and Scott, C.: A two-dimensional model of sulfur species and aerosols, *J. Geophys. Res.*, 102, 13 019–13 035, 1997.
- Zanchettin, D., Timmreck, C., Bothe, O., Lorenz, S. J., Hegerl, G., Graf, H.-F., Luterbacher, J., and Jungclaus, J. H.: Delayed winter warming: a robust decadal response to strong tropical volcanic eruptions?, *Geophys. Res. Lett.*, 40, 204–209, doi:10.1029/2012GL054403, 2012.
- Zanchettin, D., Bothe, O., Graf, H. F., Lorenz, S. J., Luterbacher, J., Timmreck, C., and Jungclaus, J. H.: Background conditions influence the decadal climate response to strong volcanic eruptions, *J. Geophys. Res.*, 118, 4090–4106, doi:10.1002/jgrd.50229, 2013.
- Zhang, D., Blender, R., and Fraedrich, K.: Volcanoes and ENSO in millennium simulations: Global impacts and regional reconstructions in East Asia, *Theor. Appl. Climatol.*, doi:10.1007/s00704-012-0670-6, 2012.

Chapter 5.

Outlook

The aim of this thesis was to explore interactions between the physical and the chemical components of the climate system in various case studies. In particular, the role of different external forcings and their interactions with the atmospheric chemistry for climate variability and climate change in the past and the future was addressed. Therefore, the CCM SOCOL was coupled to the ocean model MPIOM. The scientific questions were addressed using a number of sensitivity studies for different forcings and long-term simulations for the period 1600-2000 AD as well as simulations for the 21th century.

This thesis shows that ozone chemistry modulates the dynamic response of large volcanic eruptions and that the response is sensitive to the climate state and the eruption strengths (Muthers et al., 2014a,c). Additionally, a grand solar minima has been simulated with interactive chemistry in a future simulation for the 21th century (Anet et al., 2013b). While the effect of the solar minimum on the temperature trends is comparable to earlier studies, we could show that a future grand solar minima is expected to significantly delay the recovery of the stratospheric ozone concentrations. However, the open questions remain whether and how the atmospheric chemistry modulates the response of the climate system to a grand solar minima and whether the response differs between climate states.

Although the model has been proven useful in several simulations, a number of issues remain, which should be improved in the future. SOCOL-MPIOM is characterised by a high climate sensitivity in comparison to most CMIP5 models (Muthers et al., 2014b). The atmospheric chemistry has been found to reduce the sensitivity slightly by a negative feedback of the ozone chemistry in agreement with earlier results from Dietmüller et al. (2014). The imprint of the high sensitivity is clearly visible in the simulated transient temperature increase during the industrial period, where the GHG induced temperature increase is further amplified by additional forcings. Further analysis should explore the reasons for the high climate sensitivity of the model. An identification of underlying mechanisms, e.g. the role of clouds or convective mixing for the sensitivity (compare Webb et al., 2013; Sherwood et al., 2014), could be used to tune SOCOL-MPIOM towards a lower sensitivity. Furthermore, experience from the MPI-ESM with ECHAM6 could be used to improve the model (Mauritsen et al., 2012). Additionally, the simulated trends in the ozone chemistry during the 20th century and the small differences between the two solar forcings during the same period need further validation.

The sensitivity of SOCOL-MPIOM to non-GHG forcings has not been quantified so far. In several modelling studies (e.g., Hansen et al., 1997; Joshi et al., 2003; Cai and Tung, 2012), the differences in the models sensitivities to CO₂, solar, and ozone has been found to be small in comparison to the differences between the models. Still, depending on the spatial pattern of the forcing, response can be substantially different

(Joshi et al., 2003; Shindell, 2014). So far, the sensitivity to non-GHG forcings has been analysed only in GCMs without interactive chemistry. With increasing solar forcing the stratospheric chemistry is expected to react to the increasing UV radiation by enhanced ozone production, which adds an additional positive RF to the surface temperatures. On the other hand, however, the temperature increase is also expected to strengthen the BDC, which might reduce ozone in the lower tropical stratosphere with negative effect on the radiation balance. Two counteracting feedbacks of the chemistry are therefore possible. Results from the sensitivity simulations for the DM (Anet et al., 2013a, 2014) suggest that the direct effect of the ozone to the UV changes may dominate and lead to a slight amplification of the temperature response. In a next step the sensitivity of SOCOL-MPIOM to the solar forcing will be addressed in simulations with continuously or abrupt TSI increases, similar to the CO₂ sensitivity experiments.

The model configuration without interactive chemistry used throughout this thesis lacks a parametrization of the absorption of O₂ and O₃ in specific UV intervals. This parametrization is already implemented in the model with interactive chemistry (following Egorova et al., 2004) and should be adapted to reduce the differences between both configurations.

Another issue involves the stratosphere-troposphere coupling in SOCOL-MPIOM. Results presented in Chapter 3 indicate a reasonably coupling of wind anomalies between stratosphere and troposphere. However, in Chapter 4 and A.3 the coupling is found to be too weak in comparison to observations or earlier model simulations. With the current statistical definition of coupling events these differences in the results can not be explained. Consequently, a process-based understanding of couplings and the parametrization used in the model is needed to understand the differences.

Bibliography

- Anet, J. G., Muthers, S., Rozanov, E., Raible, C. C., Peter, T., Stenke, A., Shapiro, A. I., Beer, J., Steinhilber, F., Brönnimann, S., Arfeuille, F., Brugnara, Y., and Schmutz, W. K.: Forcing of stratospheric chemistry and dynamics during the Dalton Minimum, *Atmos. Chem. Phys.*, 13, 10 951–10 967, doi:10.5194/acp-13-10951-2013, 2013a.
- Anet, J. G., Rozanov, E. V., Muthers, S., Peter, T., Brönnimann, S., Arfeuille, F., Beer, J., Shapiro, A. I., Raible, C. C., Steinhilber, F., and Schmutz, W. K.: Impact of a potential 21st century “grand solar minimum” on surface temperatures and stratospheric ozone, *Geophys. Res. Lett.*, 40, 4420–4425, doi:10.1002/grl.50806, 2013b.
- Anet, J. G., Muthers, S., Rozanov, E. V., Raible, C. C., Stenke, A., Shapiro, A. I., Brönnimann, S., Arfeuille, F., Brugnara, Y., Beer, J., Steinhilber, F., Schmutz, W., and Peter, T.: Impact of solar vs. volcanic activity variations on tropospheric temperatures and precipitation during the Dalton Minimum, *Climate of the Past*, 10, 921–938, doi:10.5194/cp-10-921-2014, 2014.
- Cai, M. and Tung, K.-K.: Robustness of dynamical feedbacks from radiative forcing: 2% solar versus $2\times\text{CO}_2$ experiments in an idealized GCM, *J. Atmos. Sci.*, 69, 2256–2271, doi:10.1175/JAS-D-11-0117.1, 2012.
- Dietmüller, S., Ponater, M., and Sausen, R.: Interactive ozone induces a negative feedback in CO_2 driven climate change simulations, *J. Geophys. Res.*, 119, 1796–1805, doi:10.1002/2013JD020575, 2014.
- Egorova, T., Rozanov, E., Manzini, E., Schmutz, W., and Peter, T.: Chemical and dynamical response to the 11-year variability of the solar irradiance simulated with a chemistry-climate model, *Geophys. Res. Lett.*, 31, 6225–6230, doi:10.1029/2003GL019294, 2004.
- Hansen, J., Sato, M., and Ruedy, R.: Radiative forcing and climate response, *J. Geophys. Res.*, 102, 6831–6864, doi:10.1029/96JD03436, 1997.
- Joshi, M., Shine, K., Ponater, M., Stuber, N., Sausen, R., and Li, L.: A comparison of climate response to different radiative forcings in three general circulation models: towards an improved metric of climate change, *Climate Dyn.*, 20, 843–854, doi:10.1007/s00382-003-0305-9, 2003.
- Mauritsen, T., Stevens, B., Roeckner, E., Crueger, T., Esch, M., Giorgetta, M., Haak, H., Jungclaus, J., Klocke, D., Matei, D., Mikolajewicz, U., Notz, D., Pincus, R., Schmidt, H., and Tomassini, L.: Tuning the climate of a global model, *Journal of Advances in Modeling Earth Systems*, 4, M00A01, doi:10.1029/2012MS000154, 2012.
- Muthers, S., Anet, J. G., Raible, C. C., Brönnimann, S., Rozanov, E., Arfeuille, F., Peter, T., Shapiro, A. I., Beer, J., Steinhilber, F., Brugnara, Y., and Schmutz, W.: Northern hemispheric winter warming pattern after tropical volcanic eruptions: Sensitivity to the ozone climatology, *J. Geophys. Res.*, 110, 1340–1355, doi:10.1002/2013JD020138, 2014a.
- Muthers, S., Anet, J. G., Stenke, A., Raible, C. C., Brönnimann, S., Rozanov, E., Peter, T., Arfeuille, F., Shapiro, A. I., Beer, J., Steinhilber, F., Brugnara, Y., and Schmutz, W.: The coupled atmosphere-chemistry-ocean model SOCOL-MPIOM, *Geoscientific Model Development Discussions*, 7, 3013–3084, doi:10.5194/gmdd-7-3013-2014, 2014b.
- Muthers, S., Arfeuille, F., and Raible, C. C.: Dynamical and chemical ozone perturbations after large volcanic eruptions: Role of the climate state and the strength of the eruption, *J. Geophys. Res.*, submitted, 2014c.
- Sherwood, S. C., Bony, S., and Dufresne, J.: Spread in model climate sensitivity traced to atmospheric convective mixing, *Nature*, 505, 37–42, doi:10.1038/nature12829, 2014.
- Shindell, D. T.: Inhomogeneous forcing and transient climate sensitivity, *Nature Geoscience*, 4, 18–21, doi:10.1038/NCLIMATE2136, 2014.
- Webb, M. J., Lambert, F. H., and Gregory, J. M.: Origins of differences in climate sensitivity, forcing and feedback in climate models, *Climate Dyn.*, 40, 677–707, doi:10.1007/s00382-012-1336-x, 2013.

Appendix A.

A.1. Impact of a potential 21st century "grand solar minimum" on surface temperatures and stratospheric ozone

Julien G. Anet, Eugene Rozanov, Stefan Muthers, Thomas Peter, Stefan Brönnimann, Florian Arfeuille, Jürg Beer, Alexander I. Shapiro, Christoph C. Raible, Friedhelm Steinhilber, and Werner Schmutz.

Published in *Geophysical Research Letters* vol. 40, 6, p. 4420-4425, 2013.

Impact of a potential 21st century “grand solar minimum” on surface temperatures and stratospheric ozone

J. G. Anet,¹ E. V. Rozanov,^{1,2} S. Muthers,^{3,4} T. Peter,¹ S. Brönnimann,^{4,5} F. Arfeuille,^{4,5} J. Beer,⁶ A. I. Shapiro,² C. C. Raible,^{3,4} F. Steinhilber,⁶ and W. K. Schmutz²

Received 13 May 2013; revised 19 July 2013; accepted 30 July 2013; published 22 August 2013.

[1] We investigate the effects of a recently proposed 21st century Dalton minimum like decline of solar activity on the evolution of Earth’s climate and ozone layer. Three sets of two member ensemble simulations, radiatively forced by a midlevel emission scenario (Intergovernmental Panel on Climate Change RCP4.5), are performed with the atmosphere-ocean chemistry-climate model AOCCM SOCOL3-MPIOM, one with constant solar activity, the other two with reduced solar activity and different strength of the solar irradiance forcing. A future grand solar minimum will reduce the global mean surface warming of 2 K between 1986–2005 and 2081–2100 by 0.2 to 0.3 K. Furthermore, the decrease in solar UV radiation leads to a significant delay of stratospheric ozone recovery by 10 years and longer. Therefore, the effects of a solar activity minimum, should it occur, may interfere with international efforts for the protection of global climate and the ozone layer. **Citation:** Anet, J. G., et al. (2013), Impact of a potential 21st century “grand solar minimum” on surface temperatures and stratospheric ozone, *Geophys. Res. Lett.*, 40, 4420–4425, doi:10.1002/grl.50806.

1. Introduction

[2] Model simulations of 21st century climate undertaken under the CMIP5 project [e.g., Knutti and Sedláček, 2012] show global temperature increases of 1 ± 0.4 K for the RCP2.6 scenario, 1.8 ± 0.5 K for RCP4.5, 2.2 ± 0.5 K for RCP6.0, and 3.7 ± 0.7 K for RCP8.5 (Representative Concentration Pathways) [e.g., van Vuuren et al., 2011]. The ranges reflect intermodel differences for a given scenario but do not include uncertainties in future natural forcings. In the CMIP5 protocol, volcanic effects are assumed to be negligible and solar activity is chosen to mimic the last

solar cycle. Recently, the possibility of a future grand solar minimum was proposed to occur in the 21st century [Abreu et al., 2010; Lockwood et al., 2009; Steinhilber and Beer, 2013]. The cooling associated with a potential solar activity decline might have implications for global warming, atmospheric dynamics, weather patterns, and air chemistry, in general, and for stratospheric ozone, in particular. Studies using different climate models and scenarios of solar activity changes [Feulner and Rahmstorf, 2010; Rozanov et al., 2012a; Meehl et al., 2013] concluded that global warming could be partially compensated by about 0.25 to 0.5 K.

[3] Uncertainties in the magnitude of the solar contribution are partially related to different experimental designs: Feulner and Rahmstorf [2010] used a model of intermediate complexity with a simplified treatment of the stratospheric processes and obtain a reduction of the warming by 0.26 K. They adopted the greenhouse gas emissions following the Special Report on Emissions Scenarios A1B and applied solar activity changes without spectral resolution via a total solar irradiance (TSI) decrease by 0.08% and 0.25%. Resulting changes in ocean and land surface temperatures affect the entire atmosphere via the hydrological cycle. This mechanism is known as the bottom-up mechanism [e.g., Gray et al., 2010]. On the other hand, the efficiency of the top-down mechanism [e.g., Gray et al., 2010] was probably underestimated because of the very low changes in the middle atmosphere induced by the small amplitude of the ultraviolet (UV) part of the spectrum and of the missing energetic particles. To overcome this shortcoming, Rozanov et al. [2012a] applied the chemistry-climate model solar-climate-ozone links (CCM SOCOL) in the time slice mode driven by the changes of energetic particle precipitation and spectral solar irradiance (SSI) taken from the reconstructions by Shapiro et al. [2011] for Dalton minimum conditions. However, these simulations were performed without interactive ocean. Meehl et al. [2013] used the atmosphere-ocean chemistry-climate model (AOCCM) WACCM driven by a TSI drop by 0.25% during 50 years in the middle of the 21st century using the RCP4.5 emission scenario and with an SSI decrease constructed by scaling of the solar irradiance from the Naval Research Laboratory spectral solar irradiance (NRLSSI) data [Lean et al., 2005]. They obtained a reduction of global warming by 0.24 K. There is presently a lively discussion of the very uncertain SSI variations over the recent past solar cycles [Haigh et al., 2010; Lean and DeLand, 2012]. As Meehl et al. [2013] prescribed -0.25% less irradiance in the entire spectrum by taking the mean of the 1975, 1986, and 1996 solar minimum values of the NRLSSI data of Lean et al. [2005], the overall drop in UV is weaker than in the Shapiro et al. [2011] forcing, thus reducing the magnitude of the top-down mechanism.

Additional supporting information may be found in the online version of this article.

¹Institute for Atmospheric and Climate Science ETH, Zurich, Switzerland.

²Physikalisch-Meteorologisches Observatorium Davos and World Radiation Center, Davos, Switzerland.

³Climate and Environment Physics, Physics Institute, University of Bern, Bern, Switzerland.

⁴Oeschger Centre for Climate Change Research, University of Bern, Bern, Switzerland.

⁵Institute of Geography, University of Bern, Bern, Switzerland.

⁶Surface Waters Group, Eawag: Swiss Federal Institute of Aquatic Science and Technology, Surface Waters Group, Dübendorf, Switzerland.

Corresponding author: J. G. Anet, Institute for Atmospheric and Climate Science ETH, Universitaetstrasse 16, CH-8092 Zurich, Switzerland. (julien.anet@env.ethz.ch)

©2013. American Geophysical Union. All Rights Reserved.
0094-8276/13/10.1002/grl.50806

A.1. Impact of a potential 21st century "grand solar minimum" on surface temperatures and stratospheric ozone

ANET ET AL.: 21ST CENTURY SOLAR MINIMUM: TEMPERATURE AND O₃

Shapiro et al. [2011] assumed that the minimum state of the quiet Sun in time corresponds to the observed quietest areas on the present Sun, which they represented by the "model of faint supergranule cell interior" from *Fontenla et al.* [1999]. The resulting amplitudes of their secular solar irradiance change is larger than the other recently published estimates (see, e.g., discussion in *Lockwood* [2011]). This influence should be clearly seen in the ozone response and probably in the winter time temperature but not much in the annual mean temperatures.

[4] The potential drop in the solar UV activity can substantially affect the ozone layer [*Anet et al.*, 2013], which in turn affects stratospheric temperature, circulation, tropospheric climate, and the UV intensity reaching the ground. The implications of a solar activity decline for the expected stratospheric ozone recovery later in this century [*WMO*, 2011] have not yet been considered in the literature. Here we analyze the influence of a strong UV decrease [*Shapiro et al.*, 2011] and the concomitant changes in energetic particles on climate and global ozone. We use the results of transient 100 year long ensemble simulations with the AOCCM SOCOL-MPIOM (Max Planck Institute ocean model). The model is driven by three scenarios of the future spectral solar irradiance, each with two members with identical anthropogenic forcing (RCP4.5) [see *van Vuuren et al.*, 2011]. It uses a comprehensive middle-atmospheric chemical scheme and a fully coupled deep ocean. Compared to *Meehl et al.* [2013], the applied solar forcing is much stronger in the UV spectrum and lasts for a longer time, because grand minima usually last for 70 to 110 years. Moreover, we improve the approach of *Meehl et al.* [2013] keeping the 11 year solar cycle and decreasing the solar irradiance slowly to the new minimum, making it more realistic.

2. Model Description and Experimental Design

[5] The experiments are run with the AOCCM SOCOL-MPIOM which emerges from the CCM SOCOL version 3 [*Stenke et al.*, 2012] coupled to the Max Planck Institute ocean model [*Marsland et al.*, 2003] using the OASIS3 coupler [*Valcke*, 2013]. The CCM SOCOL v3 is based on the global climate model ECHAM5 [*Roeckner et al.*, 2003] and includes the chemical module MEZON (model for evaluation of ozone trends). The model is used in the middle atmosphere (MA) mode and does not include interactive vegetation. MA-ECHAM5 hands over temperature and tracer fields to MEZON, which calculates chemical transformations of 41 gas species participating in 200 gas phase, 16 heterogeneous, and 35 photolytic reactions. The resulting tendencies of chemical species are then returned to MA-ECHAM5. Our experiments are performed with T31 spectral resolution, which equals to an average grid space of 3.75° (\approx 400 km). In vertical direction, the model domain is divided into 39 layers from the ground to 0.01 hPa. For more details, see *Stenke et al.* [2012].

[6] Three experiments are carried out, each consisting of two 100 year long simulations. The only difference between the experiments is the solar forcing. One experiment, named henceforward CONST, is forced by a perpetual repetition of the solar cycles 22 and 23 until the year 2100. The second and third experiments, thenceforth called WEAK and STRONG, follow the scenario of an oncoming grand solar minimum reaching its minimum in 2090, with TSI being 4

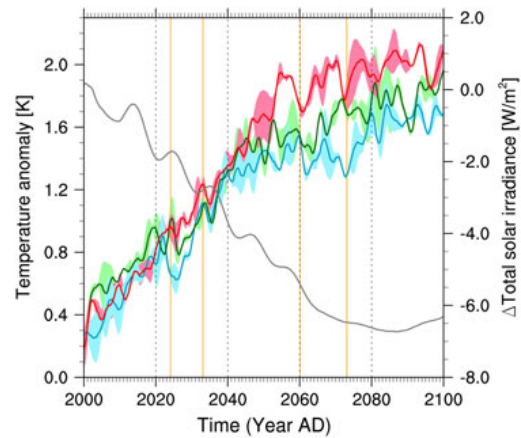


Figure 1. Globally averaged surface air temperature evolution for CONST (red), STRONG (blue), and WEAK (green) smoothed with a full width half maximum Gaussian filter over 24 months. Spread of the two runs per experiment is illustrated as pastel envelope. Anomalies (in Kelvin) are shown relative to the averaged 1986–2005 temperatures. Grey curve: total solar irradiance anomaly relative to the average TSI of the 1995–2005 period following *Shapiro et al.* [2011]. Orange vertical lines: years of hypothetical volcanic eruptions.

and 6 W/m² lower in WEAK and STRONG, respectively, as compared to CONST. In Figure 1, the grey curve shows the deviation of the total solar irradiance from the 1995–2005 averaged value [*Shapiro et al.*, 2011]. The oscillation shows the underlying 11 year solar cycle. These quantities are further used as proxies to calculate the future evolution of the SSI, the *A_p* index (describing the geomagnetic activity) and the ionization rate by galactic cosmic rays, which are necessary to drive the model [*Rozanov et al.*, 2012b]. The 4 and 6 W/m² lower TSI in WEAK and STRONG represent TSI decreases of 0.3% and 0.45%, respectively. The corresponding maximum changes of the spectral irradiance for the different bands of the ECHAM5 radiation code in WEAK are –10% for 180–250 nm, –1.5% for 240–440 nm, –0.2% for 440–690 nm, +0.01% for 690–1190 nm and 1190–2380 nm, and –0.03% for 2380–4000 nm (Figure S1 of the supporting information). The SSI changes for STRONG are larger by roughly a factor 1.5. All simulations start from the year 2000. WEAK and STRONG are initialized by restart files for this year from four 400 year long transient simulation starting from 1600, while CONST was branched from two of the 400 year long transient simulations at the year 2000. The concentrations of greenhouse gases (GHGs), ozone destroying substances (ODSs), as well as anthropogenic NO_x and CO emissions are set following the CMIP5 RCP4.5 scenario. The tropospheric aerosols are adapted from CAM3.5 simulations with a bulk aerosol model driven by CCSM3 (CMIP4) sea surface temperatures and the 2000–2100 CMIP5 emissions (S. Bauer, personal communication, 2011). Stratospheric aerosols were kept at background levels excepted for four assigned volcanic eruptions (a Fuego-like volcanic eruption in 2024, a smaller volcanic eruption in 2033, an Agung-like volcanic eruption

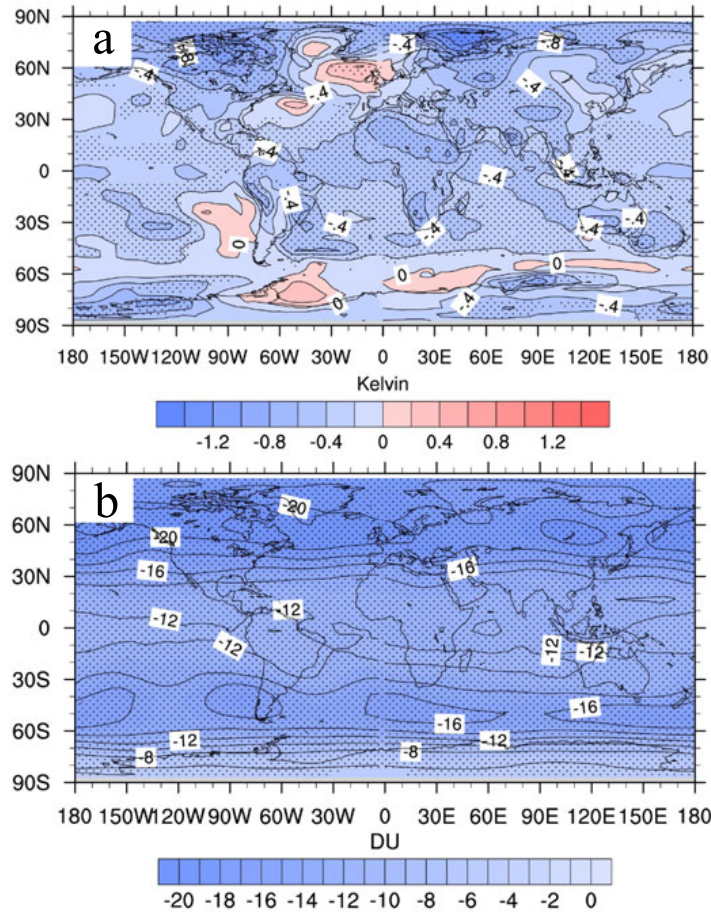


Figure 2. (a) Surface air temperature difference between STRONG and CONST, averaged over the ensemble members in the 2081–2100 period. (b) Total column ozone difference between STRONG and CONST, averaged over the ensemble members in the 2081–2100 period. Stippling denotes the areas where the differences are statistically significant at the 5% level using a t test.

in 2060, and another smaller volcanic eruption in 2073, [see *Arfeuille et al.*, 2013]).

3. Results

[7] All runs follow a distinct warming path, yielding 1.96 ± 0.12 K (CONST), 1.75 ± 0.14 K (WEAK), and 1.61 ± 0.12 K (STRONG) change in the global annual mean surface temperature, averaged over the 2081–2100 period relative to the 1986–2005 reference period, respectively (Figure 1). The results of CONST is in a good agreement with the CMIP5 RCP4.5 multimodel mean global warming of 1.8 K [*Knutti and Sedláček*, 2012]. While the warming trend of 0.24 ± 0.04 K/decade is very similar in all simulations from 2000 to 2045, the model projects a clear separation thereafter. While WEAK develops a reduced warming rate of 0.09 ± 0.04 K/decade for the second half of the century, STRONG enters a reduced warming phase of 0.08 ± 0.04 K/decade until the end of the century. Similar to WEAK, CONST shows a transition to a weaker warming rate phase of $0.11 \pm$

0.03 K/decade. The decrease of the global warming rate after 2045 in CONST is related to the declining CO₂ and CH₄ emission rates according to RCP4.5. The 2081–2100 mean temperatures are 0.21 ± 0.26 K higher in CONST than in WEAK and 0.35 ± 0.24 K higher than in STRONG. The decelerated global-averaged warming is comparable to the results of *Meehl et al.* [2013] and also compares well to the simulation with strong solar forcing (-0.25% in TSI) of *Feulner and Rahmstorf* [2010]. In our simulations, the major volcanic eruptions in 2023 and 2060 lead to a pronounced decrease in global temperatures right after the events, but temperatures recover in 2–5 years time. The two smaller eruptions have no detectable effect on temperatures. The simulated patterns of GHG warming are in good agreement with the results of other models [*Meehl et al.*, 2005; *Washington et al.*, 2009; *Knutti and Sedláček*, 2012] (Figure S2). The temperature difference between the period 2081–2100 and 1986–2005 of CONST shows the most pronounced positive differences over the Arctic due to polar amplification [e.g., *Serreze and Barry*, 2011]. Other

A.1. Impact of a potential 21st century "grand solar minimum" on surface temperatures and stratospheric ozone

ANET ET AL.: 21ST CENTURY SOLAR MINIMUM: TEMPERATURE AND O₃

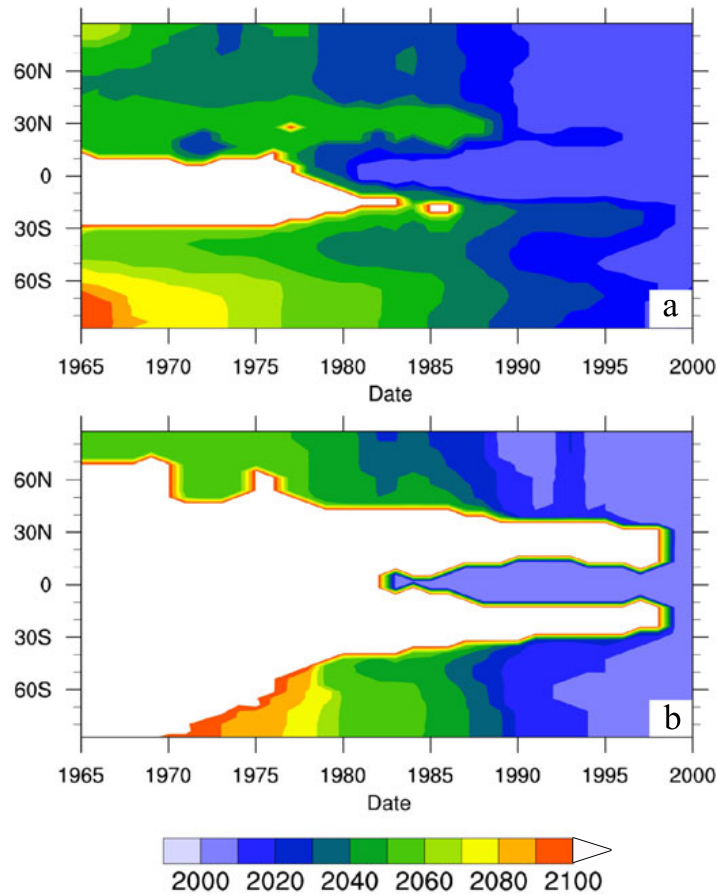


Figure 3. Timing of the total ozone column return date in the AOCCM SOCOL-MPIOM. Contours illustrate years of the simulation, in which the total ozone concentration shown on the abscissa is restored, similar to Figure 19 of *Austin et al.* [2010]. (a) Mean of CONST. (b) Mean of STRONG. Ozone column has been averaged with a running mean over 11 years (boxcar). White areas highlight ozone levels which are predicted not to recover to pre-2000 values before 2100. Reference ozone data are provided by the pre-2000 simulations.

strong temperature differences are found over Central Southern America, South Africa, the Himalayan region, and Australia.

[8] Figure 2a shows the differences in the regional pattern of surface air temperatures between STRONG and CONST for the period 2081–2100. The drop in solar activity leads to a significant cooling in the equatorial region and over most of the northern high latitudes. Due to the albedo effect from a positive sea ice anomaly, the northern polar region is cooled by up to 1 K, while the cooling over the southern polar region is less pronounced. The North Atlantic region reacts with a warming due to a 2 Sv stronger reduction of the Atlantic meridional overturning circulation in CONST compared with STRONG. The reason for this reduction is the stronger external forcing in CONST and maybe also a change in the stratosphere-troposphere coupling as suggested by *Reichler et al.* [2012]. Clearly, this needs a more detailed analysis and is beyond the scope of this study. A cooling of up to 0.4 K takes place over

large parts of the Pacific, Atlantic, and Indian Oceans. The boreal winter pattern averaged over the same period of time (Figure S3) shows an overall similar pattern as the annual mean, although the cooling over the northern polar region is stronger and temperature anomalies reach up to -1.4 K. The warming signal in the eastern part of the Antarctic Peninsula gets larger due to the sea ice melting process being stronger in CONST, leading to lower salinities. The patterns look very similar when comparing CONST to WEAK, just that the amplitudes of the temperature changes are smaller and less significant (see Figure S4). Overall, a stronger cooling signal over land is evident especially over the Arctic region compared to *Meehl et al.* [2013] due to a stronger solar forcing.

[9] The well-known pattern of recovery of the ozone layer [e.g., *WMO*, 2011] is shown in Figure S5. Up to 33 Dobson unit (DU) more ozone over the northern polar region and up to 56 DU more ozone in the southern polar region is modeled in CONST by the end of this century compared to levels

of the reference 1986–2005 period. However, the equatorial region and the subtropics of both hemispheres show much smaller or even slightly negative changes around 0 to –4 DU due to the increase of the meridional circulation in the future [e.g., *WMO*, 2011].

[10] The differences in the total column ozone averaged over the last 20 years of the 21st century between STRONG and CONST are depicted in Figure 2b. Over all regions of the world, the model simulates a highly significant decrease of ozone (Student's *t* test on the 1% significance level). The decrease is stronger over the midlatitudes than over the polar and equatorial regions, reaching negative total ozone column anomalies of up to –20 DU. Additionally, the equatorial region experiences loss of ozone of –12 DU on average, while the southern polar region suffers the smallest decrease of –8 DU. Over the northern polar region, a loss of –17 DU on average is simulated. The overall effect, illustrated in Figure S6, shows the changes in total ozone column reached by the end of the century in STRONG compared to the 1986–2005 reference period.

[11] Figure 3 shows the return date of the zonally averaged total column ozone compared to pre-2000 levels in CONST (Figure 3a) and STRONG (Figure 3b). While in CONST, nearly full recovery to the 1960 levels is reached in the extratropics and the poles, STRONG allows the total column ozone not even to reach the 1975 levels over the large areas of the northern subtropics, equatorial regions, and southern hemisphere. The recovery to the pre-1960 levels at the poles illustrated in Figure 3b thus sets in much later than in CONST.

4. Conclusions

[12] The facts that during the past 10,000 years, about 20 grand solar minima occurred, and that the past decades correspond to a long-lasting solar maximum make, it is very likely that a new grand minimum will occur. Spectral extrapolation indicates that it is likely that this minimum will occur within the next decades. However, it is not possible to predict whether it will be a Dalton or a Maunder minimum type.

[13] Yet, by assuming a Dalton minimum type solar minimum, we show in agreement with *Meehl et al.* [2013] that although the solar minimum results in a reduced global warming, it cannot compensate continuing anthropogenic impacts. Still, the modeled temperatures averaged over the last 20 years of the 21st century are lower by up to 0.3 K—depending on the details of the solar minimum scenario—than the runs with solar constant forcing. Since the duration of the grand minimum assumed in the present work is longer than that of *Meehl et al.* [2013], the apparent weakening of the global warming is more pronounced. Yet, this should not distract from the fact that the general warming is due to anthropogenic emissions and that the grand minimum can at best lead to an episodic reduction of the warming.

[14] Significant cooling pattern changes between the work of *Meehl et al.* [2013] and this one might be due to a stronger decrease in the UV spectrum—leading to a more important cooling especially over the Arctic region. In a future work, we will perform sensitivity experiments to investigate the contribution of the top-down mechanism to the temperature anomaly in the Arctic region.

[15] Although the magnitude of the solar variability is still poorly constrained [see, e.g., *Judge et al.*, 2012; *Solanki and Unruh*, 2013; *Shapiro et al.*, 2013] and remains a bottleneck for the climate studies, this study shows evidence that the strong decrease in UV radiation and in the photolysis rates leads to a significant decrease of ozone especially in the tropics. This reduction in UV slows down or even cancels the recovery of the ozone column, depending on the region. Moreover, due to the net decrease of the UV-absorbing ozone, photoactive radiation between 300 and 320 nm could be enhanced especially over the tropics and subtropics (40°S–40°N) during a future grand solar minimum. This could possibly increase the risk of skin cancer and other diseases [*Setlow*, 1974] in WEAK and STRONG with respect to CONST—and also to present conditions. Future work is needed to investigate the change in erythemal radiation in order to specify health effects.

[16] **Acknowledgments.** This project is supported by the Swiss National Science Foundation under the grant CRSI122-130642 (FUPSOL). We express our greatest thanks for this support. E. Rozanov, A. I. Shapiro, and W. Schmutz thank COST Action ES-1005 TOSCA (<http://www.tosca-cost.eu>) for the support and fruitful discussions. We would also like to thank the two anonymous reviewers for their comments.

[17] The Editor thanks two anonymous reviewers for their assistance in evaluating this paper.

References

- Abreu, J. A., J. Beer, and A. Ferriz-Mas (2010), Past and future solar activity from cosmogenic radionuclides, in *SOHO-23: Understanding a Peculiar Solar Minimum ASP Conference Series, Proceedings of a Workshop Held 21-25 September 2009 in Northeast Harbor, Maine, USA*, Vol. 428, edited by R. Steven et al., pp. 287–295, Astronomical Society of the Pacific, San Francisco.
- Anet, J. G., et al. (2013), Forcing of stratospheric chemistry and dynamics during the dalton minimum, *Atmos. Chem. Phys. Discuss.*, 13(6), 15,061–15,104, doi:10.5194/acpd-13-15061-2013.
- Arfeuille, F., D. Weisenstein, H. Mack, E. Rozanov, T. Peter, and S. Brönnimann (2013), Volcanic forcing for climate modeling: A new microphysics-based dataset covering years 1600–present, *Clim. Past Discuss.*, 9, 967–1012, doi:10.5194/cpd-9-967-2013.
- Austin, J., et al. (2010), Chemistry-climate model simulations of spring antarctic ozone, *J. Geophys. Res.*, 115, D00M111, doi:10.1029/2009JD013577.
- Feulner, G., and S. Rahmstorf (2010), On the effect of a new grand minimum of solar activity on the future climate on earth, *Geophys. Res. Lett.*, 37, L05707, doi:10.1029/2010GL042710.
- Fontenla, J., O. R. White, P. A. Fox, E. H. Avrett, and R. L. Kurucz (1999), Calculation of solar irradiances. I. Synthesis of the solar spectrum, *Astrophys. J.*, 518, 480–499, doi:10.1086/307258.
- Gray, L., et al. (2010), Solar influences on climate, *Rev. Geophys.*, 48(4), RG4001, doi:10.1029/2009RG000282.
- Haigh, J., A. Winning, R. Toumi, and J. Harder (2010), An influence of solar spectral variations on radiative forcing of climate, *Nature*, 467(7316), 696–699, doi:10.1038/nature09426.
- Judge, P. G., G. W. Lockwood, R. R. Radick, G. W. Henry, A. I. Shapiro, W. Schmutz, and C. Lindsey (2012), Confronting a solar irradiance reconstruction with solar and stellar data, *Astron. Astrophys.*, 544, A88, 6 pp., doi:10.1051/0004-6361/201218903.
- Knutti, R., and J. Sedláček (2012), Robustness and uncertainties in the new CMIP5 climate model projections, *Nat. Clim. Change*, 3, 369–373, doi:10.1038/NCLIMATE1716.
- Lean, J., G. Rottman, J. Harder, and G. Kopp (2005), Sorce contributions to new understanding of global change and solar variability, *Sol. Phys.*, 230, 27–53, doi:10.1007/s11207-005-1527-2.
- Lean, J. L., and M. T. DeLand (2012), How does the sun's spectrum vary? *J. Clim.*, 25(7), 2555–2560, doi:10.1175/JCLI-D-11-00571.1.
- Lockwood, M. (2011), Solar physics: Shining a light on solar impacts, *Nat. Clim. Change*, 1, 98–99, doi:10.1038/nclimate1096.
- Lockwood, M., A. Rouillard, and I. Finch (2009), The rise and fall of open solar flux during the current grand solar maximum, *Astrophys. J.*, 700(2), 937–944, doi:10.1088/0004-637X/700/2/937.

A.1. Impact of a potential 21st century "grand solar minimum" on surface temperatures and stratospheric ozone

ANET ET AL.: 21ST CENTURY SOLAR MINIMUM: TEMPERATURE AND O₃

- Marsland, S., H. Haak, J. Jungclaus, M. Latif, and F. Roske (2003), The Max-Planck-Institute global ocean/sea ice model with orthogonal curvilinear coordinate, *Ocean Model.*, 5, 91–27, doi:10.1016/S1463-5003(02)00015-X.
- Meehl, G. A., W. M. Washington, W. D. Collins, J. M. Arblaster, A. Hu, L. E. Buja, W. G. Strand, and H. Teng (2005), How much more global warming and sea level rise? *Science*, 307, 1769–1772, doi:10.1126/science.1106663.
- Meehl, G. A., J. M. Arblaster, and D. R. Marsh (2013), Could a future "grand solar minimum" like the Maunder minimum stop global warming? *Geophys. Res. Lett.*, 40, 1789–1793, doi:10.1002/grl.50361.
- Reichler, T., J. Kim, E. Manzini, and J. Kröger (2012), A stratospheric connection to Atlantic climate variability, *Nat. Geosci.*, 5, 783–787, doi:10.1038/ngeo1586.
- Roeckner, E., et al., (2003), The atmospheric general circulation model ECHAM5 part 1: Model description, MPI report NO 349, *Tech. rep.*, Max-Planck-Institut für Meteorologie, Hamburg.
- Rozanov, E., M. Calisto, T. Egorova, T. Peter, and W. Schmutz (2012b), Influence of the precipitating energetic particles on atmospheric chemistry and climate, *Surv. Geophys.*, 33, 483–501, doi:10.1007/s10712-012-9192-0.
- Rozanov, E. V., T. A. Egorova, A. I. Shapiro, and W. K. Schmutz (2012a), Modeling of the atmospheric response to a strong decrease of the solar activity, paper presented at International Astronomical Union, Volume 286, pp. 215–224, doi:10.1017/S1743921312004863.
- Serreze, M. C., and R. G. Barry (2011), Processes and impacts of arctic amplification: A research synthesis, *Global. Planet. Change*, 77, 85–96, doi:10.1016/j.gloplacha.2011.03.004.
- Setlow, R. B. (1974), The wavelengths in sunlight effective in producing skin cancer: A theoretical analysis, *Proc. Natl. Acad. Sci.*, 71(9), 3363–3366, doi:10.1073/pnas.71.9.3363.
- Shapiro, A. I., W. Schmutz, G. Cessateur, and E. Rozanov (2013), The place of the Sun among the Sun-like stars, *Astron. Astrophys.*, 552, A114, doi:10.1051/0004-6361/201220512.
- Shapiro, A. I., W. Schmutz, E. Rozanov, M. Schoell, M. Haberreiter, A. V. Shapiro, and S. Nyeki (2011), A new approach to the long-term reconstruction of the solar irradiance leads to large historical solar forcing, *Astron. Astrophys.*, 529, A67, 8 pp., doi:10.1051/0004-6361/201016173.
- Solanki, S., and Y. Unruh (2013), Solar irradiance variability, *Astron. Nachr.*, 334, 145–150, doi:10.1002/asna.201211752.
- Steinhilber, F., and J. Beer (2013), Prediction of solar activity for the next 500 years, *J. Geophys. Res.: Space Physics*, 118, 1861–1867, doi:10.1002/jgra.50210.
- Stenke, A., M. Schraner, E. Rozanov, T. Egorova, B. Luo, and T. Peter (2012), The SOCOL version 3.0 chemistry-climate model: Description, evaluation, and implications from an advanced transport algorithm, *Geosci. Model Dev. Discuss.*, 3419–3467, doi:10.5194/gmdd-5-3419-2012.
- Valcke, S. (2013), The OASIS3 coupler: A European climate modelling community software, *Geosci. Model Dev. Discuss.*, 6, 373–388, doi:10.5194/gmd-6-373-2013.
- van Vuuren, D. P., et al. (2011), The representative concentration pathways: An overview, *Clim. Change*, 109, 5–31, doi:10.1007/s10584-011-0148-z.
- Washington, W. M., R. Knutti, G. A. Meehl, H. Teng, C. Tebaldi, D. Lawrence, L. Buja, and W. G. Strand (2009), How much climate change can be avoided by mitigation? *Geophys. Res. Lett.*, 36, L08703, doi:10.1029/2008GL037074.
- WMO, (2011), Scientific assessment of ozone depletion: 2010, *Tech. rep.*, Global Ozone Research and Monitoring Project - Report No. 52, Geneva, Switzerland.

Supplementary material

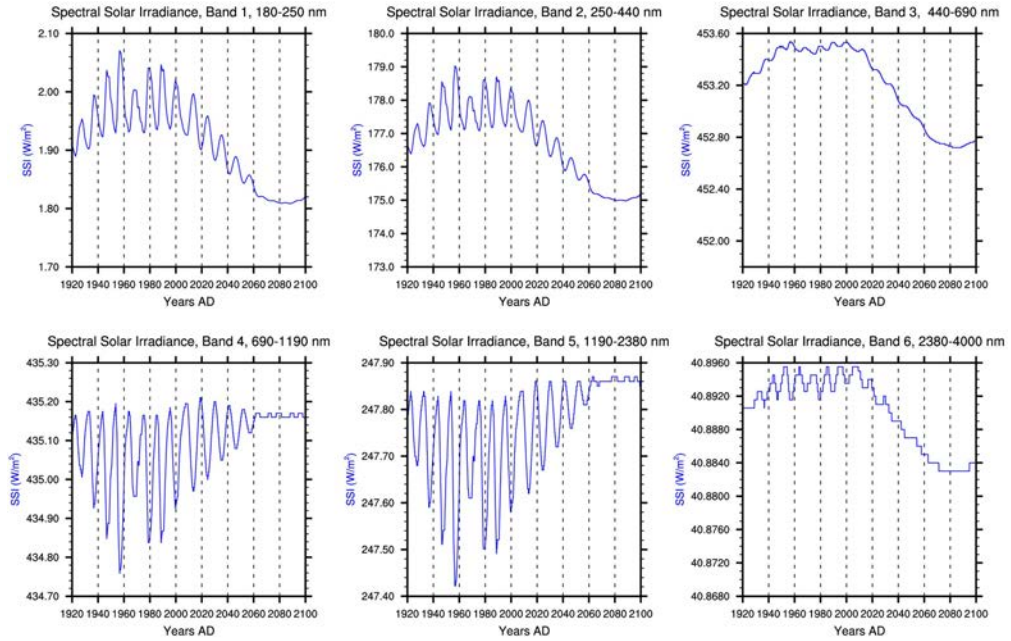


Figure S1.: Evolution of the spectral solar irradiance following Shapiro et al. (2011), split into the six ECHAM5 radiation bands.

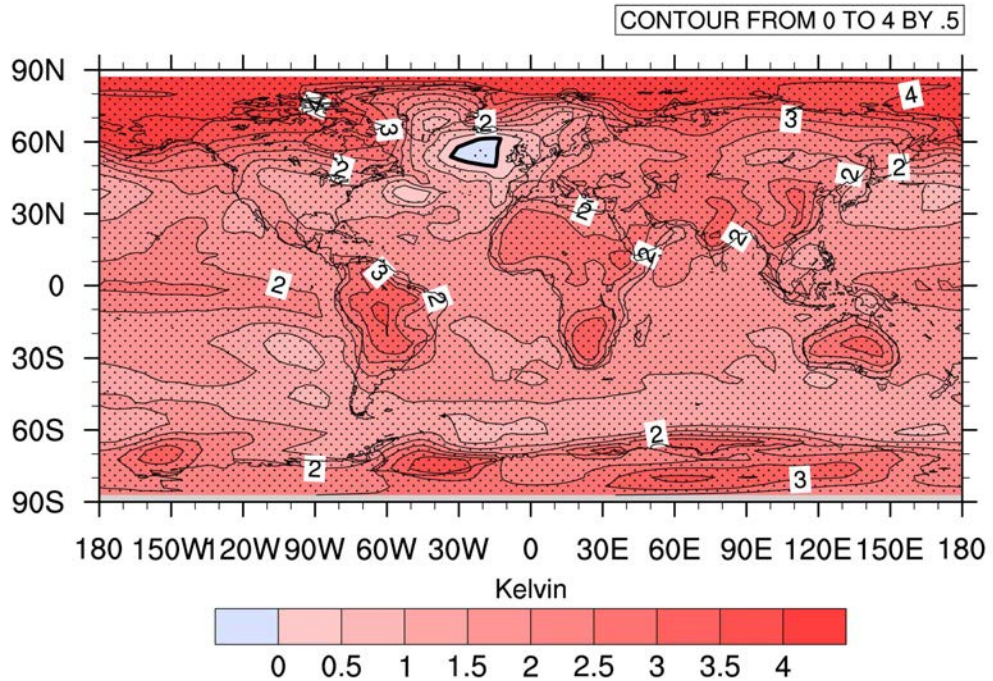


Figure S2.: Surface air temperature differences between CONST (2081-2100) and the reference period (1986-2005). Stippling: Differences significant based on a t-test with $\alpha=5\%$.

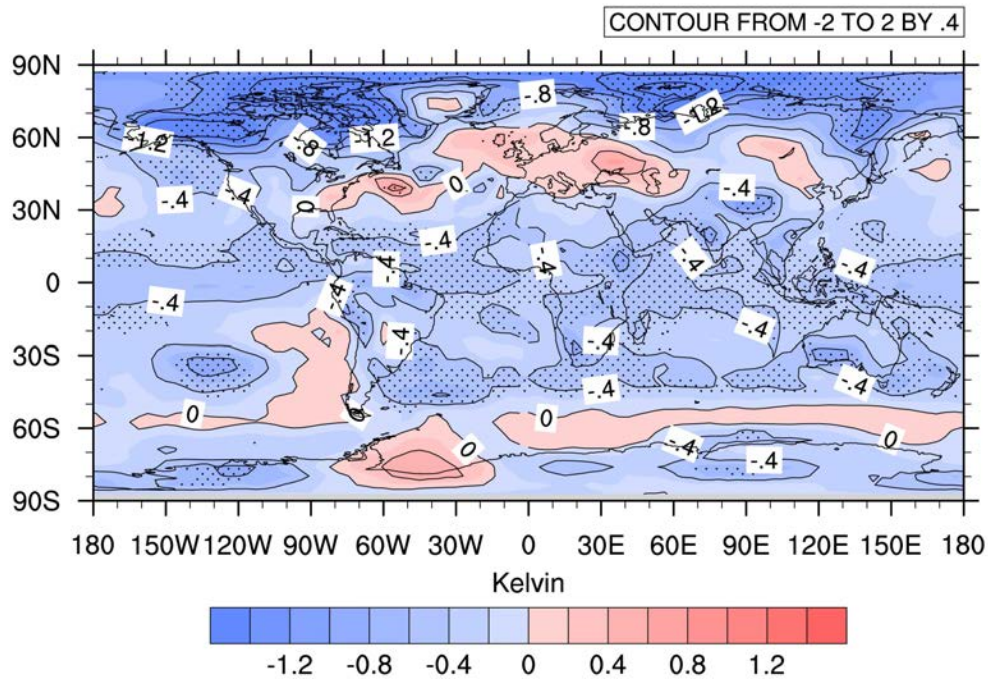


Figure S3.: 2m Temperature differences between STRONG and CONST (2081-2100) for the DJF season. Stippling: Differences significant based on a t-test with $\alpha=5\%$.

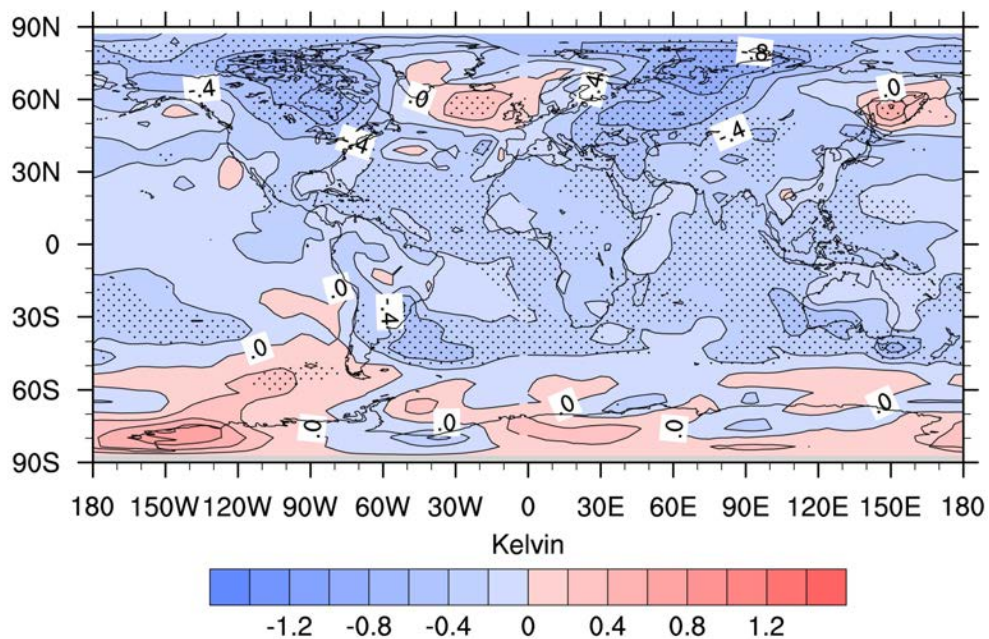


Figure S4.: Surface air temperature differences between WEAK and CONST, averaged over the ensemble members in the 2081-2100 period. Stippling: Differences significant based on a t-test with $\alpha=5\%$.

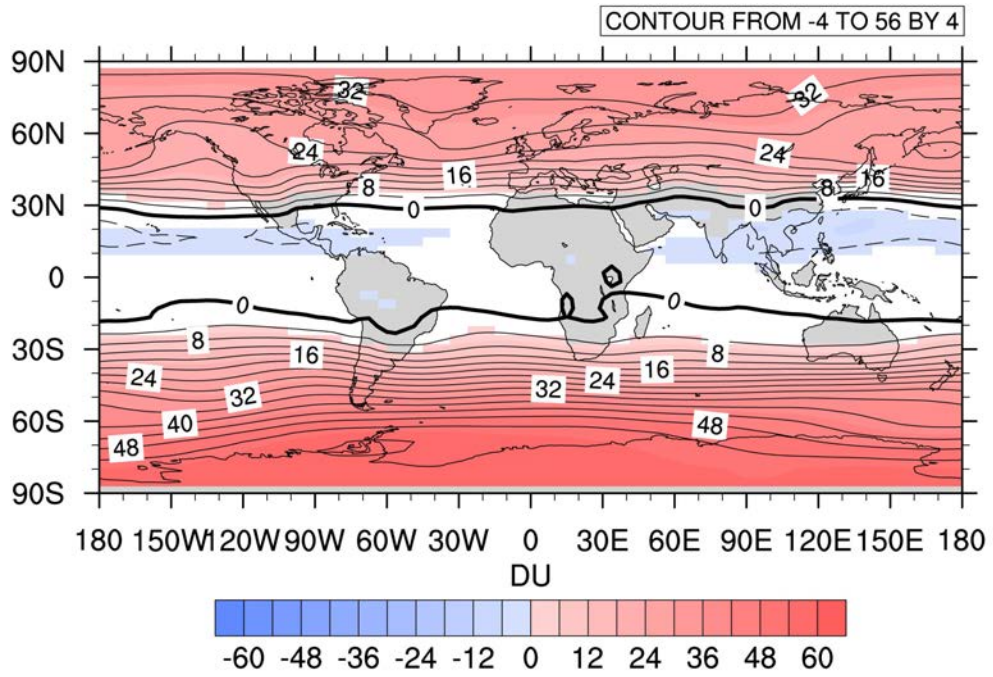


Figure S5.: Difference in total column ozone between CONST (2081-2100 period) and the reference period (1986-2005). Only areas which are significantly different on a 5% t-test are colored.

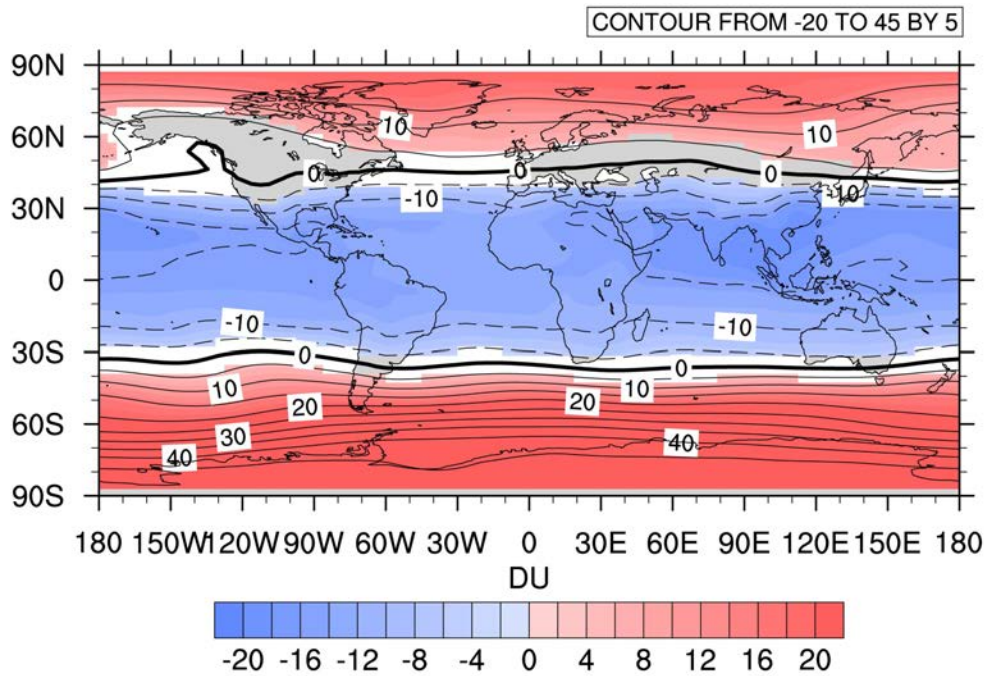


Figure S6.: Difference in total column ozone between STRONG (2081-2100 period) and the reference period (1986-2005). Only areas which are significantly different on a 5% t-test are colored.

A.2. Forcing of stratospheric chemistry and dynamics during the Dalton Minimum

Julien G. Anet, Stefan Muthers, Eugene Rozanov, Christoph C. Raible, Thomas Peter, Andrea Stenke, Alexander I. Shapiro, Jürg Beer, Friedhelm Steinhilber, Stefan Brönnimann, Florian Arfeuille, Yuri Brugnara, and Werner Schmutz.

Published in *Atmospheric Chemistry and Physics* vol. 13, p. 10951-10967, 2013.

Atmos. Chem. Phys., 13, 10951–10967, 2013
www.atmos-chem-phys.net/13/10951/2013/
doi:10.5194/acp-13-10951-2013
© Author(s) 2013. CC Attribution 3.0 License.



Atmospheric
Chemistry
and Physics
Open Access

Forcing of stratospheric chemistry and dynamics during the Dalton Minimum

J. G. Anet¹, S. Muthers^{2,3}, E. Rozanov^{1,4}, C. C. Raible^{2,3}, T. Peter¹, A. Stenke¹, A. I. Shapiro⁴, J. Beer⁵, F. Steinhilber⁵, S. Brönnimann^{3,6}, F. Arfeuille^{3,6}, Y. Brugnara^{3,6}, and W. Schmutz⁴

¹Institute for Atmospheric and Climate Science ETH, Zurich, Switzerland

²Climate and Environment Physics, Physics Institute, University of Bern, Bern, Switzerland

³Oeschger Centre for Climate Change Research, University of Bern, Bern, Switzerland

⁴Physikalisch-Meteorologisches Observatorium Davos and World Radiation Center (PMOD/WRC), Davos, Switzerland

⁵Eawag, Surface Waters Group, Kastanienbaum, Switzerland

⁶Institute of Geography, University of Bern, Bern, Switzerland

Correspondence to: J. G. Anet (julien.anet@alumni.ethz.ch)

Received: 16 April 2013 – Published in Atmos. Chem. Phys. Discuss.: 10 June 2013

Revised: 11 October 2013 – Accepted: 11 October 2013 – Published: 8 November 2013

Abstract. The response of atmospheric chemistry and dynamics to volcanic eruptions and to a decrease in solar activity during the Dalton Minimum is investigated with the fully coupled atmosphere–ocean chemistry general circulation model SOCOL-MPIOM (modeling tools for studies of Solar Climate Ozone Links-Max Planck Institute Ocean Model) covering the time period 1780 to 1840 AD. We carried out several sensitivity ensemble experiments to separate the effects of (i) reduced solar ultra-violet (UV) irradiance, (ii) reduced solar visible and near infrared irradiance, (iii) enhanced galactic cosmic ray intensity as well as less intensive solar energetic proton events and auroral electron precipitation, and (iv) volcanic aerosols. The introduced changes of UV irradiance and volcanic aerosols significantly influence stratospheric dynamics in the early 19th century, whereas changes in the visible part of the spectrum and energetic particles have smaller effects. A reduction of UV irradiance by 15%, which represents the presently discussed highest estimate of UV irradiance change caused by solar activity changes, causes global ozone decrease below the stratopause reaching as much as 8% in the midlatitudes at 5 hPa and a significant stratospheric cooling of up to 2 °C in the mid-stratosphere and to 6 °C in the lower mesosphere. Changes in energetic particle precipitation lead only to minor changes in the yearly averaged temperature fields in the stratosphere. Volcanic aerosols heat the tropical lower stratosphere, allowing more water vapour to enter the tropical stratosphere,

which, via HO_x reactions, decreases upper stratospheric and mesospheric ozone by roughly 4%. Conversely, heterogeneous chemistry on aerosols reduces stratospheric NO_x, leading to a 12% ozone increase in the tropics, whereas a decrease in ozone of up to 5% is found over Antarctica in boreal winter. The linear superposition of the different contributions is not equivalent to the response obtained in a simulation when all forcing factors are applied during the Dalton Minimum (DM) – this effect is especially well visible for NO_x/NO_y. Thus, this study also shows the non-linear behaviour of the coupled chemistry-climate system. Finally, we conclude that especially UV and volcanic eruptions dominate the changes in the ozone, temperature and dynamics while the NO_x field is dominated by the energetic particle precipitation. Visible radiation changes have only very minor effects on both stratospheric dynamics and chemistry.

1 Introduction

The fourth assessment report of the Intergovernmental Panel on Climate Change (Forster et al., 2007) noted that while the scientific understanding of the greenhouse gas (GHG) emissions and volcanic effects on climate is rather high, this is not the case for changes in solar activity. The combined forcings of GHG and tropospheric aerosols is predicted to increase until possible stabilization is reached in the second

half of the 21st century. The volcanic effect is unpredictable. Concerning solar activity, it is hypothesized that solar activity will – after a long period of high activity – drop to a new grand minimum in the 21st century (Abreu et al., 2008, 2010; Lockwood et al., 2011b; Steinhilber and Beer, 2013). Given this, an assessment of periods in the past containing grand solar minima is helpful to understand the mechanism and its implications. As an example, the Dalton Minimum (DM) was a time period lasting from 1790 to 1830 which was characterized by a significant cooling in Europe (Luterbacher et al., 2004) and the extratropical Northern Hemisphere (Ljungqvist, 2010; Auchmann et al., 2012). This unusually cold time coincides with the period of very low solar activity as expressed in low sunspot numbers (Hoyt and Schatten, 1998) and high volcanic activity due to two major volcanic eruptions in 1809 and in 1815. The exact causes of this cooling are not well defined. Some part of it can be explained by downward-propagating stratospheric perturbations (e.g. Ineson et al., 2011). We thus decided to study this period and address the solar and volcanic effects on stratospheric climate and chemistry. Up to now, studies of the DM were done to a major part with climate models with coupled interactive oceans. The novelty of our experiment setting was to include interactive chemistry to a GCM coupled with a deep layer ocean. We succeeded thus to include the most important natural forcing in a climate model simulation during the DM: (a) solar irradiance changes, which can be decomposed into the ultraviolet (UV), visible and infrared (IR) parts of the spectrum, (b) explosive tropical volcanic eruptions and (c) energetic particle precipitation (EPP).

Solar activity has been monitored for a long time (Wolf, 1861; Hoyt and Schatten, 1998). The influence of the Sun on time scales of up to hundreds of years can first be divided into two temporal classes; there is a regular, well established 11 yr cycle (Wolf, 1861; Schwabe, 1844) – which can vary in its intensity – and, on a longer time scale, there are grand minimum and maximum states of the solar activity.

Solar influence can be further classified in terms of where its largest effects can be observed in the Earth's atmosphere. This is strongly linked to the part of the spectrum with the largest variability. Kodera and Kuroda (2002) investigated the effects of the 11 yr solar cycle on atmospheric dynamics, focusing on the UV part of the spectrum. Their work suggests a downward propagation of the response in the middle atmosphere caused by heating through UV absorption and ozone increase. In solar active conditions, this additional heating leads to an increasing pole-to-equator temperature gradient, influencing also the stratospheric zonal winds (Kodera and Kuroda, 2002). This process is known as the top-down mechanism (e.g. Meehl et al., 2009; Gray et al., 2010). A different aspect is to focus rather on the visible spectrum and to follow a bottom-up approach (Meehl et al., 2009): during active solar conditions, more evaporation occurs in the subtropics. This in turn leads to an increase in the precipitation amount, which accelerates the Hadley and Walker cells (Labitzke

et al., 2002), finally leading to ENSO-like (El Niño–Southern Oscillation) anomalies and influencing stratospheric circulation. Using reconstructions of the solar irradiance like the ones from Lean et al. (1995), these two processes have been studied extensively in recent years using models of different complexity (see Gray et al., 2010 and references therein).

The fact that volcanoes can influence global climate has already been recognized in Franklin (1784) and Milham (1924). While Franklin (1784) mainly focused on the effect on the troposphere, which, after the Lakagigar (Laki) eruption, was polluted by a large amount of particles, partly leading to a constant haze, Milham (1924) focused on the Tambora eruption and the uncommon weather pattern following the eruption. In the twentieth century, partly because of four major volcanic eruptions (Agung in 1963, Fuego in 1974, El Chichón in 1982, Pinatubo in 1991), more intense scientific research was done. This research focusing especially on the radiative effects of stratospheric aerosols (see Hansen et al., 1992; Stenchikov et al., 1998; Robock, 2000, and references therein). The plume of powerful volcanic eruptions reaches the stratosphere (Halmer et al., 2002). There, SO₂ is transformed, through a number of chemical reactions, to sulfate aerosols. Aerosols at lower stratospheric altitudes (Whitten et al., 1980) are mostly spherical (Tratt and Menzies, 1994) and reflect part of the incoming solar short-wave radiation back to space. On the other hand, sulfate aerosol absorb thermal radiation. The aerosol particles also provide a medium for heterogeneous reactions facilitating the removal of reactive nitrogen oxides and the activation of halogen radicals. Thus, volcanic aerosols are important for both radiative and chemical processes in the atmosphere.

Reconstructions of the volcanic forcing (Gao et al., 2008) have been used to model past and present-day influences of volcanic events on the global climate. Generally, following observations and modelling studies, while the lower stratosphere is heated by absorption of infrared radiation by the aerosols, the troposphere and the surface usually experience a significant cooling after major volcanic eruptions (Dutton and Christy, 1992; Minnis et al., 1993; Stenchikov et al., 1998; Arfeuille, 2012). The interaction with chemistry is more complex due to the effects of enhanced halogen loading in modern times (Tie and Brasseur, 1995). In a clean preindustrial atmosphere, a significant globally averaged increase of total column ozone can be expected within one to three years after a volcanic eruption, whereas at the equator, ozone column depth is decreasing slightly (Arfeuille, 2012). In the halogen-contaminated atmosphere of today, global ozone concentration drops significantly after a volcanic eruption. The resulting heating leads to major changes in the atmospheric dynamics and large-scale oscillation patterns like El Niño, Arctic Oscillation (AO) or North Atlantic Oscillation (NAO) (Robock, 2000; Stenchikov et al., 2002; Yoshimori et al., 2005; Wagner and Zorita, 2005; Christiansen, 2007; Fischer et al., 2007; Spanghel et al., 2010).

The influence of EPP on climate is – compared to the other two aforementioned factors – a rather new subject to science and has been investigated increasingly often during the last twenty years. Its effect is still not well known and is a quite controversial issue in the climate change discussion (Marsh and Svensmark, 2000; Laut, 2003; Lockwood and Fröhlich, 2007; Erlykin et al., 2013). This disagreement is also a reason why EPP have not been included in important climate model simulation campaigns in support of WMO (World Meteorological Organization) and IPCC (Intergovernmental Panel on Climate Change) assessments (WMO, 2011; Forster et al., 2007). The EPP can be divided into three main categories: galactic cosmic rays (GCRs), solar protons, and high- and low-energy electrons (HEE, LEE). All of these types of EPP can ionize neutral molecules in the Earth's atmosphere.

The GCRs are highly energetic, charged particles. They originate from supernova explosions in our galaxy and their flux and energy spectrum at the entry of the heliosphere is very stable over millennial timescales, only being modulated by the solar activity, which is shielding the Earth from them via magnetospheric deflection (see e.g. Scherer et al., 2004). The observed GCR flux variability thus follows the cycles of the solar magnetic activity. GCRs are highly energetic particles, often relativistic with energies reaching several GeVs (Bazilevskaya et al., 2008), being capable in influencing our atmosphere in important ways: GCRs dissipate their energy mainly by ionization processes. Following a Bragg-peak (Bragg and Kleeman, 1905), the maximal ionization rate by GCR is reached at altitudes between 15 km and 20 km (Usoskin et al., 2010). The ionization is largest in the polar regions (poleward of $\pm 60^\circ$) where the geomagnetic field has the weakest shielding effect (lowest cut-off rigidity).

Solar proton events (SPEs) emerge from coronal mass ejections of the Sun, which occur very irregularly and are rarely directed towards the Earth. Hence, SPEs are very sporadic and hardly predictable. The solar wind plasma usually reach the Earth's atmosphere within 1–2 days after the ejection (Kahler, 1992). The charged particles are directed towards the poles, where they follow the lines of the geomagnetic field into the atmosphere. Only in extreme cases – when their energies reach 500 MeV or more – they can propagate down to the stratosphere (Jackman et al., 2008). As a result of the magnetic shielding, the effect of SPEs is strongly latitude dependent with an equatorward minimum of $\pm 20^\circ$ and a poleward maximum of $\pm 60^\circ$.

LEEs and HEEs originate from the interaction of the Earth's magnetospheric plasmasheet with the solar wind (Brasseur and Solomon, 2005). Solar plasma is kept trapped in the magnetosphere of the Earth and can be accelerated during periods of higher solar wind speeds. The accelerated electrons then rapidly travel along the magnetic field lines to the poles and partly penetrate the uppermost layers of the atmosphere (Bazilevskaya et al., 2008). The best evidence for their existence are the aurorae, formed by the excitation of nitrogen and oxygen atoms.

Ionization of oxygen and nitrogen lead to NO_x and HO_x production.

In the stratosphere, while HO_x has a short life time (in the range of minutes to hours) and thus affects atmospheric chemistry only locally, reactive nitrogen (NO_y) and its representative species nitric acid and chlorine nitrate have lifetimes comparable to, or even longer than, the characteristic times for vertical and horizontal mixing (which occur, for instance, via the Brewer-Dobson circulation (BDC)). In the stratosphere, NO_x and HO_x interact with ozone in a significant way, as was found by analysing important ionization events (Callis et al., 1998; Funke et al., 2011). Changes in ozone concentration inside the polar vortex modify the pole-to-equator temperature gradient and thus can have a significant influence on circulation and weather patterns (Gray et al., 2010). Different modelling studies demonstrated the influence of EPP not only on chemistry (Jackman et al., 2008; Baumgaertner et al., 2009; Egorova et al., 2011; Calisto et al., 2011; Rozanov et al., 2012b) but also on dynamics (Baumgaertner et al., 2009; Calisto et al., 2011; Rozanov et al., 2012b).

Climate during the DM minimum has already been simulated with general circulation models (GCM) in a number of studies (Bauer et al., 2003; Wagner and Zorita, 2005; Ammann et al., 2007; Spanghehl et al., 2007; Arfeuille, 2012). While Bauer et al. (2003) only used a simplified model, Wagner and Zorita (2005) and Spanghehl et al. (2007) exploited a coupled atmosphere–ocean GCM (AO-GCM). Arfeuille (2012) used the chemistry–climate model (CCM) SOCOL to simulate the effects of the Tambora volcanic eruption in 1815 on the climate and found a strong geopotential height gradient anomaly (around 250 gpm) between 55°N and 75°N at 50 hPa in the first winter after the eruption (November–April), as well as a net radiative forcing anomaly reaching -8 W m^{-2} (60°S – 60°N) during the first five months following the eruption. Thus, volcanic influences and solar Grand Minima are generally accepted as main drivers for global climate cooling. Wagner and Zorita (2005) also investigated the contribution of the slightly increasing GHG concentrations during the DM and did not find any significant impact.

In this paper, we investigate the effect of different natural factors on global stratospheric climate during the DM with a fully interactive atmosphere–ocean–chemistry climate model (AO-CCM). To the best of our knowledge, no coupled AO-CCM with EPP parameterization has yet been used for an in-depth analysis of the climate and chemistry state during the DM so far. This is also a reason why a comparison and a validation of our model simulation is nearly impossible to carry out: although investigations of the influence of EPP on the modern climate have been done (Calisto et al., 2011; Rozanov et al., 2012b), the far higher chlorofluorocarbon (CFC) content nowadays makes it difficult to compare the effect on the chemistry and especially on ozone. Concerning the effects of volcanic eruptions, e.g. the work of Arfeuille (2012) can give some hints how another model (the

former model version SOCOLv2 without interactive ocean) has simulated the Tambora eruption. Yet, exact numbers in ozone disturbance are sparse and thus also here, a validation of our results is difficult.

A description of the model framework is done in Sect. 2. In Sect. 3, we describe the chemical and dynamical changes in the stratosphere. In the last chapter, we discuss and summarize the findings of this work.

2 Description of the model and experimental set-up

2.1 AO-CCM SOCOL3-MPIOM

The AO-CCM SOCOL3-MPIOM emerges from the coupling of the CCM SOCOL3 (Stenke et al., 2013) and the ocean model MPIOM (Marsland et al., 2003) with the OASIS3 coupler (Valcke, 2013). SOCOL3 consists of the chemistry module MEZON (Model for Evaluation of oZONE trends, Rozanov et al., 1999; Egorova et al., 2003; Schraner et al., 2008) which is coupled to the GCM MA-ECHAM5 (Roeckner et al., 2003). Atmospheric temperature fields are passed to MEZON, which computes the tendencies of 41 gas species, taking into account 200 gas-phase, 16 heterogeneous, and 35 photolytical reactions. Once computed, the chemical tendencies are handed back to ECHAM5, which then takes care of the transport of species. The simulations were run in T31 spectral resolution, which is equivalent to a grid spacing of around 3.75° . The vertical spacing is irregular, as the model uses hybrid sigma pressure coordinates on 39 levels from 1000 hPa up to 0.01 hPa (80 km). The chemistry scheme is only called every two hours – simultaneously with the radiative scheme – in order to be computationally efficient.

Due to this relatively coarse vertical resolution, the Quasi-Biennial-Oscillation (QBO) is not reproduced autonomously by the GCM. To reproduce the QBO, the equatorial zonal wind field is nudged to reconstructed data in the same manner as described in Giorgetta (1996).

The original ECHAM5 radiation code does not properly treat solar spectral irradiation forcing (Forster et al., 2011): therefore, extra-heating correction factors (Zhu, 1994) for the Lyman-alpha line, the Schumann–Runge, and the Hartley and Huggins bands as well as for the Herzberg continuum were implemented. The radiation code was also modified in such a way that ECHAM5 reads in spectrally resolved solar irradiance in the six ECHAM5 short-wave bands with varying distribution instead of the standard fixed distribution of the varying total solar irradiance into the six bands.

Parameterization of the different EPPs was done identically to Rozanov et al. (2012b) and ref. therein, with the only difference being that the code has been modified for use in SOCOLv3. Highly energetic electrons (HEE) were not included in the model. To include the magnetic dependency of the ionization by EPP, a temporal, locally changing dipole

magnetic field was implemented in the model using geomagnetic proxy data as input.

2.2 Boundary conditions

The model is forced by several boundary conditions described in the following section.

The GHG concentrations for the 1780 to 1840 period of carbon dioxide, methane and nitrous oxide are based on the Palaeoclimate Modelling Intercomparison Project Phase III (PMIP3) protocol (Etheridge et al., 1996, 1998; MacFarling-Meure, 2004; Ferretti et al., 2005; MacFarling-Meure et al., 2006). Halogen-containing species were kept constant to preindustrial levels.

All forcings influenced by the activity level of the Sun were based on the solar modulation potential reconstructions produced from ^{10}Be records from ice cores: for the spectral solar irradiance forcing, we use the reconstruction of Shapiro et al. (2011). In Fig. 1, the radiative forcing data is plotted for the six bands of ECHAM5 radiation code. The main difference between this reconstruction and the former ones like Lean et al. (1995) or Bard et al. (2000) is the amplitude of the variability. For example, the difference between the maximum and the minimum total solar irradiance (TSI) value during the DM is roughly 6 W m^{-2} , whereas in, e.g. Lean et al. (1995), the drop was only by 2 W m^{-2} . For the photolysis rates, look-up tables are used, which have been generated from the spectral solar irradiance (SSI) of Shapiro et al. (2011) are used.

Several different datasets were used for the energetic particles. For the parameterization of NO_x influx, Baumgaertner et al. (2009) used the A_p index which can be reconstructed as far as back as the year 1932. The A_p index can be correlated with the A_a index, which has a longer time frame but is only based on two stations. It is available from 1868 to present. Based on sunspot numbers, the A_a and A_p indexes can be reconstructed via correlation until the year 1600. SPEs were prescribed from an existing SPE dataset (provided by Charles Jackman and covering the period 1963–2008, see Jackman et al., 2009). SPEs are very short-lived (in the order of days); thus such events cannot be reconstructed from proxies like ^{10}Be , which are usually used. Shea et al. (2006) presented a solution to reconstruct big events, like the Carrington event, from nitrates deposited in ice cores. This method, however, is very controversial (Wolff et al., 2008; Schrijver et al., 2012). In our work, SPEs are randomized for the years before 1963 by using a return-period based analysis of the last 45 yr, and weighted with the A_p index. Cosmic rays are based on the solar modulation potential (Φ), which has been reconstructed by Steinhilber et al. (2008). The dataset compares well with the neutron monitor measurements which are available for since the year 1950. Φ is an index which describes the solar modulation of the cosmic ray flux, which can be converted into pressure–latitude ionization rates using look-up tables from Usoskin et al. (2010). Palaeo-magnetic datasets

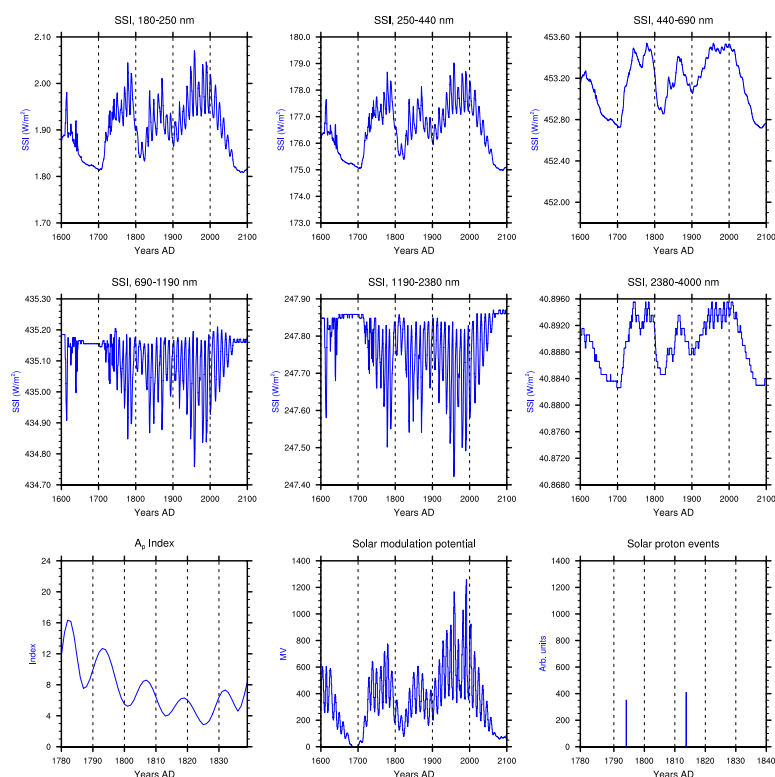


Fig. 1. Spectral solar irradiance (SSI) adapted from Shapiro et al. (2011) and A_p -index, solar modulation potential and SPE during the DM. From left to right, top to bottom: hard UV (185–250 nm, band 1), soft UV (250–440 nm, band 2), visible (440–690 nm, band 3), IR-A (690–1190 nm, band 4), IR-B (1190–2380 nm, band 5), IR-C (2380–4000 nm, band 6), A_p -index, Solar modulation potential (Φ), and SPEs.

(C. Finlay, personal communication, 2010) are applied to the model in order to take into account the geomagnetic dependency of the ionization.

Stratospheric aerosol properties are prescribed according to the approach applied by Arfeuille et al. (2013a) who used the Atmospheric and Environmental Research Inc. (AER) model (Weissenstein et al., 1997) constrained with ice-core-based estimates of sulphate aerosol mass (Gao et al., 2008, 2012). From those simulations, zonally averaged aerosol optical properties (spectrally resolved) and surface area density forcing data for SOCOL3-MPIOM were extracted. The most important volcanoes during the DM period where two weak eruptions (1 and 3 Mt SO_2) in 1794 and 1796 with unknown locations (probably extratropical), a strong unknown tropical eruption of 27 Mt SO_2 in 1809, the 55 Mt SO_2 Tambora eruption in 1815 and two eruptions (8.5 Mt and 20 Mt SO_2) – the Babuyan Claro in 1831 and the Cosigüina in 1835.

Uncertainties in historical long-term volcanic aerosol datasets can be large, and pose more challenges for representation than does the well-observed Pinatubo 1991 eruption.

Indeed, the lack of atmospheric observations leads to uncertainties arising from ice-core measurements and calibrations, and from the implementations of volcanic datasets, which generally involve further assumptions (e.g. altitude and size distributions of the aerosols). The volcanic forcing applied here is based on an aerosol model for the calculation of these variables, and the strengths of this method for the depiction of the aerosol latitude/altitude/size distributions for eruptions in the pre-satellite period are described in Arfeuille et al. (2013a). As many CCMs, also SOCOL tends to overestimate the stratospheric warming following the Pinatubo eruption (Eyring et al., 2006; Lanzante, 2007), and the AER-based SOCOL simulation of the Pinatubo eruption (Arfeuille et al., 2013b) suggests that AER-SOCOL might also overestimate the stratospheric warming due to the eruptions in the Dalton minimum. While this issue is one of the current uncertainties for the representation of volcanic impacts in the pre-satellite period, it can be noted that in the important tropical-tropopause region, SOCOL forced by AER leads to a good representation of temperature after the Pinatubo eruption,

even in better agreement with observations than many GCMs forced by satellite-based aerosol datasets.

Tropospheric aerosol properties were constructed by scaling the existing CAM3.5 simulations with a bulk aerosol model driven by CCSM3 (CMIP4) sea-surface temperatures and the 1850–2000 CMP5 emissions (S. Bauer, personal communication, 2011). For data before the year 1850, the applied scaling is a function of the world population except for 10% of the presumed 1990 biomass burning aerosols which were considered natural.

The model was forced by the standard (Hagemann et al., 1999; Hagemann, 2002) land surface datasets provided with the ECHAM5 package.

Finally, equatorial zonal mean zonal winds for nudging the QBO were generated from a backward extension of the Brönnimann et al. (2007) reconstructions using an idealized QBO cycle plus a seasonal anomaly cycle.

2.3 Experiments

To investigate the influence of solar, volcanic and the EPP forcings, we perform a series of three-members ensemble sensitivity experiments described in Table 1. We initialize our runs in the year 1780 from a transient simulation starting in 1388 AD. While the first ensemble member is run with unperturbed initial 1780 conditions, the two following members are initialized with an ocean field of the years 1781 and 1779, respectively. Every experiment covers 60 yr to reach December 1840. The analyzed period is chosen to be from 1805 to 1825 in order to reduce the noise and strengthen the signal from volcanic, solar and particle forcings. The small number of ensemble members is chosen to reduce the computational time needed for the simulations.

To address the relative roles of the UV, visible and infrared radiation, as well as the extra heating and the photolysis rates, two experiments called DM-TD (top-down) and DM-BU (bottom-up) are designed. In DM-TD, all forcing data is kept constant except (i) the first radiation band (UV) of ECHAM5 radiation code, (ii) the coefficients of extra-heating parameterization, as well as (iii) the photolysis rates. Hence, all forcing comes from the stratosphere because the response of the heating rate in the second band of ECHAM5 radiation code (240–440 nm) to the solar variability is very small (Forster et al., 2011). The opposite experiment, DM-BU, is designed in a way that all forcing is kept constant except in bands 2–6 of the ECHAM5 radiation code. Hence, DM-BU does not include any stratospheric heating or ozone production changes, meaning that all extra radiation is absorbed mostly in the troposphere and by the surface. In turn, the DM-VOLC runs are driven with all forcings except the volcanic forcing kept to constant 1780 conditions. The DM-CTRL1780 runs are performed with perpetual 1780 conditions, whereas the DM-ALL runs are driven with all forcings in transient conditions. To address the effect of energetic particles, we carry out the DM-EPP experiment which is forced

only by the parameterizations for GCR, SPE and LEE, while all other forcings are set constant or switched to background aerosol concentrations (volcanic forcing).

2.4 Method of comparison

In the next section we analyze 60 yr long time series of annual zonal mean quantities constructed from the results of three 20 yr long ensemble runs for each experiment. The statistical significances were calculated using the two-tailed Student's t test using the 5% significance level, and comparing all 60 yr long time series for each experiment. All figures illustrate the relative or absolute deviation of the results of the experiment runs relative to the control run (DM-CTRL1780). On all plots, the yellow line indicates the height of the dynamical WMO tropopause. The nonlinearities are computed in the following way: the differences of DM-TD, DM-BU, DM-VOLC and DM-EPP relative to DM-CTRL1780 are computed and added. This field is then compared to the difference field between DM-ALL and DM-CTRL1780. A positive value in the nonlinearity plot would mean that the stacked relative differences are greater than the combined differences from DM-ALL. Nonlinearities are only discussed when the sum of the contributions and the combined modelled effect are significantly different.

If not noted differently, the upper left figure of every panel illustrates the overall effect of all factors (DM-ALL), followed by the effects of UV solar irradiance (DM-TD), volcanic aerosols (DM-VOLC) and energetic particle precipitation (DM-EPP). As a reduction of the visible and infrared radiation in the DM-BU experiment has small effects on the stratospheric chemistry, these results are not shown in the chemical section.

3 Results

3.1 Atmospheric chemistry

In this section, we focus on four species: ozone, water vapour, HO_x and NO_x , as they show the most pronounced response to the considered factors.

3.1.1 Ozone

Figure 2a shows the relative effect of DM-ALL including all factors – namely the reduction of solar radiation, volcanic eruptions and EPP – with respect to the control simulation (DM-CTRL1780). Substantial ozone depletion is found almost everywhere, reaching its maximum (–8%) in the upper tropical mesosphere and middle stratosphere over the high latitudes. However, the opposite response is simulated in the polar upper mesosphere and tropical upper troposphere/lower stratosphere (UT/LS) regions where the ozone mixing ratio increases by up to 15%.

Table 1. Experiments for DM sensitivity runs: CONST values are monthly mean values from 1780. BCKGRD means that only background aerosol emissions were enabled and volcanic eruptions were turned off. TRANS means transient forcing.

Name	UV	VIS	Volcanic	EPP	Photolysis	Extra Heating
DM-CTRL1780	CONST	CONST	BCKGRD	CONST	CONST	CONST
DM-ALL	TRANS	TRANS	TRANS	TRANS	TRANS	TRANS
DM-TD	TRANS	CONST	BCKGRD	CONST	TRANS	TRANS
DM-BU	CONST	TRANS	BCKGRD	CONST	CONST	CONST
DM-VOLC	CONST	CONST	TRANS	CONST	CONST	CONST
DM-EPP	CONST	CONST	BCKGRD	TRANS	CONST	CONST

Figure 2b shows that mainly the effects of the solar UV reduction in DM-TD are responsible for the ozone loss at ozone-layer height and for the gain of ozone in the polar upper mesosphere. These ozone changes in the atmosphere can be explained mostly by three factors:

1. the decrease in solar UV irradiance which reduces the ozone production via oxygen photolysis in the stratosphere and NO_2 photolysis in the troposphere,
2. the increase of NO_x (see Fig. 5, Sect. 3.1.3), which facilitates the intensification of the NO_x cycle of ozone oxidation (Reactions R1–R3),



Net:



3. the slight compensation of the above-mentioned ozone depletion processes due to the stratospheric cooling caused by reduced solar UV and ozone mixing ratio, slowing down the ozone destruction cycles (see Sect. 3.2.1).

At the poles in lower mesospheric height (60–80 km) a surplus of ozone by up to 20 % is explained by the fact that at these heights, the UV radiation acts like a sink rather than a source of ozone. Thus, with less UV radiation, near the mesopause, ozone destruction is suppressed.

The surplus of ozone at the tropical tropopause can be explained by volcanic effects with the DM-VOLC experiment (see Fig. 2c). The main reason for the ozone increase in the tropical UT/LS after volcanic eruptions is the transformation of NO_x to N_2O_5 and the subsequent hydrolysis of N_2O_5 to HNO_3 via heterogeneous reactions on/in the sulfuric acid particles, formed in the stratosphere from the products of the volcanic eruptions. In the present day atmosphere, ozone depletion was observed after major volcanic eruptions and attributed to catalytic reactions involving reactive halogens. However, a potentially significant background of natural chlorine and bromine existed. The effect of this back-

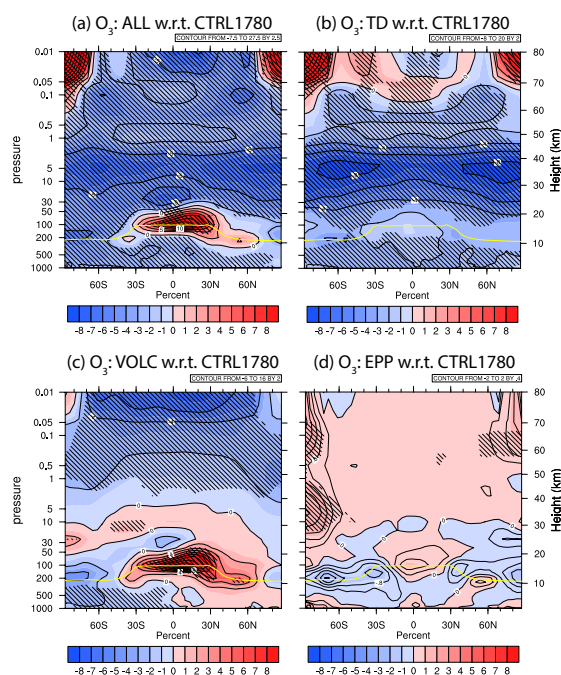


Fig. 2. Relative differences of yearly mean ozone of the DM-ALL, DM-TD, DM-VOLC and DM-EPP experiments with relation to the DM-CTRL1780 forcing run. Hatched areas are significantly different on a Student's t test with $\alpha = 5\%$. The yellow line illustrates the height of the WMO tropopause.

ground, to cause ozone depletion, would have been dominated by nitrogen deactivation on sulphate aerosol. Therefore, the heterogeneous conversion of HO_x and NO_x to relatively passive reservoir species leads to an ozone increase of up to 16 %. The decrease of ozone in the mesosphere is related to the strong increase of the HO_x species at that height (see Sect. 3.1.2), leading to an acceleration of the ozone depletion cycle.

Energetic particles can influence the ozone concentration, as shown in Rozanov et al. (2012b). Although our NO_x field looks very similar to the one from the cited work (see

Sect. 3.1.3), the ozone response to EPP in the polar mesosphere is much weaker in our simulations. The main reason for this finding is that background temperatures in the involved regions are different in SOCOLv3 from SOCOLv2. Though, the reaction of nitrogen with oxygen is highly temperature dependent (Funke et al., 2011). Thus, only a minor part of the signal seen in Fig. 2a can be attributed to EPP: the annual mean ozone anomaly shows an ozone decrease of up to 2% in the southern extratropics, which is due to the ionization of nitrogen by GCRs. The change, however, is only significant on a 10% level. Over the poles, in the lower mesosphere, a significant increase of ozone of up to 2% is simulated due to the lower ionization rates of both SPEs and LEEs, leading to less NO_x (see later). Seasonal variations are visible. The biggest effect is modelled in austral spring (SON, see Fig. S1 in the Supplement), where significant losses of ozone at UT/LS level of up to 4% are found in the southern polar latitudes.

The temporal evolution of ozone at 70 hPa (Fig. S2 in the Supplement) and at 1 hPa (Fig. S3 in the Supplement), averaged between 20°N – 20°S , are illustrated in the Supplement. They show that while the volcanic events dominate in the overall signal at the tropical-tropopause height, it is the solar signal which dominates overall at 1 hPa height (blue curve of DM-TD experiment inducing a negative anomaly visible in the pink DM-ALL curve). Other forcing factors which are not of importance at 70 hPa height have not been plotted.

3.1.2 HO_x and water vapour

In Figs. 3a and 4a the differences in water vapour and HO_x in DM-ALL and water vapour and HO_x in DM-CTRL1780 are illustrated. While water vapour concentration increases dramatically above the tropopause, HO_x is experiencing an increase in tropical UT/LS and a decrease in the mesosphere and middle tropical stratosphere.

The results of the DM-TD experiment illustrated in Fig. 3b and Fig. 4b help to attribute the H_2O increase and HO_x loss in the mesosphere to the introduced decrease of solar UV irradiance. A strong (by up to 25%) HO_x decrease in the mesosphere, coinciding with a pronounced increase of H_2O , is driven by less intensive water vapour photolysis in the Lyman-alpha line and Schumann–Runge bands. When looking at the highest levels of the model atmosphere, one recognizes that HO_x decreases less in the lower mesosphere than at stratopause levels (see Fig. 4b). This can be explained by looking at the increase of the water vapour content in Fig. 3b. As water vapour is more prominent during periods of decreasing UV radiation above 60 km due to the decrease in photodissociation, production of OH via reaction with $\text{O}(1\text{D})$ is more likely. Moreover, a cooling of the upper troposphere/lower stratosphere (UT/LS) of 0.1 K decreases the stratospheric water content by 2%. Hence, as the mean decrease of temperature at UT/LS height (shown in the dynamics section) in our DM-TD run is of around 0.2 K, a de-

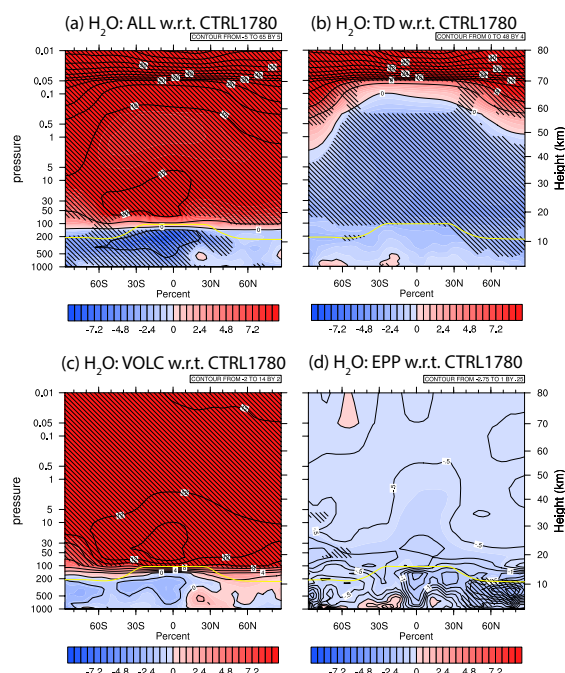
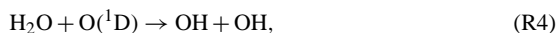


Fig. 3. Relative differences of yearly averaged water vapour of the DM-ALL, DM-TD, DM-VOLC and DM-EPP experiments with relation to the DM-CTRL1780 forcing run. Hatched areas are significantly different on a Student's t test with $\alpha = 5\%$. The yellow line illustrates the height of the WMO tropopause.

crease of roughly 4% of the stratospheric water content is to be expected – and modelled. This drop is the reason for the observed decrease in HO_x (of 4% on average) below 65 km down to the tropopause.

To explain the strong increase of water vapour above the tropopause, a look at the results of the DM-VOLC experiment (see Fig. 3c) is needed. Due to a warming signal (which will be shown in Section “Temperature”), a strong (of up to 14%) increase in the stratospheric water content is modelled even when the results are averaged over a 20 yr long period (see Robock, 2000). It is interesting to note that in the two years after Tambora, simulated water vapour contents rise by up to 60% at the tropical tropopause. Such a strong increase in water vapour content leads to an acceleration of the reactions



in the lower mesosphere and stratosphere. Hence, an increase in HO_x throughout the whole stratosphere and mesosphere (see Fig. 4c) is observed, with peak increases over the equatorial tropopause. The increase in HO_x leads to a speed-up in the oxidation of long-lived species like methane or CO.

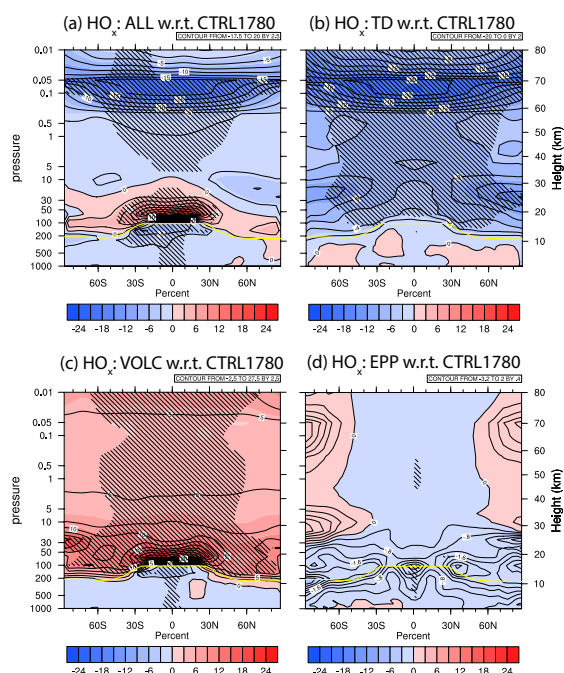


Fig. 4. Relative differences of yearly averaged HO_x of the DM-ALL, DM-TD, DM-VOLC and DM-EPP experiments with relation to the DM-CTRL1780 forcing run. Hatched areas are significantly different on a Student's t test with $\alpha = 5\%$. The yellow line illustrates the height of the WMO tropopause.

In a clean and unpolluted atmosphere, a surplus of nitrogen oxides automatically leads to the drop in HO_x concentrations. In Fig. 4d, the additional NO_x produced (see next subsection) from the GCRs decreases the amount of HO_x slightly. These changes are marginally significant on a 5% level but highly significant on a 10% level in the tropical regions of the largest ionization rates (around 100 hPa). A decrease of HO_x of up to 3% – and, during the absolute minimum of the DM, even of up to 8% – is simulated by our model. This decrease is supported by the slight additional decrease of 0.5 to 1% in the stratospheric water vapour content (Fig. 3d).

3.1.3 NO_x

In the DM-ALL experiment, the NO_x mixing ratio dramatically decreases in the polar mesosphere by up to 70% and – with much smaller magnitude – also decreases in the tropical middle stratosphere. In the tropical upper troposphere and in the stratosphere, an increase in NO_x is found (see Fig. 5a), which reaches its maximum in the upper tropical stratosphere/lower mesosphere. The latter can be explained by the smaller solar UV forcing in the DM-TD exper-

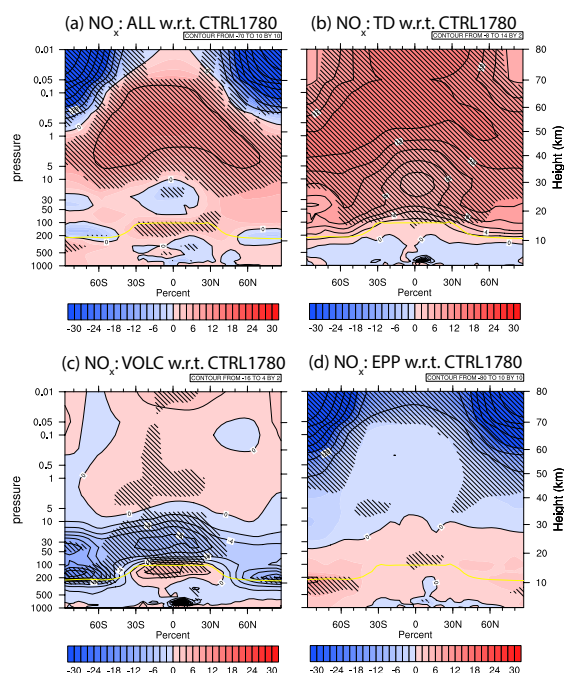


Fig. 5. Relative differences of NO_x of the DM-ALL, DM-TD, DM-VOLC and DM-EPP experiments with relation to the DM-CTRL1780 forcing run. Hatched areas are significantly different on a Student's t test with $\alpha = 5\%$. The yellow line illustrates the height of the WMO tropopause.

iment (see Fig. 5b). The reduction in the solar UV irradiance leads to a pronounced decrease of the photolysis rates for all species, including nitrogen oxide (NO). The NO absorption bands overlap with the oxygen Schumann–Runge bands (170–200 nm) and the introduced decline of the solar irradiance in this interval is one of the most pronounced (Shapiro et al., 2011). The NO photolysis ($\text{NO} + h\nu \rightarrow \text{N} + \text{O}$) plays a crucial role in the NO_y budget, providing pure loss of NO_y via the subsequent cannibalistic reaction ($\text{N} + \text{NO} \rightarrow \text{N}_2 + \text{O}$) which explain the overall NO_x increase in the DM-TD experiment.

The dipole structure in the tropical UT/LS is explained by the influence of the volcanic eruptions. The volcanic sulfate aerosols provide a media for a number of fast heterogeneous reactions. For the clean stratosphere during the DM, the most important reaction was the N_2O_5 hydrolysis, which facilitates the conversion of active nitrogen oxides to rather passive nitric acid. This effect is shown in Fig. 5c which illustrates the results of the DM-VOLC experiment. A significant NO_x decrease over the DM period is observed in this experiment above the tropopause over the tropics and at high latitudes where the aerosol abundance is at a maximum. The causes for a small NO_x increase in the tropical

upper troposphere are not clear; probably it is related to the ozone increase in this area which leads to an enhanced NO_x production via $\text{N}_2\text{O} + \text{O}(^1\text{D}) \rightarrow \text{NO} + \text{NO}$.

As expected, most of the changes in NO_x seen in Fig. 5a is dominated by energetic particles (see Fig. 5d). The NO_x influx, parameterized as the function of A_p index, weakened in intensity during the DM, leading to a NO_x decrease by up to 80%. Particles with higher energies – to a large part GCRs, whose flux was higher during the DM – penetrate deeper into the atmosphere. At tropopause levels, GCRs produce up to 6% more NO_x at the poles and up to 2% more NO_x at the equator. While an increase in NO_x concentrations above 50 km has only a small effect on the ozone layer, NO_x production at lower altitudes may lead to an acceleration of the destruction of ozone via Reactions (R1)–(R3). This insight could be of high importance for the possible future decrease in solar activity in the current century (see Anet et al., 2013). The NO_x anomalies compare well to those found in Rozanov et al. (2012b). The reason why the positive change in NO_x is not reflected in Fig. 5a is that conversion to NO_y occurs due to the additional amount of stratospheric aerosols from the volcanic eruptions. In DM-ALL, a strong decrease in NO_y is seen over the whole tropopause region.

The NO_x field is a good example to show the non-linear behaviour of atmospheric chemistry (see Fig. 6a). Superimposing all relative differences of all experiments, the mesospheric polar regions from the stacked DM-BU, DM-TD, DM-VOLC and DM-EPP result in significant differences of up to 15% more NO_x compared to DM-ALL. The NO_x field in the lower stratosphere over the northern extratropics also shows also a significant positive anomaly of 2–4% more NO_x . The analysis of the NO_y field in Fig. 6b shows an even more pronounced anomaly when superimposing all differences of all contributions together and comparing this result to the DM-ALL field: values of up to 25% more NO_y in the mesospheric polar atmosphere and in the northern polar mid-stratospheric region are reached. These differences stem partly from the NO photolysis, which was kept to constant 1780 values during the DM-EPP run. As well, the additional cooling during the DM-VOLC run resulted in NO_x deactivation over the poles, which could not happen during the DM-TD run.

The temporal evolution of NO_x at 70 hPa (Fig. S4 in the Supplement) and at 1 hPa (Fig. S5 in the Supplement), averaged between 20° N–20° S, are illustrated in the Supplement. The main signal at 70 hPa height again – as for ozone – is dominated by the volcanoes. The remaining forcings are relatively unimportant at this height and have not been plotted. At 1 hPa height, it is the solar signal which is dominant, although spikes do appear in volcanic periods. The latter anomalies, however, go back to normal values 1–2 yr after the volcanic eruptions. A negative NO_x anomaly due to EPP is not yet visible at this altitude.

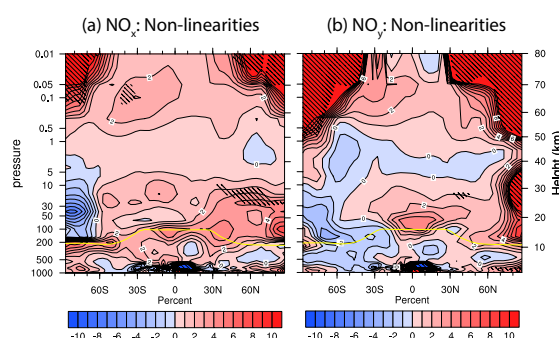


Fig. 6. Differences between the DM-ALL vs. DM-CTRL1780 field and between the (DM-TD + DM-BU + DM-VOLC + DM-EPP) vs. DM-CTRL1780 field. Positive values show a positive anomaly of the stacked differences over the DM-ALL difference field. Hatched areas are significantly different on a Student's t test with $\alpha = 10\%$. The yellow line illustrates the height of the WMO tropopause.

3.2 Stratospheric dynamics

In this section we present the changes of the stratospheric temperature and winds during the DM and identify the contribution of all considered factors.

3.2.1 Temperature

As it is shown in Fig. 7a, during the DM, the model simulates cooling in the entire atmosphere except the lower tropical stratosphere. The cooling gradually increases with altitude – from 1 K in the middle stratosphere around 25 km, up to 8 K near the mesopause. A slight enhancement of the cooling is also visible in the lower polar stratosphere. Weaker cooling of up to 0.6 K occurs below 100 hPa maximizing in the tropical upper troposphere.

Figure 7b shows the temperature changes due to implied decrease of visible and infrared solar irradiance (experiment DM-BU) and demonstrates that this factor is producing a weak cooling in the troposphere and in the upper stratosphere. The tropospheric cooling is explained by less energy income to the surface, while the cooling in the stratosphere is most likely caused by the decrease in available solar radiation for the ozone absorption in the Chappuis band. The temperature changes due to solar UV irradiance (experiment DM-TD) are illustrated in Fig. 7c which shows that this factor plays the dominant role in the cooling of the atmosphere above 25 km. The results shown in Fig. 7d demonstrate that the influence of volcanic eruptions has a more complicated spatial pattern. The volcanic aerosols produce a strong warming of up to 2 K at around 20 km in the tropical and subtropical region. The volcanic aerosol is able to absorb infrared solar and terrestrial radiation (e.g. Stenchikov et al., 1998). The obtained strong warming in the lower tropical stratosphere means that the increased absorption of the terrestrial

radiation by volcanic aerosols dominates over the absorption of the solar radiation, which should lead to a cooling due to the introduced decrease of the solar activity during the DM. As discussed in the introduction, this warming effect may be overestimated by our AO-CCM in the lower stratosphere, while at the tropopause there are good chances that our model – forced by AER data – reproduces an accurate warming right after the eruption. The warming in the UT/LS region explains the strong increase of water vapour in the stratosphere which was illustrated in Sect. 3.1.2. The cooling in the upper part of the model domain is explained by the blocking of the outgoing terrestrial radiation by the aerosol layer, leading to a decrease of the incoming energy in these layers. The dipole-like structure of the temperature changes over the polar regions would hint on the intensification of the polar night jets: this suspicion is confirmed when analysing seasonal means, which show a strong statistical significant acceleration on the 5 % level of the north polar night jet and a significant increase on the 10 % level of the southern polar night jet (see Fig. S6 in the Supplement). The blocking of the solar visible and infrared radiation by volcanic aerosols leads to a cooling in the troposphere.

Due to dilution and gravitational settling as well as washout processes, the volcanic aerosols concentration decreases over time. This has an implication on the temperature anomalies: we find that lower stratospheric temperatures revert to climatology, which is in agreement with Robock (2000).

The annual mean temperature changes from EPP are small and not statistically significant. Seasonal means, however, show significant differences: the austral winter seasonal means show a dipole pattern over the South Pole (Fig. 9a). A significant drop in temperatures (by as much as 0.7 K) between 100 hPa and 5 hPa is modelled in winter, deepening in spring to a cooling of up to 1 K. At the same time, a heating of approximately the same amplitude in a height between 1 hPa and 0.05 hPa is modelled. We explain the pattern over the southern pole by a strengthening of the polar vortex during austral winter (see next subsection) as well as a significant positive ozone anomaly of up to 3 % at 5 hPa (Fig. 2d). Ozone at these heights act as a radiative coolant. The positive temperature anomaly at mesosphere heights is due to a faster descent of air masses (BDC), leading to an increase in diabatic heating. No significant major changes in temperature can be observed during the boreal winter season.

The analyzed nonlinearities in temperatures are only significant in the troposphere and hence not shown here.

The temporal evolution of the temperatures at 70 hPa (Fig. S7 in the Supplement) and at 1 hPa (Fig. S8 in the Supplement), averaged between 20° N–20° S, are illustrated in the Supplement. The main anomalies at 70 hPa height dominating over the analyzed period are triggered by volcanic eruptions (+24 K in 1815). Other effects can be neglected. At 1 hPa height, it is the solar signal which is dominant (blue line, DM-TD). But – as for NO_x – during the volcanic peri-

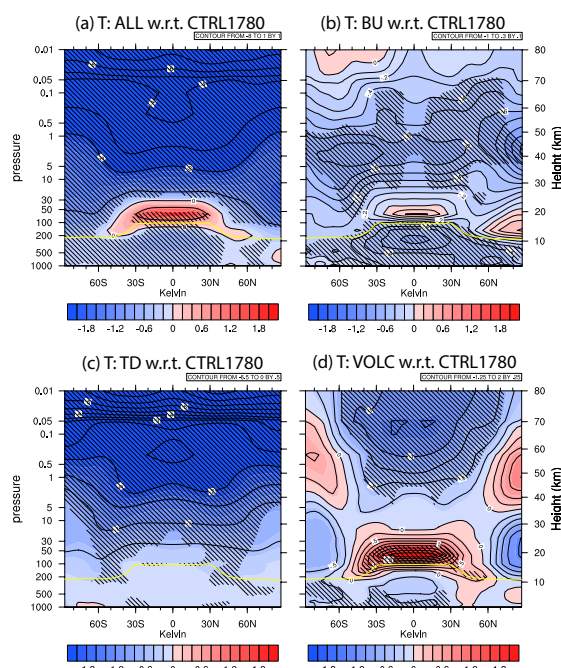


Fig. 7. Absolute differences in temperatures of the DM-ALL, DM-BU, DM-TD and DM-VOLC experiments with relation to the DM-CTRL1780 forcing run. Hatched areas are significantly different on a Student's t test with $\alpha = 5\%$. The yellow line illustrates the WMO tropopause height.

ods, slight, short-lived (1 yr) negative temperature anomalies (negative peaks of 1–2 K) are modelled. EPP or BU radiation do not influence temperatures in such a way that it would be visible on the graphs at stratopause height.

3.2.2 Wind and general circulation

The combined effect of all considered factors shown in Fig. 8a consists of a strong, although only partly significant, acceleration of the zonal winds in the subtropical stratosphere from 20 to 60 km and in the tropical stratosphere at around 50 km height. By contrast, a significant deceleration of the tropical jets and a decrease of the mesospheric extratropical zonal winds are found.

Because the introduced decrease of solar activity (DM-TD and DM-BU) does not have any wider significant influence on the annual mean zonal wind and only minor upper stratospheric influence at the southern polar region in austral winter time, the majority of the changes are attributed to the influence of the volcanic eruptions.

The model result shows a strong and significant deceleration of the zonal winds from the subtropical middle troposphere down to the surface of up to 0.8 m s^{-1} . The

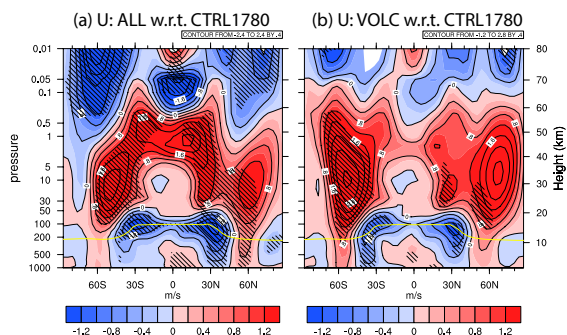


Fig. 8. Absolute differences in mean zonal wind of the DM-ALL and the DM-VOLC experiments with relation to the DM-CTRL1780 forcing run. Hatched areas are significantly different on a Student's t test with $\alpha = 5\%$. The yellow line illustrates the WMO tropopause height.

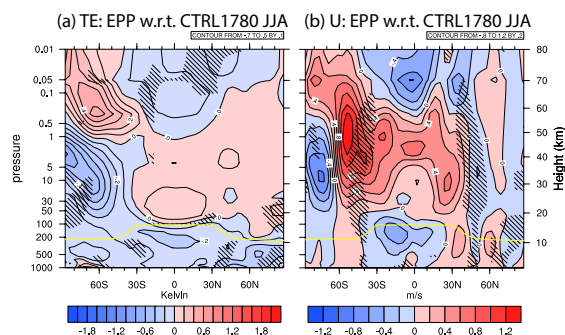


Fig. 9. Absolute JJA seasonal differences in temperature (left) and mean zonal wind (right) of the DM-EPP experiments with relation to the DM-CTRL1780 forcing run. Hatched areas are significantly different on a Student's t test with $\alpha = 5\%$. The yellow line illustrates the WMO tropopause height.

downward propagation of the signal is observed in both hemispheres. This effect comes from the strong, extended warming of the entire tropical lower stratosphere by volcanic aerosols (see Fig. 8d), leading to a smaller temperature gradient from the equator to the extratropics. This weakens the subtropical jets. By contrast, a significant strengthening of the polar jets up to 2.8 ms^{-1} is coming from the increased temperature gradient between the tropical tropopause and the polar tropopause ($\Delta T = 3.2 \text{ K}$). Moreover, in Fig. 10, a strong acceleration in vertical residual circulation (positive numbers are upwards) is observed after the 1809 and 1815 volcanic eruptions. Thus, the BDC is accelerated right after major volcanic eruptions. We explain this result by the finding that immediately after the volcanic eruption, cooling in the upper troposphere occurs. This favours the dissipation of gravity waves through the tropopause, leading to an additional gravity wave drag in the lower stratosphere, and hence an acceleration of the BDC. Following the heating of the lower stratosphere by the volcanic aerosols, the vertical residual circulation drops due to strengthening of the temperature gradient at the tropopause.

The DM-EPP experiment indicates positive – however, not significant – changes in annual zonal mean winds of up to 0.8 ms^{-1} at the stratospheric southern polar extratropics. This anomaly becomes highly significant in the austral winter seasonal mean (Fig. 9b) and reaches values of up to 1.2 ms^{-1} . The origin of this finding is the increase of adiabatic heating by descending air masses of the BDC in austral winter. The residual vertical circulation (not shown) shows a significant increase in downward motion of the air masses by up to 0.8 mms^{-1} . This in turn forms a positive temperature anomaly, leading to an increase in the pole-to-equator gradient at 60 km of height. As a consequence, the zonal wind increases. During boreal winter, a similar but less strong and non-significant pattern is found.

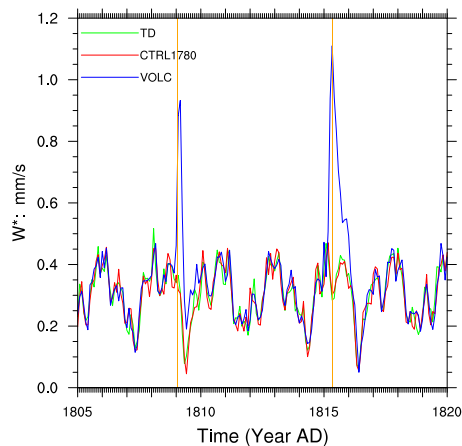


Fig. 10. Residual vertical velocity (calculation as in Andrews et al. (1987), Eqs. 3.5.1 to 3.5.3) from 1805 to 1820 for the DM-CTRL1780, DM-VOLC and DM-TD simulations at 30 hPa height averaged from $20^\circ \text{ N}/20^\circ \text{ S}$. The two major volcanic eruptions in 1809 (unknown) and 1815 (Tambora) are marked with two vertical orange lines. The data are averages of the three ensemble members and are not smoothed.

Nonlinearities in the zonal wind field are especially well visible at the southern extratropical stratopause, where a positive bias of up to 2 ms^{-1} is found (not shown). We assign this anomaly to the complex interaction between the DM-VOLC temperature gradient changes and the overall DM-TD negative temperature anomaly, which could have led to significant higher temperature gradient changes especially at the stratopause.

4 Conclusions

We present in this paper, we present a modeling study of the different forcings which could have led to the dynamical and chemical changes in the stratosphere during the DM from 1805 to 1825 AD. The contributions, analyzed with four sensitivity experiments, include decrease in visible and near infrared radiation (DM-BU), UV radiation (DM-TD), volcanic eruptions (DM-VOLC) and energetic particles, the latter including an increase of galactic cosmic rays ionization and a decrease of solar proton events and low energetic electron precipitation (DM-EPP). A comparison of DM-TD, DM-VOLC and DM-EPP to the control run showed major significant changes. However, when comparing DM-BU to the control run, we did not succeed in identifying any noticeable changes neither in stratospheric chemistry nor in the stratospheric dynamics – except for the mid-stratospheric temperature field. This is mainly due to the drop of only 1 % in the radiation band 3 from the Shapiro et al. (2011) reconstruction.

The reconstructions of the solar irradiance for past times remain highly uncertain (Judge et al., 2012; Shapiro et al., 2013; Solanki and Unruh, 2013) since no direct long-term measurements are available. We are aware of the fact that by using a strong solar forcing, the temperature, wind and chemical responses will be correspondingly strong, so that a comparison to a weaker forcing might be in place. However, in the recent work of Anet et al. (2013), we compared the ozone response using the strong forcing of Shapiro et al. (2011) – applied here – and a weaker one. Differences were not high enough to warrant the repetition of all experiments with a weaker solar forcing.

When isolating the different contributions, our simulations show the following effects on temperatures: when reducing the solar radiation in the 185–250 nm band and the photolysis rates, a temperature drop, reaching higher negative anomalies at the mesosphere than at the tropopause, is modelled. The anomalies reach 0.2 K at the tropopause and quasi-uniformly drop to values down to 6 K at the lower mesosphere. The main reason is the lower amount of absorption of radiation by ozone. A significant cooling of up to 0.6 K is observed in the middle stratosphere when reducing the irradiance of the bands 2 and 3 of the solar spectrum in our model (250–690 nm). In the volcanic scenario, the tropical tropopause is heated by up to 2.2 K due to radiative absorption by the aerosols, while a significant cooling of up to 1.2 K is modelled around the stratopause. In the DM-EPP scenario, only a seasonal significant change in temperatures could be modelled in JJA, leading to a dipole-like structure: a cold anomaly of 0.5 K in the southern polar middle stratosphere and a warming of around the same amount in the southern polar lower mesosphere.

The zonal winds did not change significantly neither in the DM-BU nor the DM-TD experiment. However, a strong significant change is modelled in the subtropics and extratrop-

ics in both hemispheres in the lower and upper stratosphere by up to 2.8 m s^{-1} when forcing the model only with volcanic aerosols. This effect is highest in the two years following an important volcanic eruption. Same as for the temperature, changes in zonal winds in the DM-EPP scenario are only significant in the JJA seasonal mean, showing a zonal wind increase of up to 1.2 m s^{-1} in the southern extratropical stratosphere, which is due to the dipole-like temperature anomalies.

The analysis of the stratospheric chemistry leads to following conclusions: ozone drops by up to 8 % in the ozone layer, HO_x decreases by up to 20 % at the stratopause and water vapour content decreases in the low stratosphere by up to 3.6 % but increases by up to 40 % at the lower mesosphere in the DM-TD scenario. In the DM-VOLC scenario, ozone increases by up to 16 % at the tropical tropopause but decreases by up to 6 % at the stratopause, HO_x increases all over by up to 25 %, as does the water vapour amount by up to 14 %. These effects are highest in the two subsequent years after a major volcanic eruption (up to 60 % more water vapour in the lower stratosphere in the 2 yr after Tambora). The DM-EPP experiment showed highly significant changes in the NO_x field: while a decrease of up to 80 % is modelled at the mesospheric poles, an increase of up to 4 % is simulated at the polar tropopause. However, no or very low effects are modelled for ozone, HO_x and water vapour.

By considering the changes in dynamics and chemistry, we conclude that only due to the complex interaction of volcanic, UV solar spectral and EPP forcing, do these contributions induce changes in the dynamics and chemistry of the stratosphere during the DM. The reduction of the visible radiation plays only a minor role in most of the fields except temperature. Thus, for future modelling studies, including an interactive chemistry with separate treatment of the different spectral bands is of great importance in order to get the climate responses on solar- and volcanic forcing as realistic as possible.

Concluding, the ozone decrease was predominantly influenced by the decrease in UV radiation in the polar mesosphere and at ozone-layer height, whereas the volcanic eruptions influenced ozone concentrations at tropical-tropopause height. EPP influenced only in a minor part the ozone concentrations in the polar mesosphere. HO_x and water-vapour increase were affected primarily by volcanic eruptions in the stratosphere and by UV in the lower mesosphere. NO_x fields were most notably influenced by EPP in the polar mesosphere and by UV in the upper stratosphere. Stratospheric winds were influenced to a major part from volcanic eruptions to a large degree. Temperatures were mainly influenced by volcanic eruptions and UV reduction, leading to a significant warming at the tropical tropopause and to a cooling in the remaining of the atmosphere.

With respect to a possible future grand solar minimum in the 21st century, a drop in ozone column by up to 7 % due to the reduction of the UV radiation is a very significant finding.

10964

J. G. Anet et al.: Changes in stratospheric chemistry and dynamics during the DM

In combination with a similar decrease in the ozone layer thickness due to ozone-depleting substances, this may become a possible health issue on Earth. As well, the effects of a reduction of UV, volcanic eruptions, and an increase of oxidation by GCRs should be thoroughly investigated in future research of the 21st century with an AO-CCM. The evolution of the ozone layer remains an important scientific topic, as e.g. crop yields or the health of living beings are subject to both anthropogenic and natural influences.

Supplementary material related to this article is available online at <http://www.atmos-chem-phys.net/13/10951/2013/acp-13-10951-2013-supplement.zip>.

Acknowledgements. This project is supported by the Swiss National Science Foundation under the grant CRSII22-130642(FUPSOL). We express our greatest thanks for this support. Moreover, we would like to acknowledge the NCL plotting tool (NCAR/CISL/VETS, 2012), which made it possible to plot the data in a nice way. E. Rozanov, A. I. Shapiro, and W. Schmutz thank COST Action ES1005TOSCA (<http://www.tosca-cost.eu>) for the support and fruitful discussions. We would also like to thank the two anonymous reviewers for their detailed and helpful comments.

Edited by: P. Jöckel

References

- Abreu, J., Beer, J., Steinhilber, F., Tobias, S. M., and Weiss, N. O.: For how long will the current grand maximum of solar activity persist?, *Geophys. Res. Lett.*, 35, L20109, doi:10.1029/2008GL035442, 2008.
- Abreu, J., Beer, J., and Ferriz-Mas, A.: Past and future solar activity from cosmogenic radionuclides, vol. 428, Past and future solar activity from cosmogenic radionuclides. Astronomical Society of the Pacific Conference Series: SOHO-23: understanding a peculiar solar minimum, 2010.
- Ammann, C., Joos, F., Schimel, D., Otto-Bliesner, B., and Tomas, R.: Solar influence on climate during the past millennium: Results from transient simulations with the NCAR Climate System Model, *P. Natl. Acad. Sci. USA*, 104, 3713–3718, doi:10.1073/pnas.0605064103, 2007.
- Andrews, D. G., Holton, J. R., and Leovy, C. B.: Middle atmosphere dynamics, Academic Press, Orlando, USA, 1987.
- Anet, J. G., Rozanov, E. V., Muthers, S., Peter, T., Brönnimann, S., Arfeuille, F., Beer, J., Shapiro, A. I., Raible, C. C., Steinhilber, F., and Schmutz, W. K.: Impact of a potential 21st century “grand solar minimum” on surface temperatures and stratospheric ozone, *Geophys. Res. Lett.*, 40, 4420–4425, doi:10.1002/grl.50806, 2013.
- Arfeuille, F.: Impacts of large volcanic eruptions on the stratosphere and climate, (Doctoral Dissertation) ETH Zürich, doi:10.3929/ethz-a-007577656, 2012.
- Arfeuille, F., Weisenstein, D., Mack, H., Rozanov, E., Peter, T., and Brönnimann, S.: Volcanic forcing for climate modeling: a new microphysics-based dataset covering years 1600-present, *Clim. Past Discuss.*, 9, 967–1012, doi:10.5194/cpd-9-967-2013, 2013a.
- Arfeuille, F., Luo, B. P., Heckendorn, P., Weisenstein, D., Sheng, J. X., Rozanov, E., Schraner, M., Brönnimann, S., Thomason, L. W., and Peter, T.: Uncertainties in modelling the stratospheric warming following Mt. Pinatubo eruption, *Atmos. Chem. Phys. Discuss.*, 13, 4601–4635, doi:10.5194/acpd-13-4601-2013, 2013b.
- Auchmann, R., Brönnimann, S., Breda, L., Bühler, M., Spadin, R., and Stickler, A.: Extreme climate, not extreme weather: the summer of 1816 in Geneva, Switzerland, *Clim. Past*, 8, 325–335, doi:10.5194/cp-8-325-2012, 2012.
- Bard, E., Raisbeck, G., Yiou, F., and Jouzel, J.: Solar irradiance during the last 1200 years based on cosmogenic nuclides, *Tellus*, 52B, 985–992, doi:10.1034/j.1600-0889.2000.d01-7.x, 2000.
- Bauer, E., Claussen, M., Brovkin, V., and Huenerbein, A.: Assessing climate forcings of the Earth system for the past millennium, *Geophys. Res. Lett.*, 30, 1276, doi:10.1029/2002GL016639, 2003.
- Baumgaertner, A. J. G., Jöckel, P., and Brühl, C.: Energetic particle precipitation in ECHAM5/MESSy1 – Part 1: Downward transport of upper atmospheric NO_x produced by low energy electrons, *Atmos. Chem. Phys.*, 9, 2729–2740, doi:10.5194/acp-9-2729-2009, 2009.
- Bazilevskaya, G., Usoskin, I., Flückiger, E., Harrison, R., Desorgher, L., Büttikofer, R., Krainev, M., Makhmutov, V., Stozhkov, Y., Svirzhevskaya, A., Svirzhevsky, N., and Kovaltsov, G.: Cosmic Ray Induced Ion Production in the Atmosphere, in: Planetary Atmospheric Electricity, edited by Leblanc, F., Aplin, K., Yair, Y., Harrison, R., Lebreton, J., and Blanc, M., vol. 30 of Space Sciences Series of ISSI, 149–173, Springer New York, doi:10.1007/978-0-387-87664-1_10, 2008.
- Bragg, W. and Kleeman, R.: On the α particles of radium, and their loss of range in passing through various atoms and molecules, *Philos. Mag.*, 10, 318–340, doi:10.1080/14786440509463378, 1905.
- Brasseur, G. and Solomon, S.: Aeronomy of the Middle Atmosphere, Springer Netherlands, Dordrecht, doi:10.1007/1-4020-3824-0, 2005.
- Brönnimann, S., Annis, J. L., Vogler, C., and Jones, P. D.: Reconstructing the quasi-biennial oscillation back to the early 1900s, *Geophys. Res. Lett.*, 34, 22, doi:10.1029/2007GL031354, 2007.
- Calisto, M., Usoskin, I., Rozanov, E., and Peter, T.: Influence of Galactic Cosmic Rays on atmospheric composition and dynamics, *Atmos. Chem. Phys.*, 11, 4547–4556, doi:10.5194/acp-11-4547-2011, 2011.
- Callis, L., Natarajan, M., Evans, D., and Lambeth, J.: Solar atmospheric coupling by electrons (SOLACE) 1. Effects of the May 12, 1997 solar event on the middle atmosphere, *J. Geophys. Res.*, 103, 28405–28419, doi:10.1029/98JD02408, 1998.
- Christiansen, B.: Volcanic Eruptions, Large-Scale Modes in the Northern Hemisphere, and the El Niño Southern Oscillation, *J. Climate*, 21, 910–922, doi:10.1175/2007JCLI1657.1, 2007.
- Dutton, E. G. and Christy, J. R.: Solar radiative forcing at selected locations and evidence for global lower tropospheric cooling following the eruptions of El Chichón and Pinatubo, *Geophys. Res. Lett.*, 19, 2313–2316, doi:10.1029/92GL02495, 1992.

- Egorova, T., Rozanov, E., Zubov, V., and Karol, I.: Model for Investigating Ozone Trends (MEZON), *Izvestiia Akademii Nauk SSSR. Seria Fizika Atmosfery i Okeana*, 39, 310–326, translated by MAIK “Nauka/Interperiodica” (Russia), 2003.
- Egorova, T., Rozanov, E., Ozolin, Y., Shapiro, A. I., Calisto, M., Peter, T., and Schmutz, W.: The atmospheric effects of October 2003 solar proton event simulated with the chemistry-climate model SOCOL using complete and parameterized ion chemistry, *J. Atmos. Sol-Terr. Phys.*, 73, 356–365, doi:10.1016/j.jastp.2010.01.009, 2011.
- Erlykin, A., Sloan, T., and Wolfendale, A.: A review of the relevance of the “CLOUD” results and other recent observations to the possible effect of cosmic rays on the terrestrial climate, *Meteorol. Atmos. Phys.*, 121, 137–142, doi:10.1007/s00703-013-0260-x, 2013.
- Etheridge, D., Steele, L., Langenfelds, R., Francey, R., Barnola, J., and Morgan, V.: Natural and anthropogenic changes in atmospheric CO₂ over the last 1000 years from air in Antarctic ice and firm, *J. Geophys. Res.*, 101, 4115–4128, doi:10.1029/95JD03410, 1996.
- Etheridge, D. M., Steele, L. P., Francey, R. J., and Langenfelds, R. L.: Atmospheric methane between 1000 A.D. and present: Evidence of anthropogenic emissions and climatic variability, *J. Geophys. Res.*, 103, 15979–15993, doi:10.1029/98JD00923, 1998.
- Eyring, V., Butchart, N., Waugh, D. W., Akiyoshi, H., Austin, J., Bekki, S., Bodeker, G. E., Boville, B. A., Brühl, C., Chipperfield, M. P., Cordero, E., Dameris, M., Deushi, M., Fioletov, V. E., Frith, S. M., Garcia, R. R., Gettelman, A., Giorgetta, M. A., Grewe, V., Jourdain, L., Kinnison, D. E., Mancini, E., Manzini, E., Marchand, M., Marsh, D. R., Nagashima, T., Newman, P. A., Nielsen, J. E., Pawson, S., Pitari, G., Plummer, D. A., Rozanov, E., Schraner, M., Shepherd, T. G., Shibata, K., Stolarski, R. S., Struthers, H., Tian, W., and Yoshiki, M.: Assessment of temperature, trace species, and ozone in chemistry-climate model simulations of the recent past, *J. Geophys. Res.*, 111, D22308, doi:10.1029/2006JD007327, 2006.
- Ferretti, D., Miller, J., White, J., Etheridge, D., Lassey, K., Lowe, D., Meure, C., Dreier, M., Trudinger, C., Van Ommen, T., and Langenfelds, R.: Unexpected changes to the global methane budget over the past 2000 years, *Science*, 309, 1714–1717, doi:10.1126/science.1115193, 2005.
- Fischer, E. M., Luterbacher, J., Zorita, E., Tett, S. F. B., Casty, C., and Wanner, H.: European climate response to tropical volcanic eruptions over the last half millennium, *Geophys. Res. Lett.*, 34, L05707, doi:10.1029/2006GL027992, 2007.
- Forster, P., Ramaswamy, V., Artaxo, P., Bernsten, T., Betts, R., Fahey, D., Haywood, J., Lean, J., Lowe, D., Myhre, G., Nganga, J., Prinn, R., Raga, G., Schulz, M., and Van Dorland, R.: Changes in Atmospheric Constituents and in Radiative Forcing, in: *Climate Change 2007: The Physical Science Basis, Contribution of Working Group I to the Fourth Assessment Report of the Intergovernmental Panel on Climate Change*, Cambridge University Press, Cambridge, United Kingdom and New York, NY, USA, 2007.
- Forster, P. M., Fomichev, V. I., Rozanov, E., Cagnazzo, C., Jonsson, A. I., Langematz, U., Fomin, B., Iacono, M. J., Mayer, B., Mlawer, E., Myhre, G., Portmann, R. W., Akiyoshi, H., Falaleeva, V., Gillett, N., Karpechko, A., Li, J., Lemennais, P., Morgenstern, O., Oberländer, S., Sigmond, M., and Shibata, K.: Evaluation of radiation scheme performance within chemistry climate models, *J. Geophys. Res.*, 116, D10302, doi:10.1029/2010JD015361, 2011.
- Franklin, B.: *Meteorological imagination’s and conjectures*, Manchester Lit. Philos. Soc., 2, 122, 1784.
- Funke, B., Baumgaertner, A., Calisto, M., Egorova, T., Jackman, C. H., Kieser, J., Krivolutsky, A., López-Puertas, M., Marsh, D. R., Reddmann, T., Rozanov, E., Salmi, S.-M., Sinnhuber, M., Stiller, G. P., Verronen, P. T., Versick, S., von Clarmann, T., Vyushkova, T. Y., Wieters, N., and Wissing, J. M.: Composition changes after the “Halloween” solar proton event: the High Energy Particle Precipitation in the Atmosphere (HEPPA) model versus MIPAS data intercomparison study, *Atmos. Chem. Phys.*, 11, 9089–9139, doi:10.5194/acp-11-9089-2011, 2011.
- Gao, C., Robock, A., and Ammann, C.: Volcanic forcing of climate over the past 1500 years: An improved ice core-based index for climate models, *J. Geophys. Res.*, 113, D23111, doi:10.1029/2008JD010239, 2008.
- Gao, C., Robock, A., and Ammann, C.: Correction to “Volcanic forcing of climate over the past 1500 years: An improved ice core-based index for climate models”, *J. Geophys. Res.*, 117, D16112, doi:10.1029/2012JD018052, 2012.
- Giorgetta, M.: *Der Einfluss der quasi-zweijährigen Oszillation: Modellrechnungen mit ECHAM4*, Ph.D. thesis, Max-Planck-Institut für Meteorologie, Hamburg, 1996.
- Gray, L. J., Beer, J., Geller, M., Haigh, J. D., Lockwood, M., Matthes, K., Cubasch, U., Fleitmann, D., Harrison, G., Hood, L., Luterbacher, J., Meehl, G. A., Shindell, D., van Geel, B., and White, W.: Solar influences on climate, *Rev. Geophys.*, 48, RG4001, doi:10.1029/2009RG000282, 2010.
- Hagemann, S.: *An improved land surface parameter dataset for global and regional climate models*, Max-Planck-Institut für Meteorologie, Hamburg, 2002.
- Hagemann, S., Botzet, M., Dümenil, L., and Machenhauer, B.: *Derivation of global GCM boundary conditions from 1 km land use satellite data*, Max-Planck-Institut für Meteorologie, 1999.
- Halmer, M., Schmincke, H.-U., and Graf, H.-F.: The annual volcanic gas input into the atmosphere, in particular into the stratosphere: a global data set for the past 100 years, *J. Volcanol. Geotherm. Res.*, 115, 511–528, doi:10.1016/S0377-0273(01)00318-3, 2002.
- Hansen, J., Lacis, A., Ruedy, R., and Sato, M.: Potential climate impact of Mount Pinatubo eruption, *Geophys. Res. Lett.*, 19, 215–218, doi:10.1029/91GL02788, 1992.
- Hoyt, D. V. and Schatten, K. H.: Group sunspot numbers: A new solar activity reconstruction, *Sol. Phys.*, 181, 491–512, doi:10.1023/A:1005007527816, 1998.
- Ineson, S., Scaife, A. A., Knight, J. R., Manners, J. C., Dunstone, N. J., Gray, L. J., and Haigh, J. D.: Solar forcing of winter climate variability in the Northern Hemisphere, *Nature*, 4, 753–757, doi:10.1038/NCEO1282, 2011.
- Jackman, C. H., Marsh, D. R., Vitt, F. M., Garcia, R. R., Fleming, E. L., Labow, G. J., Randall, C. E., López-Puertas, M., Funke, B., von Clarmann, T., and Stiller, G. P.: Short- and medium-term atmospheric constituent effects of very large solar proton events, *Atmos. Chem. Phys.*, 8, 765–785, doi:10.5194/acp-8-765-2008, 2008.

- Jackman, C. H., Marsh, D. R., Vitt, F. M., Garcia, R. R., Randall, C. E., Fleming, E. L., and Frith, S. M.: Long-term middle atmospheric influence of very large solar proton events, *J. Geophys. Res.*, 114, D11304, doi:10.1029/2008JD011415, 2009.
- Judge, P. G., Lockwood, G. W., Radick, R. R., Henry, G. W., Shapiro, A. I., Schmutz, W., and Lindsey, C.: Confronting a solar irradiance reconstruction with solar and stellar data, *Astron. Astrophys.*, 544, A88, doi:10.1051/0004-6361/201218903, 2012.
- Kahler, S.: Solar flares and coronal mass ejections, *Annu. Rev. Astron. Astr.*, 30, 113–141, doi:10.1146/annurev.aa.30.090192.000553, 1992.
- Kodera, K. and Kuroda, Y.: Dynamical response to the solar cycle, *J. Geophys. Res.*, 107, 4749–4761, doi:10.1029/2002JD002224, 2002.
- Labitzke, K., Austin, J., Butchart, N., Knight, J., Takahashi, M., Nakamoto, M., Nagashima, T., Haigh, J., and Williams, V.: The global signal of the 11-year solar cycle in the stratosphere: observations and models, *J. Atmos. Sol.-Terr. Phys.*, 64, 203–210, doi:10.1016/S1364-6826(01)00084-0, 2002.
- Lanzante, J. R.: Diagnosis of Radiosonde Vertical Temperature Trend Profiles: Comparing the Influence of Data Homogenization versus Model Forcings, *J. Climate*, 20, 5356, doi:10.1175/2007JCLI1827.1, 2007.
- Laut, P.: Solar activity and terrestrial climate: an analysis of some purported correlations, *J. Atmos. Sol.-Terr. Phys.*, 65, 801–812, doi:10.1016/S1364-6826(03)00041-5, 2003.
- Lean, J., Beer, J., and Bradley, R.: Reconstruction of solar irradiance since 1610: Implications for climate change, *Geophys. Res. Lett.*, 22, 3195–3198, doi:10.1029/95GL03093, 1995.
- Ljungqvist, F.: A new reconstruction of temperature variability in the extra-tropical northern hemisphere during the last two millennia, *Geogr. Ann. A*, 92, 339–351, doi:10.1111/j.1468-0459.2010.00399.x, 2010.
- Lockwood, M. and Fröhlich, C.: Recent oppositely directed trends in solar climate forcings and the global mean surface air temperature, *Proceedings of the Royal Society A: Mathematical, Physical and Engineering Science*, 463, 2447–2460, doi:10.1098/rspa.2007.1880, 2007.
- Lockwood, M., Owens, M., Barnard, L., Davis, C., and Steinhilber, F.: The persistence of solar activity indicators and the descent of the Sun into Maunder Minimum conditions, *Geophys. Res. Lett.*, 38, L22105, doi:10.1029/2011GL049811, 2011b.
- Luterbacher, J., Dietrich, D., Xoplaki, E., Grosjean, M., and Wanner, H.: European Seasonal and Annual Temperature Variability, Trends, and Extremes Since 1500, *Science*, 303, 1499–1503, doi:10.1126/science.1093877, 2004.
- MacFarling-Meure, C.: The natural and anthropogenic variations of carbon dioxide, methane and nitrous oxide during the Holocene from ice core analysis, Ph.D. thesis, University of Melbourne, 2004.
- MacFarling-Meure, C., Etheridge, D., Trudinger, C., Steele, P., Langenfelds, R., Van Ommen, T., Smith, A., and Elkins, J.: Law Dome CO₂, CH₄ and N₂O ice core records extended to 2000 years BP, *Geophys. Res. Lett.*, 33, L14810, doi:10.1029/2006GL026152, 2006.
- Marsh, N. and Svensmark, H.: Cosmic rays, clouds, and climate, *Space Science Reviews*, 94, 215–230, doi:10.1023/A:1026723423896, 2000.
- Marsland, S., Haak, H., Jungclaus, J., Latif, M., and Roske, F.: The Max-Planck-Institute global ocean/sea ice model with orthogonal curvilinear coordinate, *Ocean Model.*, 5, 91–27, doi:10.1016/S1463-5003(02)00015-X, 2003.
- Meehl, G. A., Arblaster, J. M., Matthes, K., Sassi, F., and van Loon, H.: Amplifying the Pacific Climate System Response to a Small 11-Year Solar Cycle Forcing, *Science*, 325, 1114–1118, doi:10.1126/science.1172872, 2009.
- Milham, W.: The year 1816 – the causes of abnormalities, *Mon. Wea. Rev.*, 52, 563–570, doi:10.1175/1520-0493(1924)52<563:TYTCOA>2.0.CO;2, 1924.
- Minnis, P., Harrison, E., Stowe, L., Gibson, G., Denn, F., Doelling, D., and Smith, W.: Radiative climate forcing by the Mount Pinatubo eruption, *Science*, 259, 1411–1415, doi:10.1126/science.259.5100.1411, 1993.
- NCAR/CISL/VETS: The NCAR Command Language (Version 6.0.0) [Software], Boulder, USA, 2012.
- Robock, A.: Volcanic Eruptions and Climate, *Rev. Geophys.*, 38, 191–219, doi:10.1029/1998RG000054, 2000.
- Roekner, E., Baeuml, G., Bonaventura, L., Brokopf, R., Esch, M., Giorgetta, M., Hagemann, S., Kirchner, I., Kornblüeh, L., Manzini, E., Rhodin, A., Schlese, U., Schulzweida, U., and Tompkins, A.: The atmospheric general circulation model ECHAM 5. PART I: Model description, Max-Planck-Institut für Meteorologie, Hamburg, Report No. 349, http://www.mpimet.mpg.de/fileadmin/publikationen/Reports/max_screp_349.pdf, 2003.
- Rozanov, E., Schlesinger, M. E., Zubov, V., Yang, F., and Andronova, N. G.: The UIUC three-dimensional stratospheric chemical transport model: Description and evaluation of the simulated source gases and ozone, *J. Geophys. Res.*, 104, 755–781, doi:10.1029/1999JD900138, 1999.
- Rozanov, E., Calisto, M., Egorova, T., Peter, T., and Schmutz, W.: Influence of the Precipitating Energetic Particles on Atmospheric Chemistry and Climate, *Surveys in Geophysics*, 33, 483–501, doi:10.1007/s10712-012-9192-0, 2012b.
- Scherer, K., Fahr, H.-J., Fichtner, H., and Heber, B.: Long-Term Modulation of Cosmic Rays in the Heliosphere and its Influence at Earth, *Solar Physics*, 224, 305–316, doi:10.1007/s11207-005-5687-x, 2004.
- Schraner, M., Rozanov, E., Schnadt Poberaj, C., Kenzelmann, P., Fischer, A. M., Zubov, V., Luo, B. P., Hoyle, C. R., Egorova, T., Fueglistaler, S., Brönnimann, S., Schmutz, W., and Peter, T.: Technical Note: Chemistry-climate model SOCOL: version 2.0 with improved transport and chemistry/microphysics schemes, *Atmos. Chem. Phys.*, 8, 5957–5974, doi:10.5194/acp-8-5957-2008, 2008.
- Schrijver, C., Beer, J., Baltensperger, U., Cliver, E., Güdel, M., Hudson, H., McCracken, K., Osten, R., Peter, T., Soderblom, D., R., D., Usoskin, I. G., and Wolff, E. W.: Estimating the frequency of extremely energetic solar events, based on solar, stellar, lunar, and terrestrial records, *J. Geophys. Res.*, 117, A08103, doi:10.1029/2012JA017706, 2012.
- Schwabe, M.: Sonnenbeobachtungen im Jahre 1843, Von Herrn Hofrath Schwabe in Dessau, *Astronomische Nachrichten*, 21, 233–236, 1844.
- Shapiro, A. I., Schmutz, W., Rozanov, E., Schoell, M., Haberleiter, M., Shapiro, A. V., and Nyeki, S.: A new approach to the long-

- term reconstruction of the solar irradiance leads to large historical solar forcing, *Astron. Astrophys.*, 529, A67, 2011.
- Shapiro, A. I., Schmutz, W., Cessateur, G., and Rozanov, E.: The place of the Sun among the Sun-like stars, *Astron. Astrophys.*, 552, A114, doi:10.1051/0004-6361/201220512, 2013.
- Shea, M., Smart, D., McCracken, K., Dreschhoff, G., and Spence, H.: Solar proton events for 450 years: The Carrington event in perspective, *Adv. Space Res.*, 38, 232–238, doi:10.1016/j.asr.2005.02.100, 2006.
- Solanki, S. and Unruh, Y.: Solar irradiance variability, *Astronomische Nachrichten*, 334, 145–150, doi:10.1002/asna.201211752, 2013.
- Spanghel, T., Cubasch, U., and Langematz, U.: Änderung der NAO im Maunder Minimum und einem zukünftigen Klima in Modellsimulationen mit EGMAM, Copernicus meetings, http://meetings.copernicus.org/dach2007/download/DACH2007_A_00360.pdf (last access: June 2013), 2007.
- Spanghel, T., Cubasch, U., Raible, C., Schimanke, S., Körper, J., and Hofer, D.: Transient climate simulations from the Maunder Minimum to present day: role of the stratosphere, *J. Geophys. Res.*, 115, D00I10, doi:10.1029/2009JD012358, 2010.
- Steinhilber, F. and Beer, J.: Prediction of solar activity for the next 500 years, *J. Geophys. Res.*, 118, 1861–1867, doi:10.1002/jgra.50210, 2013.
- Steinhilber, F., Abreu, J. A., and Beer, J.: Solar modulation during the Holocene, *Astrophys. Space Sci.*, 4, 1–6, doi:10.5194/astr-4-1-2008, 2008.
- Stenchikov, G., Kirchner, I., Robock, A., Graf, H., Antuna, J., Grainger, R., Lambert, A., and Thomason, L.: Radiative forcing from the 1991 Mount Pinatubo volcanic eruption, *J. Geophys. Res.*, 103, 837–857, doi:10.1029/98JD00693, 1998.
- Stenchikov, G., Robock, A., Ramaswamy, V., Schwarzkopf, M. D., Hamilton, K., and Ramachandran, S.: Arctic Oscillation response to the 1991 Mount Pinatubo eruption: Effects of volcanic aerosols and ozone depletion, *J. Geophys. Res.*, 107, ACL 28–1–ACL 28–16, doi:10.1029/2002JD002090, 2002.
- Stenke, A., Schraner, M., Rozanov, E., Egorova, T., Luo, B., and Peter, T.: The SOCOL version 3.0 chemistry-climate model: description, evaluation, and implications from an advanced transport algorithm, *Geosci. Model Dev.*, 6, 1407–1427, doi:10.5194/gmd-6-1407-2013, 2013.
- Tie, X. and Brasseur, G.: The response of stratospheric ozone to volcanic eruptions: Sensitivity to atmospheric chlorine loading, *Geophys. Res. Lett.*, 22, 3035–3038, 1995.
- Tratt, D. and Menzies, R.: Evolution of the Pinatubo Volcanic Aerosol Column Above Pasadena, California Observed With a Mid-Infrared Backscatter Lidar, Tech. rep., Jet Propulsion Laboratory, California Institute of Technology, <http://trs-new.jpl.nasa.gov/dspace/bitstream/2014/33312/1/94-1252.pdf>, 1994.
- Usoskin, I. G., Kovaltsov, G. A., and Mironova, I. A.: Cosmic ray induced ionization model CRAC:CRII: An extension to the upper atmosphere, *J. Geophys. Res.*, 115, D10302, doi:10.1029/2009JD013142, 2010.
- Valcke, S.: The OASIS3 coupler: a European climate modelling community software, *Geosci. Model Dev.*, 6, 373–388, doi:10.5194/gmd-6-373-2013, 2013.
- Wagner, S. and Zorita, E.: The influence of volcanic, solar and CO₂ forcing on the temperatures in the Dalton Minimum (1790–1830): a model study, *Clim. Dyn.*, 25, 205–218, 2005.
- Weisenstein, D., Yue, G., Ko, M., Sze, N., Rodriguez, J., and Scott, C.: A two-dimensional model of sulfur species and aerosols, *J. Geophys. Res.*, 102, 13019–13035, doi:10.1029/97JD00901, 1997.
- Whitten, R., Toon, O., and Rurco, R.: The stratospheric sulfate aerosol layer: Processes, models, observations, and simulations, *Pure Appl. Geophys.*, 118, 86–127, doi:10.1007/BF01586447, 1980.
- WMO: Scientific assessment of ozone depletion, Global Ozone Research and Monitoring Project – Report No. 52, Tech. rep., Geneva, Switzerland, http://montreal-protocol.org/Assessment_Panels/SAP/Scientific_Assessment_2010/index.shtml, 2011.
- Wolf, R.: Abstract of his latest results, *Mon. Not. R. Astron. Soc.*, 21, 77, 1861.
- Wolff, E. W., Jones, A. E., Bauguitte, S. J.-B., and Salmon, R. A.: The interpretation of spikes and trends in concentration of nitrate in polar ice cores, based on evidence from snow and atmospheric measurements, *Atmos. Chem. Phys.*, 8, 5627–5634, doi:10.5194/acp-8-5627-2008, 2008.
- Yoshimori, M., Stocker, T., Raible, C., and Renold, M.: Externally forced and internal variability in ensemble climate simulations of the Maunder Minimum, *J. Climate*, 18, 4253–4270, doi:10.1175/JCLI3537.1, 2005.
- Zhu, X.: An accurate and efficient radiation algorithm for middle atmosphere models, *J. Atmos. Sci.*, 51, 3593–3614, doi:10.1175/1520-0469(1994)051<3593:AAAERA>2.0.CO;2, 1994.

Supplementary material

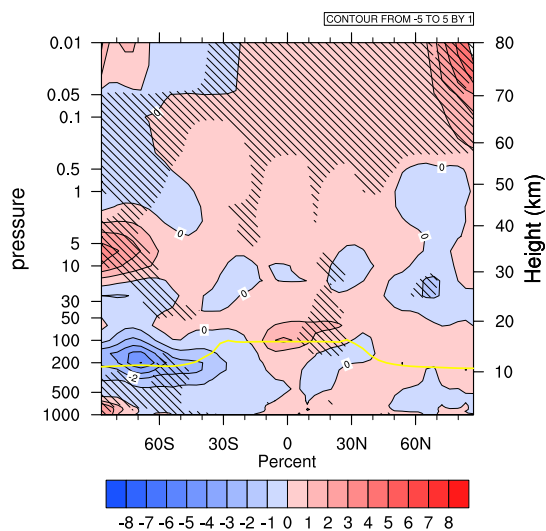


Figure S1.: Relative differences of ozone of the DM-EPP experiment with relation to the DM-CTRL1780 forcing run for the SON season. Hatched areas are significantly different on a Student's t-test with $\alpha = 5\%$. The yellow line illustrates the height of the WMO tropopause.

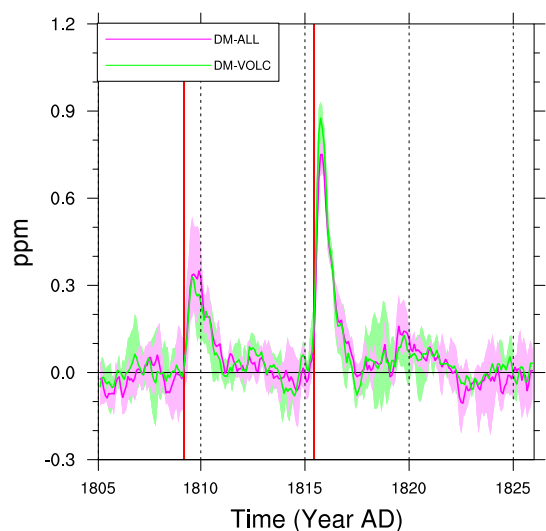


Figure S2.: Ozone mixing ratio anomalies, averaged from 20°N to 20°S , at 70 hPa height. Coloured curves show anomalies of experiments DM-ALL and DM-VOLC relative to DM-CTRL1780. The two major volcanic eruptions in 1809 (unknown) and 1815 (Tambora) are marked with two vertical red lines. The data are averages of the three ensemble members and are not smoothed.

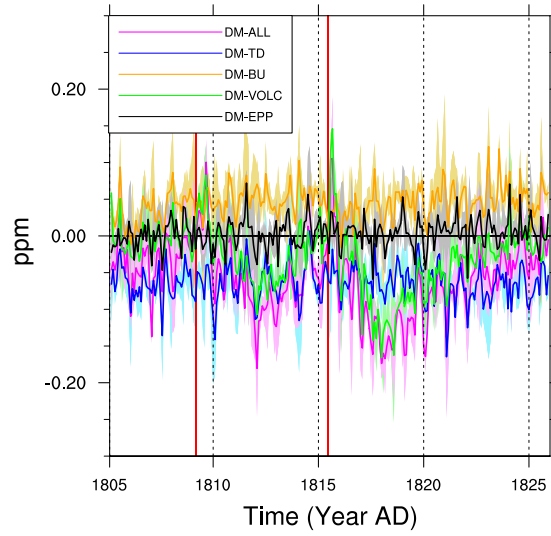


Figure S3.: Same as Figure S2, but at 1 hPa of height and illustrating the anomalies of all experiments, relative to DM-CTRL1780.

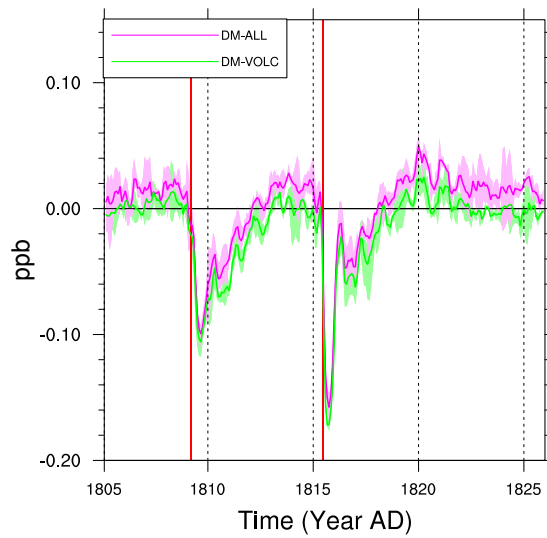


Figure S4.: Same as Figure S2, but illustrating NOx anomalies relative to DM-CTRL1780.

A.2. Forcing of stratospheric chemistry and dynamics during the Dalton Minimum

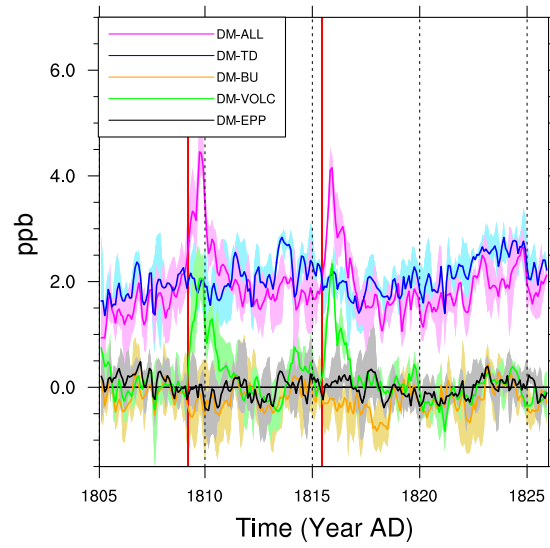


Figure S5.: Same as Figure S4, but at 1 hPa of height and illustrating the anomalies of all experiments, relative to DM-CTRL1780.

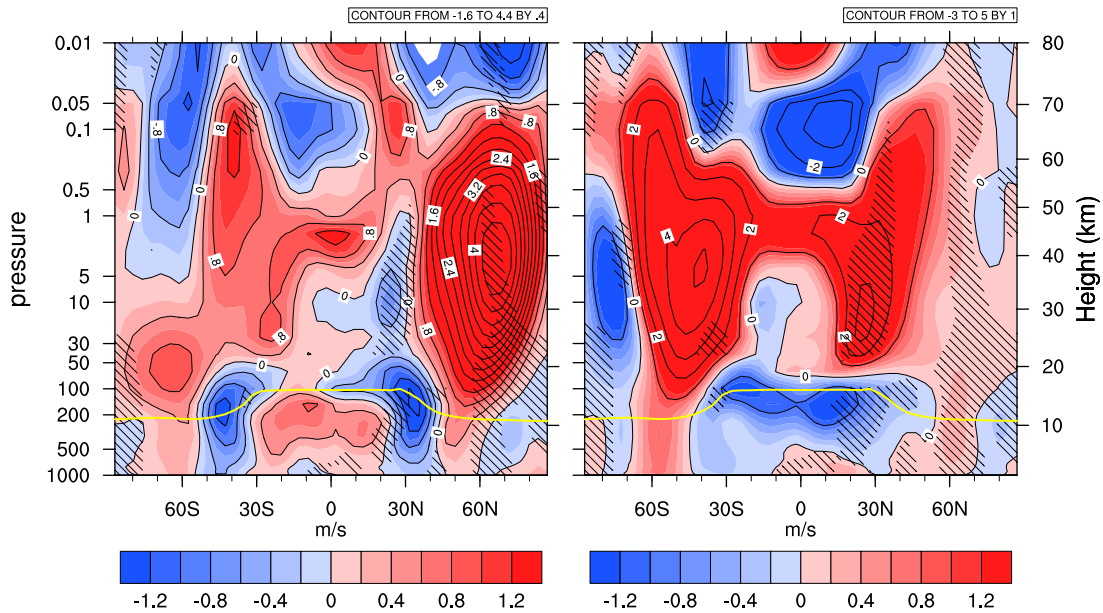


Figure S6.: Absolute differences of the zonal wind field of the DM-VOLC experiment with relation to the DM-CTRL1780 forcing run for the JJA (left) and DJF (right) season. Hatched areas are significantly different on a Student's t-test with $\alpha = 5\%$ (left) and $\alpha = 10\%$ (right). The yellow line illustrates the height of the WMO tropopause.

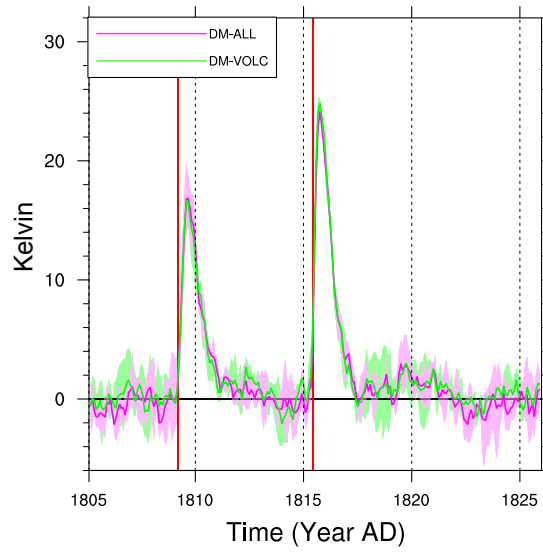


Figure S7.: Same as Figure S2, but illustrating temperature anomalies relative to DM-CTRL1780.

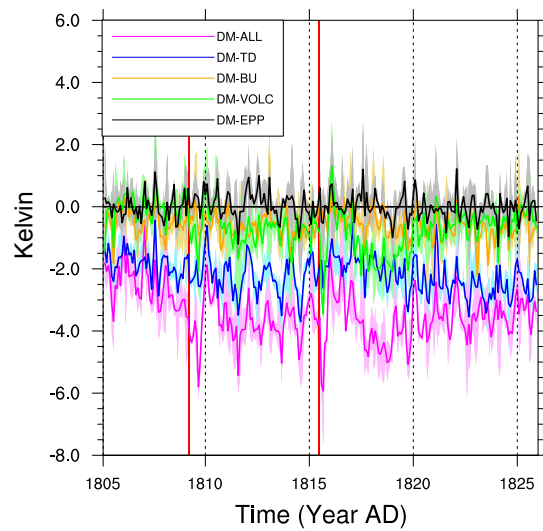


Figure S8.: Same as Figure S8, but at 1 hPa of height and illustrating the anomalies of all experiments, relative to DM-CTRL1780.

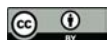
A.3. Impact of solar vs. volcanic activity variations on tropospheric temperatures and precipitation during the Dalton Minimum

A.3. Impact of solar vs. volcanic activity variations on tropospheric temperatures and precipitation during the Dalton Minimum

Julien G. Anet, Stefan Muthers, Eugene Rozanov, Christoph C. Raible, Andrea Stenke, Alexander I. Shapiro, Stefan Brönnimann, Florian Arfeuille, Yuri Brugnara, Jürg Beer, Friedhelm Steinhilber, Werner Schmutz, and Thomas Peter,

Published in *Climate of the Past*, vol. 10, 921-938, 2014.

Clim. Past, 10, 921–938, 2014
www.clim-past.net/10/921/2014/
doi:10.5194/cp-10-921-2014
© Author(s) 2014. CC Attribution 3.0 License.



Impact of solar versus volcanic activity variations on tropospheric temperatures and precipitation during the Dalton Minimum

J. G. Anet¹, S. Muthers^{2,3}, E. V. Rozanov^{1,4}, C. C. Raible^{2,3}, A. Stenke¹, A. I. Shapiro⁴, S. Brönnimann^{5,3}, F. Arfeuille^{5,3}, Y. Brugnara^{5,3}, J. Beer⁶, F. Steinhilber⁶, W. Schmutz⁴, and T. Peter¹

¹Institute for Atmospheric and Climate Science ETH, Zurich, Switzerland

²Climate and Environment Physics, Physics Institute, University of Bern, Bern, Switzerland

³Oeschger Centre for Climate Change Research, University of Bern, Bern, Switzerland

⁴Physikalisch-Meteorologisches Observatorium Davos and World Radiation Center (PMOD/WRC), Davos, Switzerland

⁵Institute of Geography, University of Bern, Bern, Switzerland

⁶Eawag, Surface Waters group, Dübendorf, Switzerland

Correspondence to: J. G. Anet (julien.anet@alumni.ethz.ch)

Received: 21 October 2013 – Published in Clim. Past Discuss.: 4 November 2013

Revised: 21 March 2014 – Accepted: 23 March 2014 – Published: 9 May 2014

Abstract. The aim of this work is to elucidate the impact of changes in solar irradiance and energetic particles versus volcanic eruptions on tropospheric global climate during the Dalton Minimum (DM, AD 1780–1840). Separate variations in the (i) solar irradiance in the UV-C with wavelengths $\lambda < 250$ nm, (ii) irradiance at wavelengths $\lambda > 250$ nm, (iii) in energetic particle spectrum, and (iv) volcanic aerosol forcing were analyzed separately, and (v) in combination, by means of small ensemble calculations using a coupled atmosphere–ocean chemistry–climate model. Global and hemispheric mean surface temperatures show a significant dependence on solar irradiance at $\lambda > 250$ nm. Also, powerful volcanic eruptions in 1809, 1815, 1831 and 1835 significantly decreased global mean temperature by up to 0.5 K for 2–3 years after the eruption. However, while the volcanic effect is clearly discernible in the Southern Hemispheric mean temperature, it is less significant in the Northern Hemisphere, partly because the two largest volcanic eruptions occurred in the SH tropics and during seasons when the aerosols were mainly transported southward, partly because of the higher northern internal variability. In the simulation including all forcings, temperatures are in reasonable agreement with the tree ring-based temperature anomalies of the Northern Hemisphere. Interestingly, the model suggests that solar irradiance changes at $\lambda < 250$ nm and in energetic particle spectra have only an insignificant impact on the climate during the Dalton Minimum. This downplays the importance of top–down

processes (stemming from changes at $\lambda < 250$ nm) relative to bottom–up processes (from $\lambda > 250$ nm). Reduction of irradiance at $\lambda > 250$ nm leads to a significant (up to 2 %) decrease in the ocean heat content (OHC) between 0 and 300 m in depth, whereas the changes in irradiance at $\lambda < 250$ nm or in energetic particles have virtually no effect. Also, volcanic aerosol yields a very strong response, reducing the OHC of the upper ocean by up to 1.5 %. In the simulation with all forcings, the OHC of the uppermost levels recovers after 8–15 years after volcanic eruption, while the solar signal and the different volcanic eruptions dominate the OHC changes in the deeper ocean and prevent its recovery during the DM. Finally, the simulations suggest that the volcanic eruptions during the DM had a significant impact on the precipitation patterns caused by a widening of the Hadley cell and a shift in the intertropical convergence zone.

1 Introduction

The Dalton Minimum (DM) was a 60 year-long period of low solar activity, lasting from AD 1780 to 1840. In addition, early in the 19th century, two major volcanic eruptions took place, injecting large amounts of sulfur dioxide into the stratosphere, which, after conversion to sulfate aerosols, increased planetary albedo, affecting the global climate. In 1816, an exceptionally cold summer was recorded in Western

Europe. This year became known as the “year without summer” (Harington, 1992; Robock, 1994). While the scientific acceptance of a significant climate impact from volcanic eruptions is high, there is ongoing debate about the contribution of the solar variability to global temperature changes in the troposphere during the DM; see for example Table 2.11 of the IPCC AR4 (IPCC, 2007).

It is well known that solar activity varies over time. This is not only documented by the sunspot number data sets (Wolf, 1861), but also by the ^{10}Be cosmogenic isotopes conserved in ice sheets (Steinhilber et al., 2008, 2009). The past evolution of the solar irradiance has been reconstructed by a number of authors (see Solanki et al., 2013, and references therein). Recently, Shapiro et al. (2011) reconstructed the spectral solar irradiance (SSI) for the last 400 years using the solar modulation potential Φ as a proxy. Their results show that the decrease in the heavily absorbed UV-C during the DM reaches 15 %, while it does not exceed 1 % in the solar spectrum with $\lambda > 250\text{ nm}$ and is negligible in the solar near infrared (NIR). This disproportionate change in the spectral solar irradiance has complex effects on the Earth’s atmospheric chemistry and climate system: on one hand, a substantial decrease in the UV-C at $\lambda < 250\text{ nm}$ (0.3 W m^{-2}) cools down the middle atmosphere and decreases the ozone production due to decelerated oxygen photolysis (Anet et al., 2013), resulting in a very small radiation anomaly on the Earth’s surface. On the other hand, the decrease at $\lambda > 250\text{ nm}$ by 6.5 W m^{-2} does not affect stratospheric chemistry, but directly influences surface temperatures.

A negative UV-C anomaly affects the state of the stratosphere and mesosphere (Rozanov et al., 2012a; Anet et al., 2013), from where it may influence the troposphere via a cascade of mechanisms: by cooling down the tropical and mid-latitude stratosphere, it decreases the pole-to-equator temperature gradient, weakens the zonal winds and accelerates the Brewer–Dobson circulation. The latter is followed by a cooling in the lower tropical stratosphere (Kodera and Kuroda, 2002), and a subsequent modulation of the Hadley cell (Haigh, 1996) impacting especially the equatorial region and alteration of the tropospheric wave pattern (Brugnara et al., 2013), propagating down to the surface. This is also known as the top-down mechanism (Meehl et al., 2009). However, in the present set of simulations the top-down mechanism is shown to be of minor importance when compared with other mechanisms discussed below.

Complementary to the top-down mechanism is the “bottom-up” mechanism, which we investigate here by separating the role of solar irradiance at $\lambda > 250\text{ nm}$: as most of this radiation is able to pass through the stratosphere without major absorption, its anomalies directly impact the radiation fluxes, energy balance and temperatures on the ground. Depending on the surface albedo, a part of this radiation is absorbed and transformed into latent or sensible heat. During periods with weak solar activity, less radiation is available in the tropics for conversion to latent heat, which is thought

to lead to a decrease in the amount of precipitation (Meehl et al., 2008) and thus a weakening of the Ferrel and Hadley cells (Labitzke et al., 2002). Both mechanisms thus finally influence the atmospheric circulation, differentiable by the time at which and where they start to influence the atmosphere. Generally, one can say that the top-down effect essentially starts to influence polar regions in hemispheric winter time, whereas the bottom-up effect literally can influence especially tropical regions during the entire year.

Besides electromagnetic radiation, a second major factor varying over time and influencing stratospheric and upper tropospheric chemistry and – regionally – tropospheric dynamics is energetic particle precipitation (EPP). These particles consist of galactic cosmic rays (GCRs), solar energetic particles (SEPs), low energy electrons (LEE) originating from the magnetosphere and high energy electrons (HEE) stemming from the Earth’s radiation belt. While SEP and LEE/HEE vary in phase with the solar activity, GCRs are partly deflected by the solar wind, and therefore are negatively correlated with solar activity. Ionization of neutral molecules like N_2 or O_2 by energetic particles facilitates the formation of NO_x and HO_x (see, e.g., Sinnhuber et al., 2012), accelerating the ozone destruction followed by a cooling inside the polar vortex and an increase in pole-to-equator temperature gradients, which in turn can change the tropospheric climate. These processes were simulated by several chemistry–climate models (CCM) and a significant response of the atmosphere to EPP was identified (Calisto et al., 2011; Semeniuk et al., 2011; Rozanov et al., 2012b). However, in our previous study (Anet et al., 2013) the net effect of particles was found to be rather weak. This is seemingly contradictory, but can be partly explained by a compensating effect of decreasing LEE and increasing GCR intensity during the DM, which above-mentioned studies could not take into account because they either investigated only one sort of the energetic particles, or they compared model runs with all EPP included against a reference run without any EPP.

A third factor, which notably influenced the stratospheric and tropospheric climate and chemistry, at least for a short time in the DM, are major volcanic eruptions, which are known for having ejected up to 60 Mt (Tambora volcanic eruption, year 1815, Gao et al., 2008) of sulfur dioxide into the atmosphere. Presumably, the plumes reached deep into the stratosphere, where the massive amounts of sulfur dioxide were converted to sulfate aerosols. As a result, the haze in the sky and colorful sunsets were reported during the period (see, e.g., Olson et al., 2004). The aerosol particles efficiently scatter a fraction of the incoming solar radiation back into space, but also absorb a part of the outgoing terrestrial infrared (IR) and incoming solar near IR (NIR). The reduction in incoming visible or NIR radiation overwhelms the IR absorption, leading to an overall global cooling, except in the polar night, where sunlight is lacking and a small warming prevails (Robock, 2000). Generally, a significant cooling of the surface occurs in the first weeks after major

volcanic eruptions, lasting for one to two years and being associated with modified patterns of precipitation, surface pressure and the teleconnection patterns, such as the Arctic Oscillation (AO), North Atlantic Oscillation (NAO) (Shindell et al., 2000; Stenchikov et al., 2002; Fischer et al., 2007) or the El Niño–Southern Oscillation (ENSO) (Robock and Mao, 1995; Adams et al., 2003), due to the downward propagation of positive anomalies in the stratospheric polar vortex strength.

Different modeling studies in the recent past show a large range of simulated climate responses to solar forcings. For instance, Wagner and Zorita (2005) showed with an atmosphere–ocean general circulation model (AO-GCM) without coupled chemistry that the combined effects of volcanic eruptions and solar irradiance decrease could significantly (by up to several tenths of a degree) modify global mean temperatures. They attributed most of this cooling to the volcanic effects, and their “solar-only” simulation without volcanic eruptions showed a decrease in global temperatures of only 0.1 K. Feulner (2011) concluded from his experiment with an intermediate complexity model that the solar contribution to the cool period during the DM was likely a smaller one. They showed that the cold climate was explained mostly by volcanic forcing. Their application of the strong solar irradiance forcing proposed by Shapiro et al. (2011) led to a substantial disagreement between their simulated and reconstructed temperature time series. Shindell et al. (2000) compared the long-term influence of volcanic eruptions to grand solar minimum conditions with a focus on the DM and on the Maunder Minimum (MM) – which occurred about 150 yr before the DM. Unfortunately, the exact solar forcing used for their modeling study remains unknown, but they concluded that volcanic eruptions have rather strong but only short-lived effects on temperatures, while the reduction of the solar irradiance during the grand minimum affects temperatures on longer timescales. They estimated a solar-induced cooling during the MM of 0.6 to 0.8 K globally. For the same period, Varma et al. (2012) investigated the Southern Hemispheric wind field response to the MM solar irradiance decrease. They estimated the stratospheric ozone change due to the reduction of solar UV irradiance from a global scaling with total solar irradiance (TSI) variations, which could lead to a shift in the Southern Hemispheric westerly winds to the north via the “top-down” mechanism consisting of a chain of complex radiative–dynamical processes (Meehl et al., 2008; Haigh, 1996). In another paper, Varma et al. (2011) concluded that the “bottom-up” mechanism via a reduction of visible irradiance had a similar effect. However, these publications (Varma et al., 2011, 2012) do not provide detailed information on changes in tropospheric temperatures. Zanchettin et al. (2013) investigated the decadal response change of the 1815 Tambora volcanic eruption to different background climate states. They found a significant dependence on background conditions when

looking at ocean dynamics, especially concerning heat transport and sea ice in the North Atlantic region.

The influence of volcanic and solar forcing on ozone chemistry, stratospheric temperatures and global circulation has become of great scientific interest in the recent years. The aim of this work is to analyze the tropospheric climate changes during the DM with a fully coupled atmosphere–ocean chemistry–climate model (AO-CCM) driven by the state-of-the-art set of climate forcings and to disentangle the contributions from changes in solar spectral irradiance, energetic particles and volcanic eruptions. To the best of our knowledge so far, such a sophisticated model and climate forcing set have not been applied for the evaluation of the tropospheric climate changes during the DM.

The work is structured as follows: after Sect. 1, which has described the state of the research and introduced some notation, Sect. 2 will provide a description of our model and our experiments. Section 3 focuses on the changes in surface temperatures and precipitation patterns caused by the different forcings. We further compare our model results to reconstructed temperature fields, and conclude in Sect. 4.

2 Sensitivity experiments and model description

2.1 AO-CCM SOCOL3-MPIOM

The AO-CCM SOCOL3-MPIOM emerges from a modification of CCM SOCOL version 3 (Stenke et al., 2013), which has been coupled with the OASIS3 coupler (Valcke, 2013) to the Max Planck Institute ocean model (MPIOM, Marsland et al., 2003). SOCOL3 is based on the GCM ECHAM5 (Roeckner et al., 2003) and includes the chemical part of the MEZON chemistry–transport model (Rozañov et al., 1999; Egorova et al., 2003; Schraner et al., 2008). SOCOL3-MPIOM is applied in middle atmosphere mode (MA) extending from the ground to 0.01 hPa or around 80 km. Simultaneously with the radiation calculation, MA-ECHAM5 hands over temperature fields to MEZON, which takes into account interactions between 41 gas species – including 200 gas phase, 16 heterogeneous and 35 photolytic reactions. Those chemical fields are then handed back to MA-ECHAM5, which calculates all components of the general circulation and tracer advection.

All simulations have been executed using the model version with T31L39 resolution, which equals an average horizontal grid space of 3.75° (~400 km) and an irregularly spaced vertical resolution of 39 levels. Due to the relatively coarse vertical resolution, the quasi-biennial oscillation is not reproduced autonomously. Hence, the equatorial zonal wind fields are nudged to reconstructed zonal mean wind data sets as in Giorgetta (1996).

It is known that the original MA-ECHAM5 code does not properly take into account radiative absorption by oxygen, either in the Lyman-alpha line or in the Schumann–Runge

A.3. Impact of solar vs. volcanic activity variations on tropospheric temperatures and precipitation during the Dalton Minimum

924

J. G. Anet et al.: Sun and volcanoes: effect on the troposphere in the DM

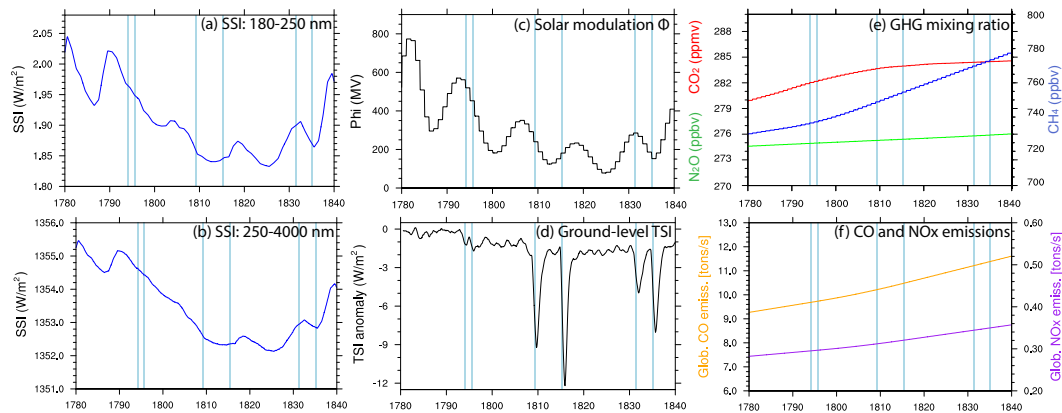


Fig. 1. Model forcing data over the Dalton Minimum (AD 1780–1840). **(a)** Spectral solar irradiance in the UV-C at $180\text{ nm} < \lambda < 250\text{ nm}$. **(b)** Spectral solar irradiance at $\lambda > 250\text{ nm}$. **(c)** Solar modulation potential following Steinhilber et al. (2008). **(d)** Ground-level TSI, showing anomalies relative to the 1780 unperturbed values. **(e)** Greenhouse gas mixing ratios for CO_2 , CH_4 and N_2O . **(f)** Anthropogenic and natural CO and NO_x emissions from fossil fuel burning. Blue vertical lines highlight the years in which a volcanic eruption occurred.

bands, and the absorption of ozone in the Hartley or Huggins bands is also only coarsely resolved (Forster et al., 2011). Hence, the heating rate calculation has been improved to add the missing parts following the approach of Egorova et al. (2004) adapted to the spectral resolution of the ECHAM5 radiation code. The parameterizations for the ionization rates by GCR, SEP and LEE were introduced identically as in Rozanov et al. (2012b) and Anet et al. (2013). HEE are not implemented due to the absence of an easily applicable parameterization.

The ocean is run in GR30 resolution (nominal resolution of around 3°). Its north pole is displaced to Greenland, making it possible to raise the resolution in the North Atlantic basin. The applied version of the AO-CCM SOCOL3-MPIOM and its performance in the representation of the climate evolution is presented by Muthers et al. (2014b).

2.2 Boundary conditions

The applied boundary conditions are described in detail by Anet et al. (2013). As a summary, the most important forcings are recapitulated subsequently.

The forcing caused by spectral solar irradiance changes is based on the mean values of the reconstruction by Shapiro et al. (2011), as illustrated in Fig. 1a and b. This determines the photolysis and heating rates due to solar irradiance absorption by various air components. Shapiro et al. (2011) assumed that the minimum state of the quiet Sun corresponds to the observed quietest area on the present Sun, and then used available long-term proxies of the solar activity (i.e., ^{10}Be isotope concentrations in ice cores, 22 year smoothed neutron monitor data) to interpolate between the present quiet Sun and the minimum state of the quiet Sun. This determines the long-term trend in the solar variability, onto which the

11 year activity cycle calculated from the sunspot number is then superposed. The time-dependent solar spectral irradiance is derived using the COSI state-of-the-art radiation code (Shapiro et al., 2010). The resulting spectral solar irradiance of this reconstruction is substantially lower during the MM than the one observed today, and the difference is larger than in the other recently published estimates. The advantage of this high-amplitude reconstruction is that it allows us to derive a maximum conceivable terrestrial climate response to solar changes, while other reconstructions leave hardly any fingerprint on the modeled climate.

For the EPPs, the A_p index reconstruction from Baumgaertner et al. (2009) is used for the LEE. For SEPs, return period-based data sets were created from an analysis of the last 45 years of the last century. The GCR ionization rates depend on the solar modulation potential Φ (Fig. 1c), which was reconstructed by Steinhilber et al. (2008). The geomagnetic dipole field strength and position are provided from paleomagnetic data sets from Finlay et al. (2010).

The volcanic forcing is based on simulations carried out with a 2-D aerosol microphysical model (Arfeuille et al., 2014). It uses total aerosol injection values from Gao et al. (2008) and information on the date/location of each eruption. The stratospheric aerosols are prescribed in terms of extinction ratios, single scattering albedos and asymmetry factors for each of the 22 ECHAM5 radiation bands and in terms of surface area densities, for each latitude–altitude band of SOCOL (zonally averaged). Aerosol optical depth values derived from this forcing are documented in Table 1. The globally averaged effect on incoming surface shortwave radiation is shown in Fig. 1d, and shows higher anomalies than that of Crowley (2000) or Robertson et al. (2001).

Table 1. Stratospheric aerosol optical depths at 550 nm derived from volcanic aerosol simulations (Arfeuille et al., 2014) using ice core measurements from Gao et al. (2008).

Year	Aerosol optical depth		Volcano, confirmed/tentative attrib.
	NH	SH	
1794	0.02	0.04	Unknown SH, no large eruption recorded
1796	0.12	0.02	Unknown NH, no large eruption recorded
1809	0.12	0.42	Unknown Tropics, eruption in February
1815	0.24	0.68	Tambora 8° S, Indonesia, 10 April
1831	0.22	0.06	Babuyan Claro 19.5° N, Philipp., date?
1835	0.36	0.23	Cosiguina 13° N, Nicaragua, 20 January

The QBO was generated by means of a backwards extension of an already existing reconstruction, using an idealized QBO cycle that is superimposed onto the regular seasonal cycle (Brönnimann et al., 2007).

The greenhouse gas forcings (Fig. 1e) for the period from 1780 to 1840 are based on the PMIP3 protocol (Etheridge et al., 1996, 1998; Ferretti et al., 2005; MacFarling-Meure et al., 2006; Meehl et al., 2009), while halogens are kept constant at preindustrial levels. The standard ECHAM5 land surface data sets by Hagemann et al. (1999) and Hagemann (2002) are used. Tropospheric aerosol fields were extracted from existing CAM3.5 simulations driven by CCSM3 (CMIP3) sea-surface temperatures and 1850–2000 CMIP5 emissions. These fields were then scaled as a function of the world population starting in the year 1850 going backwards, except for the 10 % (relative to the 1990 values) of biomass burning, which were considered constant over time.

For the global CO and NO_x emissions, the part emitted from shipping was calculated starting from the CMIP5 data sets, which were projected linearly backwards from 1850 on to the year 1800. Before 1800, no steamships existed, thus these emissions were set to zero. The natural biomass burning emissions were assumed to be constant over time, while the anthropogenic biomass burning emissions were scaled with the world population. The emissions are illustrated in Fig. 1f.

2.3 Sensitivity experiments

We performed six sensitivity experiments covering the time period from 1780 to 1840 (Table 2), each with three ensemble members. The simulations, identical to those described by Anet et al. (2013), were initialized from a long transient model run covering AD 1600–2100. The disturbances were introduced by starting the sensitivity study simulations from an ocean state one year “older” and one year “younger” than December 1779, as the time frames of December 1778, December 1779 and December 1780 provided a good mix between weak El Niño or La Niña conditions, avoiding extreme conditions in the oceanic signal (El Niño 3.4 indexes: −0.9 for December 1778, +0.8 for December 1779 and +0.6 for December 1780 of the “mother

Table 2. Dalton minimum experiments: “const” denotes constant 1780 conditions. “bckgrd” denotes background aerosol emissions and volcanic emissions off. “trans” denotes transient forcing. “Ioniz.” stands for the parametrization for SPE, LEE and GCR.

Experiment name	Process			
	ΔI ($\lambda < 250$ nm)	ΔI ($\lambda > 250$ nm)	Δ Ioniz.	Δ SAD
CTRL1780	const	const	const	bckgrd
ALL	trans	trans	trans	trans
TD	trans	const	const	bckgrd
BU	const	trans	const	bckgrd
EPP	const	const	trans	bckgrd
VOLC	const	const	const	trans

run”). The nomenclature is as follows: the run including all effects acting together on the climate system is named ALL. The “Top-Down” (TD, Meehl et al., 2008) sensitivity experiment includes only the variations of solar irradiance with $\lambda < 250$ nm and the corresponding extra heating (corrections for the Lyman- α line, the Schumann–Runge, Hartley and Huggins bands) and photolysis rates of photolytic chemical reactions. The “Bottom-Up” (BU) experiment (Meehl et al., 2008) allows only irradiance $\lambda > 250$ nm to vary over time. The EPP experiment is exclusively forced by energetic particles. In the VOLC experiment, all other forcings except the stratospheric aerosols, which affect the radiation budget and heterogeneous chemistry via changes in surface area density (SAD), were kept constant. All runs were compared to a 60 year-long control run with three ensemble members with perpetual 1780 conditions called CTRL1780. The analysis of the data was done by comparing zonally and temporally averaged ensemble mean fields to the CTRL1780 ensemble mean.

In order to focus on the strongest signals (and following Anet et al., 2013), the period from 1805 to 1825 is chosen for the temperature, precipitation and mass stream function analysis showing regional patterns on latitude–longitude or latitude–height plots, thus reducing the signal-to-noise ratio. Time evolution plots of the temperatures and ocean heat content show ensemble means of the entire simulation period. Oceanic as well as surface temperature data have been smoothed with an 12 month full width–half maximum (FWHM) Gaussian filter. The statistical significance of the global distribution of the 2 m temperature anomalies was computed using a 2-sample Student’s *t* test across all $3 \times 20 = 60$ data points, as was done in Anet et al. (2013) on a 5 % significance level, taking autocorrelation into account. The latter was done by calculating the number of independent data points over the 3×20 time steps. The statistical analysis of the hydrological cycle was done similarly, with the exception that the significance level was set to 10 % (surface temperature volcanic anomalies, precipitation, mass stream function).

3 Results

First, we discuss regional temperature differences between the specific sensitivity experiment and the CTRL1780 experiment averaged over the AD 1805–1825 period. Then we present the contribution of different forcing factors to the evolution of the mean surface temperature and ocean heat content during the entire integration period. Finally, changes in the precipitation are described in Sect. 3.3.

3.1 Temperature

The regional pattern of the annual mean 2 m temperature difference between the ALL and the CTRL1780 simulation is illustrated in Fig. 2a. In particular, the tropical and subtropical regions undergo a significant cooling by values ranging from 0.2 to 1 K. The cooling is more pronounced over the land masses than over the oceans. Three small positive temperature anomalies appear over the Bering Sea, the western Antarctic, and over the northern Atlantic regions. Significant deviations from the annual mean figure are a strong cooling during Northern Hemispheric (NH) winter over Siberia and Alaska, as well as the significant warming during polar winter over the respective polar hemisphere (Fig. S1 in the Supplement).

The cooling of the continents can be explained by the BU experiment shown in Fig. 2b, which simulates cooling patterns similar to the ALL ensemble mean, except over northern Asia and parts of Europe. The cooling is caused by the negative anomaly in solar irradiance at wavelengths $\lambda > 250$ nm and subsequently by a reduced heating of the surface. The weaker ocean response is related to the large heat capacity of the ocean, partly compensating the reduced irradiance.

The slight warm anomalies over the Bering Sea and western Antarctic Peninsula regions can be explained with the VOLC simulation (Fig. 2c). The warming pattern over the Bering Sea region, triggered by ocean upwelling (see later) is present during the whole year. In the western Antarctic Peninsula and North Atlantic regions, the patterns are predominant during the SH winter season (JJA). The western Antarctic Peninsula warming is associated with an enhanced transport of milder air masses from the subtropics, leading to a slight but significant sea ice melting (not shown). This is related to differential temperature anomalies from absorption and/or reflection of radiation by the volcanic aerosols, as shown in Anet et al. (2013). The major warming over the Bering Sea originates from a strengthening of the northward surface winds inducing a positive meridional wind stress anomaly above the northwestern Pacific and the opposite – namely a weakening of the northward surface winds inducing a negative anomaly of the meridional wind stress – in the northeastern Pacific region (not shown). This facilitates ocean upwelling via the Ekman mechanism in this region, where deep water upwelling prevails (oceanic conveyor belt).

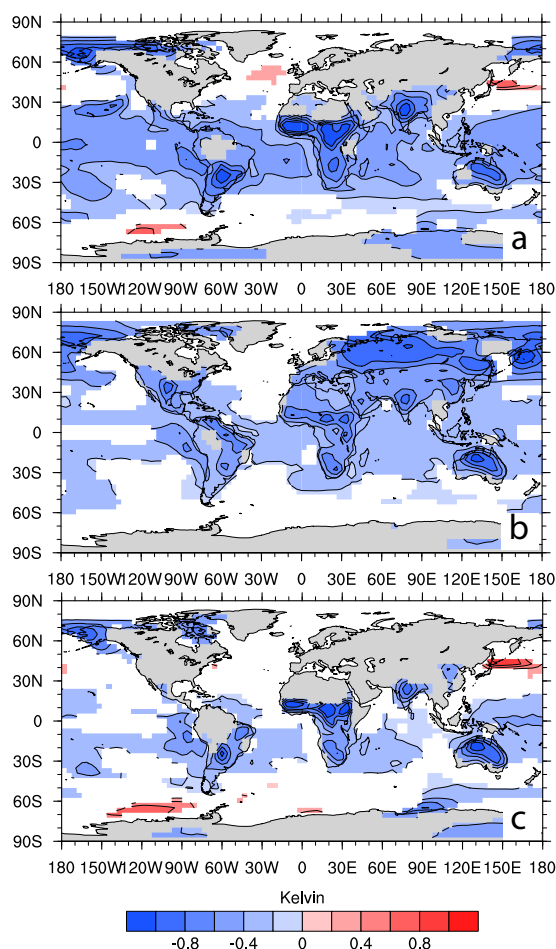


Fig. 2. (a) Ensemble mean of 2 m temperature differences, averaged over the 1805–1825 period for the ALL run. (b) Same for the “Bottom-Up” run. (c) Same for the VOLC run. Only areas that are significant at the 5 % level are colored (two-sided t test).

The surface water of the northern Bering Sea region, cooling down during the winter season, is replaced by deeper, older water from the thermocline region, which has no imprint of the volcanic signal yet, as indicated by a slight increase in the modeled vertical ocean mass transport in the winter season in that region. The warming signal is so strong that it persists throughout the year. The same warm anomaly was also found by Wang et al. (2012), which explained the finding by weakening surface westerly winds due to a strengthening polar vortex. Forming a positive surface pressure anomaly, net heat fluxes and ocean advection in the Northern Pacific region are modified. Although corroborative, these results should be confirmed by using a higher number of ensemble members to ensure its robustness, which would go beyond the scope

of this work. Both the BU and the VOLC simulations show a slight but not significant warming over the North Atlantic. One might speculate that the warming pattern shown in ALL results from a combination of volcanic and solar influences, although certain nonlinearities prohibit the direct comparison of BU+VOLC and ALL, as was already shown in Anet et al. (2013). Moreover, as illustrated in Fig. S2 in the Supplement, the response in the AMOC is relatively weak in BU, while a distinct increase in the AMOC is visible in VOLC. This finding agrees well with the work of Zanchettin et al. (2013), which finds a significant increase of 0.6 Sv in the AMOC after Tabora, while we find a significant increase of up to 1 Sv after both volcanic eruptions (beginning of the 1820s minus the pre-volcanic era). We do not find any additive effect of both eruptions, which could mean that a certain saturation effect might stop the acceleration of the AMOC. This finding however should be investigated in more detail in a future work.

The TD experiment does not reveal any statistically significant temperature anomalies either in the yearly or in the seasonal means (not shown). The EPP forcing does not produce any annual mean response; however, a strong winter warming pattern is simulated during the boreal winter over the northern polar regions (see Fig. S3 in the Supplement). The temperature response for the EPP case is much weaker and appears in a completely different location than in the previous studies (e.g., Calisto et al., 2011; Rozanov et al., 2012b). This can be explained by the fact that our EPP experiment is designed in a significantly different way: while in Calisto et al. (2011) and Rozanov et al. (2012b), the sensitivity study was done by comparing a simulation with enabled EPP parameterization to a simulation with disabled EPP parameterization, we compare a simulation with transient EPP to a simulation with constant 1780 EPP forcing. Hence the decreasing SEP and LEE ionization rates might compensate for the effect of increasing GCRs.

Compared to the climate simulations of Calisto et al. (2011) or Rozanov et al. (2012b), the lower amplitude of the simulated anomalies is attributed to a different stratosphere–troposphere coupling behavior from SOCOL3-MPIOM, whose atmospheric transport model is based on ECHAM5, compared to SOCOL2, based on ECHAM4. Especially the winter polar vortex represents a key factor determining how stratospheric influences can propagate down into the troposphere. Stratospherically induced disturbances in the polar vortex may lead to short-lived vortex breakdowns, facilitating the advection of warmer air masses from the mid-latitudes into higher latitudes at the surface. There, surface warm anomalies are the consequence. In both the before-mentioned works, strong warm 2 m temperature anomalies were found during the winter season over Europe and western Asia. This finding cannot be confirmed with our modeling results, which show a small, but significant warming over the polar region. The exact reason of this different behavior has not yet been found, but it may originate in the weaker

winter vortex in SOCOL3-MPIOM. Muthers et al. (2014a) showed that the downward propagation depends on the state of the polar vortex and can be underrepresented if the polar vortex is too weak. The deficiency is confirmed by the lack of any significant temperature response to the TD and EPP signal over Europe – which could possibly be improved by modifying the gravity wave parameterization in ECHAM5.

In agreement with Robock and Mao (1992), Kirchner et al. (1999), and Driscoll et al. (2012), or with the DM analysis of Fischer et al. (2007), we discern a slight, yet significant winter warming pattern (WWP) over Europe, Russia and parts of North America in the years following the volcanic eruptions (Fig. 3b) and a weak cool anomaly during the summer seasons following the volcanic eruptions (Fig. 3a). The signal most probably due to a too weak representation of the top-down mechanism during volcanic eruptions is weaker than in the aforementioned studies. The warming in DJF is caused by a slight shift of the NAO to a NAOplus-like phase, enhancing the mid-latitude westerlies (see Fig. 3d) and influencing the precipitation patterns (see later). The axis of the NAO pattern is slightly tilted counterclockwise (see climatology in Fig. S4 in the Supplement).

We now focus on the temporal evolution of the temperature anomalies during the DM (Fig. 4). For these illustrations, values of the CTRL1780 experiment were subtracted from the ALL, VOLC and BU time series. The internal variability of CTRL1780 is relatively small (σ global, annual ensemble mean (AEM)=0.095 K, σ NH AEM=0.154 K, σ SH AEM=0.099 K).

Compared to CTRL1780 the ALL experiment (Fig. 4a) shows a significant decrease in global mean temperatures starting in 1809. After the temperature minimum following the Tabora eruption (1815), the modeled temperatures show a slight recovery, but do not completely reach unperturbed conditions. After 1830, a second decrease in temperatures follows. We note that before 1809, all experiments show a very similar temperature evolution and that the strong volcanic eruptions (1809, 1815, 1831 and 1835) cause a clear excursion to low temperatures. These signals are clearly visible in the ocean heat content (Fig. 4b). Again, four short-term reductions in the ALL run can be recognized after the volcanic eruptions, however, with a delay of 2 to 4 years due to the thermal inertia of the ocean. Until 1830 the SH mean temperature evolution (Fig. 4c) is very similar to the global mean. However, the volcanic eruptions after 1830 have a smaller influence on SH temperatures, as the Babuyan Claro (1831) and Cosiguina (1835) eruptions are of a smaller size than the 1809 and 1815 eruptions and are also characterized by a higher aerosol loading in the NH than in the SH. Due to the smaller direct aerosol forcing and to the much higher internal variability of the climate system in the NH than in the SH, the cooling signal after 1809 is far more difficult to recognize in Fig. 4d. However, a significant decrease in temperatures of the ALL experiment is simulated after 1815 as well as a second dip to lower temperatures drop after 1830.

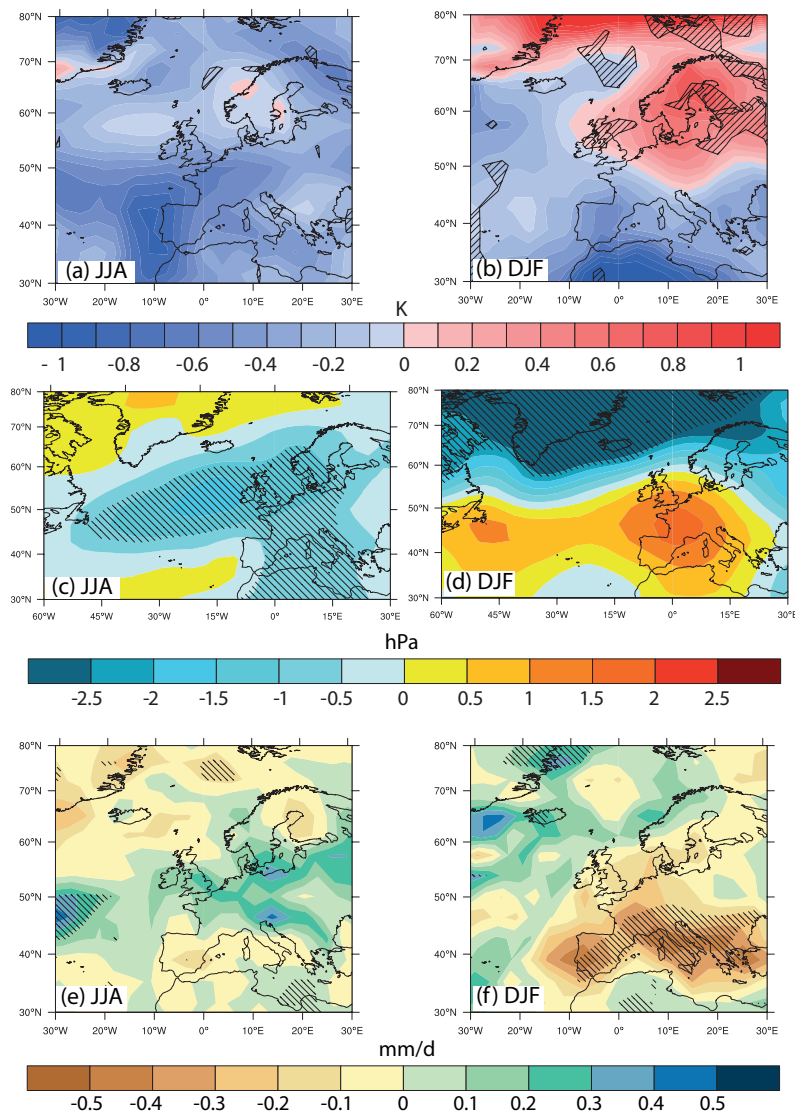


Fig. 3. Ensemble mean of post-volcanic surface temperature (a, b), sea level pressure (c, d) and precipitation (e, f) anomalies, showing the difference between VOLC (4 years: 1810, 1816, 1832 and 1836) and CTRL1780 ($3 \times 60 = 180$ years) in the JJA (left panels) and DJF (right panels) season. For all plots, dashed areas show significant changes in a 10% t test (two-sided t test).

The cooling after 1809 can be partially explained by the volcanic eruptions of 1809, 1815, 1831 and 1835. The green curve in Fig. 4a and b of the VOLC experiment shows negative excursions at exactly those years. However, a clear recovery to pre-1809 temperatures is simulated after 1817. The next decrease in temperatures appears only after the 1831 volcanic eruption. Focusing on the volcanic response a clear inter-hemispheric difference is found: while in the SH, especially the 1809 and 1815 volcanic eruptions are well

visible; the NH seems to be more responsive to the 1831 and 1835 volcanic eruptions. This is consistent with the different stratospheric aerosol loading. The temperature increases in the NH from 1813 to 1820 back to unperturbed temperature levels – and even positive anomalies in the 1820s – represent a supercompensation-like feature simulated by our model after each strong volcanic eruption. As will be shown later, this warm anomaly pattern is caused by oceanic influence, a finding that agrees with a similar study by Zanchettin et al.

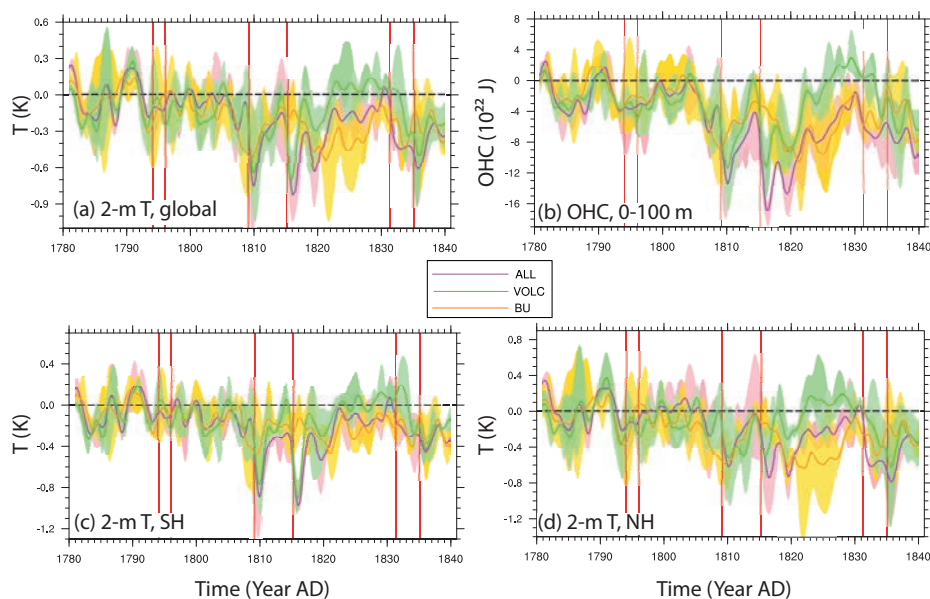


Fig. 4. (a) Ensemble means of detrended anomalies of experiments ALL, VOLC and BU relative to CTRL1780 for (a) global 2 m temperatures; (b) global ocean heat content (OHC) of the upper ocean (first 100 m in depth); (c) SH 2 m temperatures; (d) NH 2 m temperatures. For all experiments, the envelope shows the min/max values. Red vertical lines highlight the years in which a volcanic eruption occurred.

(2012). The short-term warming right after preindustrial volcanic eruptions can be explained by a small, but significant increase in tropospheric ozone concentrations after the volcanic eruptions, acting as a greenhouse gas. This increase in ozone is related to a reduction in the production rate (less radiation, less water vapor) of the hydroxyl radical OH, which is a very efficient factor in the ozone destruction. This increase is especially pronounced over the NH due to larger CO concentrations.

In order to explain the rather low temperatures of ALL between 1817 and 1830, an additional mechanism to the volcanic eruptions only has to be considered: the BU ensemble mean in Fig. 4a and b describes a negative anomaly in temperatures and OHC from 1808 on. Those below-normal conditions persist until the year 1839, and are by far stronger in the NH (Fig. 4d) than in the SH (Fig. 4c) due to a greater number of land masses. Our model results even suggest an unprecedented cool period in the NH in the 1820s following the BU scenario. This period would even have been colder than the simulated and reconstructed (see later) post-Tambora era (1816–1818), hence pointing to the importance of the volcanic eruptions during the DM, which interfered with the solar-only forcing effects.

In the ocean, a downward propagation of the signal from shallow to more deep layers is illustrated in Fig. 5a–c. While neither radiation with $\lambda < 250$ nm nor EPP (Fig. S5 in the Supplement) seems to influence the ocean heat content significantly on any level, the radiation with $\lambda > 250$ nm

(Fig. 5b) and volcanic (Fig. 5c) signals propagate down to deeper ocean layers. In Fig. 5a, we note that while the upper layers (green curves) still show a small recovery after the volcanic eruptions, taking around 5–8 years, there is no signal of recovery in the deep ocean (black curves) during the DM period. Moreover, on one hand, the bottom-up signal (Fig. 5b) takes more time to influence the ocean heat content in deeper layers than the volcanic eruptions (Fig. 5c), which is due to the lower net irradiance anomaly in the solar forcing than in the volcanic forcing. On the other hand, the BU signal among all layers is more persistent than the volcanic imprint due to the lack of “peaks” of activity. Still, the BU scenario is only the second strongest contributor to changes in the deep-layer ocean heat content, ranging behind the volcanic eruptions. One should note especially that while the uppermost layers of the VOLC experiment recover quite quickly (Fig. 5c, green curve), the signal stays memorized in the ocean, being rapidly transported into deeper layers (Fig. 5c, black curve).

Globally, a superrecovery of OHC during the 1820s is simulated for the VOLC experiment: this positive anomaly can be explained when focusing on the Bering Sea region (Fig. 5d), which can explain more than half of the global ocean heat content increase by the volcanic contribution.

Stenchikov et al. (2009) also investigated the influence of the Tambora eruption on the ocean. For all layers our simulated OHC anomaly is more pronounced, which can be explained by the lack of the 1809 volcanic eruption in the work of Stenchikov et al. (2009), but also by the fact that

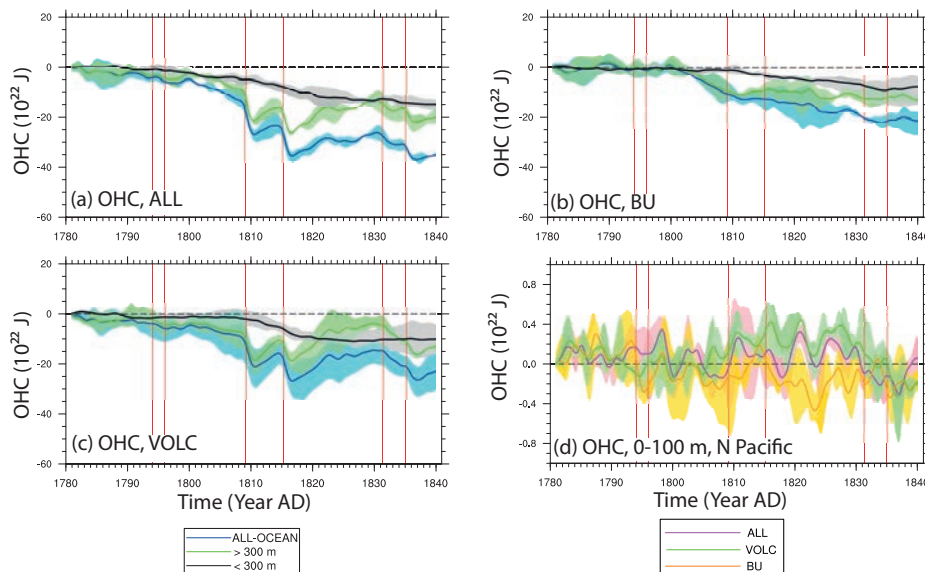


Fig. 5. Ensemble mean of detrended global ocean heat content (OHC) anomalies relative to CTRL1780, plotting technique analog to Stenchikov et al. (2009). For (a)–(c) the black curve shows global total OHC (0–6020 m), the green curve global OHC of the top 300 m, the blue curve global OHC of the layers below 300 m (300–6020 m). (a) For ALL; (b) BU; (c) VOLC. (d) Ensemble mean of local OHC anomalies relative to CTRL1780 for the layers between 0 and 100 m in depth for the northern Pacific, Bering Sea region. Envelope shows the min/max values. Red vertical lines highlight the years in which a volcanic eruption occurred.

the Tambora eruption in our study has a larger radiative impact on the SH (and thus on the oceans) than in Stenchikov et al. (2009). The half-lives of the signals, however, are comparable to each other (Stenchikov et al., 2009: 16 years for 0.5 times the total OHC recovery. VOLC-experiment: 13 years needed for 0.45 times the total OHC recovery). The imprint of the lower OHC of Stenchikov et al. (2009) seems, however, to be much smaller than ours (10×10^{22} J versus 5.5×10^{22} J), even if one would subtract the effect of the 1809 volcano in our sensitivity study. A possible explanation would be a faster deep water formation in MPI-OM than in CM2.1. This goes however beyond the scope of this work.

As neither the EPP nor the TD curves show large significant changes in the OHC (Fig. S5 in the Supplement), we conclude that although volcanic eruptions most likely kicked off the colder DM period, it was the reduction in the radiation with $\lambda > 250$ nm that maintained the low temperatures until the late 1830s.

3.2 Comparison to proxies

Back in the past, regular reliable temperature measurements were only done in some specific locations, especially in Europe, with some station records starting around 1750 (Jones et al., 2001). Further back, one has to rely on proxy-based reconstructions. Different techniques and sources for 2 m temperature reconstructions are available, and the absolute

values and variability amplitudes differ considerably from one to another data set. Most of the proxy data originate from tree rings. Not all techniques of tree ring-based (also known as “dendrochronological”) temperature reconstructions are generally accepted by the scientific community (e.g., Cecile et al., 2013). Furthermore, there is an ongoing discussion if dendrochronological proxies are at all a good basis for robust reconstructions of temperature anomalies during volcanic active periods (e.g., Tambora, 1815–1816, see also Mann et al., 2012; Anchukaitis et al., 2012). Moreover, the exact dating may not always be accurate enough to match exactly a specific (e.g., volcanic) event due to proximity effects (“wrong” exposition of the tree in that particular year, e.g., in the shade). Here, we use the best-known NH temperature reconstructions published in the IPCC (2007), in order to allow comparison with other, similar modeling studies (e.g., Wagner and Zorita, 2005). We focus on NH temperature reconstructions since the density of proxy data is higher over the NH than over the SH and, therefore, NH data are expected to be more reliable. In Fig. S4 in the Supplement, the five different reconstructions of the NH temperatures used in this work are illustrated (Jones et al., 2001; Esper et al., 2002; D’Arrigo et al., 2006; Briffa et al., 2001; Mann et al., 1999).

In Fig. 6, the temperature evolution of the NH 2 m temperatures of the ALL, VOLC and BU experiments is compared to reconstructions, represented by a grey envelope. ENSO events monitored by the Niño 3.4 index are not shown. Yet, it

still should be stated that most (over 70 %) of the events differ from one sensitivity experiment to another with a time lapse of ± 1 year. However, in the periods of interest, which are discussed later in this section, the ENSO events of BU and VOLC happened at \pm the same period. The general anomaly pattern shown for the ALL experiment, which shows positive anomalies until the beginning of the 19th century, followed by a strong cooling between 1810 and 1820, a warmer period in the 1820s and a further temperature minimum around 1835 agree very well with the reconstructed temperatures.

The first 30 years of the ALL time series are characterized by a slight temperature decrease, overlain by the 11-year solar cycle. As obvious from the sensitivity run BU, the temperatures follow the decline in solar irradiance of the Shapiro et al. (2011) forcing (Fig. 6, top panel). The cooling after the two smaller volcanic eruptions in the 1790s overcompensates the pure solar signal. While most of the reconstructions also show a 11 year-like cycle (Fig. S6 in the Supplement), the dating of the minima and maxima differs among the data sets, leading to a rather diffuse picture.

Starting from around 1805 until 1816 both the reconstructions and the modeled temperatures show a strong cooling by up to 0.6 K. During that period, the ALL experiment is in very good agreement with the composite of the reconstructions, although a slight overestimation of the 1809 volcanic induced cooling in 1811–1812 is visible. After the two major volcanic eruptions in 1809 and 1815, the temperatures in the ALL experiment show a clear recovery until the year 1826. A very similar behavior is observed in the reconstructions, although the warming in the 1820s is stronger than in the ALL simulation. As can be seen from the BU and VOLC sensitivity runs, the simulated temperature behavior can be explained as a combination of solar and volcanic effects: the BU experiment shows that the solar-only driven cooling starts already around 1803, but the overall cooling is slightly postponed by a compensating warming by the earlier volcanic eruptions. The eruption of Mt. Tambora in 1815 overcompensates the solar-induced warming after 1810, leading to a temperature minimum around 1816/1817, while the solar minimum around 1822 (BU) prevents a more pronounced warming during the 1820s, as visible in the VOLC model experiment.

The two volcanic eruptions of 1831 and 1835 with a predominant NH aerosol loading are followed by a second pronounced cold period, which is visible in the model simulations as well as in the reconstructions. Also, the simulated amplitude of this cooling, at 0.3–0.4 K, is similar to the reconstructions.

Finally, the model simulation shows a recovery from the cold anomaly after 1836, which can be explained by a general increase in solar irradiance at the end of the DM as well as dilution and removal of volcanic aerosols in the stratosphere. The warming is also found in the reconstructions.

It should be mentioned that the separation of solar and volcanic effects as done in BU and VOLC neglects non-linear feedbacks. Nevertheless, we conclude that only the

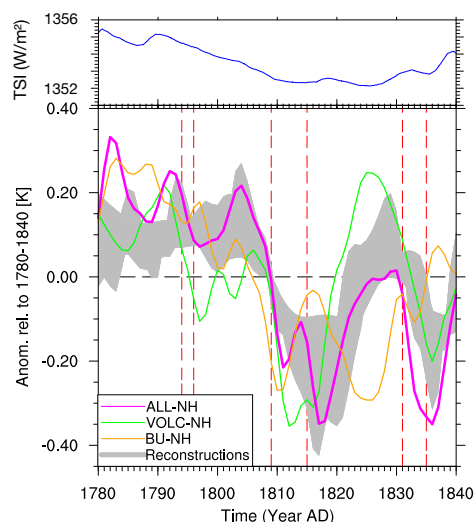


Fig. 6. Top panel: total solar irradiance from the Shapiro et al. (2011) forcing. Lower panel: model comparison with five NH temperature reconstructions of the IPCC AR4 (averaged). Magenta, green and orange lines are model curves, the grey envelope the composite of a range of tree ring-based reconstructions. Magenta thick: ensemble mean of NH temperatures (ALL-NH). Green: same, but for the VOLC experiment (VOLC-NH). Orange: same, but for the BU experiment (BU-NH). Grey region: envelope of the five NH temperature reconstructions plotted in Fig. S2 in the Supplement. Smoothing of the model results: Gaussian 3 years FWHM, centered on year 1. Red vertical dashed lines highlight the years in which a volcanic eruption occurred.

combination of both volcanic events and BU decrease is able to reproduce the reconstructed temperature patterns. Moreover, we suggest that a solar-only driven DM would have induced two cold periods in the 1810s and 1820s. Those were overcompensated by a strong VOLC warming signal in the ALL temperature pattern.

3.3 Precipitation and tropospheric circulation

Figure 7 illustrates the absolute difference in seasonal averaged precipitation (JJA and DJF) for the ALL and VOLC run relative to the CTRL1780 constant forcing run. As can be recognized, the intertropical convergence zone (ITCZ) is shifted northwards to the equatorial Atlantic. Furthermore, a sharp decrease in precipitation both during the boreal summer and winter is modeled over the Pacific warm pool region, eastern Central America, and the maritime continent.

An interesting feature is the strong increase in precipitation over the Himalayan region as well as over the eastern part of the Indian Ocean. The surplus of precipitation in the Himalayan region is due to an increased northeasterly flow, coming from a northward shift of the ITCZ. In contrast, the precipitation anomaly over the western Pacific is related to

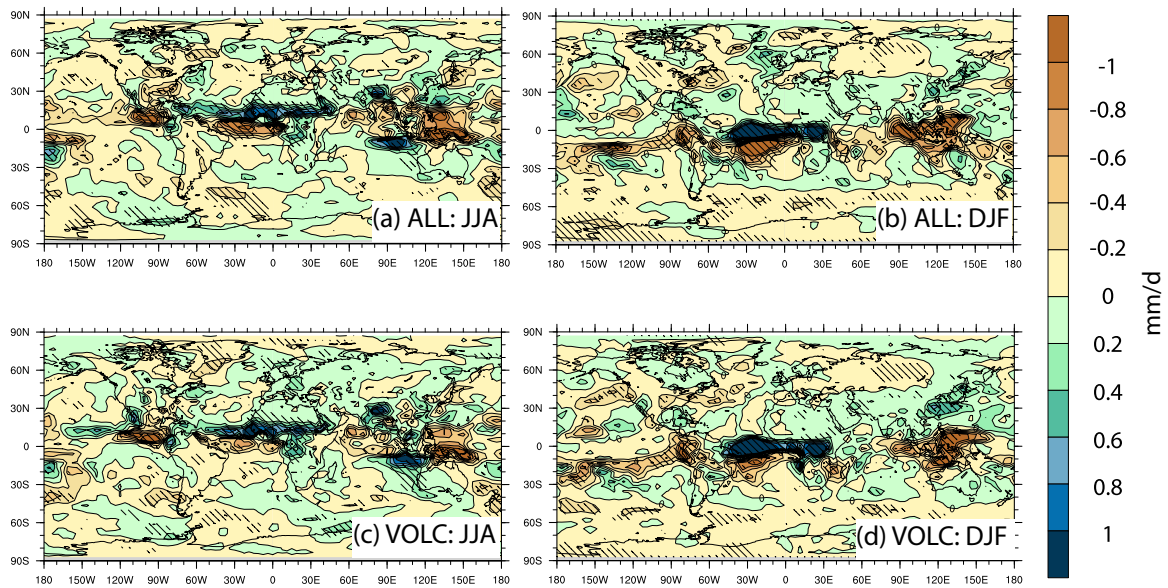


Fig. 7. (a) Ensemble mean of precipitation anomalies, averaged over the 1805–1825 period for the ALL run, JJA season. (b) Same for the DJF season. (c) Same for the VOLC run, JJA season. (d) Same for the VOLC run, DJF season. For all plots, dashed areas show significant changes in a 10 % *t* test.

a decrease in sea surface temperatures in the El Niño 3 region, which is consistent with reduced evaporation, modified circulation and significant change in the ENSO signal, also impacting – via the atmosphere the precipitation patterns in the Indopacific region – corresponding to the mechanism presented in McGregor and Timmermann (2011). The decomposition of the ALL forcing plot into the four different forcing factors (EPP, $\lambda < 250$ nm, $\lambda > 250$ nm and VOLC) shows that neither the solar forcing ($\lambda < 250$ nm, $\lambda > 250$ nm) nor the energetic particles significantly influence the seasonal or annual precipitation patterns. Hence, only the volcanic run is illustrated here (Fig. 7c and d) as it is the only run that shows a very similar precipitation anomaly pattern as in the ALL run.

A possible explanation for those precipitation anomalies lies both in the modified strength and width of the Hadley and Ferrel cells. In Fig. 8, the mass stream function (MSF) anomalies of the ALL and VOLC runs with respect to the CTRL1780 run are illustrated. During the boreal summer season (JJA), the upper branch of the Hadley cell is significantly weakened (Fig. 8a) – most probably due to the volcanic eruptions (Fig. 8c). Moreover, the Hadley cell expands in a northward direction (sharp decrease in the MSF field in Fig. 8a and c at 20° N, meaning that the background climatology illustrated as contour lines would expand towards the NH). During the winter season (DJF), we find a significant weakening of the Hadley cell (Fig. 8b and d) and a weak yet significant decrease in the Southern Hemispheric Ferrel cell.

The sizes of the cells are not significantly modified during the boreal summer season.

A similar signal has been found in Wegmann et al. (2013), who investigated the temperature and precipitation patterns after volcanic eruptions in preindustrial times. They concluded that a changed monsoon pattern and a modified behavior of the tropospheric circulation cells right after the volcanic eruptions is able to modify the global circulation, influencing short-term (some years) climate patterns over continental Europe. Although our seasonal precipitation signal is rather weak over Europe, we investigate the short-term climate pattern changes right after the different tropical volcanic eruptions (1810, 1816, 1832, 1836). Over Europe, the boreal winter SLP field (Fig. 3d) seems to switch to a more NAOplus-like situation, facilitating the transport of moist air from the Atlantic to the British islands and further to Scandinavia, while continental Europe stays in the slight influence of the anticyclonic pattern of the Azores. This NAOplus-like pattern influences the precipitation distribution, triggering a significant decrease over continental Europe and a slight increase over the British islands (Fig. 3f). The temperatures do change as well (Fig. 3b), but only marginally over continental Northern Europe, and show a slightly positive anomaly, according to the known “winter warming pattern” (see, e.g., Robock and Mao, 1992; Kirchner et al., 1999; Luterbacher et al., 2004). These results are in agreement to the work of, e.g., Iles et al. (2013), which found dryer winters and wetter summers after volcanic eruptions, as we do. During the

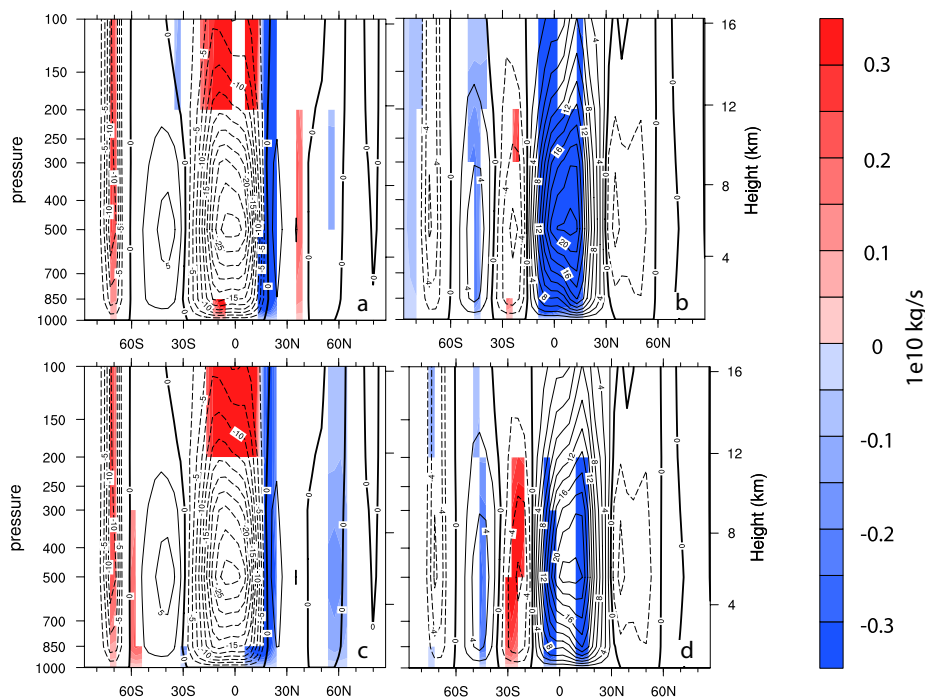


Fig. 8. (a) Ensemble mean of mass stream function anomalies, averaged over the 1805–1825 period for the ALL run, JJA season. (b) Same for the DJF season. (c) Same, but for the VOLC run, JJA season. (d) Same, but for the VOLC run, DJF season. For all plots, colored areas show significant changes in a 10 % t test. Black contour lines show the climatology for the two seasons.

summer seasons following strong volcanic eruptions, a cold anomaly signal is found (Fig. 3a), which is likely to be triggered by a significant low-pressure anomaly over continental Europe and the storm track region (Fig. 3c), leading to a signal resembling a wet anomaly over large parts of Europe (Fig. 3e).

4 Conclusions

We have performed a series of sensitivity experiments over the DM with an AO-CCM, varying successively the solar radiation with $\lambda < 250$ nm, the solar radiation with $\lambda > 250$ nm, volcanic aerosols and energetic particles.

The results show that volcanic eruptions alone cannot explain the long-lasting negative surface air temperature anomaly during the DM found in different NH temperature reconstructions. Yet, while the long-term negative temperature trend in the DM can be explained by the “bottom-up” approach when reducing only radiation with $\lambda > 250$ nm, the latter cannot explain the short and strong temperatures dips right after the volcanic eruptions. On the other hand, the volcanic eruptions experiment exaggerates the recovery of the surface temperatures in the 1820s.

We thus conclude that volcanic eruptions might have triggered the cold period from 1809 on, but that this cold time was maintained after 1816 by a lower solar irradiance. Without the decrease in solar irradiance, our model suggests that temperatures would have recovered to pre-1809 temperatures from 1820 on, except in the deep-layer ocean, in which the volcanic signal seems to dominate over the solar signal.

The obtained results indicate that the strong solar irradiance changes suggested by Shapiro et al. (2011) do not cause unrealistically large surface temperature changes during the DM, but rather help to reach a good agreement between simulated and reconstructed temperatures. This result contradicts the conclusions of Feulner (2011), which found a very large disagreement between surface temperature reconstructions and their model simulations using the solar irradiance forcing from Shapiro et al. (2011). The differences between the two studies do not arise from the selected reconstructions. Muthers et al. (2014b) compared the temperature evolution of all our four transient simulation members (1600–2000) against the Frank et al. (2010) reconstructions used by Feulner (2011), and it is clear that even if all the reconstructions of Frank et al. (2010) would have been plotted in our Fig. 6, it would not have significantly changed the overall picture. One possible explanation for this

discrepancy between the two studies is the complexity of the applied models. While Feulner (2011) used an earth system model of intermediate complexity, this study uses a much more interactive atmosphere–ocean chemistry model of high complexity.

Our model results suggest moreover that, without the two strong 1809 and 1815 volcanic eruptions, the NH would have suffered a very cold period in the 1820s, possibly putting the majority of the Earth's inhabitants in a problematic situation. Only the “overcompensation” of the cold anomaly after 1816 by the VOLC scenario in the Bering Sea region seems to have prevented this solar-induced cool period.

Our sensitivity studies show that the solar influence on the tropospheric climate is related to the bottom–up mechanism, while the efficiency of the top–down mechanism is negligible. We do not see any significant manifestations of the top–down mechanism (cooling in the lower tropical stratosphere (Anet et al., 2013), modulation of the Hadley cell and surface temperature changes in the Northern Hemisphere during boreal winter). Moreover, the simulated wintertime warming over the northern land masses after the major volcanic eruptions is not well pronounced and only marginally significant. The reasons for the weak efficiency of the top–down mechanism in our results are not clear. It can be related to model deficiencies in the simulation of the vertical coupling, of the polar vortex state or the wave generation and propagation, which become especially apparent when looking at the weak TD/EPP response. For example, Muthers et al. (2014a) showed that the efficiency of the top–down mechanism depends strongly on the climatological state of the simulated polar vortex. Further analysis should be done to understand whether the simulated polar vortex during the DM is too weak or too strong. It is moreover very possible that an interactive ocean damps the top–down and winter warming signal disproportionately, so that the signal disappears in the rather high noise of the NH temperature signal. The underestimation of the solar UV irradiance changes suggested by Shapiro et al. (2011) in comparison with the latest satellite measurements (Ermolli et al., 2013) could also be a reason, because a stronger UV forcing can make the top–down mechanism more efficient (see, e.g., Ineson et al., 2011). The other unexpected result is the weak influence of energetic particles, which can be explained by the absence of ozone response to the effects of low-energy electrons discussed by Anet et al. (2013) and probably some compensation between enhanced ionization by GCR and depressed ionization by electrons and protons during the DM.

We also show that due to volcanic eruptions, the hydrological cycle can be perturbed as such to decelerate the Hadley and Ferrel cells for timescales of 1–3 years. At the same time, the NAO is pushed into a NAOplus-like phase in the winters following a volcanic eruption, leading to an increase in precipitation in northern Europe and a negative precipitation anomaly in southern Europe. Still, the precipitation

anomaly is weaker than in the other publications cited in our manuscript.

It is possible that our chosen timing in the volcanic forcing data (date of the year) of the 1809 and 1831 eruptions is wrong. This could of course influence the results discussed in the manuscript, as the timing (in the year) of the eruption determines in which hemisphere most of the volcanic aerosol will be transported. Moreover, characteristics of the stratospheric dynamics in the DM – such as the QBO, which was nudged in our model and in the volcanic forcing calculation – are only reconstructed, and not observed. Also here, a certain margin of uncertainty persists, possibly influencing our results. The anomalies in temperature and precipitation might be more significant, as only two months of difference in the volcanic eruption lead to different results (as stated and shown in, e.g., Kravitz and Robock, 2011; Toohey et al., 2011; Driscoll et al., 2012).

This is also a reason why the upwelling mechanism in the Bering Sea region leading to the overcompensation-like temperature signal after the strong volcanic eruptions should be considered with interest, but with care. A different timing of the eruptions might lead to a different reaction not only of the tropospheric circulation cells, but also of the ocean. Also, internal variability might be a reason for the simulated response of the Bering Sea region. Also, internal variability might influence the simulated response of the Bering Sea region: Zanchettin et al. (2013) showed that internal climate variability can strongly spread the simulated decadal climate response to a strong eruption, with individual realizations differing for up to 1 K in decadal NH temperature outputs during the first two decades after the 1815 Tambora eruption. A higher number of ensembles would consolidate our findings.

Future investigations should be done focusing on the downward propagation of the stratospheric perturbations in a model with prescribed sea surface temperatures versus a model with an interactive ocean. Future research should also investigate to what extent the impact of decreasing SEP/LEE efficiency can compensate for increasing GCR influences on regional temperature changes. The upwelling signal in the Bering Sea region should be confirmed with a different timing of the volcanic eruptions and another model setup. Moreover, the statistical testing procedures should be consolidated by increasing the number of ensemble members.

Supplementary material related to this article is available online at <http://www.clim-past.net/10/921/2014/cp-10-921-2014-supplement.zip>.

Acknowledgements. Support by the Swiss National Science Foundation under grant CRSII22-130642 (FUPSOL) is gratefully acknowledged. Moreover, we would like to acknowledge the NCL plotting tool (NCAR/CISL/VETS, 2012), which enabled

efficient and appealing visualization of the model data. E. Rozanov, A. I. Shapiro, and W. Schmutz thank COST Action ES1005 TOSCA (<http://www.tosca-cost.eu>) for the support and fruitful discussions. Many thanks go also to H. Wanner (Oeschger Centre for Climate Change Research, Bern) for the efficient, creative and enthusiastic discussions. This paper profited from discussions during the PAGES/FUPSOL Workshop in 2012. Finally, we would like to thank the two anonymous reviewers for their valuable comments and Eduardo Zorita for editing.

Edited by: E. Zorita

References

- Adams, J. B., Mann, M. E., and Ammann, C. M.: Proxy evidence for an El Niño-like response to volcanic forcing, *Nature*, 426, 274–278, doi:10.1038/nature02101, 2003.
- Anchukaitis, K. J., Breitenmoser, P., Briffa, K. R., Buchwal, A., Büntgen, U., Cook, E. R., D'Arrigo, R. D., Esper, J., Evans, M. N., Frank, D., Grudd, H., Gunnarson, B. E., Hughes, M. K., Kirilyanov, A., Korner, C., Krusic, P. J., Luckman, B., Melvin, T. M., Salzer, M. W., Shashkin, A. W., Timmreck, C., Vaganov, E. A., and Wilson, R. J. S.: Tree rings and volcanic cooling, *Nat. Geosci.*, 5, 836–837, doi:10.1038/ngeo1645, 2012.
- Anet, J. G., Muthers, S., Rozanov, E., Raible, C. C., Peter, T., Stenke, A., Shapiro, A. I., Beer, J., Steinhilber, F., Brönnimann, S., Arfeuille, F., Brugnara, Y., and Schmutz, W.: Forcing of stratospheric chemistry and dynamics during the Dalton Minimum, *Atmos. Chem. Phys.*, 13, 10951–10967, doi:10.5194/acp-13-10951-2013, 2013.
- Arfeuille, F., Weisenstein, D., Mack, H., Rozanov, E., Peter, T., and Brönnimann, S.: Volcanic forcing for climate modeling: a new microphysics-based data set covering years 1600–present, *Clim. Past*, 10, 359–375, doi:10.5194/cp-10-359-2014, 2014.
- Baumgaertner, A. J. G., Jöckel, P., and Brühl, C.: Energetic particle precipitation in ECHAM5/MESSy1 – Part 1: Downward transport of upper atmospheric NO_x produced by low energy electrons, *Atmos. Chem. Phys.*, 9, 2729–2740, doi:10.5194/acp-9-2729-2009, 2009.
- Briffa, K. R., Osborn, T. J., Schweingruber, F. H., Harris, I. C., Jones, P. D., Shiyatov, S. G., and Vaganov, E. A.: Low-frequency temperature variations from a northern tree ring density network, *J. Geophys. Res.*, 106, 2929–2941, doi:10.1029/2000JD900617, 2001.
- Brönnimann, S., Annis, J. L., Vogler, C., and Jones, P. D.: Reconstructing the quasi-biennial oscillation back to the early 1900s, *Geophys. Res. Lett.*, 34, L22805, doi:10.1029/2007GL031354, 2007.
- Brugnara, Y., Brönnimann, S., Luterbacher, J., and Rozanov, E.: Influence of the sunspot cycle on the Northern Hemisphere wintertime circulation from long upper-air data sets, *Atmos. Chem. Phys.*, 13, 6275–6288, doi:10.5194/acp-13-6275-2013, 2013.
- Calisto, M., Usoskin, I., Rozanov, E., and Peter, T.: Influence of Galactic Cosmic Rays on atmospheric composition and dynamics, *Atmos. Chem. Phys.*, 11, 4547–4556, doi:10.5194/acp-11-4547-2011, 2011.
- Cecile, J., Pagnutti, C., and Anand, M.: A likelihood perspective on tree-ring standardization: eliminating modern sample bias, *Clim. Past Discuss.*, 9, 4499–4551, doi:10.5194/cpd-9-4499-2013, 2013.
- Crowley, J.: Causes of climate change over the past 1000 years, *Science*, 289, 270–277, 2000.
- D'Arrigo, R., Wilson, R., and Jacoby, G.: On the long-term context for late twentieth century warming, *J. Geophys. Res.*, 111, D03103, doi:10.1029/2005JD006352, 2006.
- Driscoll, S., Bozzo, A., Gray, L. J., Robock, A., and Stenchikov, G.: Coupled Model Intercomparison Project 5 (CMIP5) simulations of climate following volcanic eruptions, *J. Geophys. Res.-Atmos.*, 117, D17105, doi:10.1029/2012JD017607, 2012.
- Egorova, T., Rozanov, E., Zubov, V., and Karol, I.: Model for Investigating Ozone Trends (MEZON), *Seria Fizika Atmosfery i Okeana*, 39, translated by MAIK “Nauka/Interperiodica” (Russia), *Izvestiia Akademii Nauk SSSR*, 39, 310–326, 2003.
- Egorova, T., Rozanov, E., Manzini, E., Haberleiter, M., Schmutz, W., Zubov, V., and Peter, T.: Chemical and dynamical response to the 11-year variability of the solar irradiance simulated with a chemistry-climate model, *Geophys. Res. Lett.*, 31, L06119, doi:10.1029/2003GL019294, 2004.
- Ermolli, I., Matthes, K., Dudok de Wit, T., Krivova, N. A., Tourpali, K., Weber, M., Unruh, Y. C., Gray, L., Langematz, U., Pilewskie, P., Rozanov, E., Schmutz, W., Shapiro, A., Solanki, S. K., and Woods, T. N.: Recent variability of the solar spectral irradiance and its impact on climate modelling, *Atmos. Chem. Phys.*, 13, 3945–3977, doi:10.5194/acp-13-3945-2013, 2013.
- Esper, J., Cook, E. R., and Schweingruber, F. H.: Low-frequency signals in long tree-ring chronologies for reconstructing past temperature variability, *Science*, 295, 2250–2253, doi:10.1126/science.1066208, 2002.
- Etheridge, D., Steele, L., Langenfelds, R., Francey, R., Barnola, J., and Morgan, V.: Natural and anthropogenic changes in atmospheric CO₂ over the last 1000 years from air in Antarctic ice and firm, *J. Geophys. Res.*, 101, 4115–4128, doi:10.1029/95JD03410, 1996.
- Etheridge, D. M., Steele, L. P., Francey, R. J., and Langenfelds, R. L.: Atmospheric methane between 1000 A.D. and present: Evidence of anthropogenic emissions and climatic variability, *J. Geophys. Res.*, 103, 15979–15993, doi:10.1029/98JD00923, 1998.
- Ferretti, D., Miller, J., White, J., Etheridge, D., Lassey, K., Lowe, D., Meure, C., Dreier, M., Trudinger, C., Van Ommen, T., and Langenfelds, R.: Unexpected changes to the global methane budget over the past 2000 years, *Science*, 309, 1714–1717, doi:10.1126/science.1115193, 2005.
- Feulner, G.: Are the most recent estimates for Maunder Minimum solar irradiance in agreement with temperature reconstructions?, *Geophys. Res. Lett.*, 38, L16706, doi:10.1029/2011GL048529, 2011.
- Finlay, C. C., Maus, S., Beggan, C. D., Bondar, T. N., Chambodut, A., Chernova, T. A., Chulliat, A., Golovkov, V. P., Hamilton, B., Hamoudi, M., Holme, R., Hulot, G., Kuang, W., Langlais, B., Lesur, V., Lowes, F. J., Lühr, H., Macmillan, S., Mandea, M., McLean, S., Manoj, C., Menvielle, M., Michaelis, I., Olsen, N., Rauberg, J., Rother, M., Sabaka, T. J., Tangborn, A., Tøffner-Clausen, L., Thebault, E., Thomson, A. W. P., Wardinski, I., Wei, Z., and Zvereva, T. I.: International Geomagnetic Reference

A.3. Impact of solar vs. volcanic activity variations on tropospheric temperatures and precipitation during the Dalton Minimum

936

J. G. Anet et al.: Sun and volcanoes: effect on the troposphere in the DM

- Field: the eleventh generation, *Geophys. J. Int.*, 183, 1216–1230, doi:10.1111/j.1365-246X.2010.04804.x, 2010.
- Fischer, E. M., Luterbacher, J., Zorita, E., Tett, S. F. B., Casty, C., and Wanner, H.: European climate response to tropical volcanic eruptions over the last half millennium, *Geophys. Res. Lett.*, 34, L05707, doi:10.1029/2006GL027992, 2007.
- Forster, P. M., Fomichev, V. I., Rozanov, E., Cagnazzo, C., Jonsson, A. I., Langematz, U., Fomin, B., Iacono, M. J., Mayer, B., Mlawer, E., Myhre, G., Portmann, R. W., Akiyoshi, H., Falaleeva, V., Gillett, N., Karpechko, A., Li, J., Lemennais, P., Morgenstern, O., Oberländer, S., Sigmond, M., and Shibata, K.: Evaluation of radiation scheme performance within chemistry climate models, *J. Geophys. Res.*, 116, D10302, doi:10.1029/2010JD015361, 2011.
- Frank, D. C., Esper, J., Raible, C. C., Büntgen, U., Trouet, V., Stocker, B., and Joos, F.: Ensemble 25 reconstruction constraints on the global carbon cycle sensitivity to climate, *Nature*, 463, 527–530, doi:10.1038/nature08769, 2010.
- Gao, C., Robock, A., and Ammann, C.: Volcanic forcing of climate over the past 1500 years: An improved ice core-based index for climate models, *J. Geophys. Res.*, 113, D23111, doi:10.1029/2008JD010239, 2008.
- Giorgetta, M.: Der Einfluss der quasi-zweijährigen Oszillation: Modellrechnungen mit ECHAM4, Max-Planck-Institut für Meteorologie, Hamburg, Examensarbeit Nr. 40, MPI-Report 218, 1996.
- Hagemann, S.: An improved land surface parameter dataset for global and regional climate models, Max-Planck-Institut für Meteorologie, Hamburg, 2002.
- Hagemann, S., Botzet, M., Dümenil, L., and Machenhauer, B.: Derivation of global GCM boundary conditions from 1 km land use satellite data, Max-Planck-Institut für Meteorologie, Hamburg, 1999.
- Haigh, J. D.: The Impact of Solar Variability on Climate, *Science*, 272, 981–984, doi:10.1126/science.272.5264.981, 1996.
- Harington, C.: The Year without a Summer, in: *World Climate in 1816*, edited by: Harington, C., Canadian Museum of Nature, Ottawa, 1992.
- Iles, C. E., Hegerl, G. C., Schurer, A. P., and Zhang, X.: The effect of volcanic eruptions on global precipitation, *J. Geophys. Res.*, 118, 8770–8786, doi:10.1002/jgrd.50678, 2013.
- Ineson, S., Scaife, A. A., Knight, J. R., Manners, J. C., Dunstone, N. J., Gray, L. J., and Haigh, J. D.: Solar forcing of winter climate variability in the Northern Hemisphere, *Nature*, 4, 753–757, doi:10.1038/NNGEO1282, 2011.
- IPCC – Intergovernmental Panel on Climate Change: Climate change 2007: The Physical Science Basis, Contribution of Working Group I to the Fourth Assessment Report of the Intergovernmental Panel on Climate Change, in: AR4, edited by: Solomon, S., Qin, D., Manning, M., Chen, Z., Marquis, M., Averyt, K., Tignor, H., and Miller, H., Cambridge University Press, Cambridge, UK and New York, NY, USA, 2007.
- Jones, P. D., Ogilvie, A. E., Davies, T. D., and Briffa, K. R.: History and climate: memories of the future?, Springer, Berlin, 2001.
- Kirchner, I., Stenchikov, G. L., Graf, H.-F., Robock, A., and Antuna, J. C.: Climate model simulation of winter warming and summer cooling following the 1991 Mount Pinatubo volcanic eruption, *J. Geophys. Res.*, 104, 19039–19055, doi:10.1029/1999JD900213, 1999.
- Kodera, K. and Kuroda, Y.: Dynamical response to the solar cycle, *J. Geophys. Res.*, 107, 4749–4761, doi:10.1029/2002JD002224, 2002.
- Kravitz, B. and Robock, A.: Climate effects of high-latitude volcanic eruptions: Role of the time of year, *J. Geophys. Res.*, 116, D01105, doi:10.1029/2010JD014448, 2011.
- Labitzke, K., Austin, J., Butchart, N., Knight, J., Takahashi, M., Nakamoto, M., Nagashima, T., Haigh, J., and Williams, V.: The global signal of the 11-year solar cycle in the stratosphere: observations and models, *J. Atmos. Sol.-Terr. Phys.*, 64, 203–210, doi:10.1016/S1364-6826(01)00084-0, 2002.
- Luterbacher, J., Dietrich, D., Xoplaki, E., Grosjean, M., and Wanner, H.: European Seasonal and Annual Temperature Variability, Trends, and Extremes Since 1500, *Science*, 303, 1499–1503, doi:10.1126/science.1093877, 2004.
- MacFarling-Meure, C., Etheridge, D., Trudinger, C., Steele, P., Langenfelds, R., Van Ommen, T., Smith, A., and Elkins, J.: Law Dome CO₂, CH₄ and N₂O ice core records extended to 2000 years BP, *Geophys. Res. Lett.*, 33, L14810, doi:10.1029/2006GL026152, 2006.
- Mann, M., Bradley, S., and Hughes, M.: Northern hemisphere temperatures during the past millennium: inferences, uncertainties, and limitations, *Geophys. Res. Lett.*, 26, 759–762, doi:10.1029/1999GL900070, 1999.
- Mann, M. E., Fuentes, J. D., and Rutherford, S.: Underestimation of volcanic cooling in tree-ring-based reconstructions of hemispheric temperatures, *Nat. Geosci.*, 5, 202–205, doi:10.1038/ngeo1394, 2012.
- Marsland, S., Haak, H., Jungclaus, J., Latif, M., and Roske, F.: The Max-Planck-Institute global ocean/sea ice model with orthogonal curvilinear coordinate, *Ocean Model.*, 5, 91–27, doi:10.1016/S1463-5003(02)00015-X, 2003.
- McGregor, S. and Timmermann, A.: The effect of explosive tropical volcanism on ENSO, *J. Climate*, 24, 2178–2191, doi:10.1175/2010JCLI3990.1, 2011.
- Meehl, G. A., Arblaster, J., Branstator, G., and Van Loon, H.: A coupled air-sea response mechanism to solar forcing in the Pacific region, *J. Climate*, 21, 2883–2897, doi:10.1175/2007JCLI1776.1, 2008.
- Meehl, G. A., Arblaster, J. M., Matthes, K., Sassi, F., and van Loon, H.: Amplifying the Pacific Climate System Response to a Small 11-Year Solar Cycle Forcing, *Science*, 325, 1114–1118, doi:10.1126/science.1172872, 2009.
- Muthers, S., Anet, J., Raible, C., Brönnimann, S., Rozanov, E., Arfeuille, F., Peter, T., Shapiro, A., Beer, J., Steinhilber, F., Brugnara, Y., and Schmutz, W.: Northern hemispheric winter warming pattern after tropical volcanic eruptions: Sensitivity to the ozone climatology, *J. Geophys. Res.-Atmos.*, 119, 1340–1355, doi:10.1002/2013JD020138, 2014a.
- Muthers, S., Anet, J., Raible, C., Brönnimann, S., Rozanov, E., Arfeuille, F., Peter, T., Shapiro, A., Beer, J., Steinhilber, F., Brugnara, Y., and Schmutz, W.: The coupled atmosphere–chemistry–ocean model SOCOL–MPIOM, *Geosci. Model Dev. Discuss.*, 7, 3013–3084, doi:10.5194/gmdd-7-3013-2014, 2014b.
- NCAR/CISL/VETS: The NCAR Command Language (Version 6.0.0) [Software], Boulder, USA, 2012.
- Olson, D. W., Doescher, R. L., and Olson, M. S.: The blood-red sky of the scream, *American Physical Society, Maryland*, 13–14, 2004.

- Robertson, A., Overpeck, J., Rind, D., Mosley-Thompson, E., Zielinski, G., Lean, J., Koch, D., Penner, J., Tegen, I., and Healy, R.: Hypothesized climate forcing time series for the last 500 years, *J. Geophys. Res.-Atmos.*, 106, 14783–14803, doi:10.1029/2000JD900469, 2001.
- Robock, A.: Review of Year Without a Summer? World Climate in 1816, *Climatic Change*, 26, 105–108, 1994.
- Robock, A.: Volcanic Eruptions and Climate, *Rev. Geophys.*, 38, 191–219, doi:10.1029/1998RG000054, 2000.
- Robock, A. and Mao, J.: Winter warming from large volcanic eruptions, *Geophys. Res. Lett.*, 19, 2405–2408, doi:10.1029/92GL02627, 1992.
- Robock, A. and Mao, J.: The volcanic signal in surface temperature observations, *J. Climate*, 8, 1086–1103, doi:10.1175/1520-0442(1995)008<1086:TVSIST>2.0.CO;2, 1995.
- Roeckner, E., Baeuml, G., Bonaventura, L., Brokopf, R., Esch, M., Giorgetta, M., Hagemann, S., Kirchner, I., Kornblueh, L., Manzini, E., Rhodin, A., Schlese, U., Schulzweida, U., and Tompkins, A.: The atmospheric general circulation model ECHAM 5, PART I: Model description, Report No. 349, http://www.mpimet.mpg.de/fileadmin/publikationen/Reports/max_scirep_349.pdf, Max-Planck-Institut für Meteorologie, Hamburg, 2003.
- Rozanov, E. V., Schlesinger, M. E., Zubov, V., Yang, F., and Andronova, N. G.: The UIUC three-dimensional stratospheric chemical transport model: Description and evaluation of the simulated source gases and ozone, *J. Geophys. Res.*, 104, 755–781, doi:10.1029/1999JD900138, 1999.
- Rozanov, E. V., Egorova, T. A., Shapiro, A. I., and Schmutz, W. K.: Modeling of the atmospheric response to a strong decrease of the solar activity, *Proc. Int. Astron. Union*, 7, 215–224, doi:10.1017/S1743921312004863, 2012a.
- Rozanov, E. V., Calisto, M., Egorova, T., Peter, T., and Schmutz, W.: Influence of the Precipitating Energetic Particles on Atmospheric Chemistry and Climate, *Surv. Geophys.*, 33, 483–501, doi:10.1007/s10712-012-9192-0, 2012b.
- Schraner, M., Rozanov, E., Schnadt Poberaj, C., Kenzelmann, P., Fischer, A. M., Zubov, V., Luo, B. P., Hoyle, C. R., Egorova, T., Fueglistaler, S., Brönnimann, S., Schmutz, W., and Peter, T.: Technical Note: Chemistry-climate model SOCOL: version 2.0 with improved transport and chemistry/microphysics schemes, *Atmos. Chem. Phys.*, 8, 5957–5974, doi:10.5194/acp-8-5957-2008, 2008.
- Semeniuk, K., Fomichev, V. I., McConnell, J. C., Fu, C., Melo, S. M. L., and Usoskin, I. G.: Middle atmosphere response to the solar cycle in irradiance and ionizing particle precipitation, *Atmos. Chem. Phys.*, 11, 5045–5077, doi:10.5194/acp-11-5045-2011, 2011.
- Shapiro, A. I., Schmutz, W., Schoell, M., Haberreiter, M., and Rozanov, E.: NLTE solar irradiance modeling with the COSI code, *Astron. Astrophys.*, 517, A48, doi:10.1051/0004-6361/200913987, 2010.
- Shapiro, A. I., Schmutz, W., Rozanov, E., Schoell, M., Haberreiter, M., Shapiro, A. V., and Nyeki, S.: A new approach to the long-term reconstruction of the solar irradiance leads to large historical solar forcing, *Astron. Astrophys.*, 529, A67, doi:10.1051/0004-6361/201016173, 2011.
- Shindell, D., Schmidt, G., Miller, R., and Mann, M.: Volcanic and solar forcing of climate change during the preindustrial era, *J. Climate*, 16, 4094–4107, doi:10.1175/1520-0442(2003)016<4094:VASFOC>2.0.CO;2, 2000.
- Sinnhuber, M., Nieder, H., and Wieters, N.: Energetic Particle Precipitation and the Chemistry of the Mesosphere/Lower Thermosphere, *Surv. Geophys.*, 33, 1281–1334, doi:10.1007/s10712-012-9201-3, 2012.
- Solanki, S. K., Krivova, N. A., and Haigh, J. D.: Solar Irradiance Variability and Climate, *Astron. Astrophys.*, 51, 311–351, doi:10.1146/annurev-astro-082812-141007, 2013.
- Steinhilber, F., Abreu, J. A., and Beer, J.: Solar modulation during the Holocene, *Astrophys. Space Sci.*, 4, 1–6, doi:10.5194/astr-4-1-2008, 2008.
- Steinhilber, F., Beer, J., and Fröhlich, C.: Total solar irradiance during the Holocene, *Geophys. Res. Lett.*, 36, L19704, doi:10.1029/2009GL040142, 2009.
- Stenchikov, G., Robock, A., Ramaswamy, V., Schwarzkopf, M. D., Hamilton, K., and Ramachandran, S.: Arctic Oscillation response to the 1991 Mount Pinatubo eruption: Effects of volcanic aerosols and ozone depletion, *J. Geophys. Res.*, 107, ACL 28-1–ACL 28-16, doi:10.1029/2002JD002090, 2002.
- Stenchikov, G., Delworth, T. L., Ramaswamy, V., Stouffer, R. J., Wittenberg, A., and Zeng, F.: Volcanic signals in oceans, *J. Geophys. Res.*, 114, D16104, doi:10.1029/2008JD011673, 2009.
- Stenke, A., Schraner, M., Rozanov, E., Egorova, T., Luo, B., and Peter, T.: The SOCOL version 3.0 chemistry-climate model: description, evaluation, and implications from an advanced transport algorithm, *Geosci. Model Dev.*, 6, 1407–1427, doi:10.5194/gmd-6-1407-2013, 2013.
- Toohey, M., Krüger, K., Niemeier, U., and Timmreck, C.: The influence of eruption season on the global aerosol evolution and radiative impact of tropical volcanic eruptions, *Atmos. Chem. Phys.*, 11, 12351–12367, doi:10.5194/acp-11-12351-2011, 2011.
- Valcke, S.: The OASIS3 coupler: a European climate modelling community software, *Geosci. Model Dev.*, 6, 373–388, doi:10.5194/gmd-6-373-2013, 2013.
- Varma, V., Prange, M., Lamy, F., Merkel, U., and Schulz, M.: Solar-forced shifts of the Southern Hemisphere Westerlies during the Holocene, *Clim. Past*, 7, 339–347, doi:10.5194/cp-7-339-2011, 2011.
- Varma, V., Prange, M., Spanghel, T., Lamy, F., Cubasch, U., and Schulz, M.: Impact of solar-induced stratospheric ozone decline on Southern Hemisphere westerlies during the Late Maunder Minimum, *Geophys. Res. Lett.*, 39, L20704, doi:10.1029/2012GL053403, 2012.
- Wagner, S. and Zorita, E.: The influence of volcanic, solar and CO₂ forcing on the temperatures in the Dalton Minimum (1790–1830): a model study, *Clim. Dynam.*, 25, 205–218, 2005.
- Wang, T., Otterå, O., Gao, Y., and Wang, H.: The response of the North Pacific Decadal Variability to strong tropical volcanic eruptions, *Clim. Dynam.*, 39, 2917–2936, doi:10.1007/s00382-012-1373-5, 2012.
- Wegmann, M., Brönnimann, S., Bhend, J., Franke, J., Folini, D., Wild, M., and Luterbacher, J.: Volcanic influence on European summer precipitation through monsoons: Possible cause for “Years Without a Summer”, *J. Climate*, doi:10.1175/JCLI-D-13-00524.1, in press, 2013.

A.3. Impact of solar vs. volcanic activity variations on tropospheric temperatures and precipitation during the Dalton Minimum

938

J. G. Anet et al.: Sun and volcanoes: effect on the troposphere in the DM

Wolf, R.: Abstract of his latest results, *Mon. Not. R. Astron. Soc.*, 21, 77, 1861.

Zanchettin, D., Timmreck, C., Graf, H.-F., Rubino, A., Lorenz, S., Lohmann, K., Krüger, K., and Jungclaus, J.: Bi-decadal variability excited in the coupled ocean–atmosphere system by strong tropical volcanic eruptions, *Clim. Dynam.*, 39, 419–444, doi:10.1007/s00382-011-1167-1, 2012.

Zanchettin, D., Bothe, O., Graf, H. F., Lorenz, S. J., Luterbacher, J., Timmreck, C., and Jungclaus, J. H.: Background conditions influence the decadal climate response to strong volcanic eruptions, *J. Geophys. Res.-Atmos.*, 118, 4090–4106, doi:10.1002/jgrd.50229, 2013.

Supplementary material

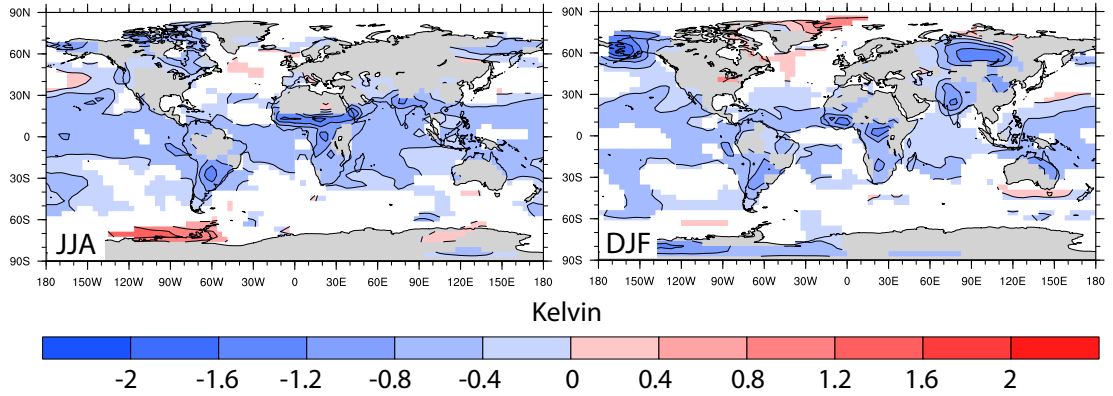


Figure S1.: Ensemble mean of 2m-Temperature differences, averaged over the 1805-1825 period for the ALL run, JJA (left) and DJF (right) seasons. Only areas which are significant at the 5% level are colored (two sided t-test).

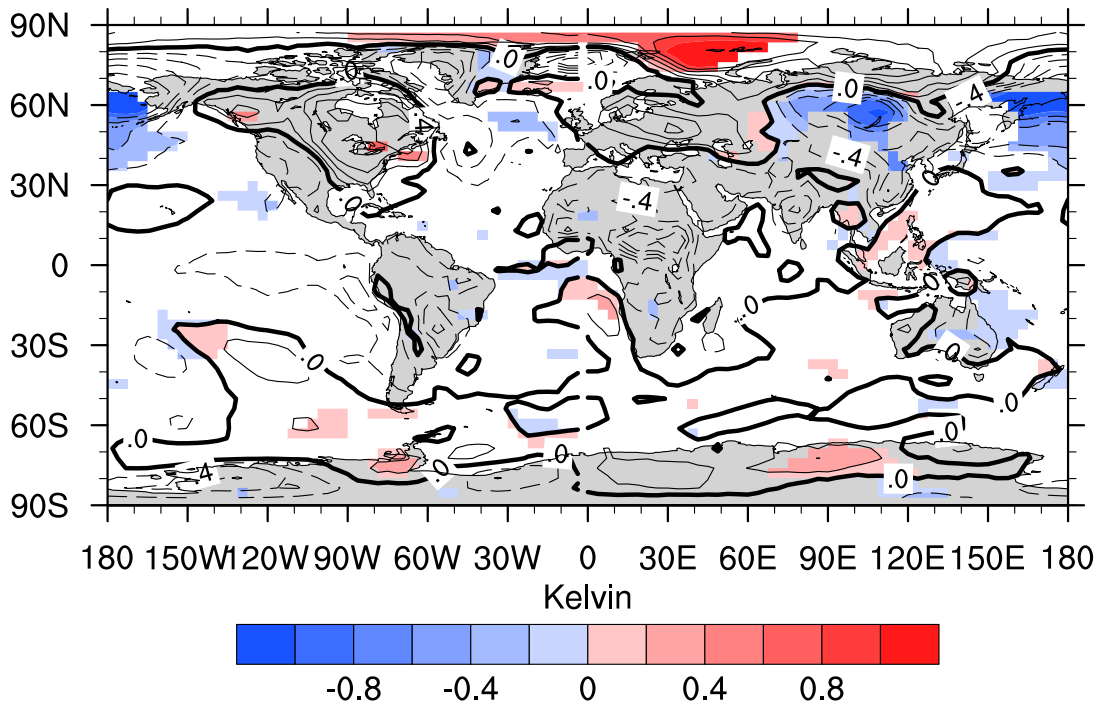


Figure S2.: Ensemble mean of 2m-Temperature differences, averaged over the 1805-1825 period for the EPP run, boreal winter season (DJF). Only areas which are coloured at the 5% level are coloured (two sided t-test).

A.3. Impact of solar vs. volcanic activity variations on tropospheric temperatures and precipitation during the Dalton Minimum

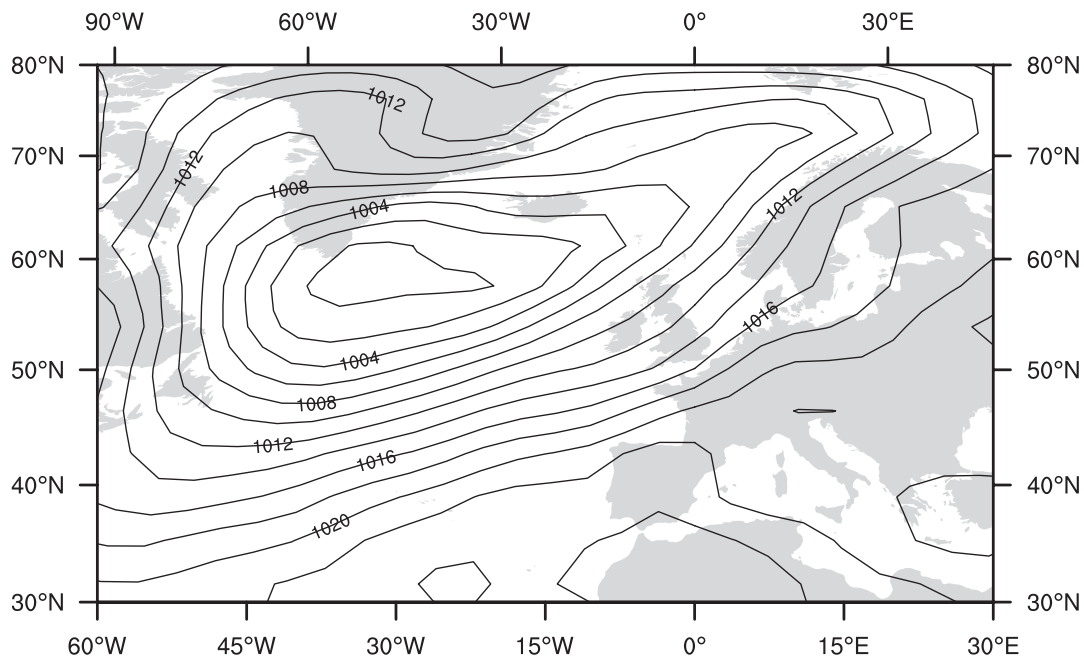


Figure S3.: Climatology of the sea level pressure patterns during the boreal winter season (DJF) of the ALL experiment.

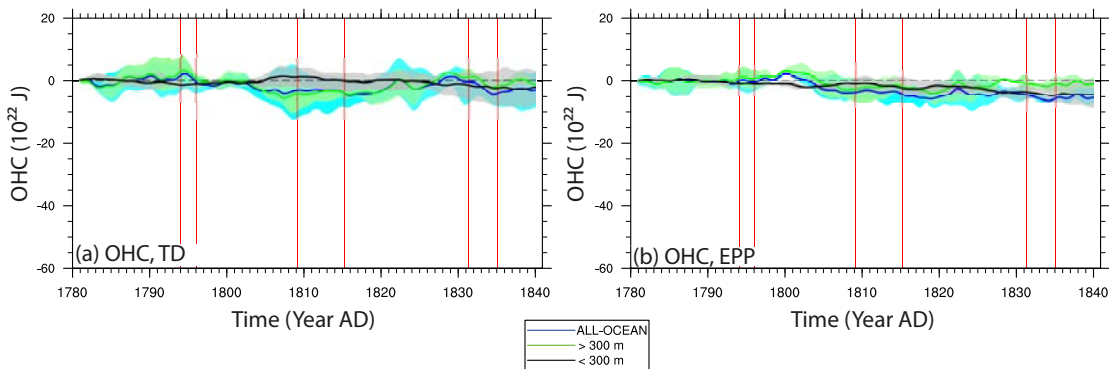


Figure S4.: Ensemble mean of detrended global ocean heat content (OHC) anomalies relative to CTRL1780, plotting technique analogue to Stenchikov 2009. For a and b: Black curve shows global total OHC (0 m-6020 m), green curve global OHC of the top 300 m, blue curve global OHC of the layers below 300 m (300 m-6020 m). Envelope shows the min/max values. (a): For TD; (b): for EPP. Red vertical lines highlight the years, at which a volcanic eruption occurred.

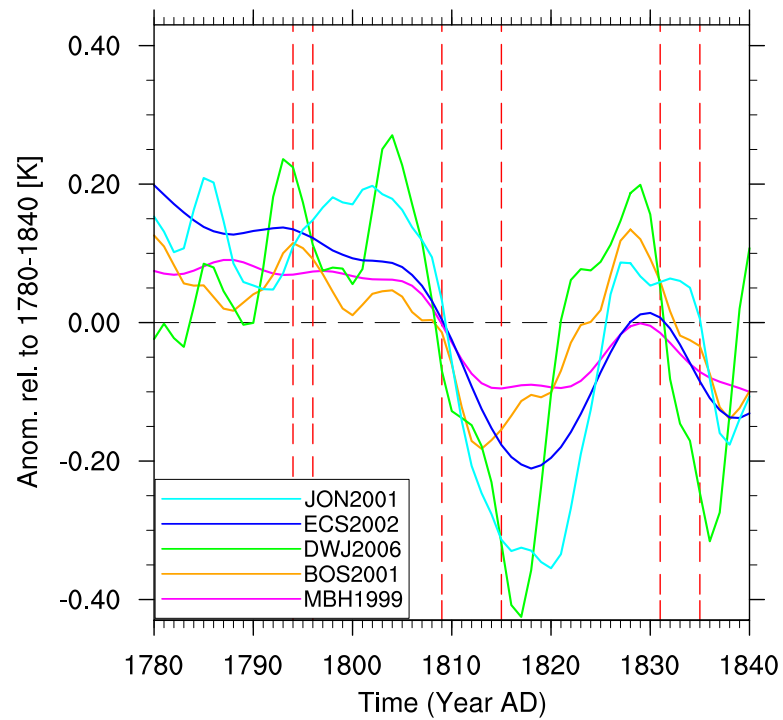


Figure S5.: Northern hemispheric temperature reconstructions following IPCC AR4. Cyan, JON2001: Jones et al. (2001); Blue, ECS2002: Esper et al. (2002); Green, DWJ2006: d'Arrigo et al. (2006); Orange, BOS2001: Briffa et al. (2001); Magenta, MBH1999: Mann et al. (1999). Red, dashed vertical lines highlight the years, at which a volcanic eruption occurred.

Acknowledgements

I would like to thank all the people who supported me in the last 3.5 years and made this thesis possible.

First of all, I express my thank to PD. Dr. Christoph Raible for supervising this thesis and the tremendous amount of time he spend in discussing my problems and ideas. I would also like to show my gratitude to Prof. Dr. Thomas Stocker for being the co-supervisor. A big thank also to Prof. Dr. Thomas Peter for the external review of this thesis.

This thesis is part of the Synergia Project FUPSOL (future and past solar influence on the terrestrial climate) and benefits substantially from the input from the people of this project. In particular, I would like to thank Julien G. Anet, who worked with me on the coupling of SOCOL-MPIOM, Eugene Rozanov and Andrea Stenke for answering my layman's questions on atmospheric chemistry and SOCOL, Florian Arfeuille for explaining me everything about volcanic forcings, and Stefan Brönnimann, Jürg Beer, Alexander Shapiro, Florian Steinhilber, Yuri Brugnara, and Werner Schmutz for fruitful discussions at our FUPSOL meetings and beyond.

IT support is often forgotten if the technical infrastructure is running smoothly, and that is what it did, thanks to Kay Bieri and Dr. René Bleisch (both KUP), Urs Beyerle (IAC), Andrey Martynov (GUIB), and the IT support team of the ubelix cluster at the University of Bern, as well as the brutus cluster at the ETH in Zurich.

Furthermore, I would like to express my thank to Cevahir Kilic, Andreas Born, Niklaus Merz, Flavio Lehner, Juliette Mignot, Basil Neff, and all my other colleagues for the pleasant time. Many thanks also for the not-so anonymous reviewers of the Introduction: at least 50% of the commas of this thesis belong to you!

Nicht zuletzt danke ich meinen Eltern, für die langjährige Unterstützung ohne die es diese Dissertation nie gegeben hätte. Aniela, dir schulde ich ein unbeschreibbar grosses Dankeschön für die Unterstützung in den letzten Monaten und überhaupt die letzten Jahre mit dir. Danke! Und Luca, dir verdanke ich es, dass ich spätestens Abends, wenn ich nach Hause kam, die Dissertation schnell vergessen hatte, wobei... eigentlich auch tagsüber immer wieder.

Publications

submitted / in review

- **Muthers, S.**, J. G. Anet, A. Stenke, C. C. Raible, E. Rozanov, S. Broennimann, T. Peter, F. X. Arfeuille, A. I. Shapiro, J. Beer, F. Steinhilber, Y. Brugnara, and W. Schmutz (2014): “The coupled atmosphere-chemistry-ocean model SOCOL-MPIOM”, *Geosci. Model Dev. Disc.*, vol. 7, p. 3013-3084, doi:10.5194/gmdd-7-3013-2014 (in review for *Clim. Past*)
- **Muthers, S.**, F. Arfeuille, C. C. Raible (2014): “Dynamical and chemical ozone perturbations after large volcanic eruptions: Role of the climate state and the strength of the eruption”. *J. Geophys. Res.* (in review)

reviewed journals (in reversed chronological order)

11. Anet, J. G., **S. Muthers**, E. Rozanov, C. C. Raible, T. Peter, A. Stenke, A. Shapiro, J. Beer, F. Steinhilber, S. Broennimann, F. Arfeuille, Y. Brugnara, and W. Schmutz (2014): “Impact of solar vs. volcanic activity variations on tropospheric temperatures and precipitation during the Dalton Minimum”, *Clim. Past*, vol. 10, p. 921-938, doi:10.5194/cp-10-921-2014
10. Gosling, S., E. Bryce, P. Dixon, K. Gabriel, J. Hanes, D. Hondula, L. Liang, P. MacLean, **S. Muthers**, S. Nascimento, M. Petralli, and J. Vanos (2014): “A glossary for biometeorology”, *Int. J. Biomet.*, vol. 58, 2, p. 277-308, doi:10.1007/s00484-013-0729-9
9. Shiue, I., **S. Muthers**, and N. Bearman (2014): “The role of cold stress in predicting extra cardiovascular and respiratory admissions.”, *Int. J. Cardiol.*, vol. 171, 1, p. e109-e110, doi:10.1016/j.ijcard.2013.12.122.
8. **Muthers, S.**, J. G. Anet, C. C. Raible, S. Broennimann, E. Rozanov, F. Arfeuille, T. Peter, A. I. Shapiro, J. Beer, F. Steinhilber, Y. Brugnara, W. Schmutz (2014): “Sensitivity of the winter warming pattern following tropical volcanic eruptions to the background ozone climatology”, *J. Geophys. Res.*, vol. 199, 3, p. 1340-1355, doi:10.1002/2013JD020138.
7. Anet, J. G., **S. Muthers**, E. Rozanov, C. C. Raible, T. Peter, A. Stenke, A. Shapiro, J. Beer, F. Steinhilber, S. Broennimann, F. Arfeuille, Y. Brugnara, and W. Schmutz (2013): “Which forcing was responsible for the change in stratospheric chemistry and dynamics during the Dalton Minimum”, *Atmos. Chem. Phys.*, vol. 13, p. 10951-10967, doi:10.5194/acp-13-10951-2013.
6. Anet, J.G., E.V. Rozanov, **S. Muthers**, C.C. Raible, S. Broennimann, F. Arfeuille, T. Peter, J. Beer, F. Steinhilber, and W. Schmutz (2013): “Impact of a potential 21st century ‘Grand Solar Minimum’ on climate and stratospheric ozone”, *Geophys. Res. Lett.*, vol. 40, 16, p. 4420-4425, doi:10.1002/grl.50806.

5. Matzarakis, A., M. Hämmerle, C. Endler, **S. Muthers**, E. Koch, (2012): “Assessment of tourism and recreation destinations under climate change conditions in Austria”. *Met. Zeitschr.*, vol. 21, 2, p. 157-165, doi:10.1127/0941-2948/2012/0342.
4. Matzarakis, A., **S. Muthers**, and E. Koch (2011): “Human-biometeorological evaluation of heat-related mortality in Vienna”. *Theor. Appl. Climatol.*, vol. 105, 1-2, p. 1-10, doi:10.1007/s00704-010-0372-x.
3. **Muthers, S.** and A. Matzarakis (2010): “The use of beanplots in applied climatology - A comparison with boxplots”. *Met. Zeitsch.*, vol. 19, 6, p. 639-642, doi:10.1127/0941-2948/2010/0485.
2. **Muthers, S.**, A. Matzarakis, and E. Koch (2010): “Summer Climate and mortality in Vienna - A human-biometeorological approach of heat related mortality during the heat waves in 2003”. *Wien. klin. Wochenschr.*, vol. 122, 17-18 p. 525-531, doi:10.1007/s00508-010-1424-z
1. **Muthers, S.**, A. Matzarakis, and E. Koch (2010): “Climate change and mortality in Vienna - A human biometeorological analysis based on regional climate modeling.” *Int. J. Environ. Res. Public Health*, vol. 7, 7, p. 2965-2977, doi: 10.3390/ijerph7072965.

other scientific publications

2. Marktl, W., **S. Muthers**, A. Matzarakis, and E. Koch (2010): “Klima beeinflusst Mortalität”. *Österreichische Ärztezeitung*, vol. 10, p. 64-69.
1. **Muthers, S.** (2010): “Untersuchung des Zusammenhangs von thermischem Bioklima und Mortalität in Österreich auf der Grundlage von Messdaten und regionalen Klimamodellen”. Master’s thesis (Magisterarbeit) at the Albert-Ludwigs-University of Freiburg, Germany.

Erklärung

gemäss Art. 28 Abs. 2 RSL 05

Name/Vorname:

Matrikelnummer:

Studiengang:

Bachelor Master Dissertation

Titel der Arbeit:

.....

.....

LeiterIn der Arbeit:

.....

Ich erkläre hiermit, dass ich diese Arbeit selbständig verfasst und keine anderen als die angegebenen Quellen benutzt habe. Alle Stellen, die wörtlich oder sinngemäss aus Quellen entnommen wurden, habe ich als solche gekennzeichnet. Mir ist bekannt, dass andernfalls der Senat gemäss Artikel 36 Absatz 1 Buchstabe r des Gesetzes vom 5. September 1996 über die Universität zum Entzug des auf Grund dieser Arbeit verliehenen Titels berechtigt ist.

.....
Ort/Datum

.....
Unterschrift

Curriculum Vitæ

Personal Data

Name	Stefan Muthers
Date of Birth	October 06, 1980
Place of Origin	Trier, Germany

Education

1987-1991	Primary School, Kenn, Germany
1991-2001	Max-Planck-Gymnasium, Trier, Germany
2002-2006	University of Trier, Germany: Studies of Applied Geography
2006-2010	Albert-Ludwigs University Freiburg, Germany: Physical Geography
2009-2010	Master Thesis ("Magisterarbeit") at the Institute for Meteorology in Freiburg, Germany (Thesis advisors: Prof. Dr. Andreas Matzarakis and Dr. Helmut Saurer)
2010	"Magister Scientiarum" in Physical Geography, Meteorology, and Computer Science
2010-2014	Ph.D. at the division for Climate and Environmental Physics, Physics Institute, University of Bern, Switzerland (Thesis advisors: PD Dr. Christoph Raible and Prof. Dr. Thomas Stocker)

Conferences, Workshops, Seminars

- | | |
|------|---|
| 2009 | COST training school: Universal Thermal Climate Index (UTCI), University of Warsaw, Poland |
| 2010 | BIOMET-7, Freiburg, Germany (poster and talk) |
| 2010 | DACH, Bonn, Germany (talk) |
| 2011 | EaSyMS11 – 4. Earth System Modelling School, Max-Planck-Institute for Meteorology, Hamburg, Germany |
| 2011 | ResClim Summerschool, Svalbard, Norway (poster) |
| 2012 | EGU General Assembly, Vienna, Austria (poster) |
| 2012 | FUPSOL PAGES Workshop, Davos, Switzerland (poster and talk) |
| 2012 | NCCR Summerschool, Monte Verità, Switzerland (poster) |
| 2013 | EGU General Assembly, Vienna, Austria (poster) |
| 2013 | NCCR Summerschool, Grindelwald, Switzerland (poster) |
| 2013 | Seminar of "Climate and Environmental Physics", Bern, Switzerland (invited talk) |
| 2014 | FUPSOL II PAGES Workshop, Davos, Switzerland (talk) |